USE OF RADAR ESTIMATED PRECIPITATION FOR FLOOD FORECASTING

USE OF RADAR ESTIMATED PRECIPITATION FOR FLOOD FORECASTING

By DAYAL WIJAYARATHNE, M.Sc., B.Sc.

Faculty of Science

School of Earth, Environment and Society

A Thesis Submitted to the School of Graduate Studies

in Partial Fulfillment of the Requirements for the Degree

DOCTOR OF PHILOSOPHY

November 2020

DOCTOR OF PHILOSOPHY (2020)	McMaster University
School of Earth, Environment and Society	Hamilton, Ontario
TITLE:	Use of Radar Estimated Precipitation for Flood Forecasting
AUTHOR:	Dayal Wijayarathne M.Sc. (Bowling Green State University) B.Sc. (University of Peradeniya)
SUPERVISOR:	Dr. Paulin Coulibaly
NUMBER OF PAGES:	xxviii, pp. 300

Lay Abstract

Floods are common and increasing deadly natural hazards in the world. Predicting floods in advance using Flood Early Warning System (FEWS) can facilitate flood mitigation. Radar Quantitative Precipitation Estimates (QPEs) can provide real-time, spatially, and temporally continuous precipitation data. This research focuses on bias-correcting and evaluating radar QPEs for hydrologic forecasting. The corrected QPE are applied into a framework connecting hydrological and hydraulic models for operational flood forecasting in urban watersheds in Canada. The key contributions include: (1) Dual-polarized radar QPEs is a useful precipitation input to calibrate, validate and run hydrological models; (2) Radar-gauge merging enhance accuracy and reliability of radar QPEs; (3) Floods could be more accurately predicted by integrating hydrological and hydraulic models in one framework using bias-corrected Radar QPEs; and (4) Gauge-calibrated hydrological models can be run effectively using the bias-corrected radar QPEs. This research will benefit future applications of real-time radar QPEs in operational FEWS.

Abstract

Flooding is one of the deadliest natural hazards in the world. Forecasting floods in advance can significantly reduce the socio-economic impacts. An accurate and reliable flood forecasting system is heavily dependent on the input precipitation data. Real-time, spatially, and temporally continuous Radar Quantitative Precipitation Estimates (QPEs) is useful precipitation information source. This research aims to investigate the efficacy of American and Canadian weather radar QPEs on hydrological model calibration and validation for flood forecasting in urban and semi-urban watersheds in Canada.

A comprehensive review was conducted on the weather Radar network and its' hydrological applications, challenges, and potential future research in Canada. First, radar QPEs were evaluated to verify the reliability and accuracy as precipitation input for hydrometeorological models. Then, the radar-gauge merging techniques were assessed to select the best method for urban flood forecasting applications. After that, merged Radar QPEs were used as precipitation input for the hydrological models to assess the impact of radar QPEs on hydrological model calibration and validation. Finally, a framework was developed by integrating hydrological and hydraulic models to produce flood forecasts and inundation maps in urbanized watersheds.

Results indicated that dual-polarized radar QPEs could be effectively used as a source of precipitation input to hydrological models. The radar-gauge merging enhances both the accuracy and reliability of Radar QPEs, and therefore, the accuracy of streamflow simulation is also improved. Since flood forecasting agencies usually use

hydrological models calibrated and validated using gauge data, it is recommended to use bias-corrected Radar QPEs to run existing hydrological models to simulate streamflow to produce flood extent maps. The hydrological and hydraulic models could be integrated into one framework using bias-corrected Radar QPEs to develop a successful flood forecasting system.

Acknowledgment

I would like to express my heartfelt gratitude to my supervisor Prof. Paulin Coulibaly for his continuous guidance, motivation, support, and patience over the past four years. It would have been impossible to accomplish this landmark in my lifespan without his utmost help. I would also like to express my sincere gratitude to the other supervisory committee members, Prof. Altaf Arain, and Dr. David Sills, for their support and contributions, which have improved my research.

I would like to extend my heartfelt gratitude to all my colleagues at McMaster Water Resources and Hydrologic Modeling Lab (WRHML) for their help and making my graduate life pleasurable and exciting. I would like to thank the following individuals who were eager to share their time and knowledge to guide me throughout my Ph.D. research: Mr. S. Boodoo, Dr. A.A. Khan, Dr. N. Kouwen, Mr. M. Khayer, Prof. D. Hudak, Dr. O. Champagne, Dr. H. Tolossa.

Many thanks to the Natural Sciences and Engineering Research Council of Canada (NSERC), the School of Graduate Studies (SGS), and the School of Earth, Environment and Society (SEES) at McMaster University for the financial and official supports. I acknowledge Toronto and Region Conservation Authority (TRCA), Environment and Climate Change Canada (ECCC), Water Survey of Canada (WSC), Canadian Surface Prediction Archive (CaSPAr), Water Resources Management Division (WRMD)-NL, and NOAA National Weather Service (NWS) for providing me hydrological models and data throughout this work. I also want to thank Hydrologic

Forecasting and Water Management Division in Manitoba Infrastructure, Department of Municipal Affairs and Environment-NL, and ECCC Observations-Based Research Section at King City for hosting me as an intern graduate student.

Last and foremost, I owe a big thanks to an exceptional person, my wife, P. Rupasinghe, for her unconditional love, encouragement, and understanding throughout my pursuit of the Ph.D. degree. I am genuinely grateful to my parents and all family members in Sri Lanka for their continued emotional and financial support. Finally, my deep and sincere gratitude to Sri Lankan friends in Canada, mostly Ms. C. Wimalasena, Mr. H. Melanson, and G. Amaradasa, for their support and generous care over the past few years. This journey would not have been possible without the help of my family and friends.

Thank you all.

.

Table of Content

Table of Contents

List of Figures

List of Tables

List of Abbreviations

AEP	Annual Exceedance Probability
CAFFEWS	Canadian Adaptive Flood Forecasting and Early Warning System
CaLDAS	Canadian Land-Data Assimilation System
CaPA	Canadian Precipitation Analysis
CAPPI	Constant Altitude Plan Position Indicator
CASA	Collaborative Adaptive Sensing of the Atmosphere
CaSPAr	Canadian Surface Prediction ARchive
CDFM	Cumulative Distribution Function Matching
CHPS	Community Hydrologic Prediction System
CLASS	Environment Canada Canadian LAnd Surface Scheme
CONUS	CONterminous United States
CRAFT	Collaborative Radar Acquisition Field Test
CWRN	Canadian Weather Radar Network
CWRRP	Canadian Weather Radar Replacement Program
CWSR	Canadian Weather Station Radar
DDS	Dynamically Dimensioned Search
DND	Department of National Defense
DPA	Digital Precipitation Array
DP-QPEs	Dual-polarimetric rain-rate algorithms
EC	Environment Canada
ECCC	Environment and Climate Change Canada
EFFS	European Flood Forecasting System
EPS	Ensemble Prediction Systems
FEWS	Flood Early Warning System
FIC	Frequency and Intensity Correction
GDPS	Global Deterministic Prediction System

GR4J	modèle du Génie Rural à 4 paramètres Journalier
GRU	Group Response Units
GTA	Greater Toronto Area
GUI	Graphical User Interface
HEC-2	Hydrologic Engineering Center - 2
HEC-DSS	Hydrologic Engineering Center-Data Storage System
HEC-DSSVue	Hydrologic Engineering Center Data Storage System Visual Utility Engine
HEC-HMS	Hydrologic Engineering Center's Hydrologic Modeling System
HEC-RAS	Hydrologic Engineering Center River Analysis System
HEC-RTS	Hydrologic Engineering Center-Real Time Simulation
HPC	High-Performance Computing
HRAP	Hydrologic Rainfall Analysis Projection
HRU	Hydrological Response Units
HSPF	Hydrological Simulation Program - Fortran
HYMO	HYdrological MOdel
IQR	Inter-Quartile Range
KGE	Kling-Gupta Efficiency
KRE	Kriging with Radar-based Error correction
LiDAR	Light Detection and Ranging
LOCI	Local intensity scaling
MAC-HBV	McMaster University Hydrologiska Byråns Vattenbalansavdelning
MAE	Mean Absolute Error
MAPLE	McGill Algorithm for Precipitation nowcasting by the Lagrangian Extrapolation
MBSA	Modified Brandes Spatial Adjustment
MC2	Mesoscale Compressible Community
MFB	Mean Field Bias correction

MPFC	Modified Peak Flow Criterion
MRC	Multiplicative Random Cascade
MRMS	Multi-Radar Multi-sensor QPEs
MRO	McGill weather Radar Observatory
MRR	Micro Rain Radars
MSC	Meteorological Service of Canada
NCEI	National Centers for Environmental Information
NCEP	National Centers for Environmental Prediction
NEXRAD	NEXt-generation weather RADar
NEXRAD-VC	NEXRAD Validation and Calibration software
NFFS	National Flood Forecasting System
NMQ	National Mosaic and Multi-Sensor QPE
NOAA	National Oceanic and Atmospheric Administration
NSE	Nash Sutcliffe Efficiency
NSERC	Natural Science and Engineering Research Council
NWP	Numerical Weather Prediction
NWS	National Weather Services
OHA	One-Hour Precipitation
OK	Ordinary Kriging
OSTRICH	Optimization Software Toolkit
PBIAS	Percent Bias
PFC	Peak Flow Criterion
PMM	Probability Matching Method
POLPPI	POLarimetric Plan Position Indicator
POSS	Precipitation Occurrence Sensor System
PPS	Precipitation Processing System
QPEs	Quantitative Precipitation Estimates
QUALHYMO	Quality/Quantity Simulation Model

Radar	Radio detection and ranging
RADOLAN	Radar-Online-Aneichung
RainFARM	Rainfall Filtered Autoregressive Model
RDA	Range-dependent bias adjustment
RMSE	Root Mean Square Error
RSR	RMSE-observations standard deviation ratio
SAC-SMA	Sacramento Soil Moisture Accounting
SCS	Soil Conservation Service
SHARP	Short-term Automated Radar Predictions
SMOS	Soil Moisture and Ocean Salinity
SNODAS	Snow Data Assimilation System
SWE	Snow Water Equivalent
TRCA	Toronto and Region Conservation Authority
UTM	Universal Transverse Mercator
VE	Volume Error
VPR	Vertical Profile of Reflectivity
WATFLOOD	University of Waterloo Flood Forecasting System
WCT	Weather and Climate Toolkit
WMO	World Meteorological Organization
WPMM	Window Probability Matching Method
WRF	Weather Research and Forecasting
WRMD	Water Resources Management Division

List of Symbols

adimp	additional impervious area
ai	impervious sub-basin area
ak	infiltration coefficient-bare ground
ak2	recharge coefficient-bare ground
ak2fs	recharge coefficient-snow covered ground
akfs	infiltration coefficient-snow covered ground
alpha	non-linearity coefficient
as	sub-basin area
athorn	coefficient of a simplified version of Thornthwaite's formula
b1r	baseflow 1 number of reservoirs
b1s	baseflow 1 storage coefficient
b2r	baseflow 2 number of reservoirs
b2s	baseflow 2 storage coefficient
base	base temperature for melt calculations
beta	non-linear parameter controlling runoff generation
cperc	constant percolation rate parameter
C_{RDA}	range dependent multiplicative factor
C_i	correction factor
C_{maf}	MFB mean assessment factor
C_{mfb}	MFB single adjustment factor
cdf_G	CDF of the historical gauge data
cdf_R	CDF of the radar rainfall
ddf	degree day factor
dff	degree day factor
fc	maximum soil box water content
flp	limit for potential evaporation
fm	melt factor
$F_G(x)$	observed intensity distribution
$F_R(x)$	truncated radar rainfall intensity distribution
g1c	ground water 1 storage coefficient
g1i	initial ground water 1 storage
g1p	ground water 1 percolation rate
g1s	groundwater 1 storage capacity
g2c	groundwater 2 percolation rate
g2i	initial groundwater 2 storage
g2p	groundwater 2 percolation capacity
if	infiltration rate

is	initial soil storage
k0	flow recession coefficient
k1	flow recession coefficient in the upper soil reservoir
k2	flow recession coefficient in the lower soil reservoir
kcond	conductivity of the wetland (bank)-channel interface
lsuz	threshold value to control response routing
lzf	lower zone drainage function parameter
lzfpm	lower-zone free water primary maximum storage
lzfsm	lower-zone free water supplemental maximum storage
lzpk	lower-zone primary free water lateral depletion rate
lzsk	lower-zone supplemental free water lateral depletion rate
lztwm	lower-zone tension water maximum storage
maxbas	runoff distribution parameter
mr	snowmelt rate
pctim	impervious fraction of the watershed area
pfree	fraction percolating from upper to lower zone free water storage
pwr	lower zone drainage function exponent
P	coefficients of the polynomial models
$\bar{P}_G$	average hourly rain gauge measurement
$\bar{P}_R$	average hourly radar estimated rainfall
P_G	hourly precipitation observed by gauge
P_R	hourly radar estimated precipitation
$\bar{\hat{Q}}$	mean simulated flow
$\hat{Q}_{pi}$	simulated peak flows
$\hat{Q}_i$	simulated flow at i^{th} data point
$\bar{Q}$	mean observed flow
Q_i	observed flow at i^{th} data point
Q_{pi}	observed peak flows
R	rain rate/ radar rainfall
R2n	river channel Manning's n
rcr	rainfall correction factor
rec	interflow coefficient
retn	upper zone retention
rexp	exponent of the percolation equation
rq	residence time parameters of quick flow
scf	snow correction factor
si	number of sub-reaches
so	storage-outflow
sp	soil percolation rate
ss	surface storage capacity

st	storage coefficient
sublime_rate	sublimation rate
SW	spectrum width
tc	time of concentration
tcrt	critical temperature for snowmelt
theta	porosity the wetland or channel bank
tmax	upper temperature threshold
tmin	lower temperature threshold
tr	upper threshold temperature to distinguish rainfall and snowfall
ts	tension zone capacity
us	soil storage capacity
uzfwm	upper-zone free water maximum storage
uzk	upper-zone free water lateral depletion rate
uztwm	upper-zone tension water maximum storage
V	velocity
wh	wet hour
x2	water exchange coefficient
x3	capacity of the routing store
x4	time parameter for unit hydrographs
xl	capacity of the production soil store
$\tilde{x}$	the minimum observed rainfall amount
$\tilde{x}_R$	threshold radar rainfall value
$\tilde{x}_{R,h}$	wet-hour threshold
x'	transformed radar rainfall data
Z	horizontal reflectivity/ reflectivity factor
zperc	maximum percolation rate
α	measure of relative variability
β	bias (ratio of simulated and observed values)
$\gamma(h)$	parametric variogram
$\varepsilon_R(s)$	the deviation between observed and interpolated radar values
μ	mean intensity
μ_1	lagrange multiplier

Declaration of Academic Achievement

This thesis was prepared in a sandwich style following the regulations provided by the School of Graduate Studies at McMaster University. It includes the published and submitted papers listed below:

Chapter 2: Application of weather Radar for operational hydrology in Canada – A review, by D. Wijayarathne and P. Coulibaly, Canadian Water Resources Journal, under review, manuscript number TCWR-2020-0005.R2.

Chapter 3: Evaluation of Radar Quantitative Precipitation Estimates (QPEs) as an Input of Hydrological Models for Hydrometeorological Applications, by D. Wijayarathne, S. Boodoo, P. Coulibaly and D. Sills, Journal of Hydrometeorology, 21(8), 1847-1864, https://doi.org/10.1175/JHM-D-20-0033.1, 2020. (© American Meteorological Society. Used with permission.)

Chapter 4: Evaluation of Radar-Gauge Merging Techniques to be Used in Operational Flood Forecasting in Urban Watersheds, by D. Wijayarathne, P. Coulibaly, S. Boodoo and D. Sills, Water, 12(5), 1494, https://doi.org/10.3390/w12051494, 2020. (Under license)

Chapter 5: Integration of Radar QPEs into HEC-RTS Framework for Improved Hydrological Model Calibration for Streamflow Simulation and Flood Inundation Mapping, by D. Wijayarathne, P. Coulibaly, S. Boodoo and D. Sills, Journal of Hydrometeorology, under review, manuscript number JHM-D-20-0267.

Appendix A: Identification of hydrological models for operational flood forecasting in St. John's, Newfoundland, Canada, by D.B. Wijayarathne and P. Coulibaly, Journal of Hydrology: Regional Studies, 27, 100646. https://doi.org/10.1016/j.ejrh.2019.100646, 2020. (With permission from the publisher)

D. Wijayarathne wrote all the articles. Prof. P. Coulibaly, as the supervisor, guided research planning and helped in manuscript preparation by reviewing and editing. For Chapter 2, D. Wijayarathne conducted the literature review of the current radar network in Canada and how it has been applied from a hydrological context. D. Wijayarathne wrote the manuscript, and Prof. P. Coulibaly reviewed and edited it. The paper was submitted to the Canadian Water Resources Journal in 2020. For Chapter 3 and 4, D. Wijayarathne conducted the formal analysis and computational work with the guidance and supervision of Prof. P. Coulibaly, and Mr. S. Boodoo. D. Wijayarathne wrote the manuscript. Prof. P. Coulibaly, Mr. S. Boodoo, and Dr. D. Sills reviewed and edited it. Chapter 3 was published in the Journal of Hydrometeorology in 2020, and chapter 4 was published in Water journal in 2020. For Chapter 5, D. Wijayarathne conducted the modeling and computational work with the guidance and supervision of Prof. P. Coulibaly and Mr. S. Boodoo. D. Wijayarathne wrote the manuscript. Prof. P. Coulibaly, Mr. S. Boodoo, and Dr. D. Sills reviewed and edited it, and the paper was submitted to the Journal of Hydrometeorology in 2020. For Appendix A, D. Wijayarathne conducted the modeling and computational work with the guidance and supervision of Prof. P. Coulibaly. D. Wijayarathne wrote the manuscript. Prof. P. Coulibaly reviewed

and edited it, and the paper was published in the Journal of Hydrology: Regional Studies in 2020. The work reported here was undertaken from September 2016 to November 2020.

Chapter 1. Introduction

1.1. Background

Floods have been recognized as the world's deadliest natural disasters after earthquakes and tsunamis, given its potential for catastrophic socio-economic impacts (Balica et al., 2013; Jonkman & Vrijling, 2008). During the 21st century, the frequency of flooding has increased mainly due to climate change and population growth (Jonkman & Kelman, 2005; Tol, 2016). Meteorological extremes led by climate change accelerate the hydrological cycle increasing discharge in streams leading to floods (Han & Coulibaly, 2017). The population increase exacerbates both frequency and impact of flooding due to the paving over of natural areas and increasing the pressure on sewer systems (Zhang et al., 2018). Recently occurred unprecedented floods such as the 2017 Texas floods (USA), 2013 Toronto flood (Canada), and 2007 Scotland flood (UK) have brought attention to flood mitigation measures all around the world (Reggiani et al., 2009). In Canada, the frequency of floods and associated human and economic losses have been increased over the past 50 years (Bowering et al., 2014). Therefore, floods are identified as one of the most common natural hazards to life, property, economy, and the Canadian environment. The estimated total cost of massive floods in Canada is approximately 36 billion CAD from 1900 to 2016, as reported by Public Safety Canada (2019). Therefore, flood mitigation measures are essential for flood-prone regions to minimize the damages.

The generally implemented flood mitigation strategies are classified as structural and nonstructural (Thampapillai & Musgrave, 1985). Structural measures reduce flood probability by altering physical characteristics (Heidari, 2009). These measures include

constructing structures such as dams, levees, and culverts, requiring a significant capital investment (Mays, 2010). On the contrary, less expensive nonstructural measures that involve administrative measures are more effective and affordable approaches to reduce the negative impact of flooding (Faisal et al., 1999). The United Nations identifies flood forecasting and warning as an effective nonstructural flood mitigation approach as it can reduce the flood damage up to 35% (Nagai, 2003; Pilon, 2002). Many developed countries have implemented flood forecasting and early warning systems to issue real-time flood forecasts for effective flood management and mitigation. For example, National Flood Forecasting System (NFFS) in England (Werner et al., 2009); Community Hydrologic Prediction System (CHPS) in the USA (Roe et al., 2010); European Flood Forecasting System (EFFS) in Europe (De Roo et al., 2003); Flood Early Warning System (FEWS) in Scotland (Cranston & Tavendale, 2012). Flood forecasting and early warning systems utilize hydrological and hydraulic models to predict floods using hydrometeorological data as inputs (Jain et al., 2018). Even though hydrological and hydraulic modeling has been used for flood forecasting in Canada (Moradkhani & Sorooshian, 2008; Zahmatkesh et al., 2019), currently, there is no nationwide flood forecasting system (*FloodNet*, 2020).

The accuracy and reliability of flood forecasts heavily depends on the accuracy and reliability of input precipitation data (Larson & Peck, 1974). The precipitation input for hydrological models is collected through conventional rain-gauges and weather Radio detection and ranging (Radar) (Gilewski & Nawalany, 2018). The calibration and validation of hydrological models embedded in flood forecasting systems mostly rely on

in-situ rain gauge data (McMillan et al., 2011; Shakti et al., 2019). Rain-gauges are believed to be providing accurate point rainfall measurements even though they suffer from both random and systematic errors (Sevruk, 1982). The point gauge data must be interpolated into a grid to represent the spatial distribution of rainfall before use into distributed hydrological models for flood forecasting purposes (Rabiei & Haberlandt, 2015). In contrast to rain-gauges, operational weather radar produces real-time, spatially, and temporally continuous Quantitative Precipitation Estimates (QPEs) over an area within the Radar range, capturing variations of precipitation in both space and time (Dhiram & Wang, 2016; Thorndahl et al., 2016). Gridded precipitation estimates with high temporal resolution can enhance flood forecasting, especially in urban watersheds, where response time is low as hours due to the impervious ground (Benjamin, 2016; Chen et al., 2017).

At present, different countries produce commercial weather Radar products that are extensively used in operational hydrology: e.g., NEXt-generation weather RADar (NEXRAD) in the USA, Nimrod in the UK, and Radar-Online-Aneichung (RADOLAN) in Germany (Krajewski et al., 2010; Marx et al., 2006; Moore et al., 2004). The first weather Radar station in Canada was established in the 1950s, and since then, the Radar network was progressively expanded (Mekis et al., 2018). The current Canadian Weather Radar Network (CWRN) is a mixed network of conventional and dual-polarized Doppler Radar and includes 31 Radar stations covering Canada's most populated areas (Joe & Lapczak, 2002). Both base reflectivity data (Horizontal reflectivity: Z) and dual-polarized reflectivity data (Differential Reflectivity: Z_{DR} and Specific Differential Phase: K_{DP}) are

collected in about 1 min intervals with 0.25 km × 0.5-degree range and azimuthal resolution using POLarimetric Plan Position Indicator (POLPPI) scans at 0.5-degree elevation by ECCC Radar (Dufton, 2016; Ryzhkov et al., 2005). Radar QPEs are then estimated using different rain rate estimators (Z-R algorithms) such as R (Z), R (Z, Z_{DR}), R (Z, K_{DP}), and R (K_{DP}, Z_{DR}) (Brandes et al., 2002; Bringi et al., 2011; Fulton et al., 1998; Marshall & Palmer, 1948; Richards & Crozier, 1983). Most of the Canadian ground-based Radars are C-band Radar; however, the existing ECCC C-band Radar network is currently being upgraded into S-bands, with an expected completion date of 2023. Other than the Canadian weather Radar systems, the American Radar system, NEXRAD, covers areas close to the USA – Canada border where most of the Canadian population reside. The NEXRAD Radar system is a Doppler weather Radar network developed by National Weather Services (NWS) and uses both single-polarimetric rain rate algorithms R(Z) and Dual-polarimetric rain-rate algorithms (DP-QPEs) to produce Radar QPEs (Fulton et al., 1998; Ryzhkov et al., 2005). There are two levels of NEXRAD products where both Level II (three meteorological base data: reflectivity, mean radial velocity, and spectrum width) and Level III (Radar QPEs) are available publicly in the National Centers for Environmental Information (NCEI) archives (Chen & Farrar, 2007; Xie et al., 2006). Therefore, USA NEXRAD S-band Radar QPE is a potential precipitation data source for Canadian watersheds.

Instead of direct precipitation measurements, Radar uses the attenuation of microwave from precipitation targets measured as reflectivity. The measured reflectivity values are converted into precipitation volumes using the predefined relationship between

Radar reflectivity and the Rainfall rate (Austin, 1987; Marshall & Palmer, 1948). Therefore, Radar QPEs suffer from errors induced during the reflectivity measurements and reflectivity-rain intensity conversion process (Dai et al., 2018). The ground clutter (Hubbert et al., 2009), bright band contamination (Cao et al., 2019), Radar instrument miscalibration (Collier, 1986), attenuation (Park et al., 2005), range degradation (Gabella et al., 2011), the variability of the raindrop size distribution (Williams et al., 2005), anomalous propagation (Moszkowicz et al., 1994), etc., induce errors to reflectivity measurements and consequently in Radar QPEs. As a result of these numerous errors that can profoundly affect final Radar QPEs, their use as an input for hydrological models is limited (Rabiei & Haberlandt, 2015; Wang et al., 2015).

The dual-polarized Radar produces better QPEs than conventional single polarized Radar (Bringi et al., 2011; Chandrasekar et al., 2013; Hall et al., 2015; Sugier et al., 2006). Also, increasing the Radar network's density reduces the uncertainties in Radar QPEs by reducing the Radar stations' distance. However, these modifications are challenging due to Canada's complex geography, and both methods require significant capital investment. As a solution, previous research has proven that adjusting Radar QPEs to match with gauge observations (radar-gauge merging) could significantly improve the accuracy and reliability of Radar QPEs. (Goudenhoofdt & Delobbe, 2009; Ochoa-Rodriguez et al., 2019; Vieux & Bedient, 2004; Wang et al., 2015). The performance of radar-gauge merging methods and, ultimately, merged Radar QPEs depend on the quality of raw Radar reflectivity and corresponding Radar only QPEs. Therefore, Radar only QPEs must be evaluated before applying radar-gauge merging at the resolution required

for urban hydrological applications. After evaluating and applying radar-gauge merging, Radar QPEs can be used as precipitation input for the hydrological model to assess the impact of Radar QPEs on hydrological model calibration, validation, and run for operational flood forecasting. A Flood Early Warning System (FEWS) can be developed by integrating hydrological and hydraulic models into a one-framework capable of collecting, computing, viewing, and bias-correcting Radar QPEs. Hence, further research is needed to evaluate, bias-correct, and examine the effect of Radar QPEs on hydrological model calibration, validation, and operational run for flood forecasting.

1.2. Problem Statement and Motivations

Radar estimated precipitation data has gained significant attention over conventional rain gauges in operational hydrology. Even though Radar QPEs have been used in hydrological context for decades in Canada, there has been no literature summarizing the state-of-the-art use of Radar QPEs in operational hydrology. A comprehensive literature review summarizing the current Canadian Radar network, available Radar QPEs, application in hydrology, challenges, and potential future research is required.

The American NEXRAD QPEs is a potential Radar QPE for hydrological applications in Canadian watersheds. Even though both Canadian and US weather Radar has been used for decades in hydrological applications, their accuracy and reliability are uncertain due to intrinsic errors during measurements and reflectivity-rain rate conversions. Therefore, a comprehensive evaluation of Radar QPEs at high spatial (a few

km) and temporal (hourly or sub-hourly) resolutions is essential before using them as precipitation input for hydrometeorological models.

Following the evaluation, a vigorous method to adjust Radar QPEs to match with gauge observations (radar-gauge merging) should be applied to improve the accuracy and reliability before using Radar QPEs in operational hydrology with confidence. Previous studies have shown a significant improvement in the accuracy and reliability of Radar QPEs after radar-gauge merging. However, the application of radar-gauge merging to improve new dual-polarized Radar QPEs is yet to be implemented in operational flood forecasting in urban and semi-urban watersheds in Canada.

Establishing a system to predetermine flood events is necessary to mitigate flood damage. A flood forecasting system involves hydrological models representing different hydrological processes and hydraulic models to simulate flood extent and inundation depths. Therefore, implementing a system that connects hydrological and hydraulic models in one framework using bias-corrected Radar QPEs as the precipitation input is essential to issue flood warnings to make proper decisions and take immediate actions to reduce flood damage.

1.3. Scope of the research

The study presented here addressed the use of Radar QPEs for hydrological model calibration, validation, and flood forecasting in Canadian urban watersheds. To accomplish the overall objective, the following secondary objectives were achieved:

- A literature review on the application of weather Radar for operational hydrology in Canada.

- Evaluation of available Radar QPEs.
- Assessment of radar-gauge merging techniques.
- Integration of hydrological and hydraulic models into one framework to develop flood extent maps using merged Radar QPEs.

Four journal articles have been completed from the research and are presented in chapter 2-5 of the thesis. Each of the objectives forms the basis of papers published or in the review process in peer-reviewed journals.

Apart from the primary research, a case study was performed to propose a suitable flood forecasting method at the Waterford River watershed in St. John's, Newfoundland (Appendix A).

1.4. Thesis Outline

This thesis consists of six chapters. Chapter 1 is an overview describing the background, research motivations, scope of the research, and thesis outline. Chapter 2 presents a comprehensive literature review of Canada's weather Radar network and its application from a hydrological context. The third chapter evaluates two KBUF NEXRAD S-band Radar QPEs at Buffalo, New York, USA, and seven WKR C-band dual-polarized Radar QPEs at King City, ON, Canada. The fourth chapter compares several radar-gauge merging techniques and identifies the best technique that suits the Humber River (semi-urban) and Don River (urban) watersheds in Canada. Chapter 5 integrates HEC-HMS hydrological model and HEC-RAS hydraulic models into the HEC-RTS model framework to examine the impact of Radar QPEs on hydrological model

calibration, validation, and flood mapping in Mimico Creek watershed (urban) in the GTA. Finally, chapter 6 includes conclusions and recommendations for future research.

1.5. References

Austin, P. M. (1987). Relation between measured radar reflectivity and surface rainfall. *Monthly Weather Review*, *115*(5), 1053–1070. https://doi.org/10.1175/1520-0493(1987)115<1053:RBMRRA>2.0.CO;2.

Balica, S. F., Popescu, I., Beevers, L., & Wright, N. G. (2013). Parametric and physically based modelling techniques for flood risk and vulnerability assessment: A comparison. *Environmental Modelling & Software*, *41*, 84–92. https://doi.org/10.1016/j.envsoft.2012.11.002.

Benjamin, M. R. (2016). *The use of radar and hydrological models for flash flood evaluation and prediction*.

Bowering, E. A., Peck, A. M., & Simonovic, S. P. (2014). A flood risk assessment to municipal infrastructure due to changing climate part I: Methodology. *Urban Water Journal*, *11*(1), 20–30. https://doi.org/10.1080/1573062X.2012.758293.

Brandes, E. A., Zhang, G., & Vivekanandan, J. (2002). Experiments in rainfall estimation with a polarimetric radar in a subtropical environment. *Journal of Applied Meteorology*, *41*(6), 674–685. https://doi:10.1175/1520-0450(2002)041<0674:EIREWA>2.0.CO;2.

Bringi, V. N., Rico-Ramirez, M. A., & Thurai, M. (2011). Rainfall estimation with an operational polarimetric C-band radar in the United Kingdom: Comparison with a gauge network and error analysis. *Journal of Hydrometeorology*, *12*(5), 935–954. https://doi:10.1175/JHM-D-10-05013.1.

Cao, Y., Su, D., Fan, X., & Chen, H. (2019). Evaluating the Algorithm for Correction of the Bright Band Effects in QPEs with S-, C-and X-Band Dual-Polarized Radars.

Advances in Atmospheric Sciences, *36*(1), 41–54. https://doi.org/10.1007/s00376-018-8032-7.

Chandrasekar, V., Keränen, R., Lim, S., & Moisseev, D. (2013). Recent advances in classification of observations from dual polarization weather radars. *Atmospheric Research*, *119*, 97–111. https://doi.org/10.1016/j.atmosres.2011.08.014.

Chen, D., & Farrar, A. (2007). Evaluation of NARAD Precipitation Data for Rainfall Monitoring in Eastern Ontario, Canada. *Geomatics Solutions for Disaster Management*, 103–116. https://doi.org/10.1007/978-3-540-72108-6_8.

Chen, Y., Li, J., Wang, H., Qin, J., & Dong, L. (2017). Large-watershed flood forecasting with high-resolution distributed hydrological model. *Hydrology and Earth System Sciences*, *21*(2), 735. https://doi: 10.5194/hess-21-735-2017.

Collier, C. G. (1986). Accuracy of rainfall estimates by radar, Part I: Calibration by telemetering raingauges. *Journal of Hydrology*, *83*(3–4), 207–223. https://doi:10.1016/0022-1694(86)90152-6.

Cranston, M. D., & Tavendale, A. C. (2012). Advances in operational flood forecasting in Scotland. *Proceedings of the Institution of Civil Engineers-Water Management*, *165*(2), 79–87. https://doi.org/10.1680/wama.2012.165.2.79.

Dai, Q., Yang, Q., Zhang, J., & Zhang, S. (2018). Impact of Gauge Representative Error on a Radar Rainfall Uncertainty Model. *Journal of Applied Meteorology and Climatology*, *57*(12), 2769–2787. https://doi.org/10.1175/JAMC-D-17-0272.1.

De Roo, A. P., Gouweleeuw, B., Thielen, J., Bartholmes, J., Bongioannini-Cerlini, P., Todini, E., Bates, P. D., Horritt, M., Hunter, N., & Beven, K. (2003). Development of a European flood forecasting system. *International Journal of River Basin Management*, *1*(1), 49–59. https://doi.org/10.1080/15715124.2003.9635192.

Dhiram, K., & Wang, Z. (2016). Evaluation on Radar Reflectivity-Rainfall Rate (ZR) Relationships for Guyana. *Sciences*, *6*, 489–499. https://doi.org/10.4236/acs.2016.64039.

Dufton, D. R. L. (2016). *Quantifying uncertainty in radar rainfall estimates using an X-band dual polarisation weather radar* [PhD Thesis]. University of Leeds.

Faisal, I. M., Kabir, M. R., & Nishat, A. (1999). Non-structural flood mitigation measures for Dhaka City. *Urban Water*, *1*(2), 145–153. https://doi.org/10.1016/S1462-0758(00)00004-2.

FloodNet. (2020). Retrieved October 28, 2020, from https://www.nsercfloodnet.ca/

Fulton, R. A., Breidenbach, J. P., Seo, D.-J., Miller, D. A., & O'Bannon, T. (1998). The WSR-88D rainfall algorithm. *Weather and Forecasting*, *13*(2), 377–395. https://doi.org/10.1175/1520-0434(1998)013<0377:TWRA>2.0.CO;2.

Gabella, M., Morin, E., & Notarpietro, R. (2011). Using TRMM spaceborne radar as a reference for compensating ground-based radar range degradation: Methodology verification based on rain gauges in Israel. *Journal of Geophysical Research: Atmospheres*, *116*(D2). https://doi:10.1029/2010JD014496.

Gilewski, P., & Nawalany, M. (2018). Inter-comparison of Rain-Gauge, Radar, and Satellite (IMERG GPM) precipitation estimates performance for rainfall-runoff modeling in a mountainous catchment in Poland. *Water*, *10*(11), 1665. https://doi:10.3390/w10111665.

Goudenhoofdt, E., & Delobbe, L. (2009). Evaluation of radar-gauge merging methods for quantitative precipitation estimates. *Hydrology and Earth System Sciences*, *13*(2), 195–203. https://doi: 10.5194/hess-13-195-2009.

Hall, W., Rico-Ramirez, M. A., & Krämer, S. (2015). Classification and correction of the bright band using an operational C-band polarimetric radar. *Journal of Hydrology*, *531*, 248–258. https://doi.org/10.1016/j.jhydrol.2015.06.011.

Han, S., & Coulibaly, P. (2017). Bayesian Flood Forecasting Methods: A Review. *Journal of Hydrology*, *551*, *340-351*. https://doi.org/10.1016/j.jhydrol.2017.06.004.

Heidari, A. (2009). Structural master plan of flood mitigation measures. *Natural Hazards & Earth System Sciences*, *9*(1). https://doi.org/10.5194/nhess-9-61-2009.

Hubbert, J. C., Dixon, M., Ellis, S. M., & Meymaris, G. (2009). Weather radar ground clutter. Part I: Identification, modeling, and simulation. *Journal of Atmospheric and Oceanic Technology*, *26*(7), 1165–1180. https://doi.org/10.1175/2009JTECHA1159.1.

Jain, S. K., Mani, P., Jain, S. K., Prakash, P., Singh, V. P., Tullos, D., Kumar, S., Agarwal, S. P., & Dimri, A. P. (2018). A Brief review of flood forecasting techniques and their applications. *International Journal of River Basin Management*, *16*(3), 329–344. https://doi.org/10.1080/15715124.2017.1411920.

Joe, P., & Lapczak, S. (2002). Evolution of the Canadian operational radar network. *ERAD, Nov., Delft, Netherlands*. http://copernicus.org/erad/online/erad-370.pdf

Jonkman, S. N., & Vrijling, J. K. (2008). Loss of life due to floods. *Journal of Flood Risk Management*, *1*(1), 43–56. https://doi.org/10.1111/j.1753-318X.2008.00006.x.

Jonkman, S. N., & Kelman, I. (2005). An analysis of the causes and circumstances of flood disaster deaths. *Disasters*, *29*(1), 75–97. https://doi.org/10.1111/j.0361-3666.2005.00275.x.

Krajewski, W. F., Kruger, A., Smith, J. A., Lawrence, R., Gunyon, C., Goska, R., Seo, B.-C., Domaszczynski, P., Baeck, M. L., & Ramamurthy, M. K. (2010). Towards better utilization of NEXRAD data in hydrology: An overview of Hydro-NEXRAD. *Journal of Hydroinformatics*, *13*(2), 255–266. https://doi.org/10.2166/hydro.2010.056.

Larson, L. W., & Peck, E. L. (1974). Accuracy of precipitation measurements for hydrologic modeling. *Water Resources Research*, *10*(4), 857–863. https://doi.org/10.1029/WR010i004p00857.

Marshall, J. S., & Palmer, W. M. K. (1948). The distribution of raindrops with size. *Journal of Meteorology*, *5*(4), 165–166. https://doi.org/10.1175/1520-0469(1948)005x003C;0165:tdorwsx0003e;2.0.co;2.

Marx, A., Kunstmann, H., Bárdossy, A., & Seltmann, J. (2006). Radar rainfall estimates in an alpine environment using inverse hydrological modelling. *Advances in Geosciences*, *9*, 25–29. hal-00296952.

Mays, L. W. (2010). *Water resources engineering*. John Wiley & Sons.

McMillan, H., Jackson, B., Clark, M., Kavetski, D., & Woods, R. (2011). Rainfall uncertainty in hydrological modelling: An evaluation of multiplicative error models. *Journal of Hydrology*, *400*(1–2), 83–94. https://doi.org/10.1016/j.jhydrol.2011.01.026.

Mekis, E., Donaldson, N., Reid, J., Zucconi, A., Hoover, J., Li, Q., Nitu, R., & Melo, S. (2018). An overview of surface-based precipitation observations at Environment and Climate Change Canada. *Atmosphere-Ocean*, *56*(2), 71–95. https://doi.org/10.1080/07055900.2018.1433627.

Moore, R. J., Jones, A. E., Jones, D. A., Black, K. B., & Bell, V. A. (2004). Weather radar for flood forecasting: Some UK experiences. *Sixth International Symposium on Hydrological Applications of Weather Radar*, 2–4.

Moradkhani, H., & Sorooshian, S. (2008). General review of rainfall-runoff modeling: Model calibration, data assimilation, and uncertainty analysis. *Hydrological Modelling and the Water Cycle*, 1–24. https://doi.org/10.1007/978-3-540-77843-1_1.

Moszkowicz, S., Ciach, G. J., & Krajewski, W. F. (1994). Statistical detection of anomalous propagation in radar reflectivity patterns. *Journal of Atmospheric and*

Oceanic Technology, *11*(4), 1026–1034. https :doi:10.1175/1520-0426(1994)011<1026:SDOAPI>2.0.CO;2.

Nagai, A. (2003). Hydrologic Modeling of Rainfall-runoff Process and Its Application to Real-time Flood Forecasting. *Present Situation OnThe Water Resources and Water Related Disaster, and The Role of Agro-Environmental Education*, 111–118. [Available online at https://pdfs.semanticscholar.org/cc11/b928840c5e5573df97473a59e26bcda8d750.pdf].

Ochoa-Rodriguez, S., Wang, L.-P., Willems, P., & Onof, C. (2019). A review of radar-rain gauge data merging methods and their potential for urban hydrological applications. *Water Resources Research*. https://doi:10.1029/2018WR023332.

Park, S. G., Bringi, V. N., Chandrasekar, V., Maki, M., & Iwanami, K. (2005). Correction of radar reflectivity and differential reflectivity for rain attenuation at X band. Part I: Theoretical and empirical basis. *Journal of Atmospheric and Oceanic Technology*, *22*(11), 1621–1632. https://doi.org/10.1175/JTECH1803.1.

Pilon, P. J. (2002). *Guidelines for reducing flood losses*. United Nations International Strategy for Disaster Reduction (UNISDR).

Public Safety Canada, 2019: The Canadian Disaster Database, Accessed 28 October 2020, https://www.publicsafety.gc.ca/cnt/rsrcs/cndn-dsstr-dtbs/index-en.aspx.

Rabiei, E., & Haberlandt, U. (2015). Applying bias correction for merging rain gauge and radar data. *Journal of Hydrology*, *522*, 544–557. https://doi.org/10.1016/j.jhydrol.2015.01.020.

Reggiani, P., Renner, M., Weerts, A. H., & Van Gelder, P. (2009). Uncertainty assessment via Bayesian revision of ensemble streamflow predictions in the operational river Rhine forecasting system. *Water Resources Research*, *45*(2). https://doi.org/10.1029/2007WR006758.

Richards, W. G., & Crozier, C. L. (1983). Precipitation measurement with a C-band weather radar in southern Ontario. Atmosphere-Ocean, 21(2), 125–137. https://doi: 10.1080/07055900.1983.9649160.

Roe, J., Dietz, C., Restrepo, P., Halquist, J., Hartman, R., Horwood, R., Olsen, B., Opitz, H., Shedd, R., & Welles, E. (2010). NOAA's community hydrologic prediction system. *Proceedings from the 4th Federal Interagency Hydrologic Modeling Conference*.

Ryzhkov, A. V., Schuur, T. J., Burgess, D. W., Heinselman, P. L., Giangrande, S. E., & Zrnic, D. S. (2005). The Joint Polarization Experiment: Polarimetric rainfall measurements and hydrometeor classification. *Bulletin of the American Meteorological Society*, *86*(6), 809–824. https://doi: 10.1175/BAMS-86-6-809.

Sevruk, B. (1982). *Methods of correction for systematic error in point precipitation measurement for operational use*.

Shakti, P.C.., Nakatani, T., & Misumi, R. (2019). The Role of the Spatial Distribution of Radar Rainfall on Hydrological Modeling for an Urbanized River Basin in Japan. *Water*, *11*(8), 1703. https://doi.org/10.3390/w11081703.

Sugier, J., Tabary, P., Gourley, J., & Friedrich, K. (2006). Evaluation of dual-polarisation technology at C-band for operational weather radar network. *EUMETNET Opera*, *2*.

Thampapillai, D. J., & Musgrave, W. F. (1985). Flood damage mitigation: A review of structural and nonstructural measures and alternative decision frameworks. *Water Resources Research*, *21*(4), 411–424. https://doi.org/10.1029/WR021i004p00411.

Thorndahl, S., Einfalt, T., Willems, P., Nielsen, J. E. ek, ten Veldhuis, M.-C., Arnbjerg-Nielsen, K., Rasmussen, M. R., & Molnar, P. (2016). Weather radar rainfall data in urban hydrology. *Hydrology and Earth System Sciences & Discussions*, 1–37. https://doi.10.5194/hess-21-1359-2017.

Tol, R. S. (2016). The impacts of climate change according to the IPCC. *Climate Change Economics*, *7*(01), 1640004. https://doi.org/10.1142/S2010007816400042.

Vieux, B. E., & Bedient, P. B. (2004). Assessing urban hydrologic prediction accuracy through event reconstruction. *Journal of Hydrology*, *299*(3), 217–236. https://doi: 10.1016/j.jhydrol.2004.08.005.

Wang, L.-P., Ochoa-Rodríguez, S., Van Assel, J., Pina, R. D., Pessemier, M., Kroll, S., Willems, P., & Onof, C. (2015). Enhancement of radar rainfall estimates for urban hydrology through optical flow temporal interpolation and Bayesian gauge-based adjustment. *Journal of Hydrology*, *531*, 408–426. https://doi: 10.1016/j.jhydrol.2015.05.049.

Werner, M., Cranston, M., Harrison, T., Whitfield, D., & Schellekens, J. (2009). Recent developments in operational flood forecasting in England, Wales and Scotland. *Meteorological Applications: A Journal of Forecasting, Practical Applications, Training Techniques and Modelling*, *16*(1), 13–22. https://doi.org/10.1002/met.124.

Williams, C. R., Gage, K. S., Clark, W., & Kucera, P. (2005). Monitoring the reflectivity calibration of a scanning radar using a profiling radar and a disdrometer. *Journal of Atmospheric and Oceanic Technology*, *22*(7), 1004–1018. https://doi.org/10.1175/JTECH1759.1

Xie, H., Zhou, X., Hendrickx, J., Vivoni, E., Guan, H., Tian, Y., & Small, E. (2006). Comparison of NEXRAD Stage III and gauge precipitation estimates in central New Mexico. *Journal of the American Water Resources Association*, *42*(1), 237–256. https://doi: 10.1111/j.1752-1688.2006.tb03837.x.

Zahmatkesh, Z., Kumar Jha, S., Coulibaly, P., & Stadnyk, T. (2019). An overview of river flood forecasting procedures in Canadian watersheds. *Canadian Water Resources Journal/Revue Canadienne Des Ressources Hydriques*, 1–17. https://doi.org/10.1080/07011784.2019.1601598.

Zhang, W., Villarini, G., Vecchi, G. A., & Smith, J. A. (2018). Urbanization exacerbated the rainfall and flooding caused by hurricane Harvey in Houston. *Nature*, *563*(7731), 384–388. https://doi.org/10.1038/s41586-018-0676-z.

Chapter 2. Application of weather Radar for operational hydrology in Canada – A review

Summary of Paper 1: Wijayarathne, D., and Coulibaly, P. (2020). Application of weather Radar for operational hydrology in Canada – A review. *Canadian Water Resources Journal*, under review.

This research work provides a comprehensive literature review of the weather Radar network in Canada and how it has been applied from a hydrological context in Canada since the 1950s.

The main topics include:

- Canadian weather Radar network.
- Accessible Radar data.
- Radar QPEs.
- Application of weather Radar in operational hydrology.
- Challenges in the use of Radar QPEs in operational hydrology.
- Potential future research.

Key results of this research include:

- In Canada, the application of weather Radar in hydrology had been increased in last decade; however, further research is necessary to address the niche areas.
- Radar only QPEs and multi-radar QPEs are used in Canada to issue operational weather warnings, to determine the type of precipitation, precipitation features,

and structure, in operational forecasting such as weather forecasts and snow depth predictions, and as a tool to validate atmospheric models.

- The use of Radar QPEs is limited by the random and systematic errors, variability in *Z-R* relationship, poorly gauged precipitation network, the ongoing development of Radar infrastructure, existing C-band single radar network, and the complex geography.
- Further research is crucial to evaluate Radar QPEs, to verify radar-gauge merging methods, and to incorporate real-time Radar QPEs to hydrological models.

2.1. Abstract

Weather Radar provides real-time, spatially and temporally continuous precipitation data over a large area, and therefore it has been used for operational hydrology in Canada over the past decades. Recently, the focus on weather Radar in Canada has increased since the existing Environment and Climate Change Canada (ECCC) C-band Radar network is replaced with S-band dual-polarized Radar. This paper aims to provide a wide-ranging literature review of the current Radar network in Canada and how it has been applied from a hydrological context. The review starts with an overview of the Canadian weather Radar network, emphasizing current and future developments. Next, the application of weather Radar in hydrology is summarized, including specific research and operational examples. Finally, some recommendations are provided for future studies based on new developments in Canada's weather Radar network.

Keywords: Radar, Canadian weather Radar, *Z-R* relationship, C-band Radar, Hydrology

Utilisation des Radars météorologiques en hydrologie opérationnelle au Canada - Etat de l'art

Résumé

Les Radars météorologiques fournissent des données de précipitations spatialement et temporellement continues, en temps réel et sur de grandes distances. Depuis une dizaine d'années, ces données ont été largement utilisées en prévisions hydrologiques opérationnelles. L'intérêt porté sur les Radars météorologiques a récemment augmenté au Canada suite au remplacement du réseau de Radars en bande C d'Environnement et Changement Climatique Canada (ECCC) par des Radars en bande S à double polarité. Cet article a pour objectif de fournir un large état de l'art du réseau de Radars météorologiques au Canada et comment il a été utilisé en hydrologie. La revue commence par un aperçue du réseau de Radars météorologiques canadien, puis met l'accent sur les récents et futurs développements. Ensuite, l'utilisation du réseau de Radars en hydrologie est décrite en donnant des exemples de travaux de recherche et d'utilisation opérationnelle. Pour finir, cet article donne des recommandations pour des travaux futurs sur la base des nouvelles avancées du réseau de Radars météorologiques canadien.

2.2. Introduction

Radio detection and ranging (Radar) was first used and named by S.M Taylor and F.R Furth of the US Navy in 1940 and adopted universally in 1943 (Doviak 1993). The Radar emits electromagnetic radiation in the microwave domain of the electromagnetic spectrum and detects the echo returned from the targets. Radar uses five different separate

band/wavelength ranges in the electromagnetic spectrum; S-band (~10 cm), C-band (~5 cm), X-band (~3 cm), W band (~3 mm), and K_a /K_u (~1 cm) (Bluestein et al. 2014; Einfalt et al. 2004; Whiton et al. 1998). Information about the targets can be determined by analyzing the return signal (Skolnik 1962).

Radar is used for various applications such as military, nautical, aviation, marine, meteorology, biology, and weather surveillance. The use of Radar in weather surveillance was initiated in April 1944 with the beginning of weather observing and reporting at two Harbor Defense Cristobal installations (Whiton et al. 1998; Best Jr 1973). Since then, the applications of weather Radar in a hydrological context have evolved significantly, especially with the advances in Radar infrastructure, computer power, data processing techniques, and hydrological and climate models (Thorndahl et al. 2016). Recently, there has been a significant focus on real-time precipitation information derived from weather Radar to complement conventional rainfall gauges since it provides real-time, spatially, and temporally continuous data over a large area (Thorndahl et al. 2016). Due to the Radar signal's ability to penetrate clouds and rain, it can be used to provide information on the internal structure of a storm (Hasler and Morris 1986). These capabilities contribute to Radar playing an essential role in meteorological studies (Doviak 1993). Different countries use their weather Radar systems that produce different commercial Radar products such as Radar-Online-Aneichung (RADOLAN) in Germany (Marx et al. 2006), Nimrod in the UK (Moore et al. 2004), and Next Generation Weather Radar (NEXRAD) in the USA (Krajewski et al. 2010). Those products provide a fixed Cartesian

grid with rainfall accumulation data summarized over a given time period (Thorndahl et al. 2016).

Precipitation estimates based on weather Radar have been used for hydrological applications for decades in Canada as an alternative to conventional gauge measurements. In Canada, research on Radar began in 1931 and continued to operational research under the project Stormy Weather in 1943 (Sills and joe 2019; Douglas 1990; Middleton 1981). Since then, the application of weather Radar from a hydrological perspective has evolved significantly (Sills and Joe 2019). Interest in Canadian weather Radar has been increased due to the recent announcement made by the Canadian government regarding the replacement of the entire existing Environment and Climate Change Canada (ECCC) C-band Radar network with S-band dual-polarized Radar ("The Government of Canada Invests to Modernize Weather-Forecasting Infrastructure" 2017). To date, there has been no literature summarizing the state-of-the-art of Canadian weather Radar for operational hydrology.

The purpose of this review paper is to provide a detailed description of the current weather Radar network in Canada and to encapsulate the previous hydrological applications that used weather Radar in Canada since the 1950s. The first half of the paper provides a detailed description of the existing Radar network, including novel developments that have yet to be implemented. The second half of the article provides a review on the state-of-the-art in the applications of Radar estimated precipitation in Canadian operational hydrology and is structured based on the critical areas of research that are recognized as being significant in the published literature. Additionally, the

challenges involved in using current weather Radar products and the potential direction of future research are also discussed.

2.3. Canadian Weather Radar Network (CWRN)

The first individual weather Radars in Canada were established in the 1950s (Mekis et al. 2018). Since then, the Radar network has been gradually expanded over the past few decades to the current state. An overview of the evaluation of the CWRN, together with hardware and software upgrades, can be found in Joe and Lapczak (2002) , Mekis et al. (2018) and Sills and Joe (2019). Canada's current Radar network includes 31 Radar stations at a full conventional reflectivity measurement range of 256 km in a radius around the site and a dual-polarized Doppler range of 120 km around the site (Figure 2-1 and Table 2-1) (Mekis et al. 2018). ECCC maintains 29 Canadian Radar stations, while the other two (The Jimmy Lake and Lac Castor) are maintained and operated by the Department of National Defense (DND) ("ARCHIVED - Environment and Climate Change Canada - Weather Monitoring Infrastructure" 2012). The CWRN is a diverse network of non-Doppler Radar (24 elevation angle reflectivity-only scans) and Doppler Radar (three elevation angle Doppler scans) (Joe and Lapczak 2002) and covers most of the populated areas in Canada (Figure 2-1). Besides, McGill University operates the McGill university Radar (WMN) (Table 2-1). It is located near the Macdonald Campus at Ste. Anne de Bellevue, on the western tip of the island of Montreal (Damant et al. 1983a). WMN Radar is a dual-polarized S-band Radar, and their characteristics are presented in Damant et al. (1983a).

All Canadian ground-based Radars were C-band Radar until 2017, except for the J.S. Marshall Radar Observatory (MRO) near Montreal (McGill Radar), an S-band Radar (Mekis et al. 2018). For the past few decades, research was conducted to determine the possible benefits of shifting to a dual-polarization S-band Radar network in future upgrades. Many of these studies were directed towards validating data processing algorithms (Huang et al. 2010; Shi et al. 2010; Hudak, Rodriguez, and Donaldson 2008). Consequently, Canada is currently upgrading its C-band Doppler Radars with dual-polarized S-bands starting with Radisson station (XRA), Saskatchewan. Once the system becomes adequately replaced, the target requirement is to install 20 new Radars by 31 March 2023. The replacement project was started on 28 February 2017. Fourteen C-band Radar stations were replaced with S-band Radar as of October 2020 (Table 2-1). Updates on the ongoing project to upgrade Canadian weather Radar can be found on the Government of Canada Radar overview webpage (https://www.canada.ca/en/environment-climate-change/services/weather-general-tools-resources/radar-overview.html).

Aside from the C and S-band Radar, X-band Radar was also used in Canada (Lee et al. 2007; Hudak et al. 2002). Besides S-band Radar, the Marshall Radar Observatory operates continuous-wave, bi-static X-band Doppler Radar using Precipitation Occurrence Sensor System (POSS). The X-band dual-polarization Doppler Radar on the seashore of the Beaufort Sea at Tuktoyaktuk at Northwest territories was set up by the Hokkaido University under the Beaufort and Arctic Storms Experiment (BASE) project carried out in 1994 (Asuma et al. 1998). Even though dense X-band radar networks

[e.g., Collaborative Adaptive Sensing of the Atmosphere (CASA) network in Dallas/Fort Worth] are successfully deployed in urban areas around the world to improve the spatial and temporal resolution of Radar (Chen and Chandrasekar 2015), X-band Radar is seldom used in Canada. The use of dense X-band Radar could be a viable approach to produce high-resolution Radar in densely populated southern Canada.

On top of ground-based Radar, portable Radar was also used for various applications in Canada (Hudak et al. 2002). For example, the McMaster University X-and dual-polarization portable Radar (IPIX) was deployed to several field experiments that advanced the use of dual-polarization Radar (Hudak et al. 2004; Stewart et al. 2004).

Other than the Canadian Radar systems, the American NEXRAD Radar system covers Canada's parts close to the USA – Canada border, where most populated regions in Canada are located (Figure 2-1). For example, NEXRAD Radar stations at Buffalo (KBUF), Cleveland (KCLE), and Detroit (KDTX) cover the Greater Toronto Area (GTA) in Canada. NEXRAD is an S-band Doppler weather Radar network operated by US National Weather Services (NWS) and the US Military. Even though its usable range is 180 km, data can be used to estimate precipitation up to 230 km away from the station (Vieux and Bedient 2004).

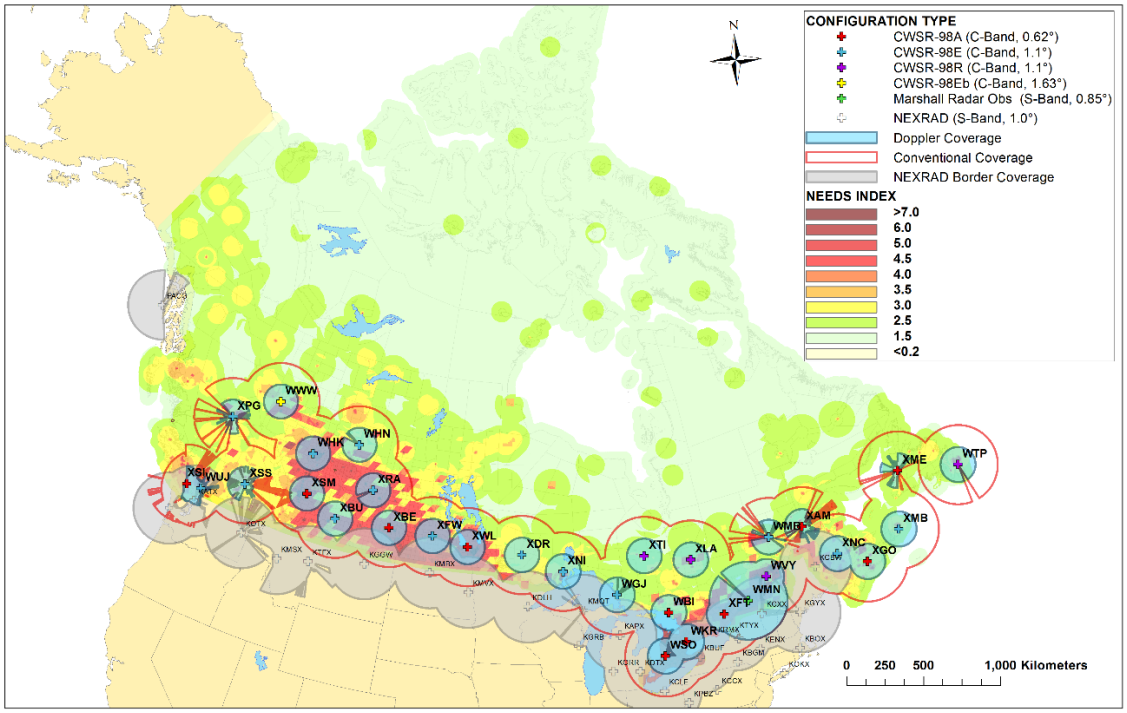

Figure 2-1 *The Conventional and Doppler coverage of the Canadian operational WKR C-band and NEXRAD S-band Radar. (Note: the map shows the status before the Canadian Weather Radar Replacement Program (CWRRP). The coverage includes blockages. The background consists of a Needs Index map prepared using ranking and weighting of hydrometeorological monitoring factors such as weather and climate-related risks and socio-economic impacts. Different colored cross marks represent different Canadian Weather Station Radar (CWSR) based on beam widths and antennas. Source: An overview of surface-based precipitation observations at Environment and Climate Change Canada, Mekis et al., Atmosphere-Ocean, 27 March, 2018, Taylor & Francis Ltd, reprinted by permission of the publisher Taylor & Francis Ltd, http://www.tandfonline.com)*

Table 2-1 *Canadian weather Radar network.*

Province	Site	ID	System upgrade/ in operation	Band
Alberta	Carvel	WHK	2000	C
	Schuler	XBU	2002	S
	Spirit River	WWW	2019	S
	Strathmore	XSM	2001	S
British Columbia	Aldergrove	WUJ	1997	C
	Mount Sicker (Victoria)	XSI	2000	C
	Mount Silver Star	XSS	2002	C
	Prince George	XPG	2003	C
Manitoba	Foxwarren	XFW	2018	S
	Woodlands	XWL	1999	C
New Brunswick	Chipman	XNC	2019	S
Newfoundland and Labrador	Holyrood	WTP	1931	C
	Marble Mountain	XME	2001	C
Nova Scotia	Gore	XGO	2001	C
	Marion Bridge	XMB	2019	S
Ontario	Britt	WBI	2002	C
	Dryden	XDR	2003	S
	Exeter	WSO	2019	S
	Franktown	XFT	2015	C
	King City	WKR	2000	C
	Lasseter Lake	XNI	2002	C
	Montreal River Harbour	WGJ	2000	C
	Timmins	XTI	2018	S
Quebec	Lac Castor	WMB	1999	C
	Landrienne	XLA	2001	S
	McGill	WMN	1993	S
	Val d'Irène	XAM	2009	C
	Villeroy	WVY	2017	C
	Blainville	ASB	2018	S
Saskatchewan	Bethune	XBE	2019	S
	Jimmy Lake	WHN	1999	C
	Radisson	XRA	2018	S

2.4. Radar Quantitative Precipitation Estimates (QPEs)

2.4.1. Radar only QPEs

Radar products have two main categories: Radar reflectivity maps at the observational heights (Figure 2-2a) and precipitation accumulations derived from instantaneous rate summaries (Figures 2-2b and 2-2c). Microwave attenuation and

scattering from precipitation targets are converted into precipitation intensity and accumulation using empirical relationships between the Radar reflectivity factor (Z) and the Rainfall rate (R) (Marshall and Palmer 1948). In Canada, three primary methods have been used to derive Z-R relationships (Xin, Reuter, and Larochelle 1997); (1) Probability Matching Method (PMM), (2) Optimal curve fitting by measuring the Radar reflectivity and surface rainfall rate using gauges, and (3) compute Z and R by integrating over the observed raindrop size spectrum. Choosing the best Z-R relationship for a selected watershed in the hydrological application in Canada is always a challenge because it depends on the geographical location, rain type, synoptic types, storm types, climate region, time of the storm, the condition of thermodynamic stability, and environment (Richards and Crozier 1983). The authentic Marshall-Palmer relationship ($Z=200R^{1.6}$) has been widely used in studies conducted in Canada (Gad and Tsanis 2003; Tsanis, Gad, and Donaldson 2002; Schell et al. 1992; Kouwen and Garland 1989; Tao and Kouwen 1989; Bellon and Austin 1984; Damant et al. 1983a; Bellon, Lovejoy, and Austin 1980; Barge et al. 1979; Austin and Austin 1974). In 1983, Richards and Crozier developed a new relationship ($Z=295R^{1.43}$) for instantaneous rainfall rates for small areas by correlating seasonal C-band Radar at Woodbridge, Ontario, with raindrop disdrometer. It was proposed that the relationship suggested by Richards and Crozier (1983) is capable of producing more accurate rain rates using reflectivity compared to other existing relationships for southern Ontario, Canada. It was often used for the research in south Ontario watersheds (Fassnacht 2003; Benoit et al. 2000; Dalezios 1988; Kouwen 1988;

Richards and Crozier 1983). Besides those mentioned above, other Z-R relationships that were used in the past hydrological studies in Canada are listed in Table 2-2.

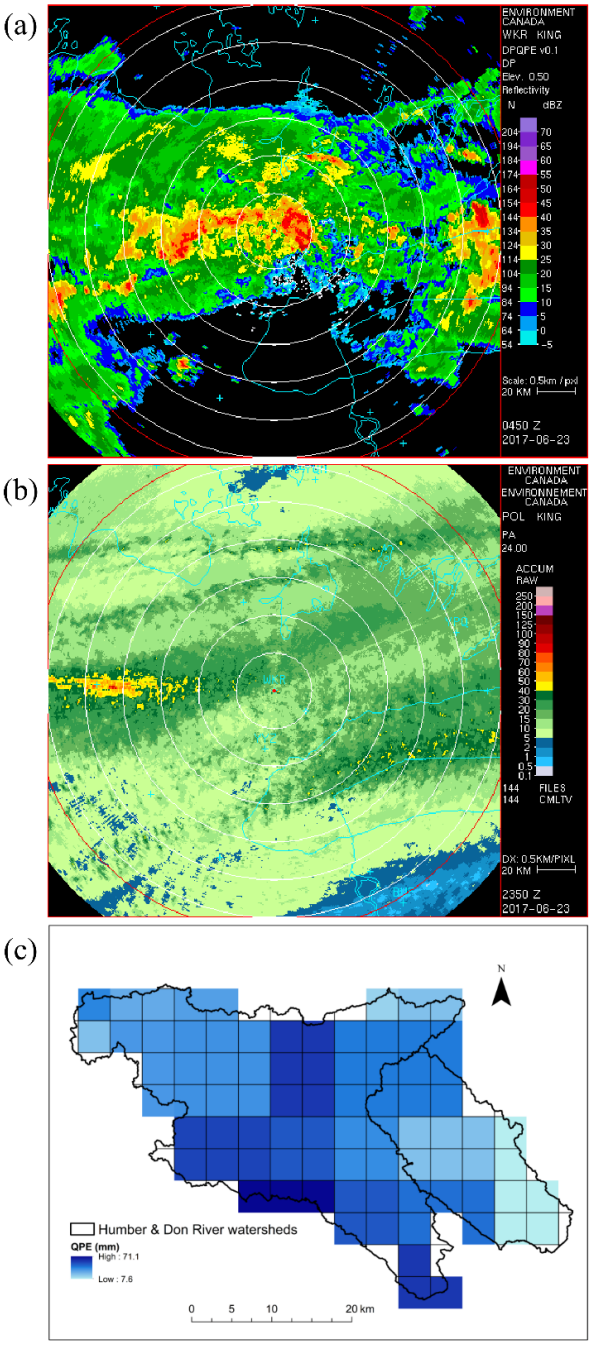

Figure 2-2 *Radar products. (a) WKR C-band Radar POLarimetric Plan Position Indicator (POLPPI)'s of reflectivity image at 0450Z on 20170623 (source: Observations-Based Research Section, King City, ECCC), (b) 24-hour accumulation at the end of the UTC day 2017-06-23 (2350Z) (Source: Observations-Based Research Section, King City, ECCC), and (c) NEXRAD Level III Digital Precipitation Array (DPA) Radar precipitation field from 8 July, 2013, 1800 UTC to 9 July, 2013, 0200 UTC over the Humber River watershed in GTA (Wijayarathne et al. 2020a)*

Table 2-2 *Z-R relationships used in hydrological applications in Canada.*

Reference	**Key Objective**	**Study area**	***Z-R* relation**	**Type of Radar**	**Contribution/conclusions/major findings**
Dalezios and Kouwen 1990	Study the affecting factors and sources of error at the preprocessing stage of the raw Radar reflectivity on Radar QPEs	Grand River watershed, Southern Ontario	$Z = 485R^{1.43}$	Woodbridge C-band	Deterministic corrective techniques are required to address non-rainfall echoes, signal attenuation, and wind effect during preprocessing of reflectivity
Xin et al. 1997	*Z-R* relationship for summertime convective rainfall	Edmonton	$Z=32.5R^{1.65}$	Carvel C-band	A new *Z-R* relationship is developed using the Window Probability Matching Method (WPMM)
Fassnacht et al. 2001	To improve weather Radar estimated precipitation using surface temperature	Range of King City Radar	$Z=1780R^{2.21}$	King City C-band	Radar adjustment using the near-surface air temperature is suitable for mixed precipitation
Fassnacht 2003	Compare weather Radar vs. gridded gauge data for hydrological model	Upper Grand River basin, Ontario	$Z=1780R^{2.21}$	King City C-band	Radar performs better for simulated runoff volumes than gauge data
Lee et al. 2007	Model the variability of Drop Size Distributions in Space and Time	Range of McGill Radar	$Z=206R^{1.55}$	McGill S-band POSS X-band	Space-time variability of the distributions of the size of raindrops is developed
Berenguer and Zawadzki 2009	Quantify the sources of uncertainty affecting Radar rainfall estimates	Montreal, Quebec	$Z=237R^{1.55}$	McGill S-band Radar	Developed error covariance matrix of Radar rainfall estimates at the ground
Boodoo et al. 2015	Evaluate C-band Radar QPEs and algorithms based on different dual-polarized products	The city of Toronto	$R = 0.0365\mathrm{Z}^{0.625}$, $R = 0.017\mathrm{Z}^{0.714}$, $R = 0.0058\mathrm{Z}^{0.91}10^{-0.209Z_{DR}}$, $R =37.9K_{DP}^{0.89}10^{-0.209Z_{DR}}$, $R = 294\mathrm{A}^{0.89}$, $R = 25K_{DP}^{0.81}$, $R = 29K_{DP}^{0.85}$, $R = 33.8K_{DP}^{0.79}$, $R = \mathrm{sign}(K_{DP})\ 33.8\lvert K_{DP}\rvert^{0.79}$	King City C-band NEXRAD S-band	The algorithms based on K_{DP} and specific attenuation at horizontal polarization perform better than the ones based on reflectivity and differential reflectivity
Wijayarathne et al. 2020b	Evaluate C-band and NEXRAD QPEs over	Humber River and Don River	$R = 0.0365Z^{0.625}$, $R = 0.017Z^{0.714}$, $R = 33.8K_{DP}^{0.79}$,	King City C-band NEXRAD S-band	• NEXRAD QPEs performs the best • QPEs derived from C-band multi-parameter rain rate estimator using K_{DP}

	Canadian urban watersheds	watersheds, GTA	$R = 37.9K_{DP}^{0.89}10^{-0.072Z_{DR}}$, $R = 0.0058Z^{0.91}10^{-0.209Z_{DR}}$	and Z_{DR} performs equally as NEXRAD • Adjustment with gauge data is necessary before using Radar QPEs for hydrometeorological studies

The single polarized Radar transmits and receives Radar with a single horizontal plane and produces standard variables such as reflectivity (Z), velocity (V), and spectrum width (SW). The dual-polarized Radar emits and receives Radar signals in horizontal and vertical polarization and produces additional variables by comparing the horizontal and vertical channels' signal strength phase. The main dual-polarized variables measured by the Radar are Differential Reflectivity (Z_{DR}), Correlation Coefficient (CC), Specific Differential Phase (K_{DP}), and specific attenuation at horizontal polarization (A) (Boodoo et al. 2015). According to the literature, dual-polarization enhances precipitation estimates' accuracy and leads to more accurate forecasts (Boodoo et al. 2015; Ryzhkov et al. 2005a). Dual-polarization helps to mitigate attenuation and anomalous propagation (Ryzhkov et al. 2005a). Dual polarized parameters can be used to distinguish precipitation from non-precipitation targets such as birds and therefore enable better removal of non-precipitation targets (Berenguer et al. 2006). For example, the polarimetric variable CC is how similarly the horizontal and vertical pulses behave in the pulse volume. The variable CC is an essential discriminator between liquid rain and other targets because it is typically very close to one for rain (Dufton 2016). Dual-polarized Radar variables can provide additional information on precipitation, such as the size, shape, and type of precipitation targets (Hall et al. 1984). Moreover, dual-polarization will enhance the capability of distinguishing non-uniform precipitation (hail, melting snow) from uniform meteorological targets (rain, snow). For instance, Z_{DR} is a measure of the difference between the horizontal and vertical reflectivity factor and helps to identify the shape of the precipitation target (Hall et al. 1984). Therefore, it can be used to differentiate rain,

snow, and hail. The K_{DP} gives better rain rate estimates in heavy rainfall because, differently to reflectivity, it is immune to attenuation. The product K_{DP} represents the range deviation of the differential phase shift that enables better precipitation estimates, especially in intense rainfall events (Ryzhkov et al. 2005b). Application of dual-polarization Radar technology in hydrology has been carried out regularly (Wijayarathne et al. 2020b; Boodoo et al. 2015; Boodoo et al. 2010).

The NEXRAD uses both single-polarimetric R(Z) and Dual-polarimetric (DP-QPEs) rain-rate algorithms to derived Radar QPEs (Ryzhkov et al. 2005a). The Precipitation Processing System (PPS) algorithm proposed by Fulton et al. (1998) ($R= 0.017Z^{0.714}$) was widely used in hydrological studies in USA. Details of processing NEXRAD QPEs can be found in Berkowitz et al. (2013). Mainly, two levels of NEXRAD products are available in the National Centers for Environmental Information (NCEI) archives. Reflectivity, mean radial velocity, and spectrum width are available as Level II NEXRAD data, and Radar QPEs derived from Level II data are available as Level III NEXRAD data (Zhang et al. 2019; Chen and Farrar 2007; Xie et al. 2006).

Replacement of existing C-band Radar with S-band dual-polarized Radar is expected to improve the performance due to transferring single-polarized to dual-polarized and wavelength change. The partial attenuation of the Radar signal is the main problem of C-band Radar. Nevertheless, with the dual-polarized S-band Radar, the reduction of the signal's amplitude is significantly low and leads to a better estimation of rainfall. Also, recently developed Radar algorithms are mainly derived for dual-polarized S-band NEXRAD Radar in the USA (Cifelli et al. 2011). New technologies are also

designed to process, download, and archive, based on dual-polarized S-band NEXRAD Radar. Several toolkits, such as the NOAA toolkit, are only capable of handling dual-polarized Radar. Freely available software that can be used for retrieval, computing, processing, viewing, and managing real-time Radar, such as Get real-time ("GetMyRealtime Water Data" 2020), are developed to work with S-band dual-polarized Radar data. Therefore, the proposed transition from C-band to S-band provides the opportunity to use these recent technological advances made for NEXRAD for Canada. Additionally, the broader operating range of S-band Radar compared to the C-band will expand the usable spatial coverage of Radar.

Besides new S-band Radar, Micro Rain Radars (MRR) are now being deployed across the ECCC network and being tested across Canada. The MRR is vertically pointing Doppler Radar, which operates at 24.23 GHz. Further information regarding MRR could be found at www.metek.de. MRR would help the hydrological community by monitoring the origin of raindrops and frozen hydrometeors and identifying the bright band level. Also, MRR can detect small amounts of rainfall, even lower than the minimum amount that conventional rain gauges can measure (Wang, Lei, and Yang 2017).

2.4.2. Radar assimilated QPEs

Today, different commercial Radar QPEs that are corrected with rain gauge network data are produced by fusing multiple QPEs with Radar to improve the accuracy of the precipitation estimates (Nasab 2017). Those products provide a fixed Cartesian grid with rainfall accumulation data summarized over time. The integration of multi-radar can

alleviate deficiencies in the single Radar and provides more accurate detection of physical processes and QPEs. Both national and international organizations produce different high-resolution QPEs by fusing multiple Radar QPEs with gauge measurements, analyses from the weather prediction models, and satellite observations.

2.4.2.1. Canadian Precipitation Analysis (CaPA)

CaPA is a precipitation product developed by the Meteorological Service of Canada (MSC) and provides nation-wide interpolated precipitation analysis for 6 and 24-hour accumulations at resolutions of 10 km (operational) (Fortin et al. 2018; Boluwade et al. 2017; Fortin et al. 2015). CaPA uses an optimal interpolation procedure that blends different precipitation sources, such as precipitation estimates from the Numerical Weather Prediction (NWP) model, point gauge measurements, satellite data, and Radar data (Boluwade et al. 2017). The assimilation of Canadian Radar precipitation into CaPA precipitation estimates started in 2014. However, the assimilation is limited to rainfall only because of winter challenges with the bias correction of Radar data, such as potential bright band contamination. Also, the Radar assimilation is limited to the Doppler range of C-band Radar because the signal is contaminated by non-meteorological targets, and the Radar samples the volume above clouds beyond the Doppler range (Fortin et al. 2018). Since November 2016, US NEXRAD Radar covering Canada or the Great Lakes watershed is also included in CaPA (Fortin et al. 2015). Apart from the operational CaPA product with a 10 km resolution, a newly developed 2 km resolution CaPA data product is now available for research communities with an archive going back to early July 2016. Further details of CaPA can be found in Fortin et al. (2018). CaPA data were used in

Canada for environmental prediction applications such as hydrological modeling (Lespinas et al. 2015; Eum et al. 2014), hydrological forecasting (Mahfouf et al. 2007), and snow depth predictions (Carrera et al. 2010). Also, CaPA data were used by the Canadian Land-Data Assimilation System (CaLDAS) to estimate soil moisture, soil temperature, and snow depths in real-time over Canada (Carrera et al. 2015; Lespinas et al. 2015).

2.4.2.2. National Mosaic and Multi-Sensor QPE (NMQ)

The NMQ is a multi-radar, multi-sensor system which assimilates Radar mosaic grids along with other observational network data such as satellite, gridded model analyses, or forecast fields to increase the significance of Radar data in operational forecasting (Zhang et al. 2011; Xu et al. 2008; Gourley et al. 2001). This system is demonstrated by the Collaborative Radar Acquisition Field Test (CRAFT) project of the US National Weather Services and consumes base data from more than 140 WAR-88D Radars and 31 Canadian C-band weather Radars (Zhang et al. 2011; Droegemeier et al. 2000). NMQ assimilates level II data from the WSR-88D network with different data sources such as ECCC weather Radar and regional rain gauge network (Zhang et al. 2011). The fully automated NMQ system generates 3D Radar reflectivity mosaic grids and a suite of severe weather and QPE products for the conterminous United States (CONUS) at a 1-km horizontal resolution and 2.5-minute update cycle (Zhang et al. 2011).

2.4.2.3. Multi-Radar Multi-Sensor QPEs (MRMS)

The MRMS system was recently developed by the National Centers for Environmental Prediction (NCEP) to address seamless national Radar information requirements for model-data assimilation and QPEs in the USA (Zhang et al. 2016). The MRMS system currently integrates about 180 operational Radars, about 7000 gauges, and generates QPEs across the CONUS and southern Canada at a very high spatial and temporal resolution of 1-km and 2 minutes (Zhang et al. 2016). Operational Radar used by MRMS includes 146 S-band WSR -88D and 30 C-band Radars operated by ECCC. The MRMS also provides other high-resolution national products such as 3D reflectivity mosaic, seamless hybrid scan reflectivity, and surface precipitation rate and types (Zhang et al. 2016).

2.5. Use of weather Radar data in operational hydrology

2.5.1. Operational forecasting

The precipitation input for numerical forecasting models mainly comes from conventional rain gauges. There is significant attention to real-time precipitation information derived from Radar to complement traditional rainfall gauges as it provides real-time, spatially, and temporally continuous data that can enhance operational forecasting. Different aspects were used in the past to produce operational forecasts using weather Radars in Canada. Using McGill S-band weather Radar, the Short-term Automated Radar Predictions (SHARP) method was developed to generate 0 to 3-hour interval precipitation forecasts (Bellon and Austin 1984, 1978). The mean absolute

deviation between Radar and gauge precipitation calculated over the catchment varies from 49% to 60% for 0.5 to 3-hr forecasts. Nearly a decade after the verification against the rain gauges, the MRO began providing real-time rainfall estimates using the linear extrapolation of the Radar image (Bellon and Zawadzki 1994). The linear extrapolation method was frequently used by researchers to make nowcasts in Canada (Bellon and Zawadzki 1994; Bellon and Austin 1984). In this method, the Radar echoes were translated by the same amount proportional to a calculated past motion. One-hour forecast rainfall accumulation was transformed at a spatial and temporal resolution of 1 km and 5 minutes based on the linear extrapolation of the latest Constant Altitude Plan Position Indicator (CAPPI) data. An attempt to use spatial and temporal averaging (smoothing) was taken to improve the skill of this technique by researchers at MRO (Bellon and Austin 1984). A 10% reduction of Root Mean Square Error (RMSE) was observed after smoothing for 1 hour ahead precipitation forecasts compared to the unsmoothed Radar data. Another study conducted in 1980 developed an algorithm that yields the likelihood of rain from combining satellite imagery and McGill S-band Radar data obtained in eastern Canada (Bellon et al. 1980). The algorithm acquired two bivariate frequency distributions from infrared and visible satellite images and then collocated with Radar, which was used to discriminate rain and non-rain clouds. An operational version called Rainsat was developed after this study and was used in real-time operational forecasting since 1981. Damant et al. (1983b) examined the errors involved in Radar QPEs using linear extrapolation forecasting technique to generate precipitation forecast. The unadjusted radar-gauge comparison showed an average bias of 3%, RMSE of 87%, and

an absolute difference of 50%. After adjusting Radar QPEs to the storm-bias, bias, RMSE, and absolute differences were reduced to -2%, 67%, and 33%, respectively.

Germann and Zawadzki (2004) took the first approach of probabilistic forecasts using Radar images in Canada. In this study, the McGill Algorithm for Precipitation nowcasting by the Lagrangian Extrapolation (MAPLE) method was used to generate probabilistic precipitation rate forecasts. A three stepped MAPLE method was proposed by Germann and Zawadzki (2002) to forecast potential precipitation. The MAPLE method first uses variational Radar echo tracking to determine the motion field of precipitation. Second, a semi-Lagrangian advection scheme is used to advect Radar reflectivity. Finally, various predictability measures such as the lifetime are calculated by comparing Eulerian and Lagrangian persistence forecasts with observations. In 2004, Germann and Zawadzki used continental-scale Radar images along with the MAPLE method to derive a lifetime of precipitation patterns in Eulerian and Lagrangian space, and those patterns were used as a measure of predictability.

At present, hydrological modeling plays a vital role in operational forecasting (Nester et al. 2016). Conventional hydrological modeling requires a dense gauge network, which is, at times, not practical due to the operational cost and relatively large size of Canadian watersheds (McMillan et al. 2011). The precipitation from gauges produces point data, which should be interpolated to a grid before using it as gridded precipitation input for distributed hydrological models (Rabiei and Haberlandt 2015). Previous studies showed that gridded precipitation derived using real-time weather Radar could provide accurate flow simulations using hydrological models to facilitate operational forecasting

(Chen et al. 2017; Benjamin 2016; Fan et al. 2014). A significant improvement in nowcasting and real-time forecasting in urban areas was observed by coupling the hydrological models with nowcasting techniques that use Radar QPEs (Poletti et al. 2017).

Compared to the USA, studies on Radar estimated rainfall as an input of the hydrological models in Canada are sparse. In general, Radar is applied to hydrological modeling in two ways: (1) quantitative and (2) qualitative. In Canada, previous studies have only addressed the quantitative approaches. Nearly all of the studies in Canada were performed using the University of Waterloo Flood Forecasting System (WATFLOOD) model (Table 2-3). The application of Radar QPEs for hydrological modeling requires semi or fully distributed hydrological models. WATFLOOD was frequently used at the time because it is capable of ingesting gridded Radar inputs on a temporal scale. A detailed description of the WATFLOOD model can be found in Wijayarathne and Coulibaly 2020 and Kouwen 2016. WATFLOOD has been used since 1988 for diverse hydrological modeling applications in Canada using weather Radar data (Table 2-3).

Table 2-3 *Hydrological modeling studies using WATFLOOD.*

Reference	Key Objective	Study area	*Z-R* relation	Type of Radar	Contribution/conclusions/major findings
Kouwen et al. 1988	Describe a real-time flood forecasting system	Grand River watershed, Southern Ontario	$Z=295R^{1.43}$	King City C-band	Use of real-time Radar along with conventional data sources in WATFLOOD
Kouwen et al. 1993	Test GRU approach to represent the heterogeneity of a watershed using Radar rainfall	Grand River, Saugeen, and Humber River, Eastern Toronto	-	King City C-band	The model parameters are uniquely related to land cover. Hence, the model parameters are transferable to watersheds in physiographically similar areas
Fassnacht et al. 1999	Use of Radar to estimate snowfall as precipitation input for hydrological modeling	Grand River watershed, Southern Ontario	-	King City C-band	Radar data are adjusted to consider the occurrence of mixed precipitation, shape of snow particles, and a site-specific scaling phenomenon
Benoit et al. 2000	Develop a new tool to validate and interpret results from atmospheric models through assimilation of meteorological and hydrological models	Southern Ontario watershed	$Z=295R^{1.43}$	King City S-band	Hydrological models are adequately sensitive to improve atmospheric models
Cranmer et al. 2001	Examine the effects of modeling the nonlinearities of hydrological response to various storm intensities	Duffins Creek drainage basin, southern Ontario	-	King City C-band	WATFLOOD model can amplify observed floods of lesser magnitude to produce flood forecasts
Bingeman et al. 2006	Calibration, validation, and sensitivity analysis of the WATFLOOD model for hydrological processes	Boreal Ecosystem Atmosphere Study (BOREAS) study area	-	King City C-band	Presents a simple split-sample stream flow calibration-validation, followed by validations of internal state variables
Tao and Kouwen 1989	Examine the advantages of using Landsat-derived land cover information for the flood-flow forecasting model	The Grand River, south-western Ontario	$Z=200R^{1.6}$	King City C-band	Watershed elements can be made significant than a typical homogeneous hydrologic unit by calculating runoff for each land cover class separately
Kouwen and Garland 1989	Examine the effects of the spatial resolution of radar-derived rainfall on hydrology to show the impact of discretization of Radar data on hydrological modeling for flood forecasting	Grand River watershed, Southern Ontario	$Z=200R^{1.6}$	Woodbridge Radar	• Spatial averaging reduces the effects of erroneous Radar readings and give comparable results with those obtained using finer resolutions • The appropriate level of discretization depends on the area being modeled

			• There is no significant effect of the level of discretization of Radar precipitation data on the generation of hydrographs

Apart from WATFLOOD, few other hydrological models were used for research and operational applications in Canadian watersheds using Radar QPEs as precipitation input (Table 2-4). The main application was to assess the capability of Radar estimated rainfall to enhance the hydrological model simulations of storm hydrographs. Other applications included explaining precipitation features, structure, and moisture transport, evaluating Radar QPEs, explaining hydrological processes, quantifying errors associated with Radar QPEs, etc. For further details on the use of different hydrological models along with weather Radar in Canadian hydrology, see Table 2-4. Also, the use of weather Radar to forecast gridded snowfall as an input of hydrological models were summarized by Woo et al. (2000). Moreover, Tsanis et al. (2002) compared the rain-gauge tracking technique and Radar storm tracker to obtain storm kinematics into rainfall input to calculate runoff for hydrological applications.

Table 2-4 *Hydrological applications of weather Radar using different hydrological models.*

Reference	Key Objective	Study area	Hydrological Model	Type of Radar	Contribution/conclusions/major findings
Schell et al. 1992	Assess the capability of radar-measured rainfall to enhance the storm hydrographs simulation	St. Dominique watershed, south-western Quebec	HYMO	McGill S-band	Radar estimated rainfalls produced minor improvements for short duration, high intensity, spatially variable rainfall events
Fabry et al. 1994	Determine the magnitude of sampling errors for high-resolution Radar data	Range of McGill Radar	Empirical model	McGill S-band	Sampling errors affect both accuracies of Radar rainfall and calibration with gauges
Asuma et al. 1998	Explain the precipitation features, structure, and moisture transport associated with two different weather conditions using Radar	Tuktoyaktuk, Northwest Territories	A conceptual model	Aircraft-based Radar Tuktoyaktuk X-band	The structure of the storm is strongly affected by the topography of the region and the presence of open water
Hunter et al. 2002	Examine landscape-scale linkages between storm meteorology and hydrology	Vanguard, Saskatchewan	convective indices MSC trajectory model	Bethune C-band	• The meteorology of the storm is described • The origin of the air masses that contributed to the event are identified
Shi et al. 2010	Test the Goddard cloud microphysics scheme in WRF and compare in-situ and Radar measured snowfall	CARE site located near Egbert, Ontario	WRF	King City C-band	Demonstrates the feasibility of using WRF at cloud-resolving resolution (1-km or finer) for high-latitude snow events
Boodoo et al. 2010	A previously developed algorithm was refined for identifying the height of the Radar bright band	Great Lakes region, southern Ontario	The numerical weather prediction model	King City C-band	Less intense bright bands are detectable
McKee et al. 2018	• Assess the effect of radar-gauge merging techniques in hydrology • To determine the effect of influencing factors on Radar QPEs	Upper Thames River Basin, Ontario	HEC-HMS	Canadian WSO experimental C-band	• Radar-gauge merging increases the accuracy of QPEs as well as predicted stream flows • Radar QPEs can be affected by gauge density, rainfall intensity, and time-step of adjustment technique

The integration of different hydrological models in one framework to simulate watershed responses was tested for years using weather Radar QPEs, and those models are still in progress, mainly due to its complexity (Che and Mays 2015). The WATCLASS model (Soulis et al. 2000), which is a linkage of the WATFLOOD and the Environment Canada Canadian LAnd Surface Scheme (CLASS), was used by Fassnacht et al. (1999) to examine the effectiveness of weather Radar to estimate precipitation for five winters (1993 to 1997) in southern Canada as forcing to hydrological models. Both gridded gauge precipitations and raw and adjusted weather Radar precipitations were used as input to the linked WATCLASS models to compare the performances by comparing simulated stream flows. WATCLASS was also implemented and run to investigate and examine the use of Radar estimated rainfall and interpolated gauge measurements as the precipitation input to hydrological models by comparing peak stream flows and cumulative runoff volumes in the Upper Grand River basin in central, south-western Ontario, Canada (Fassnacht 2003). Moreover, WATFLOOD was merged with an atmospheric model, Mesoscale Compressible Community (MC2), by Bacchi and Ranzi (2003) to make a new tool to validate and interpret stream flows produced by atmospheric models.

Moreover, the ArcView GIS environment was used to process and analyze weather Radar QPEs in the previous literature. For example, Gad and Tsanis (2003) developed a GIS multi-component module to read geo-referenced weather Radar data, calibrate against gauges, estimate the kinematics of precipitation patterns, and derive rainfall depths.

2.5.2. Solid precipitation estimation

Many of the previous applications of weather Radar involved rainfall. However, several studies were conducted to estimate solid precipitation rates using reflectivity. Hassan, Taylor, and Isaac (2019) developed two snowfall rate-estimation methods using a nonlinear regression analysis with King City C-band reflectivity factor (Z) and differential reflectivity (Z, Z_{DR}). Both algorithms outperformed the algorithms used by the Canadian Radar network enabling better snowfall accumulations for hydrological applications. A methodology to derive Radar reflectivity factor–liquid-equivalent snow rate power-law relation was introduced by Huang et al. (2010) using King City C-band operational Radar to improve the fall speed quality. The normalized bias of 2.1% and the normalized fractional standard error of 26% were reported between the estimated liquid-equivalent accumulations and gauge amounts for seven snow days during the validation. In 2008 Hudak et al. used the ECCC C-band weather Radar at King City as a reference to assess the ability of satellite CloudSat to detect precipitation during the cold season. Additional research conducted by Hudak et al. (2002) compared Radar signatures of two ground-based polarimetric Radars to detect winter storm conditions in southern Canada using McGill S-band and McMaster University IPIX X-band Radar in the survey. The results suggested that X-band K_{DP} performed better than the S-band for detecting winter precipitation. Also, Z_{DR} and K_{DP} Radar reflectivity products provided valuable information to differentiate mixed phase from glaciated conditions. A new approach to detect Radar composite coverage area of shallow convective lake-effect snowstorms using negative elevation angles was tested over Lake Ontario using both NEXRAD S-

band and Canadian C-band Radar by Brown et al. (2007). The Radar composite coverage area was increased from 40% to 85% in the lower half (0–1 km) of the lake-effect snowstorm using downward Radar scans toward the lake's surface.

2.5.3. Evaluation of weather Radar QPEs

Evaluation of Radar QPEs as an alternative precipitation source for in-situ rain gauge measurements was performed using different weather Radar products across Canada in the past literature. In 1974, Austin and Austin studied both McGill S-band Radar QPEs and gauge measurements to detect rainfall, leading to the flooding of house basements in the City of Ottawa, Ontario. After evaluating nine summer storm events, the study concluded that weather Radar could make a useful contribution to urban hydrology by supplementing it with gauge measurements. Barge et al. (1979) assessed the benefits of weather Radar over rain gauges in hydrological studies. The accumulated precipitation for Red Deer River Basin, Alberta estimated by Alberta Research Council's S-band Radar and an independent gauge data throughout a stormy 6-day period (for 1400- 2000 MDT from July 26-31, 1977) agreed to within 15%. The authors suggested that the best possible rainfall over a basin could be estimated using the combination of precipitation data from both gauge and weather Radar because the gauges accurately measure the surface rainfall at a point. In contrast, the weather Radar determines the spatial variability of precipitation. The authors also suggested the weather Radar as a potentially useful hydrology tool because of much faster availability and accounting for spatial variability than gauge data. Damant et al. (1983a) evaluated the widely used Thiessen interpolation technique using average Radar estimated QPEs as a reference over the Yamaska River

watershed using McGill S-band Radar. Analysis of thirteen summer storms revealed errors between 3% and 69% for the whole basin. The associated errors depend heavily on the type of rainfall (convective or stratiform). After a comprehensive evaluation of four rainfall analysis methods over the Grand River basin above Cambridge (Gait) in southern Ontario using Woodbridge C-band Radar, Dalezios (1988) suggested that weather Radar generally underestimates heavy rainfall and overestimates light rainfall.

Besides Canadian C-band Radar QPEs, a few studies evaluated NEXRAD Radar QPEs as a potential precipitation source for hydrological applications in Canadian watersheds. Chen and Farrar (2007) evaluated NEXRAD S-Band Radar QPEs in Eastern Ontario for potential flood monitoring and water budget analysis. A relatively high correlation of 0.78 was observed during heavy rainfall events between daily NEXRAD QPEs and gauge measurements. Also, 62% of Radar data underestimated the observed precipitation by gauges, and the underestimation was more significant for less intense rainfall. In comparison to the interpolated rainfall surface from rain gauges, NEXRAD showed a more continuous pattern. As a part of a study that focused on Lake Simcoe's water quality in southern Ontario, Ramkellawa et al. (2009) proposed using NEXRAD S-band Radar QPEs to represent rainfall after adjusting with local rain gauges. The Radar QPEs better represented localized rainfall, with most correlation coefficients being over 0.90. Another study emphasized the usefulness of weather Radar as a precipitation source in the areas where gauge density is sparse to provide additional insight on extreme rainfall events over southern Ontario using NEXRAD S-Band Radar QPEs (Paixao et al. 2015).

The authors also emphasized the importance of incorporating weather Radar and gauge measurements in identifying homogeneous regions of extreme rainfall.

2.5.4. Radar-gauge merging

Integrating weather Radar and gauge measurements to enhance the space-time quality of the precipitation is called radar-gauge merging (Wijayarathne et al. 2020a; McKee and Binns 2016; Thorndahl et al. 2016; Wang et al. 2013). The purpose is to merge strengths while diminishing the limitations of both Radar and gauge measurements (Wijayarathne et al. 2020a McKee and Binns 2016). McKee and Binns (2016) described and compared eight radar-gauge merging methods with the complexity ranging from simple mean-field bias correction to Bayesian data combination. The authors concluded that merging methods are primarily affected by several factors, such as gauge network design, storm type, and the adjustment technique's time step. The authors also brought up the lack of research on the near real-time application of radar-gauge merging methods in Canada. Therefore, further research was recommended to evaluate Radar QPEs and adjustment techniques especially for operational hydrological modeling for flood forecasting in Canadian watershed.

Hessami, Anctil, and Viau (2004) performed a statistical-like approach based on artificial neural networks to combine McGill S-band and rain gauge observations for hourly accumulation. The study mapped the weather Radar (input space) to the rain gauges (output space) using different artificial neural network models for a post-calibration of the Radar QPEs. The Levenberg-Marquardt algorithm using Bayesian regularization was introduced as an accurate and reliable method for radar-gauge

merging, especially for real-time urban hydrological applications. McKee et al. (2018) evaluated several radar-gauge merging techniques with single-polarized Canadian WSO experimental C-band over the Upper Thames River Basin, Ontario, to determine the effect of radar-gauge merging on the accuracy of QPEs as well as predicted stream flows. The authors concluded that radar-gauge merging increased the accuracy of QPEs and predicted streamflow. The gauge density, rainfall intensity, and time-step of adjustment technique showed a profound effect on radar-gauge merging. A recent study conducted by Wijayarathne et al. (2020a) evaluated several radar-gauge merging techniques focusing on hydrological model run for operational flood forecasting in urban watersheds. Methods were deployed using four types of Radar QPEs with hourly temporal resolution (two dual-polarized King City C-band and two KBUF NEXRAD S-band) over Semi-urban Humber River and urban Don River watersheds in the GTA, Canada. Surprisingly, the simple Cumulative Distribution Function Matching (CDFM) method outperformed Kriging with radar-based error correction (KRE) method even though geostatistical methods are known to be the best for radar-gauge merging. The performances were better for low- to medium-intensity rainfall during the summer, where convective rainfall events prevail.

2.6. Challenges in the use of Radar QPEs in operational hydrology in Canada

Even though weather Radar produces real-time, spatially, and temporally continuous precipitation data, the operational use of Radar QPEs in hydrology is rare in Canada. The intrinsic errors linked to Radar measurements and, subsequently, Radar QPEs, are considered the main disadvantages. As weather Radar does not measure the

precipitation directly, Radar-based rainfall estimates are known to be subject to errors from different sources such as variability of the drop size distribution, evaporation, attenuation, advection, vertical air motion, ground clutter, radome wetting, Radar instrument miscalibration, partial beam blocking, and beam filling (Boodoo et al. 2015; Wang et al. 2015). Variability in *Z-R* relationships also induce errors for the Radar rainfall estimates. Those errors cause consistent over or underestimating Radar estimated rainfall compared to the rain gauges (Vallabhaneni et al. 2005).

A significant improvement of Radar estimated rainfall was observed when polarimetric signals were used for the Canadian basins (Boodoo et al. 2015). Also, the uncertainties in Radar QPE significantly decreased when the distance to the Radar stations was reduced by increasing the Radar network density. Both methods require significant investment, and hence, the adjustment based on rain gauges is still needed (Thorndahl et al. 2016). It is difficult to recommend one radar-gauge merging method because it depends on the application and the basin characteristics (Goudenhoofdt and Delobbe 2009). Therefore, choosing the best method for a selected watershed is always a compromise. Also, a high quality, dense gauge network is required for a reliable Radar rainfall adjustment. Therefore, frequently observed defects in gauge measures such as missing data, time shift, clogging of the gauge, calibration errors, wind effect, etc. need to be eliminated for accurate QPEs (Thorndahl et al. 2016; Gires et al. 2014; Ciach et al. 2007).

As mentioned before, Canada's current Radar network includes 31 Radar stations covering only populated areas and does not contain all watersheds in Canada. Canada is

geographically large, and hence the basins are also relatively large (Figure 2-3). According to the Data Resource Centre of the University of Guelph Library, there are 1480 stations with climate normal in Canada; however, only 496 stations meet the United Nation's World Meteorological Organization (WMO) standards. In Canada, the existing hydrometric network is lacking in all main watersheds compared to the WMO standards. The most deficient hydrometric networks are identified in Alberta (North Saskatchewan, Oldman, and Red Deer basins), Northern Ontario (Hudson Bay basin), and the Northwest Territories (Mishra and Coulibaly 2010). It was also found that the southernmost urban and suburban catchments are too poorly equipped and do not meet the WMO guidelines for hydrological studies (Coulibaly et al. 2013). Dramatic reduction of the hydrometric stations was noticed recently in Canada, and the main reason was identified as the budgetary cutbacks and shifts in government priorities in the 1990s (Mishra and Coulibaly 2009; Pilon et al. 1996). Since adjusting Radar to match with rain gauges is crucial in Radar hydrometry, the poorly gauged network remains a significant challenge in Canada.

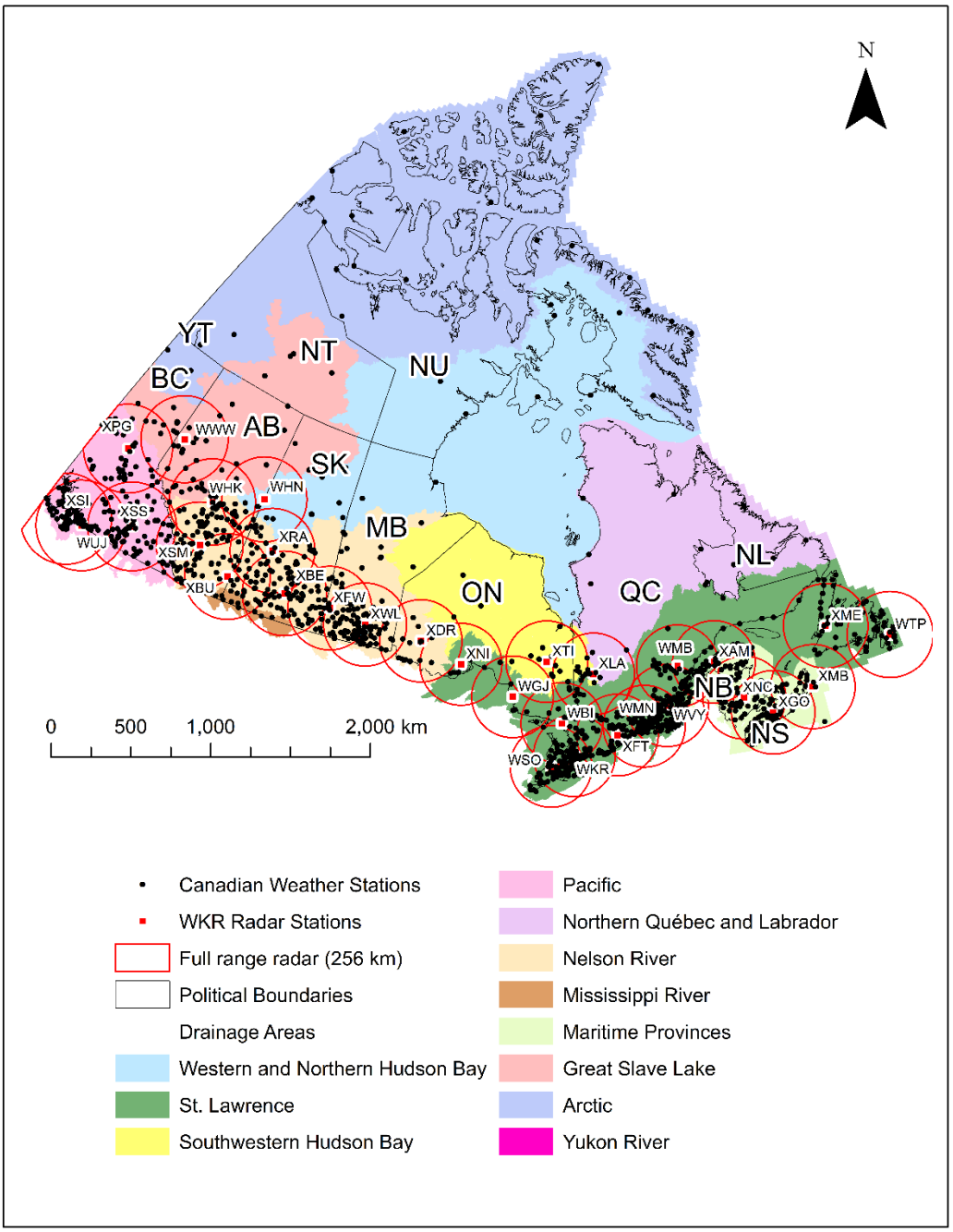

Figure 2-3 *Canadian gauge network, hydrometric delineations (major river basins and hydrography), and Radar gauge coverage (Gauge network data source: Data Resource Centre, University of Guelph Library)*

Another reason for the limited use of Radar in Canadian hydrology is still ongoing development of the Radar infrastructure. Radar stations must cover a broad range, including Doppler scans, to increase the overlaps with neighboring Radar stations. However, broadening the Doppler range will involve considerable investment. Also, the country varies geographically, and very few Radar stations are placed on remote and mountainous sites (e.g., the Val d'Irene Radar site located on top of the Chic-Choc Mountains in the south shore of the St Lawrence River). These factors limit the establishment of the Radar sites and hence, the use of Radar in operational hydrology in Canada.

Additional significant challenge the Canadian meteorologists and hydrologists face is the variability in the Vertical Profile of Reflectivity (VPR). The error due to VPR is significant in Canada because large parts of the country are located beyond the Doppler range (120 km) from the nearest Radar. Since Radar performs a volumetric scan at different elevation angles, precipitation is detected at different heights from the Earth's surface. The measurements are taken aloft because the distance from the Earth's surface increases as the Radar beam travels away from the Radar station. Therefore, VPR correction is necessary to measure the precipitation intensity at the Earth's surface based on the scans performed aloft.

Bright band contamination during the cold seasons remains a challenge in the use of weather Radar in hydrology. At high latitudes, the freezing level is typically at low altitude (e.g., less than 2 km) even during summertime rainfall. However, many studies were limited to the summer period, where the bright band effect is minimal (Wijayarathne

et al. 2020b; Boodoo et al. 2015). Even though a few studies attempted to correct the Radar QPEs for bright band contaminations in Canada, the issue remains a challenge (Boodoo et al. 2010; Fabry and Zawadzki 1995; Humphries and Barge 1979). Methods to find the areas, type of rainfall, and timing of the year where bright band contamination is possible is vital to apply an adequate correction to weather Radar measurements during QPE generation. The newly deployed MRR would help in future research focusing on bright band contamination because of the ability to detect the bright band's level.

Associated computational power and storage in Radar data collection, processing, management, and archiving are always challenging. Because of the high spatial and temporal resolution of weather Radar data and associated QPE products, higher storage and memory allocation are required compared to the gauge data.

2.7. Conclusions and future work

Precipitation information derived from weather Radar has drawn significant attention in Canada because it provides real-time, spatially and temporally continuous data over a large area. This paper presents a thorough review of the existing Canadian weather Radar network and summarizes the previous studies in the hydrological context. Despite the good progress achieved in the use of weather Radar in hydrological studies in Canada, there is much work ahead.

According to the previous literature, Radar QPEs were used to determine the type of precipitation, precipitation features, structure, and moisture transport. Radar precipitation estimates were also used for operational forecasting such as weather forecasts, snow depth predictions, operational weather warnings, and flood forecasting.

Furthermore, it was an excellent tool to validate and interpret results produced by the atmospheric models. The use of radar-derived rainfall as precipitation forcing to hydrological models was not a typical application in Canada compared to the USA. Most of the studies in Canada were performed using the model WATFLOOD. The linear extrapolation of Radar images was frequently used by researchers to make nowcasts in Canada. Even though Radar provides gridded precipitation estimates, intrinsic errors associated with Radar, variability in *Z-R* relationship, the poorly gauged precipitation network, the ongoing development of the Radar infrastructure, existing C-band single-polarized Radar network, and the complex geography in Canada were identified as the most challenging tasks in the use of weather Radar in Canadian hydrology.

Considering the challenges mentioned above and looking into the future, further research should be conducted to address the gaps. Evaluating newly developed Radar QPE products is necessary to verify their reliability and accuracy as an additional precipitation data source for operational hydrology. The added value of dual-polarized Radar over single-polarized Radar to generate QPE products for operational application should be investigated. In particular, the added value of dual-polarized Radar into hydrological models to simulate streamflow in real-time should be thoroughly examined using newly developed hydrological models. Different Radar adjustment techniques and their impacts have been studied for years, and it is difficult to recommend one method over others since it depends on the application and basin characteristics. Further research is needed to look for the best adjustment techniques using the existing rain gauge network to adjust both Canadian and NEXRAD Radar data before their use. Even though the

application of Radar QPEs as precipitation input to hydrological models was tested in research, the operational application is relatively sparse. Therefore, the current research findings need to be tested for operational use, such as flood forecasting. Arc-GIS provides a platform for automated processing of the Radar data and allows rapid data display. Hydrological studies are significantly improved in recent years with the linkage of Radar with the GIS system in the USA and Europe and are highly recommended for Canada. A few studies investigated the use of weather Radar QPEs in mountainous regions where errors are highly likely. Radar measurements in mountainous regions are affected by ground echoes, beam blockage, bright band interception, VPR variability, and frequent rainfall. The potential of using weather Radar in mountainous regions remains a challenge in Canada, and further research is recommended. As discussed in this review, In Canada, hydrological modeling using radar QPEs has only addressed the quantitative approaches. Even though qualitative applications of hydrological modeling were addressed in other parts of the world (Joss and Germann 2000), this remains a niche for future research in Canada.

In conclusion, the use of weather Radars in hydrology has matured steadily in Canada. However, further research is essential to fill the gaps summarized herein to facilitate and enhance hydrological applications of radar-derived precipitation in the Canadian context.

2.8. Acknowledgments

This work was financially supported by the Natural Science and Engineering Research Council (NSERC) Canadian FloodNet under grant number: NETGP-451456.

The authors would like to thank Prof. D. Hudak and Dr. J. Leach for their suggestions and valuable comments that helped improve the manuscript. The authors are grateful to Dr. O. Champagne for translating the abstract into French. The authors also acknowledge Mr. S. Boodoo and Dr. E. Mekis (ECCC) for providing illustrations.

2.9. References

Asuma, Yoshio, Soshi Iwata, Katsuhiro Kikuchi, GW Kent Moore, Ryuji Kimura, and Kazuhisa Tsuboki. 1998. "Precipitation Features Observed by Doppler Radar at Tuktoyaktuk, Northwest Territories, Canada, during the Beaufort and Arctic Storms Experiment." *Monthly Weather Review* 126 (9): 2384–2405. doi:10.1175/1520-0493(1998)126<2384:PFOBDR>2.0.CO;2.

Austin, G. L., and L. B. Austin. 1974. "The Use of Radar in Urban Hydrology." *Journal of Hydrology* 22 (1–2): 131–142. doi:0.1016/0022-1694(74)90100-0.

Bacchi, Baldassare, and Roberto Ranzi. 2003. "Hydrological and Meteorological Aspects of Floods in the Alps: An Overview." *Hydrology and Earth System Sciences Discussions* 7 (6): 785–798. doi: 10.5194/hess-7-785-2003.

Barge, B. L., R. G. Humphries, S. J. Mah, and W. K. Kuhnke. 1979. "Rainfall Measurements by Weather Radar: Applications to Hydrology." *Water Resources Research* 15 (6): 1380–1386. doi:10.1029/WR015i006p01380.

Bellon, A., and G. L. Austin. 1978. "The Evaluation of Two Years of Real-Time Operation of a Short-Term Precipitation Forecasting Procedure (SHARP)." *Journal of Applied Meteorology* 17 (12): 1778–1787. doi.org/10.1175/1520-0450(1978)017<1778:TEOTYO>2.0.CO;2.

———. 1984. "The Accuracy of Short-Term Radar Rainfall Forecasts." *Journal of Hydrology* 70 (1–4): 35–49. doi: 10.1016/0022-1694(84)90112-4.

Bellon, A., S. Lovejoy, and G. L. Austin. 1980. “Combining Satellite and Radar Data for the Short-Range Forecasting of Precipitation.” *Monthly Weather Review* 108 (10): 1554–1566. doi: 10.1175/1520-0493(1980)108<1554:CSARDF>2.0.CO;2.

Bellon, A., and I. Zawadzki. 1994. “Forecasting of Hourly Accumulations of Precipitation by Optimal Extrapolation of Radar Maps.” *Journal of Hydrology* 157 (1–4): 211–233. doi: 10.1016/0022-1694(94)90106-6.

Benjamin, Michael Richard. 2016. “The Use of Radar and Hydrological Models for Flash Flood Evaluation and Prediction.” Master Thesis, University of the Witwatersrand.

Benoit, Robert, Pierre Pellerin, Nick Kouwen, Harold Ritchie, Norman Donaldson, Paul Joe, and E. D. Soulis. 2000. “Toward the Use of Coupled Atmospheric and Hydrologic Models at Regional Scale.” *Monthly Weather Review* 128 (6): 1681–1706. doi: 10.1175/1520-0493(2000)128<1681:TTUOCA>2.0.CO;2.

Berenguer, Marc, Daniel Sempere-Torres, Carles Corral, and Rafael Sánchez-Diezma. 2006. “A Fuzzy Logic Technique for Identifying Nonprecipitating Echoes in Radar Scans.” *Journal of Atmospheric and Oceanic Technology* 23 (9): 1157–1180. doi: 10.1175/JTECH1914.1.

Berenguer, Marc, and Isztar Zawadzki. 2009. “A Study of the Error Covariance Matrix of Radar Rainfall Estimates in Stratiform Rain. Part II: Scale Dependence.” *Weather and Forecasting* 24 (3): 800–811. doi: 10.1175/2008WAF2222210.1.

Berkowitz, D. S., J. A. Schultz, S. Vasiloff, K. L. Elmore, C. D. Payne, and J. B. Boettcher. 2013. “Status of Dual Pol QPE in the WSR-88D Network. 27th Conf. on Hydrology, Austin, TX.” *Amer. Meteor. Soc* 2.

Best Jr, William H. 1973. “Radars over the Hump: Recollections of the First Weather Radar Network.” *Bulletin of the American Meteorological Society* 54 (3): 205–208.

Bingeman, A. Kouwen, N. Kouwen, and E. D. Soulis. 2006. “Validation of the Hydrological Processes in a Hydrological Model.” *Journal of Hydrologic Engineering* 11 (5): 451–463. doi: 10.1061/(ASCE)1084-0699(2006)11:5(451).

Bluestein, Howard B., Robert M. Rauber, Donald W. Burgess, Bruce Albrecht, Scott M. Ellis, Yvette P. Richardson, David P. Jorgensen, Stephen J. Frasier, Phillip Chilson, and Robert D. Palmer. 2014. "Radar in Atmospheric Sciences and Related Research: Current Systems, Emerging Technology, and Future Needs." *Bulletin of the American Meteorological Society* 95 (12). American Meteorological Society: 1850–1861. doi.org/10.1175/BAMS-D-13-00079.1.

Boluwade, A., K.Y. Zhao, T. A. Stadnyk, and P. Rasmussen. 2017. "Towards Validation of the Canadian Precipitation Analysis (CaPA) for Hydrologic Modeling Applications in the Canadian Prairies." *Journal of Hydrology* 556: 1244-1255. doi: 10.1016/j.jhydrol.2017.05.059.

Boodoo, S., D. Hudak, N. Donaldson, and M. Leduc. 2010. "Application of Dual-Polarization Radar Melting-Layer Detection Algorithm." *Journal of Applied Meteorology and Climatology* 49 (8): 1779–1793. doi: 10.1175/2010JAMC2421.1.

Boodoo, Sudesh, David Hudak, Alexander Ryzhkov, Pengfei Zhang, Norman Donaldson, David Sills, and Janti Reid. 2015. "Quantitative Precipitation Estimation from a C-Band Dual-Polarized Radar for the 8 July 2013 Flood in Toronto, Canada." *Journal of Hydrometeorology* 16 (5): 2027–2044. doi: 10.1175/JHM-D-15-0003.1.

Brown, Rodger A., Thomas A. Niziol, Norman R. Donaldson, Paul I. Joe, and Vincent T. Wood. 2007. "Improved Detection Using Negative Elevation Angles for Mountaintop WSR-88Ds. Part III: Simulations of Shallow Convective Activity over and around Lake Ontario." *Weather and Forecasting* 22 (4): 839–852. doi: 10.1175/WAF1019.1.

Carrera, Marco L., Stéphane Bélair, and Bernard Bilodeau. 2015. "The Canadian Land Data Assimilation System (CaLDAS): Description and Synthetic Evaluation Study." *Journal of Hydrometeorology* 16 (3): 1293–1314. doi: 10.1175/JHM-D-14-0089.1.

Carrera, Marco L., Stéphane Bélair, Vincent Fortin, Bernard Bilodeau, Dorothée Charpentier, and Isabelle Doré. 2010. "Evaluation of Snowpack Simulations over

the Canadian Rockies with an Experimental Hydrometeorological Modeling System." *Journal of Hydrometeorology* 11 (5): 1123–1140. doi: 10.1175/2010JHM1274.1.

Che, Daniel, and Larry W. Mays. 2015. "Development of an Optimization/Simulation Model for Real-Time Flood-Control Operation of River-Reservoirs Systems." *Water Resources Management* 29 (11): 3987–4005. doi: 10.1007/s11269-015-1041-8.

Chen, Dongmei, and Andrew Farrar. 2007. "Evaluation of NARAD Precipitation Data for Rainfall Monitoring in Eastern Ontario, Canada." *Geomatics Solutions for Disaster Management*, 103–116. doi: 10.1007/978-3-540-72108-6_8.

Chen, Haonan, and Venkatachalam Chandrasekar. 2015. "The quantitative precipitation estimation system for Dallas–Fort Worth (DFW) urban remote sensing network." *Journal of Hydrology* 531: 259-271. https://doi.org/10.1016/j.jhydrol.2015.05.040.

Chen, Yangbo, Ji Li, Huanyu Wang, Jianming Qin, and Liming Dong. 2017. "Large-Watershed Flood Forecasting with High-Resolution Distributed Hydrological Model." *Hydrology and Earth System Sciences* 21 (2): 735. doi: 10.5194/hess-21-735-2017.

Ciach, Grzegorz J., Witold F. Krajewski, and Gabriele Villarini. 2007. "Product-Error-Driven Uncertainty Model for Probabilistic Quantitative Precipitation Estimation with NEXRAD Data." *Journal of Hydrometeorology* 8 (6): 1325–1347. doi: 10.1175/2007JHM814.1.

Cifelli, Robert, V. Chandrasekar, S. Lim, P. C. Kennedy, Y. Wang, and S. A. Rutledge. 2011. "A New Dual-Polarization Radar Rainfall Algorithm: Application in Colorado Precipitation Events." *Journal of Atmospheric and Oceanic Technology* 28 (3): 352–364. doi: 10.1175/2010JTECHA1488.1.

Coulibaly, Paulin, Jos Samuel, Alain Pietroniro, and David Harvey. 2013. "Evaluation of Canadian National Hydrometric Network Density Based on WMO 2008

Standards." *Canadian Water Resources Journal* 38 (2): 159–167. doi: 10.1080/07011784.2013.787181.

Cranmer, A. J., N. Kouwen, and S. F. Mousavi. 2001. "Proving WATFLOOD: Modelling the Nonlinearities of Hydrologic Response to Storm Intensities." *Canadian Journal of Civil Engineering* 28 (5): 837–855. doi: 10.1139/l01-049.

Dalezios, Nicolas R. 1988. "Objective Rainfall Evaluation in Radar Hydrology." *Journal of Water Resources Planning and Management* 114 (5): 531–546. doi: 10.1061/(ASCE)0733-9496(1988)114:5(531).

Dalezios, Nicolas R., and Nicholas Kouwen. 1990. "Radar Signal Interpretation in Warm Season Rainstorms." *Hydrology Research* 21 (1): 47–64. doi: 10.2166/nh.1990.0004.

Damant, C., G. L. Austin, A. Bellon, and R. S. Broughton. 1983a. "Errors in the Thiessen Technique for Estimating Areal Rain Amounts Using Weather Radar Data." *Journal of Hydrology* 62 (1–4): 81–94. doi: 10.1016/0022-1694(83)90095-1.

Damant, C., G. L. Austin, A. Bellon, M. Osseyrane, and N. Nguyen. 1983b. "Radar Rain Forecasting for Wastewater Control." *Journal of Hydraulic Engineering* 109 (2): 293–297. doi: 10.1061/(ASCE)0733-9429(1983)109:2(293).

Douglas, R. H. 1990. "The Stormy Weather Group (Canada)." *In Radar in Meteorology*, 61–68. Springer. doi: 10.1007/978-1-935704-15-7_8.

Doviak, Richard J. 1993. Doppler Radar and Weather Observations. Courier Corporation.

Droegemeier, Kelvin K., J. D. Smith, S. Businger, C. Doswell III, J. Doyle, C. Duffy, E. Foufoula-Georgiou, et al. 2000. "Hydrological Aspects of Weather Prediction and Flood Warnings: Report of the Ninth Prospectus Development Team of the US Weather Research Program." *Bulletin of the American Meteorological Society* 81 (11): 2665–2680.

Dufton, David Richard Lloyd. 2016. “Quantifying Uncertainty in Radar Rainfall Estimates Using an X-Band Dual Polarisation Weather Radar.” PhD Thesis, University of Leeds.

Einfalt, Thomas, Karsten Arnbjerg-Nielsen, Claudia Golz, Niels-Einar Jensen, Markus Quirmbach, Guido Vaes, and Baxter Vieux. 2004. “Towards a Roadmap for Use of Radar Rainfall Data in Urban Drainage.” *Journal of Hydrology* 299 (3): 186–202. doi: 10.1016/j.jhydrol.2004.08.004.

Environment and Climate Change Canada. 2012. “ARCHIVED - Environment and Climate Change Canada - Weather Monitoring Infrastructure.” 20 January. http://www.ec.gc.ca/default.asp?lang=En&n=592AB94B-1&news=06F87D0A-4EC0-41F2-99EE-729855FCEA65.

Environment and Climate Change Canada. 2017. “The Government of Canada Invests to Modernize Weather-Forecasting Infrastructure.” News releases. Gcnws. 28 February. https://www.canada.ca/en/environment-climate-change/news/2017/02/the_government_ofcanadainveststomodernizeweather-forecastinginfr.html.

Eum, Hyung-Il, Yonas Dibike, Terry Prowse, and Barrie Bonsal. 2014. “Inter-Comparison of High-Resolution Gridded Climate Data Sets and Their Implication on Hydrological Model Simulation over the Athabasca Watershed, Canada.” *Hydrological Processes* 28 (14): 4250–4271. doi: 10.1002/hyp.10236.

Fabry, Frederic, Aldo Bellon, Mike R. Duncan, and Geoffrey L. Austin. 1994. “High Resolution Rainfall Measurements by Radar for Very Small Basins: The Sampling Problem Reexamined.” *Journal of Hydrology* 161 (1–4): 415–428. doi: 10.1016/0022-1694(94)90138-4.

Fabry, Frederic, and Isztar Zawadzki. 1995. “Long-Term Radar Observations of the Melting Layer of Precipitation and Their Interpretation.” *Journal of the Atmospheric Sciences* 52 (7): 838–851. doi.org/10.1175/1520-0469(1995)052<0838:LTROOT>2.0.CO;2.

Fan, Fernando Mainardi, Paulo Rógenes Monteiro Pontes, L. F. S. Beltrame, Walter Collischonn, and Diogo Costa Buarque. 2014. "Operational Flood Forecasting System to the Uruguay River Basin Using the Hydrological Model MGB-IPH." ICFM-6 Proceedings. São Paulo, Brasil.

Fassnacht, S. R. 2003. "Radar Precipitation for Winter Hydrological." In Weather Radar Information and Distributed Hydrological Modelling: Proceedings of an International Symposium (Symposium HS03) Held During IUGG 2003, the XXIII General Assembly of the International Union of Geodesy and Geophysics: At Sapporo, Japan, from 30 June to 11 July, 2003, 35. International Assn of Hydrological Sciences.

Fassnacht, S. R., N. Kouwen, and E. D. Soulis. 2001. "Surface Temperature Adjustments to Improve Weather Radar Representation of Multi-Temporal Winter Precipitation Accumulations." *Journal of Hydrology* 253 (1): 148–168. doi: 10.1016/S0022-1694(01)00479-6.

Fassnacht, S. R., E. D. Soulis, and N. Kouwen. 1999. "Algorithm Application to Improve Weather Radar Snowfall Estimates for Winter Hydrologic Modelling." *Hydrological Processes* 13 (18): 3017–3039. doi: 10.1002/(SICI)1099-1085(19991230)13:18<3017::AID-HYP13>3.0.CO;2-K.

Fortin, V., G. Roy, T. Stadnyk, K. Koenig, N. Gasset, and A. Mahidjiba. 2018. "Ten Years of Science Based on the Canadian Precipitation Analysis: A CaPA System Overview and Literature Review." *Atmosphere-Ocean* 56 (3): 178–196. doi.org/10.1080/07055900.2018.1474728.

Fortin, Vincent, Guy Roy, Norman Donaldson, and Ahmed Mahidjiba. 2015. "Assimilation of Radar Quantitative Precipitation Estimations in the Canadian Precipitation Analysis (CaPA)." *Journal of Hydrology* 531: 296–307. doi: 10.1016/j.jhydrol.2015.08.003.

Fulton, Richard A., Jay P. Breidenbach, Dong-Jun Seo, Dennis A. Miller, and Timothy O'Bannon. 1998. "The WSR-88D Rainfall Algorithm." *Weather and Forecasting* 13 (2): 377–395. doi.org/10.1175/1520-0434(1998)013<0377:TWRA>2.0.CO;2.

Gad, M. A., and I. K. Tsanis. 2003. "A GIS Methodology for the Analysis of Weather Radar Precipitation Data." *Journal of Hydroinformatics* 5 (2): 113–126. doi: 10.2166/hydro.2003.0009.

Germann, Urs, and Isztar Zawadzki. 2002. "Scale-Dependence of the Predictability of Precipitation from Continental Radar Images. Part I: Description of the Methodology." *Monthly Weather Review* 130 (12): 2859–2873. doi: 10.1175/1520-0493(2002)130<2859:SDOTPO>2.0.CO;2.

Germann, U., and I. Zawadzki. 2004. "Scale Dependence of the Predictability of Precipitation from Continental Radar Images. Part II: Probability Forecasts." *Journal of Applied Meteorology* 43 (1): 74–89. doi: 10.1175/1520-0450(2004)043<0074:SDOTPO>2.0.CO;2

"GetMyRealtime Water Data." 2020. Accessed 18 April. http://getmyrealtime.com/.

Gires, Auguste, Ioulia Tchiguirinskaia, Daniel Schertzer, Alma Schellart, Alexis Berne, and Shaun Lovejoy. 2014. "Influence of Small Scale Rainfall Variability on Standard Comparison Tools between Radar and Rain Gauge Data." *Atmospheric Research* 138: 125–138. doi: 10.1016/j.atmosres.2013.11.008.

Goudenhoofdt, E., and L. Delobbe. 2009. "Evaluation of Radar-Gauge Merging Methods for Quantitative Precipitation Estimates." *Hydrology and Earth System Sciences* 13 (2): 195–203. doi: 10.5194/hess-13-195-2009.

Gourley, Jonathan J., J. Zhang, R. A. Maddox, C. M. Calvert, and K. W. Howard. 2001. "A Real-Time Precipitation Monitoring Algorithm–Quantitative Precipitation Estimation and Segregation Using Multiple Sensors (QPE-SUMS)." In Symp. on Precipitation Extremes: Prediction, Impacts, and Responses, 57–60.

Hall, Martin PM, John WF Goddard, and Stephen M. Cherry. 1984. “Identification of Hydrometeors and Other Targets by Dual-Polarization Radar.” *Radio Science* 19 (1): 132–140. doi: 10.1029/RS019i001p00132.

Hasler, A. Frederick, and K. Robert Morris. 1986. “Hurricane Structure and Wind Fields from Stereoscopic and Infrared Satellite Observations and Radar Data.” *Journal of Climate and Applied Meteorology* 25 (6): 709–727. doi: 10.1175/1520-0450(1986)025<0709:HSAWFF>2.0.CO;2.

Hassan, Diar, Peter A. Taylor, and George A. Isaac. 2019. “Solid Snowfall Rate Estimation Using a C-Band Radar.” *Meteorological Applications* 26 (1): 64–73. doi: 10.1002/met.1737.

Hessami, Masoud, Francois Anctil, and Alain A. Viau. 2004. “Selection of an Artificial Neural Network Model for the Post-Calibration of Weather Radar Rainfall Estimation.” *Journal of Data Science* 2 (2): 107–124.

Huang, Gwo-Jong, V. N. Bringi, Robert Cifelli, David Hudak, and W. A. Petersen. 2010. “A Methodology to Derive Radar Reflectivity–Liquid Equivalent Snow Rate Relations Using C-Band Radar and a 2D Video Disdrometer.” *Journal of Atmospheric and Oceanic Technology* 27 (4): 637–651. doi: 10.1175/2009JTECHA1284.1.

Hudak, D., B. Currie, P. Rodriguez, S. G. Cober, I. Zawadzki, G. A. Isaac, and M. Wolde. 2002. “Cloud Phase Detection in Winter Stratiform Clouds Using Polarimetric Doppler Radar.” In Proc. ERAD, 90–94.

Hudak, D., B. Currie, R. Stewart, P. Rodriguez, J. Burford, N. Bussières, and B. Kochtubajda. 2004. "Weather systems occurring over Fort Simpson, Northwest Territories, Canada, during three seasons of 1998–1999: 1. Cloud features." *J. Geophys. Res.* 109, D22108. doi: 10.1029/2004JD004929

Hudak, David, Peter Rodriguez, and Norman Donaldson. 2008. “Validation of the CloudSat Precipitation Occurrence Algorithm Using the Canadian C Band Radar

Network." *Journal of Geophysical Research: Atmospheres* 113 (D8). doi: 10.1029/2008JD009992.

Humphries, Robert G., and Brian L. Barge. 1979. "Polarization and Dual-Wavelength Radar Observations of the Bright Band." *IEEE Transactions on Geoscience Electronics* 17 (4). IEEE: 190–195. doi: 10.1109/TGE.1979.294648.

Hunter, Fraser G., David B. Donald, Brian N. Johnson, Wayne D. Hyde, Ron F. Hopkinson, John M. Hanesiak, Markus OB Kellerhals, and Bart W. Oegema. 2002. "The Vanguard Torrential Storm (Meteorology and Hydrology)." *Canadian Water Resources Journal* 27 (2): 213–227. doi: 10.4296/cwrj2702213.

Joe, Paul, and Steve Lapczak. 2002. "Evolution of the Canadian Operational Radar Network." ERAD, Nov., Delft, Netherlands. http://copernicus.org/erad/online/erad-370.pdf.

Joss, J., and U. Germann. 2000. "Solutions and Problems When Applying Qualitative and Quantitative Information from Weather Radar." Physics and Chemistry of the Earth, Part B: *Hydrology, Oceans and Atmosphere* 25 (10–12). Elsevier: 837–841. doi.org/10.1016/S1464-1909(00)00112-X.

Kouwen, N. 2016. "WATFLOOD/CHARM Canadian Hydrological And Routing Model." Department of Civil Engineering, University of Waterloo, Waterloo, Ontario, Canada.

Kouwen, N., and G. Garland. 1989. "Resolution Considerations in Using Radar Rainfall Data for Flood Forecasting." *Canadian Journal of Civil Engineering* 16 (3): 279–289. doi: 10.1139/l89-053.

Kouwen, N., E. D. Soulis, A. Pietroniro, J. Donald, and R. A. Harrington. 1993. "Grouped Response Units for Distributed Hydrologic Modeling." *Journal of Water Resources Planning and Management* 119 (3): 289–305. doi: 10.1061/(ASCE)0733-9496(1993)119:3(289).

Kouwen, Nicholas. 1988. “WATFLOOD: A Micro-Computer Based Flood Forecasting System Based on Real-Time Weather Radar.” *Canadian Water Resources Journal* 13 (1): 62–77. doi: 10.4296/cwrj1301062.

Krajewski, Witold F., Anton Kruger, James A. Smith, Ramon Lawrence, Charles Gunyon, Radoslaw Goska, Bong-Chul Seo, Piotr Domaszczynski, Mary Lynn Baeck, and Mohan K. Ramamurthy. 2010. “Towards Better Utilization of NEXRAD Data in Hydrology: An Overview of Hydro-NEXRAD.” *Journal of Hydroinformatics* 13 (2): 255–266. doi: 10.2166/hydro.2010.056.

Lee, Gyu Won, Alan W. Seed, and Isztar Zawadzki. 2007. “Modeling the Variability of Drop Size Distributions in Space and Time.” *Journal of Applied Meteorology and Climatology* 46 (6): 742–756. doi: 10.1175/JAM2505.1.

Lespinas, Franck, Vincent Fortin, Guy Roy, Peter Rasmussen, and Tricia Stadnyk. 2015. “Performance Evaluation of the Canadian Precipitation Analysis (CaPA).” *Journal of Hydrometeorology* 16 (5): 2045–2064. doi: 10.1175/JHM-D-14-0191.1.

Mahfouf, Jean-François, Bruce Brasnett, and Stéphane Gagnon. 2007. “A Canadian Precipitation Analysis (CaPA) Project: Description and Preliminary Results.” *Atmosphere-Ocean* 45 (1): 1–17. doi: 10.3137/ao.v450101.

Marshall, John S., and W. Mc K. Palmer. 1948. “The Distribution of Raindrops with Size.” *Journal of Meteorology* 5 (4): 165–166. doi: 10.1175/1520-0469(1948)005<0165:TDORWS>2.0.CO;2.

Marx, A., H. Kunstmann, A. Bárdossy, and J. Seltmann. 2006. “Radar Rainfall Estimates in an Alpine Environment Using Inverse Hydrological Modelling.” *Advances in Geosciences* 9: 25–29. doi: 10.5194/adgeo-9-25-2006.

McKee, Jack L., and Andrew D. Binns. 2016. “A Review of Gauge–Radar Merging Methods for Quantitative Precipitation Estimation in Hydrology.” *Canadian Water Resources Journal* 41 (1–2): 186–203. doi: 10.1080/07011784.2015.1064786.

McKee, Jack L., Andrew D. Binns, Mark Helsten, and Mark Shifflett. 2018. "Evaluation of Gauge-Radar Merging Methods Using a Semi-Distributed Hydrological Model in the Upper Thames River Basin, Canada." *JAWRA Journal of the American Water Resources Association* 54 (3): 594–612. doi: 10.1111/1752-1688.12625.

McMillan, Hilary, Bethanna Jackson, Martyn Clark, Dmitri Kavetski, and Ross Woods. 2011. "Rainfall Uncertainty in Hydrological Modelling: An Evaluation of Multiplicative Error Models." *Journal of Hydrology* 400 (1–2): 83–94. doi: 10.1016/j.jhydrol.2011.01.026.

Mekis, Eva, Norman Donaldson, Janti Reid, Alex Zucconi, Jeffery Hoover, Qian Li, Rodica Nitu, and Stella Melo. 2018. "An Overview of Surface-Based Precipitation Observations at Environment and Climate Change Canada." *Atmosphere-Ocean* 56 (2): 71–95. doi: 10.1080/07055900.2018.1433627.

Middleton, W. E. K. 1981. "Radar development in Canada: The radio branch of the National Research Council of Canada." Wilfrid Laurier University Press, ISBN 0-88920-106-4.

Mishra, A. K., and P. Coulibaly. 2010. "Hydrometric Network Evaluation for Canadian Watersheds." *Journal of Hydrology* 380 (3): 420–437. doi: 10.1016/j.jhydrol.2009.11.015.

Mishra, Ashok K., and Paulin Coulibaly. 2009. "Developments in Hydrometric Network Design: A Review." *Reviews of Geophysics* 47 (2). doi: 10.1029/2007RG000243.

Moore, Robert J., Anne E. Jones, David A. Jones, Kevin B. Black, and Vicky A. Bell. 2004. "Weather Radar for Flood Forecasting: Some UK Experiences." In Sixth International Symposium on Hydrological Applications of Weather Radar, 2–4. Citeseer.

Nasab, Arezoo Rafieei. 2017. "Improving Hydrologic Prediction Via Data Assimilation, Data Fusion and High-Resolution Modeling." PhD Thesis, University of Texas at Arlington.

Nester, Thomas, Jürgen Komma, and Günter Blöschl. 2016. “Real Time Flood Forecasting in the Upper Danube Basin.” *Journal of Hydrology and Hydromechanics* 64 (4): 404–414. doi: 10.1515/johh-2016-0033.

Paixao, Edson, M. Monirul Qader Mirza, Mark W. Shephard, Heather Auld, Joan Klaassen, and Graham Smith. 2015. “An Integrated Approach for Identifying Homogeneous Regions of Extreme Rainfall Events and Estimating IDF Curves in Southern Ontario, Canada: Incorporating Radar Observations.” *Journal of Hydrology* 528: 734–750. doi: 10.1016/j.jhydrol.2015.06.015.

Pilon, P. J., T. R. Yuzyk, R. A. Hale, and T. J. Day. 1996. “Challenges Facing Surface Water Monitoring in Canada.” *Canadian Water Resources Journal* 21 (2): 157–164. doi: 10.4296/cwrj2102157.

Poletti, Maria Laura, Flavio Pignone, Nicola Rebora, and Francesco Silvestro. 2017. “Probabilistic Hydrological Nowcasting Using Radar Based Nowcasting Techniques and Distributed Hydrological Models: Application in the Mediterranean Area.” In EGU General Assembly Conference Abstracts, 19:14367.

Rabiei, E., and U. Haberlandt. 2015. “Applying Bias Correction for Merging Rain Gauge and Radar Data.” *Journal of Hydrology* 522: 544–557. doi: 10.1016/j.jhydrol.2015.01.020.

Ramkellawan, Jeffrey, Bahram Gharabaghi, and Jennifer G. Winter. 2009. “Application of Weather Radar in Estimation of Bulk Atmospheric Deposition of Total Phosphorus over Lake Simcoe.” *Canadian Water Resources Journal* 34 (1): 37–60. doi: 10.4296/cwrj3401037.

Richards, W. G., and C. L. Crozier. 1983. “Precipitation Measurement with a C-Band Weather Radar in Southern Ontario.” *Atmosphere-Ocean* 21 (2): 125–137. doi: 10.1080/07055900.1983.9649160.

Ryzhkov, Alexander V., Scott E. Giangrande, Valery M. Melnikov, and Terry J. Schuur. 2005a. “Calibration Issues of Dual-Polarization Radar Measurements.” *Journal of*

Atmospheric and Oceanic Technology 22 (8): 1138–1155. doi: 10.1175/JTECH1772.1.

Ryzhkov, Alexander V., Terry J. Schuur, Donald W. Burgess, Pamela L. Heinselman, Scott E. Giangrande, and Dusan S. Zrnic. 2005b. "The Joint Polarization Experiment: Polarimetric Rainfall Measurements and Hydrometeor Classification." *Bulletin of the American Meteorological Society* 86 (6): 809–824. doi: 10.1175/BAMS-86-6-809.

Schell, G. S., C. A. Madramootoo, G. L. Austin, and R. S. Broughton. 1992. "Use of Radar Measured Rainfall for Hydrologic Modelling." *Canadian Agricultural Engineering* 34 (1): 41–48.

Shi, J. J., W. K. Tao, T. Matsui, R. Cifelli, A. Hou, S. Lang, A. Tokay, N. Y. Wang, C. Peters-Lidard, and G. Skofronick-Jackson. 2010. "WRF Simulations of the 20–22 January 2007 Snow Events over Eastern Canada: Comparison with in Situ and Satellite Observations." *Journal of Applied Meteorology and Climatology* 49 (11): 2246–2266. doi: 10.1175/2010JAMC2282.1.

Sills, D. M., and P. I. Joe. 2019." From pioneers to practitioners: A short history of severe thunderstorm research and forecasting in Canada." Atmosphere-Ocean 57, 249–261. https://doi.org/10.1080/07055900.2019.1673145.

Skolnik, Merrill I. 1962. "Introduction to Radar." Radar Handbook 2.

Soulis, E. D., K. R. Snelgrove, N. Kouwen, F. Seglenieks, and D. L. Verseghy. 2000. "Towards Closing the Vertical Water Balance in Canadian Atmospheric Models: Coupling of the Land Surface Scheme CLASS with the Distributed Hydrological Model WATFLOOD." *Atmosphere-Ocean* 38 (1): 251–269. doi: 10.1080/07055900.2000.9649648.

Stewart, R. E., J. E. Burford, D. Hudak, D, B. Currie, B. Kochtubajda, P. Rodriguez, and J. Liu. 2004. "Weather systems occurring over Fort Simpson, Northwest

Territories, Canada, during three seasons of 1998–1999: 2. Precipitation features." *J. Geophys. Res* 109, D22109. doi: 10.1029/2004JD004929

Tao, Tao, and Nicholas Kouwen. 1989. "Remote Sensing and Fully Distributed Modeling for Flood Forecasting." *Journal of Water Resources Planning and Management* 115 (6): 809–823. doi: 10.1061/(ASCE)0733-9496(1989)115:6(809).

Thorndahl, Søren, Thomas Einfalt, Patrick Willems, Jesper Ellerb\a ek Nielsen, Marie-Claire ten Veldhuis, Karsten Arnbjerg-Nielsen, M. R. Rasmussen, and Peter Molnar. 2016. "Weather Radar Rainfall Data in Urban Hydrology." *Hydrology and Earth System Sciences & Discussions*, 1–37. doi: 10.5194/hess-21-1359-2017.

Tsanis, I. K., M. A. Gad, and N. T. Donaldson. 2002. "A Comparative Analysis of Rain-Gauge and Radar Techniques for Storm Kinematics." *Advances in Water Resources* 25 (3): 305–316. doi: 10.1016/S0309-1708(02)00003-9.

Vallabhaneni, S., B. E. Vieux, and T. Meeneghan. 2005. "Radar-Rainfall Technology Integration into Hydrologic and Hydraulic Modeling Projects." Chapter in Practical Modeling of Urban Water Systems, Monograph 12.

Vieux, Baxter E., and Philip B. Bedient. 2004. "Assessing Urban Hydrologic Prediction Accuracy through Event Reconstruction." *Journal of Hydrology* 299 (3): 217–236. doi: 10.1016/j.jhydrol.2004.08.005.

Wang, Hong, Hengchi Lei, and Jiefan Yang. 2017. "Microphysical Processes of a Stratiform Precipitation Event over Eastern China: Analysis Using Micro Rain Radar Data." *Advances in Atmospheric Sciences* 34 (12). Springer: 1472–1482. doi.org/10.1007/s00376-017-7005-6.

Wang, Li-Pen, Susana Ochoa-Rodríguez, Nuno Eduardo Simões, Christian Onof, and Čedo Maksimović. 2013. "Radar–Raingauge Data Combination Techniques: A Revision and Analysis of Their Suitability for Urban Hydrology." *Water Science and Technology* 68 (4): 737–747. doi: 10.2166/wst.2013.300.

Wang, Li-Pen, Susana Ochoa-Rodríguez, Johan Van Assel, Rui Daniel Pina, Mieke Pessemier, Stefan Kroll, Patrick Willems, and Christian Onof. 2015. "Enhancement of Radar Rainfall Estimates for Urban Hydrology through Optical Flow Temporal Interpolation and Bayesian Gauge-Based Adjustment." *Journal of Hydrology* 531: 408–426. doi: 10.1016/j.jhydrol.2015.05.049.

Whiton, Roger C., Paul L. Smith, Stuart G. Bigler, Kenneth E. Wilk, and Albert C. Harbuck. 1998. "History of Operational Use of Weather Radar by US Weather Services. Part I: The Pre-NEXRAD Era." *Weather and Forecasting* 13 (2): 219–243. doi: 10.1175/1520-0434(1998)013<0219:HOOUOW>2.0.CO;2.

Wijayarathne, Dayal Buddika, and Paulin Coulibaly. 2020. "Identification of Hydrological Models for Operational Flood Forecasting in St. John's, Newfoundland, Canada." *Journal of Hydrology: Regional Studies* 27. Elsevier: 100646. doi.org/10.1016/j.ejrh.2019.100646.

Wijayarathne, Dayal, Paulin Coulibaly, Sudesh Boodoo, and David Sills. 2020a. "Evaluation of Radar-Gauge Merging Techniques to Be Used in Operational Flood Forecasting in Urban Watersheds." *Water* 12 (5): 1494. doi.org/10.3390/w12051494.

Wijayarathne, Dayal, Sudesh Boodoo, Paulin Coulibaly, and David Sills. 2020b. "Evaluation of Radar Quantitative Precipitation Estimates (QPEs) as an Input of Hydrological Models for Hydrometeorological Applications." *Journal of Hydrometeorology*. 21(8): 1847-1864. doi: 10.1175/JHM-D-20-0033.1.

Woo, Ming-ko, Philip Marsh, and John W. Pomeroy. 2000. "Snow, Frozen Soils and Permafrost Hydrology in Canada, 1995–1998." *Hydrological Processes* 14 (9): 1591–1611. doi: 10.1002/1099-1085(20000630)14:9<1591::AID-HYP78>3.0.CO;2-W.

Xie, H., X. Zhou, J. Hendrickx, E. Vivoni, H. Guan, Y. Tian, and E. Small. 2006. "Comparison of NEXRAD Stage III and Gauge Precipitation Estimates in Central

New Mexico." *Journal of the American Water Resources Association* 42 (1): 237–256. doi: 10.1111/j.1752-1688.2006.tb03837.x.

Xin, Lingyan, Gerhard Reuter, and Bruno Larochelle. 1997. "Reflectivity-Rain Rate Relationships for Convective Rainshowers in Edmonton: Research Note." *Atmosphere-Ocean* 35 (4): 513–521. doi: 10.1080/07055900.1997.9649602.

Xu, Xiaoyong, Kenneth Howard, and Jian Zhang. 2008. "An Automated Radar Technique for the Identification of Tropical Precipitation." *Journal of Hydrometeorology* 9 (5): 885–902. doi: 10.1175/2007JHM954.1.

Zhang, Guifu, Vivek N. Mahale, Bryan J. Putnam, Youcun Qi, Qing Cao, Andrew D. Byrd, Petar Bukovcic, Dusan S. Zrnic, Jidong Gao, and Ming Xue. 2019. "Current Status and Future Challenges of Weather Radar Polarimetry: Bridging the Gap between Radar Meteorology/Hydrology/Engineering and Numerical Weather Prediction." *Advances in Atmospheric Sciences* 36 (6). Springer: 571–588. doi.org/10.1007/s00376-019-8172-4.

Zhang, Jian, Kenneth Howard, Carrie Langston, Brian Kaney, Youcun Qi, Lin Tang, Heather Grams, et al. 2016. "Multi-Radar Multi-Sensor (MRMS) Quantitative Precipitation Estimation: Initial Operating Capabilities." *Bulletin of the American Meteorological Society* 97 (4): 621–638. doi: 10.1175/BAMS-D-14-00174.1.

Zhang, Jian, Kenneth Howard, Carrie Langston, Steve Vasiloff, Brian Kaney, Ami Arthur, Suzanne Van Cooten, et al. 2011. "National Mosaic and Multi-Sensor QPE (NMQ) System: Description, Results, and Future Plans." *Bulletin of the American Meteorological Society* 92 (10): 1321–1338. doi: 10.1175/2011BAMS-D-11-00047.1.

Chapter 3. Evaluation of Radar Quantitative Precipitation Estimates (QPEs) as an Input of Hydrological Models for Hydrometeorological Applications

Summary of Paper 2: Wijayarathne, D., Boodoo, S., Coulibaly, P., and Sills, D. (2020). Evaluation of Radar Quantitative Precipitation Estimates (QPEs) as an Input of Hydrological Models for Hydrometeorological Applications. *Journal of Hydrometeorology*, 21(8), 1847-1864. https://doi.org/10.1175/JHM-D-20-0033.1.

The objective of this study is to verify the reliability and accuracy of Radar QPEs as precipitation input for hydrometeorological models. Nine hourly Radar QPEs from rain-rate relationships using Horizontal reflectivity (Z), Differential reflectivity (Z_{DR}), and Specific differential phase (K_{DP}) for twenty rainfall events over two watersheds; Humber River (semi-urban) and Don River (urban) watersheds, were used in this study. Two KBUF NEXRAD S-band Radar QPEs at Buffalo, New York, USA, and seven WKR C-band dual-polarized Radar QPEs at King City, ON, Canada were evaluated.

Key results of this research include:

- KBUF NEXRAD S-band QPEs can be used as precipitation forcing for hydrological models in Canadian watersheds.
- WKR C-band Radar QPEs with a multi-parameter rain rate estimator using K_{DP} and Z_{DR} performs equally well as KBUF NEXRAD S-band Radar QPEs.
- Continuous time series could be generated using WKR radar QPEs, which has a high temporal resolution, long-term data archive, and good percent detection.

- Persistent spatial variation of all verification matrices indicates the potential of Radar QPEs as gridded precipitation input for distributed hydrological models.

3.1. Abstract

Weather radar provides real-time, spatially distributed precipitation estimates, whereas traditional gauge data are restricted in space. The use of Radar Quantitative Precipitation Estimates (QPEs) as an input of hydrological models for hydrometeorological applications has increased with the development of weather radar worldwide. New dual-polarization technology and algorithms are showing improvements to radar QPEs.

This study evaluates radar QPEs from C-band radar at King City, Canada (WKR), and NEXRAD S-band radar at Buffalo, USA (KBUF) to verify the reliability and accuracy for operational use in the Humber River (semi-urban) and Don River (urban) watersheds in the Greater Toronto Area (GTA), Canada. Twenty rainfall events that occurred from 2011 to 2017 were determined from hourly gauge measurements and compared with nine radar QPEs. Rain rates were estimated with different algorithms using three dual-polarized reflectivity values: Horizontal reflectivity (Z), Differential reflectivity (Z_{DR}), and Specific differential phase (K_{DP}). The correlation coefficient, bias, detection, and root mean square error were calculated and averaged over all events for each gauge station to show the spatial distribution and in a similar pattern to represent the variation by the event.

The quality of the results in terms of accuracy and reliability indicates that the radar QPEs from KBUF S-band and WKR C-band multi-parameter rain rate estimators can be effectively used as precipitation forcing of hydrological models for hydrometeorological applications. The high spatio-temporal resolution, long term data archive, and good percent detection of radar QPEs can facilitate hydrometeorological applications by providing a continuous time series for hydrological models.

3.2. Introduction

There is ample evidence of an increase in extreme weather events during the 21st century, mainly due to climate change (Jentsch et al. 2007; Pachauri et al. 2014). After earthquakes and tsunamis, floods have been the deadliest natural disaster in the world over recent decades (Balica et al. 2013). Enhanced meteorological extremes accelerate the hydrological cycle and cause fluctuations in the discharge that cause floods (Han and Coulibaly 2017; Reggiani and Weerts 2008). In Canada, floods are identified as the most frequent natural hazard to life, property, economy, and environment in the past century and show an increasing trend over time (Bowering et al. 2014). As reported by Public Safety Canada, the estimated total costs of massive floods in Canada from 1900 to 2016 were estimated at almost 36 billion CADs (The Canadian Disaster Database 2019). Therefore, flood mitigation measures are vital for flood-prone regions, and an enhanced flood forecasting system is an essential part of flood mitigation.

A proper flood forecasting system can deliver precise and reliable forecasts with adequate lead time (Cloke and Pappenberger 2009). Over the past few decades in Canada, flood forecasting and nowcasting had been conducted based on hydrological modeling

using lumped, semi-distributed, and distributed models (Moradkhani and Sorooshian 2008). Different hydrological models are being used across Canada for flood forecasting (Zahmatkesh et al. 2019). Even though different static and dynamic precipitation data are available in Canada, the precipitation input of hydrological models rely mostly on in-situ rain gauge data (Unduche et al. 2018; Zahmatkesh et al. 2019). Point data from gauges use different interpolation techniques to make spatially distributed precipitation grids for hydrological modeling applications (Nerini et al. 2015). Widely used interpolation techniques introduce errors to precipitation estimates, mainly due to their inability to quantify interpolation uncertainty (Boluwade et al. 2017; Tabios III and Salas 1985). In operational hydrology, spatially distributed precipitation estimates with a high temporal resolution are preferred to use as the meteorological input for hydrological models.

Nowadays, with the worldwide development of weather radar infrastructure, there is considerable interest in real-time, spatially distributed precipitation information derived from radar over conventional rain-gauge data for hydrometeorological applications such as flood forecasting (Thorndahl et al. 2016). Also, the use of hydrological models in combination with radar estimated Quantitative Precipitation Estimates (QPEs) as a substitute to rain gauges has evolved recently mainly with the advances in radar hardware, data processing, and numerical models (Şensoy et al. 2016). Rain gauges are reliable instruments for rainfall point measurements, but the rainfall varies both in space and time, which is not captured by typical rain gauge networks (Dhiram and Wang 2016). Unlike gauges, radar produces real-time, spatially, and temporally continuous data that enhances hydrometeorological applications (e.g., flood forecasting) in small urban

watersheds (Thorndahl et al. 2016). In relatively large watersheds with sparse rain gauge density, weather radar provides a reliable source of precipitation input for hydrological models that facilitate hydrometeorological applications (Price et al. 2014).

The concept of radar estimated QPEs for hydrological applications first appeared at the urban storm drainage conference in Sweden, 1984 (Einfalt et al. 2004). In conjunction with the advances in radar systems, computer power, and hydrological models over the past decades, the application of radar QPEs as precipitation input for hydrological models has been increased since then (Beneti et al. 2019; Khan et al. 2019; Meischner 2005; Ran et al. 2018). Different countries produce commercial weather radar QPEs providing a grid with precipitation accumulation over time (e.g., Next Generation Weather Radar (NEXRAD) in the USA, NIMROD in the UK and Radar-Online-Aneichung (RADOLAN) in Germany) (Krajewski et al. 2010a; Marx et al. 2006; Moore et al. 2004; Wijayarathne et al. 2020). Also, the accuracy and reliability of weather radar QPEs have been significantly improved with the use of dual-polarized radar products such as Specific Differential Phase (K_{DP}) and Differential Reflectivity (Z_{DR}) (Bringi et al. 2011; Chandrasekar et al. 2013; Hall et al. 2015; Park et al. 2005; Sugier et al. 2006; Dufton 2016; Ryzhkov et al. 2005). Hydrometeorological applications in urban and semi-urban watersheds are benefited mostly from real-time operational weather radar QPEs. For example, local operational warning systems based on weather radar QPEs have been developed to help emergency planning worldwide (Thorndahl et al. 2017; Vivoni et al. 2006; Krajewski et al. 2017; Hapuarachchi et al. 2011). For example, the Weather Research and Forecasting (WRF) model, which is a fully coupled atmospheric-land-

surface/hydrologic model, has been used to forecast heavy precipitation events by assimilating conventional observations and weather radar products (Mazzarella et al. 2020). However, the use of radar QPEs in operational hydrology is yet to be implemented in Canada.

Research in Canadian weather radar began under the project Stormy Weather at the end of the Second World War in 1943 (Sills and Joe 2019; Douglas 1990). Since then, the radar network was gradually expanded, and the application of weather radar in hydrometeorological applications has evolved significantly. The current Canadian radar network includes 31 radar stations and covers most of the populated areas (Joe and Lapczak 2002). This radar network provides reflectivity measurement at a range of 256 km in a radius around the radar site and a Doppler coverage at a range of 120 km around the site (Mekis et al. 2018). The King City weather radar (WKR) facility located in the north of Toronto, Ontario is the first Doppler radar system to be designed and operated in Canada specifically for the weather radar observations (Crozier et al. 1991). In 2004, King City C-band radar (~5 cm) was upgraded to dual-polarization technology and operates in simultaneous transmit and receive mode (Boodoo et al. 2015).

Other than the Canadian weather radar systems, the American radar system NEXRAD covers areas close to the USA – Canada border where most of the Canadian population resides (Fortin et al. 2015). For example, the NEXRAD radar station at Buffalo (KBUF) covers the Greater Toronto Area (GTA) in Canada. NEXRAD is a Doppler weather radar network developed by National Weather Services (NWS) of the United States that comprises 160 weather surveillance radar across the United States

(Mekis et al. 2018; Weber et al. 2007). Currently, both single-polarimetric rain rate R(Z) algorithms and Dual-polarimetric (DP-QPEs) rain-rate algorithms are used by NWS for the NEXRAD radar in the USA (Ryzhkov et al. 2005; Berkowitz et al. 2013). Two levels of NEXRAD products are available to the public in the National Centers for Environmental Information (NCEI) archives (National Climatic Data Center 2018). Level II NEXRAD data are the three meteorological base data: reflectivity, mean radial velocity, and spectrum width. Level III NEXRAD, which is mostly used in hydrological studies, are derived from Level II data from multiple weather radars covering the area (Chen and Farrar 2007; Xie et al. 2006).

Even though the radar QPEs had been used for nearly 30 years in hydrological applications, the use of radar QPEs as an input of hydrological models is still controversial mainly due to the associated errors (Rabiei and Haberlandt 2015; Wang et al. 2015). The accuracy is contentious due to errors in measurements and reflectivity-rain intensity conversions and causes uncertainties in hydrological models (Dai et al. 2018). Since radar provides indirect rainfall measurements, errors can be induced by the variability of the drop size distribution (Maki et al. 2005), attenuation (Park et al. 2005), ground clutter (Hubbert et al. 2009), radar miscalibration (Ayat et al. 2018), partial beam blocking (PC et al. 2013), evaporation, advection, vertical air motion, radome wetting, and beam filling (Thorndahl et al. 2016; Wang et al. 2015). Therefore, evaluation is essential before using radar QPEs in hydrometeorological applications.

When compared to the USA, studies on the radar QPE evaluation in Canada is relatively sparse. The first study was conducted to assess the benefits of weather radar in

hydrological studies in the Red Deer River Basin, Alberta using Alberta Research Council's S-band radar (Barge et al. 1979). The estimated precipitation using the Marshall-Palmer Z-R relation for the James River sub-basin by the two methods only agreed to within 15% throughout a stormy 6-day period. Another study compared the mean areal rainfall computed using the Theissen polygon method and weather radar in the Yamaska river watershed using McGill S-band radar data (Damant et al. 1983). The error between 3% and 69% were reported for thirteen storms compared to the gauge data. A performance assessment of Woodbridge C-band radar QPEs using the $Z = 295R^{1.43}$ algorithm for the Grand River basin above Cambridge in Southern Canada was conducted over six storm events from 1975 to 1978 by Dalezios in 1988. A systematic mean storm radar bias, which varies from 0.37-2.56, was observed between gauge and radar storm accumulations. In 1992, Schell et al. examined the capability of radar QPEs to enhance the storm hydrographs simulation for six rainfall events occurring in 1986 and 1987 over St. Dominique watershed (8.13 km^2) in south-western Quebec using McGill weather radar ($Z=200R^{1.6}$). A minor improvement in hydrograph simulation was observed for high-intensity rainfall events when radar QPEs were used as input to the HYdrological MOdel (HYMO). In 2003, Fassnacht investigated the radar QPEs versus gridded gauge data as precipitation input to hydrological model WATCLASS for the Upper Grand River basin in central, southwestern Ontario, Canada using King City C-band for five winters from 1993 to 1997. The radar QPEs outperformed the gauge data in the model simulating runoff volumes with reported underestimation of 41.7% and 0.3% for gauge and radar QPE, respectively. Most recently, Boodoo et al. (2015) evaluated several radar QPEs

from the King City C-band dual-polarized radar for a flash flooding in the city of Toronto after a heavy rainfall event over a 2-h period on 8 July 2013. This study evaluated total storm accumulations of WKR C-band QPE algorithms based on different dual-polarized products, horizontal reflectivity (Z), differential reflectivity (Z_{DR}), specific differential phase (K_{DP}), and specific attenuation at horizontal polarization (A). KBUF NEXRAD S-band dual-polarized radar at Buffalo, New York, and gauges were used as the reference. The study demonstrated good performance from the algorithms based on K_{DP} and A. The only evaluation of NEXRAD radar QPEs in Canadian watersheds (to the best of our knowledge) was conducted in 2007 by Chen and Farrar in 2007. A correlation of 0.78 was reported between the daily accumulation NEXRAD radar QPEs and rain gauge measurements. Also, 62% of NEXRAD radar QPEs underestimated the precipitation, especially for small rainfall events. Nevertheless, a more continuous pattern of rainfall was observed in radar precipitation surface than the interpolated gauge surface.

Currently, a satisfactory technique to incorporate radar QPEs for hydrological models in Canadian watersheds in real-time or near real-time does not exist. Also, a robust method to correct biases in radar QPEs before using them as precipitation input to hydrological models has not been evaluated to date. Both bias correction of radar using radar-gauge merging and eventually incorporating radar QPEs into hydrological models depends on the accuracy and reliability of radar QPEs (Wijayarathne et al. 2020). A few studies have evaluated radar QPEs in Canadian watersheds but were limited to a single Z-R rain rate relationship, mostly Marshall-Palmer (Barge et al. 1979; Damant et al. 1983; Dalezios 1988; Schell et al. 1992). Also, many of the past studies have evaluated

monthly, daily, or accumulations over storms (Barge et al. 1979; Dalezios 1988; Boodoo et al. 2015). However, hydrometeorological applications such as operational flood forecasting requires high temporal (hourly or sub-hourly) precipitation inputs. Therefore, an extensive evaluation of existing radar QPEs in Canadian watersheds using high temporal (hourly) radar QPEs is necessary. Floods can be triggered either by high intense rainfall occurring in short periods or persistent low intense rain for a more extended period (Diakakis et al. 2016). Therefore, a wide range of rainfall intensities needs to be considered to draw more reliable conclusions. Evaluating the accuracy and reliability of different radar QPEs would help develop Ensemble Prediction Systems (EPS) by using various precipitation ensembles derived from different R-Z algorithms to force the hydrological models (Cloke and Pappenberger 2009; Moradkhani and Sorooshian 2008). Thus, a comprehensive evaluation is necessary before using radar QPEs as input to hydrological models with high confidence.

This study is the first attempt to evaluate nine hourly radar QPEs for twenty rainfall events that reported in spring, summer, and fall periods from 2011 to 2017 over two watersheds in the GTA, Canada: Humber River (semi-urban) and Don River (urban) watersheds. Two KBUF NEXRAD S-band radar QPEs at Buffalo, New York, USA, and seven WKR C-band dual-polarized radar QPEs at King City, ON, Canada are used for the study. The goals of this study are; 1) to evaluate hourly radar QPEs/ algorithms to assess which best suits the urban watersheds in GTA, Canada; 2) to illustrate the performance of radar QPEs for different rainfall events. 3) to assess the performance of radar QPEs at different rain intensities and in different seasons. The outcome of this research will help

to identify the best radar QPE to be implemented in the two urban watersheds in GTA, Ontario, Canada. Also, the evaluation of radar QPEs will facilitate the radar-gauge merging and, subsequently, hydrometeorological applications such as real-time flood forecasting.

3.3. Study area

The Humber River watershed and Don River watershed are the two watersheds of interest (Figure 3-1). Both watersheds are in the Greater Toronto Area and are currently managed by the Toronto and Region Conservation Authority (TRCA). These watersheds are urban and encompass many impervious areas; hence they are considered flood-prone. Recent flood events (e.g., 2013 Toronto flash flood) have emphasized the need for enhanced flood forecasting systems that deliver precise and reliable forecasts with appropriate lead time.

The Humber River watershed is a part of the Great Lakes basin and is considered the largest watershed in the GTA. The watershed encompasses an area of 911 km^2. Land uses consist of approximately 54% rural land, 33% urban land, and the remaining 13% urbanizing land (Watershed Features - Humber River n.d.). This watershed is semi-urban and home to over 800,000 residents. A detailed description of the Humber River watershed can be found in the TRCA Watershed Features - Humber River website (Watershed Features - Humber River n.d.).

The Don River watershed is considered a fully urbanized watershed with approximately 80% developed areas and the remaining area being wetlands, forest, croplands, and pasture (Natural Resources Canada 2009). The watershed is approximately

350 km^2 in size, and the catchment is home to over 1 million residents. For further details of the Don River watershed, readers are referred to the TRCA Don River website (Don River n.d.).

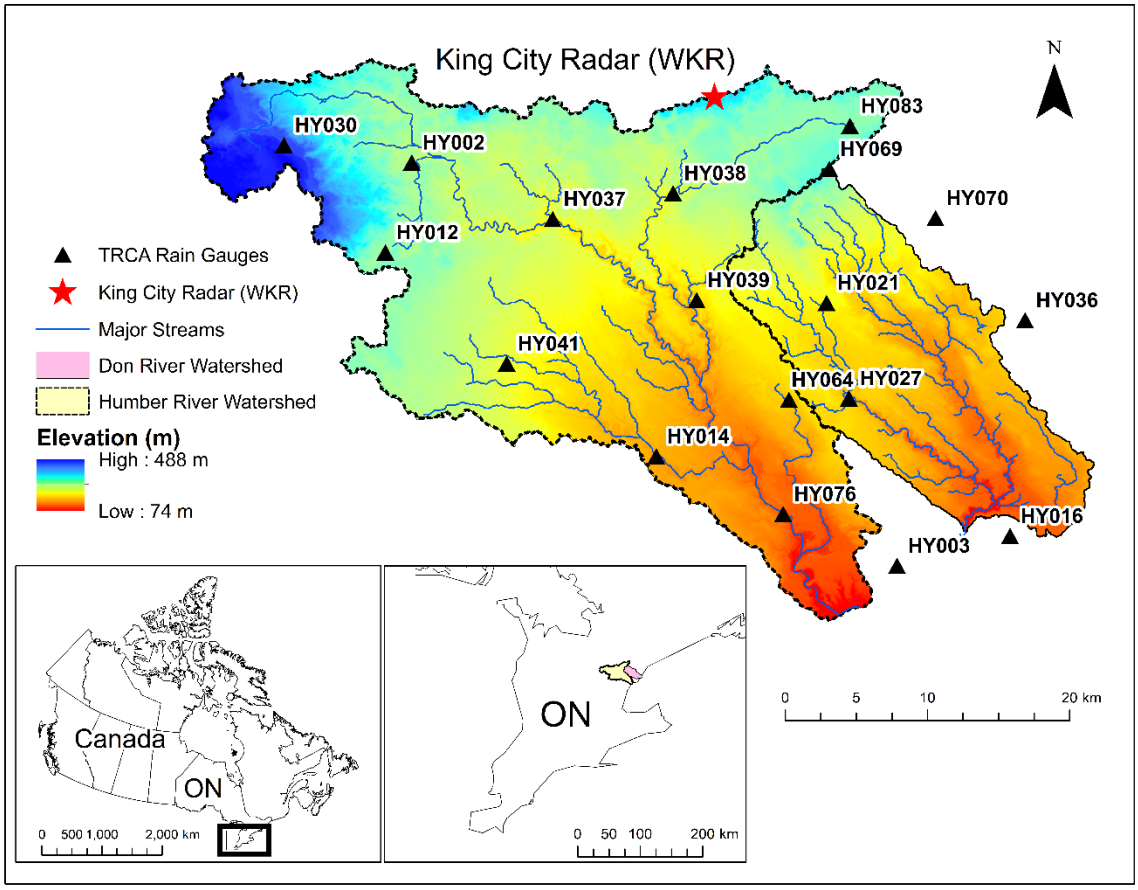

Figure 3-1 *Humber River and Don River watersheds in GTA*

3.4. Materials and methods

3.4.1. Data Description

3.4.1.1. Rain gauge

One-hour accumulations of surface rainfall data provided by tipping-bucket rain gauges from 2011- 2017 were gathered from TRCA data archives. The temporal

resolution of received rainfall data ranges from 5 to 60 min. TRCA operates eighteen real-time tipping-bucket rain gauges distributed across the two watersheds. All gauges are located within the ~40 km radius range of King City (WKR) Canadian C-band radar station (Figure 3-2). Apart from Canadian radar, both watersheds have an excellent radar spatial coverage from the Buffalo (KBUF) NEXRAD S-band radar. All TRCA gauge stations are located within the usable range (<180 km) of KBUF NEXRAD S-band radar station (Figure 3-2).

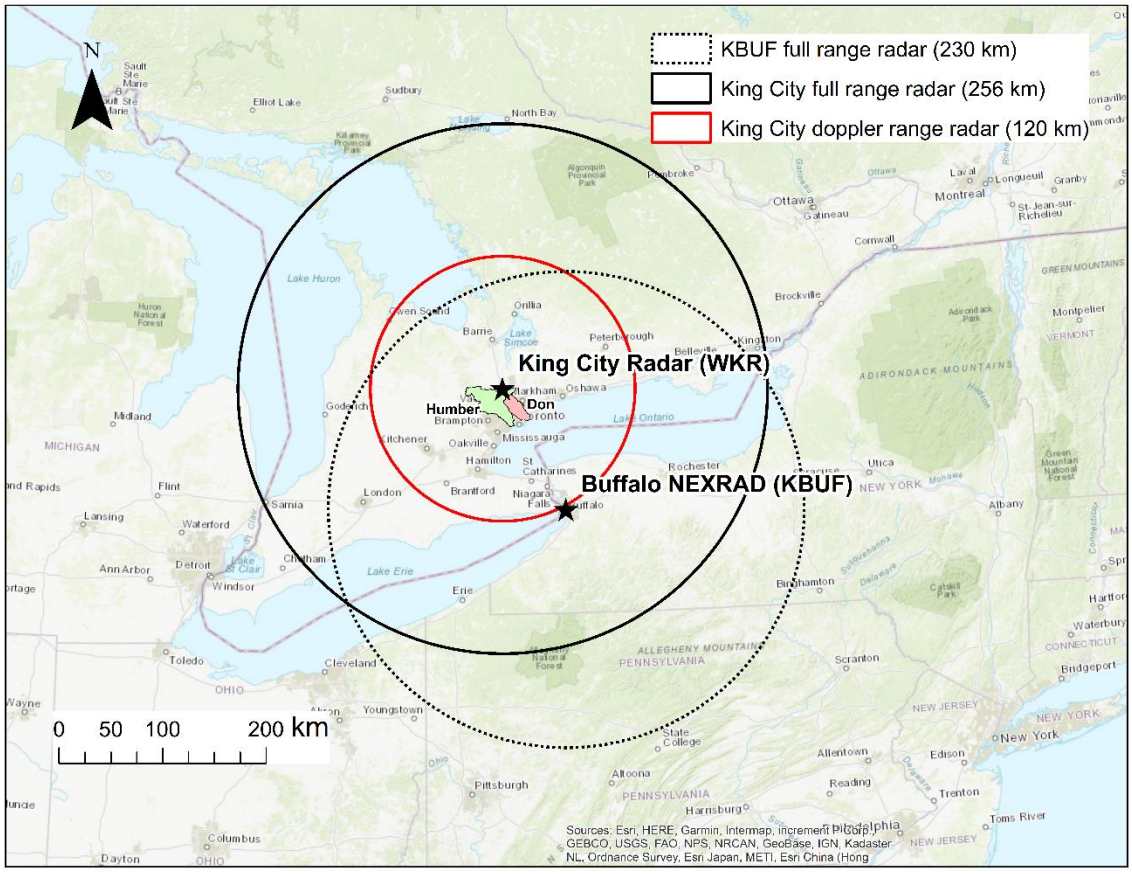

Figure 3-2 *Spatial coverage of radar from King City Canadian C-band radar (WKR) and Buffalo USA NEXRAD S-band radar (KBUF)*

3.4.1.2. KBUF NEXRAD S-band radar QPEs

NEXRAD Level III S-Band radar estimated precipitation data recorded at the Buffalo radar (Lat 42.94639 Lon -78.72278) for the same period as gauge data were downloaded from the National Centers for Environmental Information (NCEI) archives (National Climatic Data Center 2018). Two NEXRAD Level III QPE products, One-Hour Precipitation (N1P/78), and Digital Precipitation Array (DPA/81), were used in this study. N1P/78 is a radar estimated one-hour precipitation accumulation at the volume scan time on a 1.1-nm by a 1-degree grid. The DPA/81 is a radar estimated one-hour precipitation accumulation on the 4.7625 km Hydrologic Rainfall Analysis Projection (HRAP) grid.

3.4.1.3. King City WKR C-band QPEs

POLarimetric Plan Position Indicator (POLPPI) scans at 0.5-degree elevation completed in ~1 min with 0.25 km × 0.5-degree range and azimuthal resolution and repeated in a 10-min cycle were collected from Environment and Climate Change Canada (ECCC) data archives.

3.4.2. Data preprocessing and derivation of rainfall time series

3.4.2.1. KBUF NEXRAD S-band radar

Both NEXRAD N1P/78 and DPA/81 products have been calculated using the Precipitation Processing System (PPS) algorithm using $R= 0.017Z^{0.714}$ Z-R relationship (Fulton et al. 1998). Raw data are stored as ASCII format. The NEXRAD S-band radar QPEs comprise an accumulation of precipitation over 1 hour. The NEXRAD S-band radar QPEs at 1-hour intervals were exported into ASCII format using NOAA's Weather

and Climate Toolkit (WCT). The Binary NEXRAD radar QPE data were then converted into GeoTIFF files using batch processing capability of the terminal version of WCT. Several scripts were written in MATLAB, Python, and batch files to facilitate data processing (Guzman et al. 2013). ArcGIS 10.6.1 was used to re-project gridded NEXRAD data into Universal Transverse Mercator (UTM) coordinate system. Re-projected NEXRAD grids were then clipped into watershed boundaries with the use of modeling tools in ArcGIS.

3.4.2.2. WKR C-band radar

Radar QPEs were estimated for each of the POLPPI scans at 10 min intervals using different rain rate estimator algorithms listed in Table 3-1. In this study, the modified ZPHI attenuation correction, which depends on identified hotspots, was used to correct Z and Z_{DR} for attenuation. For further details on ZPHI attenuation correction, readers refer to Ryzhkov et al. (2006, 2007) and Boodoo et al. (2015). After attenuation correction, rain rates are calculated using R (Z), R (Z, Z_{DR}), R (Z, K_{DP}), and R (K_{DP}, Z_{DR}) algorithms. Rain rates using both raw and attenuation corrected Z and Z_{DR} were estimated using conventional Marshall Palmer ($R = 0.0365Z^{0.625}$) algorithm (Marshall and Palmer 1948). Also, the US-derived Z-R relationship by Fulton et al. (1998) was used to derive radar QPEs using WKR C-band radar (Z) to compare the rainfall accumulation in the overlapping radar (NEXRAD and WKR) coverage with the same Z-R relationship. Since the coefficients of the Z-R relationship by Fulton et al. (1998) are much similar to the Z-R relationship suggested by Richards and Crozier (1983) for WKR radar, the effects of attenuation, height difference and other factors in the resulting accumulations can be

compared. Moreover, a combined Z and K_{DP} algorithm using a threshold on K_{DP} and Z was estimated using algorithms $R = 0.017Z^{0.714}$ and $R = 33.8K_{DP}^{0.79}$, suggested by Brandes et al. (2002). Furthermore, two multi-parameter rain-rate estimators, R (Z, Z_{DR}) and R (K_{DP}, Z_{DR}), were used to estimate rainfall for the evaluation (Bringi et al. 2011).

Table 3-1 *List of rain-rate estimators for radar QPEs.*

Product	Description	Formula	Reference
C1	standard Marshall Palmer with uncorrected Z	$R = 0.0365Z^{0.625}$	(Marshall and Palmer, 1948)
C2	standard Marshall Palmer with attenuation corrected Z	$R = 0.0365Z^{0.625}$	(Marshall and Palmer, 1948)
C3	attenuation corrected Z but using NEXRAD R(Z)	$R = 0.017Z^{0.714}$	(Fulton et al. 1998)
C4	combined Z and K_{DP} algorithm using a threshold on K_{DP}	$R = 0.017Z^{0.714}$ $R = 33.8K_{DP}^{0.79}$	(Brandes et al. 2002)
C5	combined Z and K_{DP} algorithm using a threshold on Z	$R = 0.017Z^{0.714}$ $R = 33.8K_{DP}^{0.79}$	(Brandes et al. 2002)
C6	Multi parameter rain rate estimator using Z and Z_{DR}	$R = 0.0058Z^{0.91}10^{-0.209Z_{DR}}$	(Bringi et al. 2011)
C7	Multiparameter rain rate estimator using K_{DP} and Z_{DR}	$R = 37.9K_{DP}^{0.89}10^{-0.072Z_{DR}}$	(Bringi et al. 2011)
N1	NEXRAD Level III (N1P)	$R = 0.017Z^{0.714}$	(Fulton et al. 1998)
N2	NEXRAD Level III (DPA)	$R = 0.017Z^{0.714}$	(Fulton et al. 1998)

An averaging window of 11 × 11 in range and azimuth of radar-derived accumulations centered over the nearest gauge location was used to compare with rain gauge amounts. Pixel averaging permits restraining the effect of wind drift that can be very significant (Lack and Fox 2007). Since range bins are 0.25 km and azimuth are 0.5-degree resolutions, 11 pixels in range = 11 × 0.25 km = 2.75 km and 11 pixels in azimuth = 11 × 0.5 = 5.5 degrees, at an average gauge distance of 40 km, this works out to about

3.8 km. Radar estimated rain rates are assumed to be constant over the scanning time interval of 10 min. The 10-min radar rainfall measurements are accumulated to obtain the total hourly rainfall time series.

3.4.3. Evaluation of radar QPEs

Twenty rainfall events, totaling 297 h of rainfall that occurred in spring, summer, and fall periods from 2011 to 2017 (Table 3-2), were identified from hourly rain gauge data and used as a ground reference. Winter precipitation was excluded from this study because the algorithms are only valid for liquid precipitation and do not account for possible bright band contamination (Boodoo et al. 2015; Wijayarathne et al. 2020). Several criteria such as intensity, speed, storm size, availability of both gauge and radar precipitation, missing values, satisfactory accumulation of rainfall, suitable duration, coverage of the watershed, and adequate discharge at the outlet of the watershed were considered for event selection. The duration of an event was determined as the time wherein at least half of the gauges recorded a precipitation amount > 0 mm to the time where half of the gauges start re-recording zero (Krajewski et al. 2010b; Wijayarathne et al. 2020). Hourly accumulations from gauges and nine radar QPEs listed in Table 3-1 for each event were calculated. The summary statistics were computed between each gauge-pixel pair, and missing values were ignored during the comparison. The correlation coefficient (Eq. 3-1), bias (Eq. 3-2), radar detection (Young and Brunsell 2008) (Eq. 3-3), and RMSE (Eq. 3-4) were calculated between radar QPEs and gauge for each event separately. These metrics were averaged over all events for each gauge station to show the spatial distribution and in a similar pattern to represent the variation by the event.

Correlation (r)

$$r = \frac{\sum(P_G - \bar{P}_G)(P_R - \bar{P}_R)}{\sqrt{\sum (P_G - \bar{P}_G)^2 \sum (P_R - \bar{P}_R)^2}} \quad (3\text{-}1)$$

BIAS (b)

$$b = \frac{\sum P_R - \sum P_G}{\sum P_G} \times 100 \quad (3\text{-}2)$$

Detection (d)

$$d = \frac{n_{P_R} > 0, P_G > thresh}{n_{P_G} > thresh} \times 100 \quad (3\text{-}3)$$

RMSE (rmse)

$$rmse = \sqrt{\frac{\sum_{i=1}^{n} (P_G - P_R)^2}{n}} \quad (3\text{-}4)$$

Where,

P_G is hourly precipitation observed by gauge, $\bar{P}_G$ is average hourly rain gauge measurement, P_R is hourly radar estimated precipitation, $\bar{P}_R$ is average hourly radar estimated rainfall, $n_{P_R} > 0, P_G > thresh$, number of radar-gauge pairs that the radar reports precipitation and the corresponding rain gauge observation exceeds a specified threshold (0 mm); and $n_{P_G} > thresh$, number of radar-gauge pairs where the rain gauge observation exceeds a specified threshold (> 0 mm).

Table 3-2 *Description of events.*

Event No	Start date	UTC	End date	UTC	Season	Rainfall (mm)			Duration (Hours)
						Avg	Max	Min	
1	11/29/2011	4:00	11/29/2011	22:00	Fall	36.2	53.4	4.6	19
2	6/1/2012	8:00	6/1/2012	23:00	Summer	27.7	39	7.6	16
3	5/28/2013	20:00	5/29/2013	8:00	Spring	33.95	60	3	14
4	7/8/2013	18:00	7/9/2013	2:00	Summer	44.92	93.8	0	9
5	7/31/2013	19:00	8/1/2013	10:00	Summer	34.76	50	1	16
6	7/28/2014	0:00	7/28/2014	12:00	Summer	28.74	85	0	13
7	9/6/2014	0:00	9/6/2014	10:00	Fall	26.6	52.6	0	11
8	4/20/2015	3:00	4/20/2015	19:00	Spring	20.45	32	0	17
9	5/30/2015	15:00	5/31/2015	23:00	Spring	42.34	66	10	33
10	6/8/2015	0:00	6/8/2015	13:00	Summer	28.33	44.2	0	14
11	6/27/2015	17:00	6/28/2015	21:00	Summer	39.07	57	16	29
12	10/28/2015	7:00	10/28/2015	23:00	Fall	30.12	49.8	0	17
13	11/10/2015	19:00	11/11/2015	11:00	Fall	13.2	20.4	0	17
14	8/13/2016	16:00	8/14/2016	1:00	Summer	24.44	45.2	0	10
15	8/16/2016	8:00	8/16/2016	19:00	Summer	16.32	34.4	1	12
16	6/23/2017	5:00	6/23/2017	14:00	Summer	37.33	65.2	1	10
17	7/20/2017	15:00	7/20/2017	17:00	Summer	19.86	41.6	0	3
18	7/27/2017	0:00	7/27/2017	15:00	Summer	9.91	15.2	2	16
19	8/22/2017	12:00	8/22/2017	23:00	Summer	11.8	24.2	0	14
20	11/18/2017	22:00	11/19/2017	8:00	Fall	11.62	20	0	11

In this study, it is essential to notice that there is always a spatial mismatch in the precipitation estimates between radar and gauges because different volumes are sampled by rain gages and weather radar (Grayman and Eagleson 1971). Rain gauges record time-integrated precipitation over an eight-inch diameter surface area, whereas radar instantly samples a significant volume above approximately 4×4 km surface (Young and Brunsell 2008). This spatial mismatch can contribute to differences in precipitation values. Also, gauges that are used as the ground truth can be unreliable due to random and systematic errors (Mekonnen et al. 2015). Random errors can be resulted by irregularities of topography and vegetation around the gauge site, poor gauge site conditions, human errors, inadequate network density, and by the disclosure to prevailing winds. Systematic errors in precipitation due to wind-induced under-catch, wetting, and evaporation losses also affect the gauges (Sevruk 1982). There is also a known low bias for tipping bucket gauges in high precipitation events where the bucket tipping cannot keep up.

3.5. Results and discussion

Average precipitation detections with WKR C-band and KBUF NEXRAD S-band radar QPEs for each event are presented in Figure 3-3-a. Overall, the detection is relatively higher for all WKR C-band radar QPEs than KBUF NEXRAD QPEs and varies from event to event. This is not surprising as the study area is much closer to the C-band radar than the S-band, although it suffers from attenuation of return echoes (Borga et al. 2002). The range of detections reported for WKR C-band radar QPEs ranges from 53.5 – 96.6 %, and KBUF S-band radar QPE ranges from 3.0 – 92.3%. The KBUF NEXRAD

measures the precipitation relatively far (~ 106 km) from the watershed, while WKR radar measures the precipitation just below the storm at a distance of 37 km at the furthest edge of the watershed. NEXRAD Level III (DPA) (hereafter N2) is competitive with all C-band radar QPEs, but detection for NEXRAD Level III (N1P) (hereafter N1) is not as good as N2. As pointed out by Young and Brunsell (2008), low detection of NEXRAD can be partially responsible for problems in both bias and correlation when compared to the gauge accumulations. It is also challenging to address the lack of detection during the calibration of hydrologic models (Zhang et al. 2012; Young and Brunsell 2008). Since detection is high in WKR C-band radar QPEs, it is possible to formulate a continuous time series with a smaller number of missing data, which is often required for hydrological model calibration. Additionally, dual-polarization data from WKR are available starting in 2004; therefore, it is possible to generate a continuous time series with sub-hourly resolutions for hydrological models. The box plots in Figure 3-3-b show an average detection for C-band radar QPEs is ~ 80%. The interquartile range (IQR) is relatively low for all C-band radar QPEs, and therefore, they can detect all events successfully compared to the NEXRAD QPEs.

The average correlation between radar-estimated precipitation amounts and gauge observations is reported in Figure 3-3-c. The average correlation for QPEs from NEXRAD (0.38 – 0.98) is superior to all C-band QPEs (0.20 – 0.97). The average correlation for the N2 (0.71) is better than N1 (0.63). The path attenuation is a significant influence on radar-estimated QPEs in heavy rain events (Boodoo et al. 2015), as C-band radar beams attenuate more rapidly than KBUF NEXRAD S-band radar because of its

shorter wavelength (~ 10 cm for NEXRAD and ~ 5 cm for WKR). The multi-parameter rain rate estimator using K_{DP} and Z_{DR} (hereafter C7) and combined Z and K_{DP} algorithm using a threshold on K_{DP} (hereafter C4) are competitive with NEXRAD radar QPEs with reported average correlations of 0.60 and 0.56, respectively. The C4 and combined Z and K_{DP} algorithm using a threshold on Z (hereafter C5) show better correlation compared to other C-band radar QPEs using only Z: standard Marshall Palmer with uncorrected Z (hereafter C1), standard Marshall Palmer with attenuation corrected Z (hereafter C2), and attenuation corrected Z using rain-rate estimator for NEXRAD (hereafter C3). Previously conducted research suggests that K_{DP} is advantageous over Z for quantitative precipitation estimates (Vivekanandan et al. 1999; Brandes et al. 2001). The K_{DP} is not a power measurement; therefore, radar QPEs derived from K_{DP} are less affected by anomalous propagation, attenuation, beam blockage, and radar miscalibration (Ryzhkov et al. 2014). Also, these QPEs are known to be less sensitive to variations in drop size distributions and the existence of hail (Sachidananda and Zrnić 1987; Aydin et al. 1995). Even though K_{DP} is resilient to the radar errors as mentioned above, the vulnerability of Z to these errors may be limiting the quality of rainfall estimates using combined algorithms. Combining radar QPEs using thresholds on K_{DP} shows better performances than combined radar QPEs using thresholds on Z. All other C-band radar estimated QPEs (C1, C2, and C3) show relatively low average correlation (0.41, 0.43, and 0.46, respectively). After attenuation correction, the correlation between the gauge and radar QPEs has been improved but does not show considerable improvement. The attenuation correction may be overshadowed by the extensive radome attenuation at WKR, resulting in poor rainfall

estimates (Germann 1999; Boodoo et al. 2015). C3 shows better performances with the reported correlation of 0.46 than using Marshall Palmer on Z (C1, 0.41 and C2, 0.43). IQRs for those QPEs (Figure 3-3-d) are relatively higher, implying that the correlation varies from event to event considerably. The correlation values are better for events in summer than fall and spring, especially for N2, N1, C7, and C4. For example, summer events 14 to 19 show $r > 0.83$ while the fall and spring events 1, 3, and 7 show $r < 0.5$ for N2. Even though the correlation is relatively low, the values are relatively persistent (mean value ranges between 0.40 and 0.60) for all the events for other C-band radar QPEs. N2, N1, C7, and C4 radar QPEs are more reliable for summer events than events in fall and spring. The bright band effect during early spring and late fall has affected the quality of radar QPEs for both KBUF NEXRAD S-band radar and WKR C-band radar (Austin and Bemis 1950, Fabry and Zawadzki 1995). For the rest of the C-band radar QPEs (C1, C2, C3, C5, and C6), the correlation is less, but they capture all events regardless of the period or intensity of the event. The reported correlation values are approximately similar for all radar QPEs for the less intense (< 5 mm/h) events (e.g., events 9 and 11). In contrast, correlation considerably varies between different radar QPEs for high-intensity ($\geq$ 5mm/h) events (e.g., events 4 and 17). For high-intensity events, N2, N1, C7, and C4 perform better than other WKR C-band radar QPEs (C1, C2, C3, C5, and C6). Since these correlations are not optimum for both WKR C-band and KBUF NEXRAD QPEs for hydrological models, bias correction is necessary before using radar QPEs as a precipitation input.

Figure 3-3-e shows the average RMSE between radar-gauge hourly accumulation pairs for all the events. Errors follow the same trend as the reported correlation. The least RMSE errors are reported for N2 (2.8 mm) followed by C7 (3.2 mm), and errors vary considerably from event to event. Error is high for high-intensity events (e.g., events 4 and 17) and relatively small in low-intensity events (e.g., events 9 and 11). For example, average RMSE for event 4 (10.4 mm/h) and 17 (13.9 mm/h) are 8.6 mm and 10.5 mm, respectively whereas for event 9 (2.0 mm/h) and 11 (2.0 mm/h) are 2.7 mm and 2.3 mm, individually. In Figure 3-3-f, the least mean and IQR were reported for N2, which implies that errors incorporated are low, constant, and independent from the event for N2. According to Seo et al. (2015), radar calibration errors, technical limitations such as non-uniform beam filling, wind effect, growth of precipitation, anomalous propagation, variations in the Z-R relationship, presence of hail, or other hydrometeors can affect the accuracy of radar QPEs. Even though attenuation and ground clutter is taken care of during signal processing, the limitations mentioned above restrict the efficiency of radar QPEs.

The event-to-event variations in r and RMSE could be attributed to the differences in storm type and magnitude (Stellman et al. 2001; McKee and Binns 2016). The accuracy and reliability of radar QPEs vary along with the season (Prat and Nelson 2014). According to the results, the added value to QPEs from the radar is considerable during the summer when convective rainfall events prevail. Convective rainfall is produced through local scale lifting of air parcels and is characterized by moderate to heavy rainfalls of short duration (high intensity). Convective cells are often mischaracterized by

rain gauges, but captured by weather radar (McKee and Binns 2016). On the contrary, stratiform rainfall is produced through larger-scale, regional lifting of air parcels (e.g., a low-pressure system), resulting in light to moderate rainfall over a large area for a relatively long duration. Rain gauges can characterize the stratiform precipitation relatively well compared to weather radar (McKee and Binns 2016).

Figure 3-3-g and 3-3-h show the distribution of bias values and boxplots over the events. All radar QPEs underestimate the reported gauge precipitation for all events except for events 1, 12, 13, and 20. This underestimation is reported because radar QPEs are subject to both random and systematic errors. For instance, an order of 4 to 5% of radar underestimation was stated due to wind under catch by Duchon and Essenberg (2001). The radar underestimation is relatively less for N2, C7, and C4. All radar QPEs over predicts events 1, 12, 13, and 20, which were taken place in late fall / early winter and could be possibly bright band contaminated. NEXRAD over predictions in spring and fall may also be due to the bright band effect. The discrepancy in sampling heights between KBUF NEXRAD S-band and WKR C-band measurements could be a complicating factor that affects the bias as NEXRAD and WKR radar do not measure the same volume in the space and time. Besides possible errors during radar measurements, the variations in the individual event biases can be attributed to storm type and magnitude (McKee and Binns 2016). The weather radar underestimates precipitation during convective summer events and overestimates stratiform events in late fall / early winter (Kalinga and Gan 2006; McKee and Binns 2016).

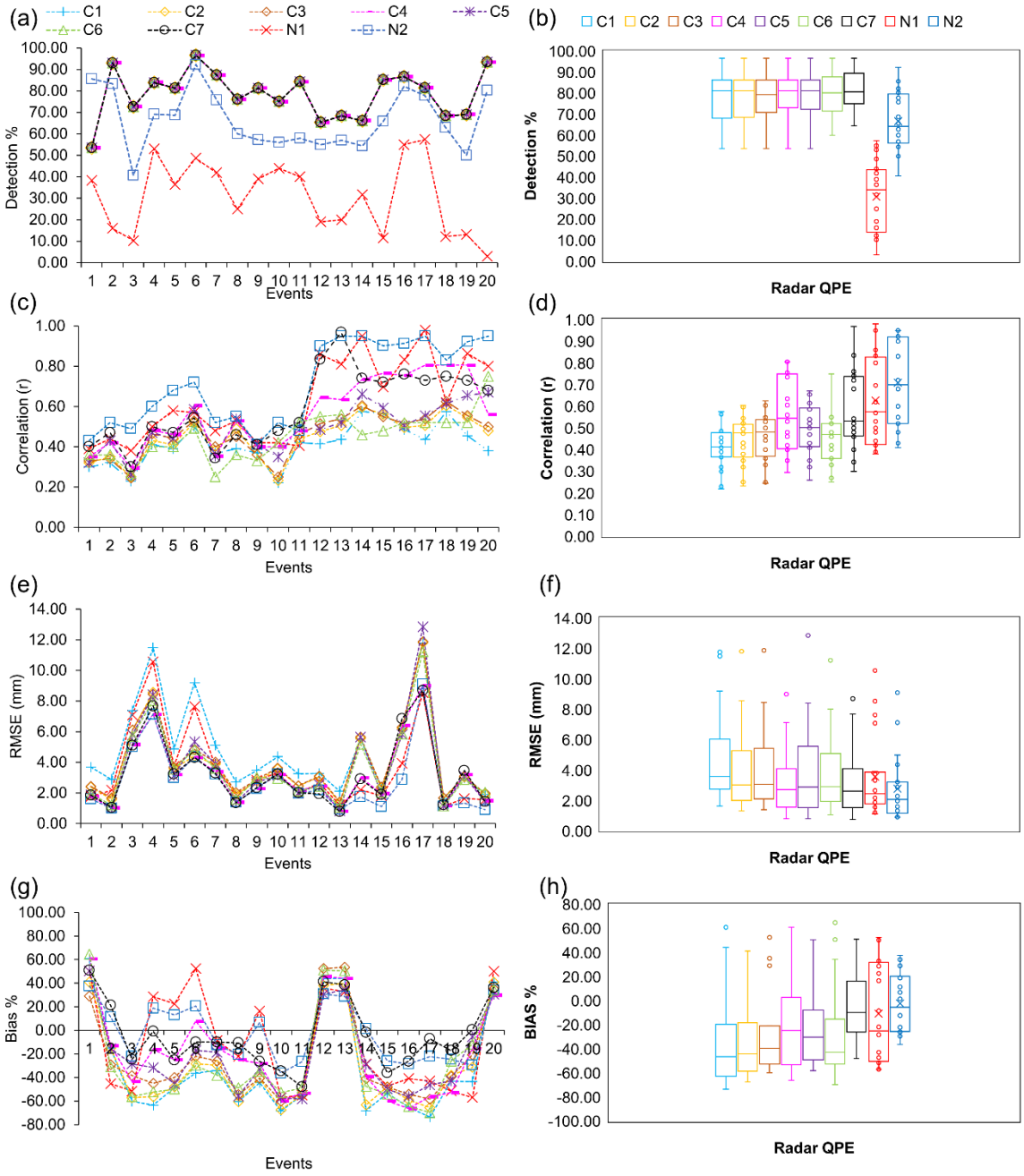

Figure 3-3 *Average detection (a & b), correlation (c & d), RMSE (e & f), and bias (g & h) between hourly accumulation of radar QPEs and gauge measurements for each event*

Figure 3-4-a shows the radar QPE detection for each station across the basin. For all radar QPEs, the detection is reasonably constant across the basin. As shown in the box

plots in Figure 3-4-b, WKR C-band radar detects all events effectively with low IQR. The detection ranges from 65 to 85 % for all WKR C-band radar QPEs at each TRCA rain gauge station. The C7 shows the best average detection of 81.55 % among all the radar QPEs along with the least reported IQR in figure 3-4-b. NEXRAD S-band radar detection is relatively small compared to WKR C-band radar. N2 detection (56.24 – 68.15 %) is better than N1 (20.31 – 27.37 %). As mentioned before, the detection is affected by the distance to the radar station from the gauge stations. N2 is competitive with WKR C-band radar, whereas N1 shows relatively low detection.

Figure 3-4-c shows the correlation between the hourly accumulations of radar-gauge pairs for each station across the basin. The average correlation for radar QPEs from KBUF NEXRAD (0.34 – 0.60) is greater to all C-band radar QPEs (0.20 – 0.52). The reported average correlation for N2 of 0.54 is superior to N1 (0.44). The WKR C-band, C7, and C4 are also competitive with NEXRAD radar QPEs with relatively good reported correlations of 0.42 and 0.40, respectively. Contrasting to events, there is no dramatic variability in correlation for each station across the two watersheds. As shown in Figure 3-4-d, the correlation does not significantly vary from station to station. Reported IQRs for those QPEs are relatively lower, implying that at all stations, all radar QPEs perform equally well.

As shown in Figure 3-4-e, the average RMSE between the hourly accumulations of radar-gauge pairs at each gauge stations across the two watersheds approximately ranges from 2.5 – 4.6 mm and 2.8 – 4.4 mm for WKR C-band and KBUF NEXRAD S-band, respectively. Error-values are reasonably constant across the basin, and the RMSE

follows the same trend as the correlation. The least average error of 2.5 mm is reported for radar QPE using C7, followed by N2 (2.6 mm). Since spatial distribution of correlation and errors is constant across the two watersheds, so they can be used as gridded precipitation input for hydrologic models, especially for semi- and fully distributed hydrologic models. On the other hand, relatively high IQR values of reported RMSEs for all radar QPEs (Figure 3-4-f) indicate that errors associated with different events at the same station are considerably different.

Figure 3-4-g and 3-4-h show the distribution of bias values and boxplots over the stations for each radar's QPEs. As shown in Figure 3-4-g, all radar QPEs are less than the gauge precipitation except for N2. The bias is fluctuating around the zero line for N2. The underestimation is relatively less for N1(-15.17 to -63.10), C7 (-37.76 to -1.41), and C4 (-4.02 to -39.47). The reported bias is relatively high for the rest of the C-band (C1, C2, C3, C5, and C6) radar QPEs. Therefore, a correction is necessary before using them as precipitation input for hydrological models. Even though bias values are high, they are consistent with relatively low IQR (Figure 3-4-h), especially for C1, C2, and C3. The constant bias can be addressed and adjusted during the calibration of hydrological models by incorporating a bias constraint into the objective function (Chiew et al. 2009; Madsen et al. 2002; Viney et al. 2009).

Overall, there is no dramatic variability amongst matrices across the two watersheds. The reasonably similar matrices across the two watersheds can be attributed to the similar characteristics shared by the two watersheds. A relatively high-density gauge network (one gauge per ~75 km^2 in Humber River and one gauge per ~116 km^2 in

the Don River) with a uniform distribution of gauges across the two basins helps to capture the spatial distribution of rainfall adequately. Also, all gauges are located within ~40 km radius range of WKR Canadian C-band radar station and ~ 106 km KBUF NEXRAD S-band radar station. Therefore, the effect of distance (range) from the radar towers to the gauges nearly the same for both watersheds. Hence, the effect of range to radar QPEs is minimal and nearly the same throughout both the two watersheds. As can be seen in Figure 3-1, the elevation in most of the area is relatively similar and, thus, no high barriers that hinder the radar signals affecting radar reflectivities and, subsequently, the radar QPEs. The C-band radar station is located in an elevated area and therefore provides better coverage for both watersheds. As the region seen by the both WKR C-band and NEXRAD S-band radar shares similar characteristics, the observed constant errors and correlations between gauges and radar QPEs is reasonable.

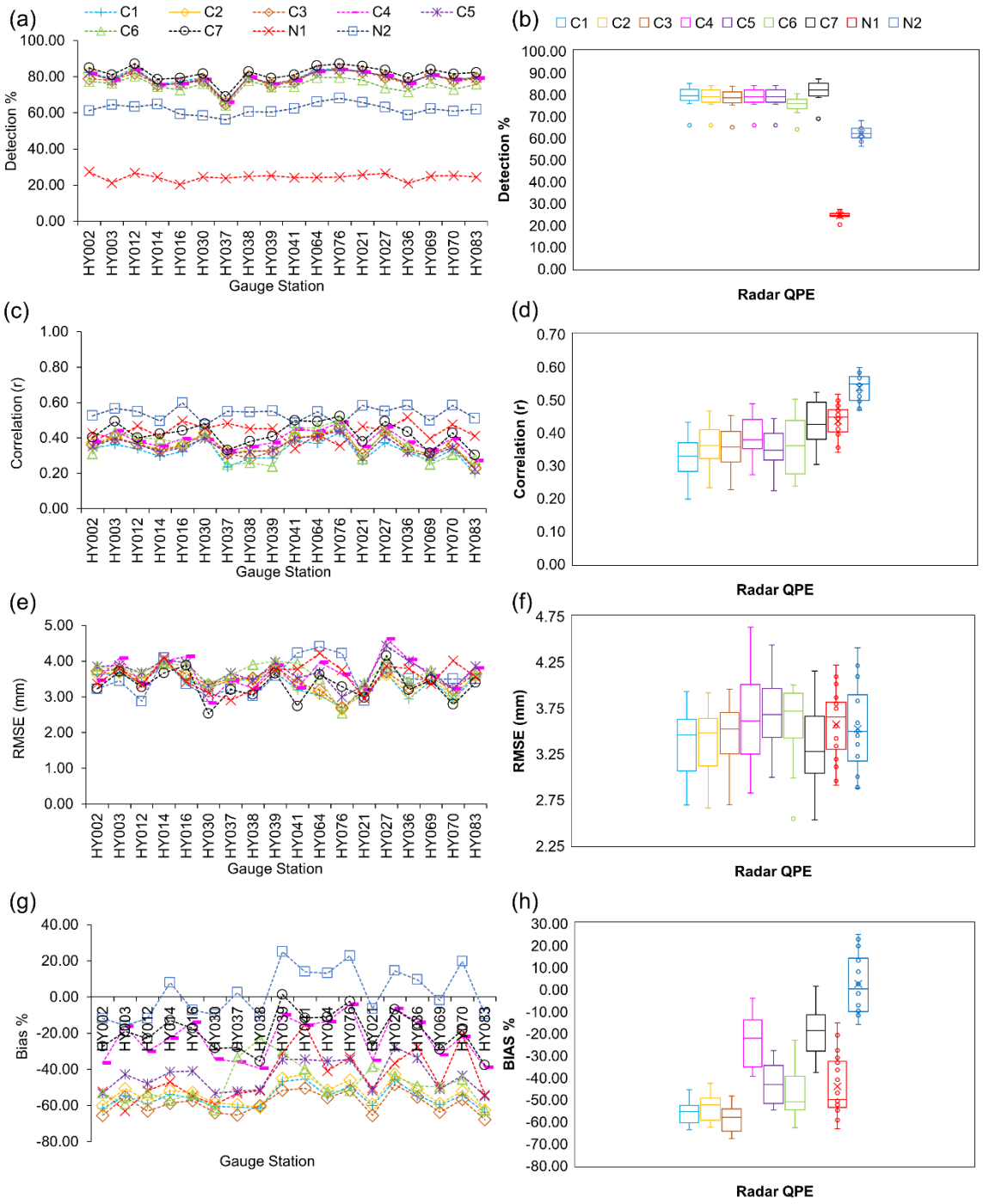

Figure 3-4 *Average detection (a & b), correlation (c & d), RMSE (e & f), and bias (g & h) between hourly accumulation of radar QPEs and gauge measurements for each TRCA gauge station*

To further assess the radar QPE performances, scatter plots between the hourly accumulations of radar (R) -gauge (G) pairs for all events (i.e., for the 297 h) for each radar QPE are shown in Figure 3-5. The solid line in the figure represents the one-to-one line. The dotted lines in the figure represent the least absolute deviation fits for the form of $R = aG + b$ for the hourly radar-gauge pairs for all events. The R (Z), R (Z, K_{DP}), R (Z, Z_{DR}), and R (K_{DP}, Z_{DR}) radar QPEs with and without attenuation correction of WKR C-band radar and KBUF NEXRAD S-band radar are shown in figure 3-5. For all radar QPEs, the best fit line is well below one, except for the C7 and N2. The average correlation coefficient reported for the C7 and N2 is 0.60 and 0.71, respectively. Average RMSE reported as 3.2 mm and 2.8 mm for C7 and N2, respectively. Data are also more clustered along the one-to-one line, and C7 and N2 radar QPEs generally perform well compared to the gauge observation. Those two radar QPEs perform reasonably well for most of the accumulations except for underestimation at lower accumulation amounts. Both C7 and N2 perform reasonably well for higher accumulation amounts. All other QPEs show some inconsistencies at the medium and higher accumulations. The scatterplots also show that the results are more dispersed from the one-to-one line with the increasing accumulations for all the radar QPEs. In general, the C7 and the N2 show better agreement with the gauges for all accumulation amounts.

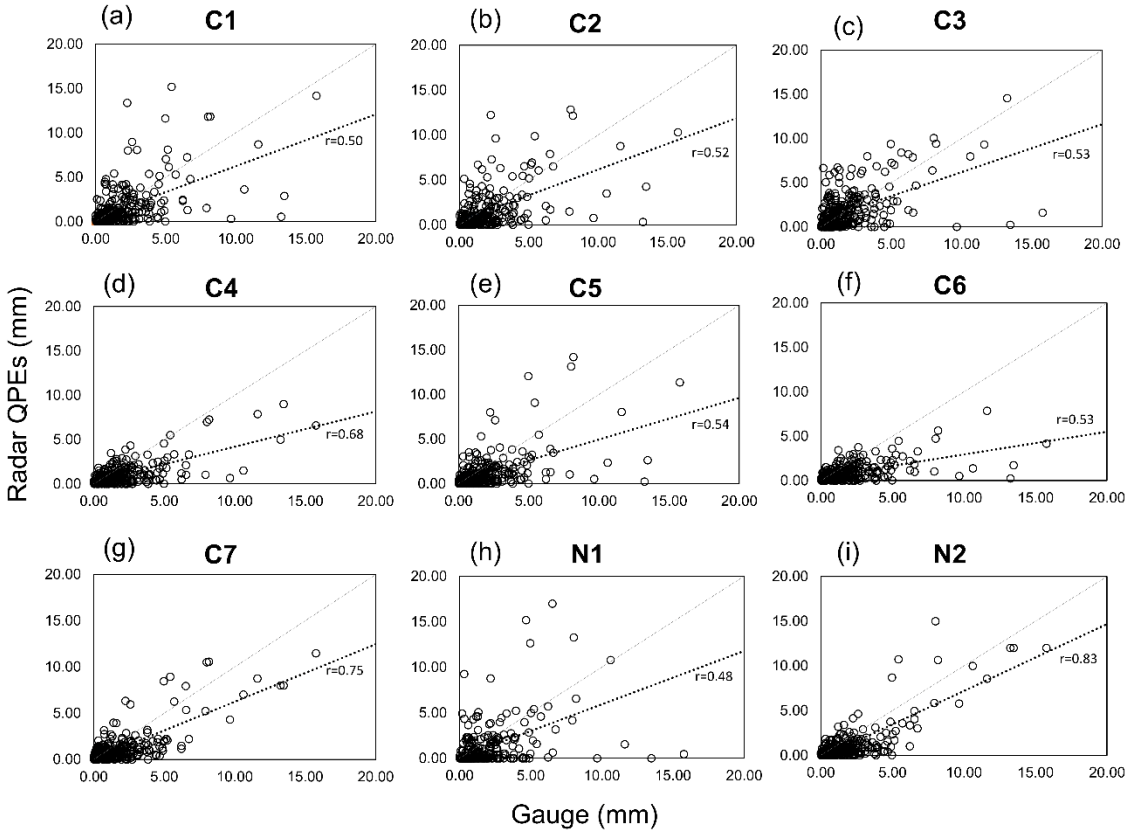

Figure 3-5 *Scatterplots of hourly accumulations of radar estimated QPEs against the gauge for the radar QPE estimators listed in table 3-1*

Hourly accumulation of precipitation values is summed for each radar QPE and each event to produce radar totals (R_T) to compare with gauge totals (G_T). A scatterplot of the gauge totals against radar totals is shown in Figure 3-6. The solid line in the figure represents the least absolute deviation fits for the form of $R_T = aG_T + b$ for the 20 event totals. The dashed line is the one-to-one line. In contrast to the high degree of scattering between radar QPEs and gauge reported precipitation for hourly data (Figure 3-5), the event totals graphed in Figure 3-6 show a definite linear relationship, but less scatter in the longer-term radar estimates. The spread between all radar QPEs and gauge

observations decreases with more extended temporal accumulation. For example, the correlation coefficient increases from hourly to event total of 0.63 to 0.76 for N2. Reduction in the spatial variability of the rainfall field due to time averaging minimizes the inconsistencies in radar and gauge sampling areas.

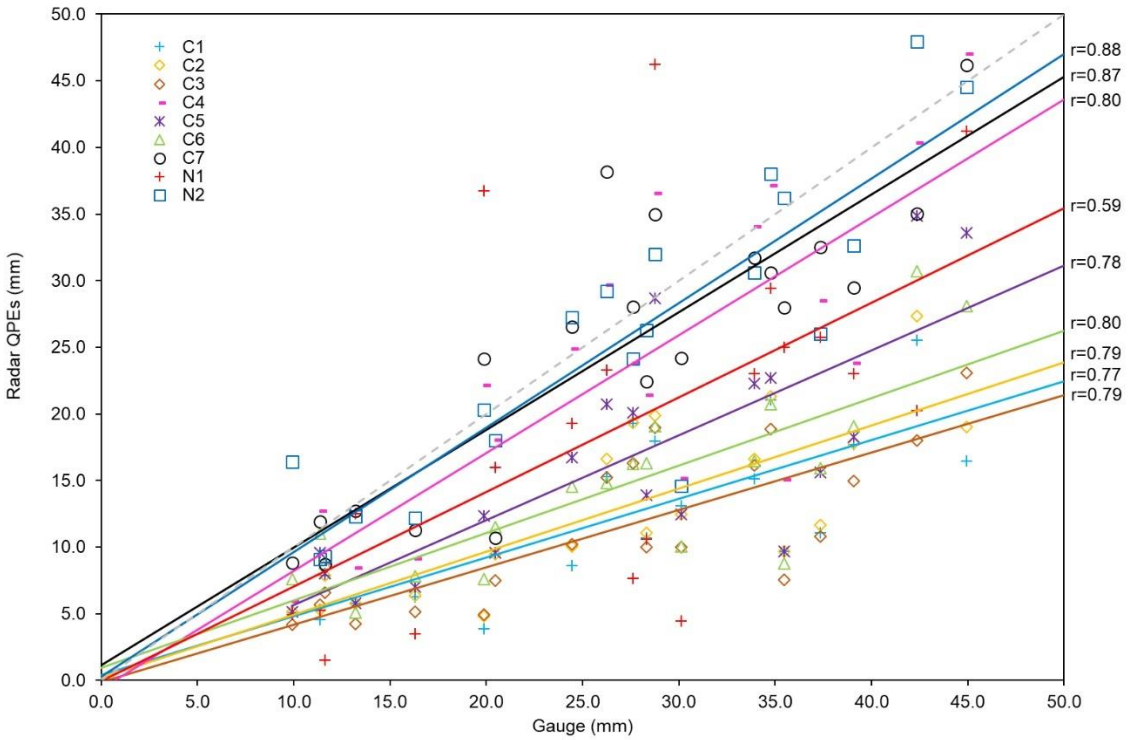

Figure 3-6 *Scatterplots of radar estimated totals against the gauge totals for 20 events.*

The radar-gauge ratios are calculated for the hourly rainfall accumulations estimated by each rain-rate algorithms for the 297 h of analysis (i.e., all events) and plotted (Figure 3-7) as a function of the gauge hourly accumulations to illustrate the relative strengths of each algorithm at high and low rain rates. The ratio of one indicates unbiased radar estimates. For hourly accumulations, the ratios are much less or higher than one for all radar QPEs for lower precipitation amounts ranging from 1 to 5 mm.

However, the ratio has become progressively better with higher precipitation amounts, especially for C7 and N2. Both C7 and N2 have ratios much closer to one for high hourly gauge accumulation amounts from 10 to 15 mm.

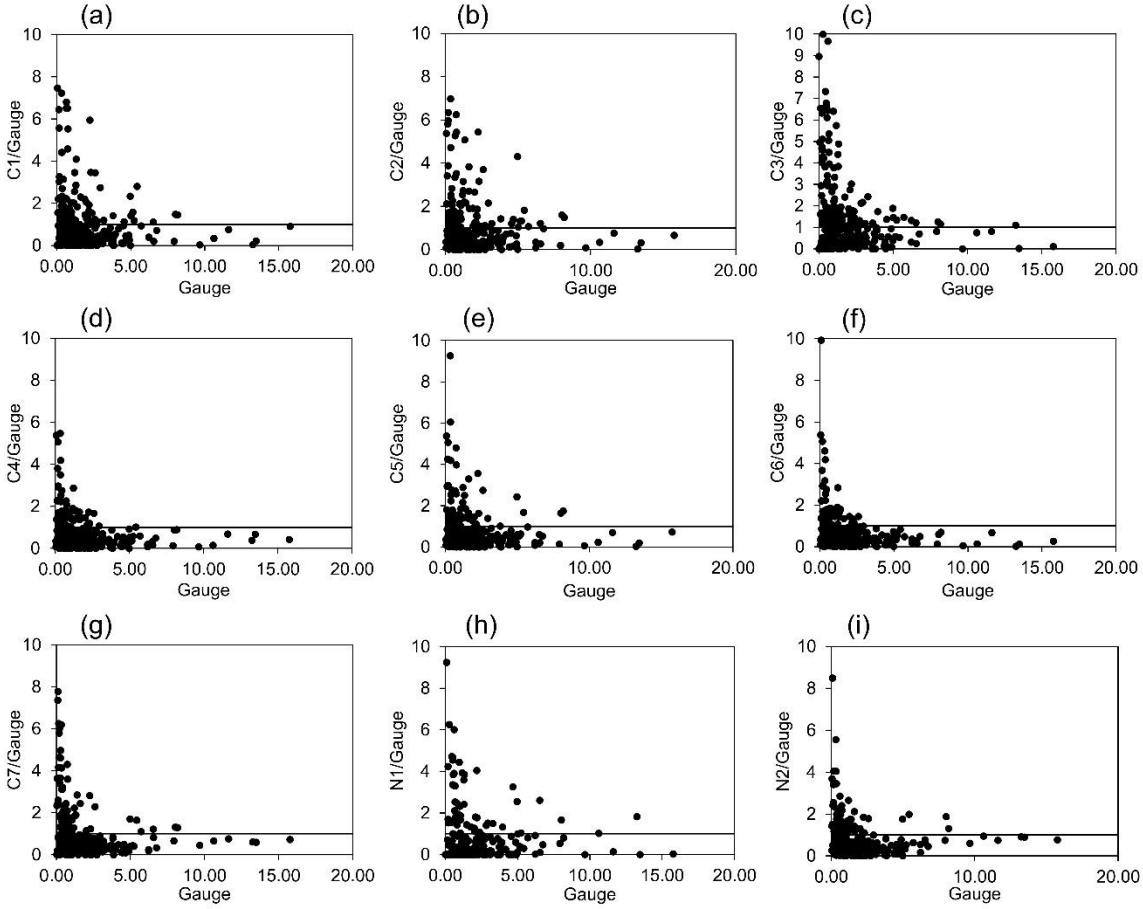

Figure 3-7 *Ratios of radar-gauge hourly accumulations as a function of the hourly gauge accumulations for the radar QPE estimators listed in table 3-1*

For further analysis, Taylor diagrams are drawn to select the best performing radar QPE based on three statistical parameters; standard deviation, correlation coefficient, and centered root mean square error for both hourly accumulations for 297 h (Figure 3-8-a) and total event accumulations (Figure 3-8-b). Comparable to the results discussed above,

the N2, C7, and C4 QPEs perform comparatively well as they are plotted closest to the black arc as well as the point observation ('OBS' in the figure).

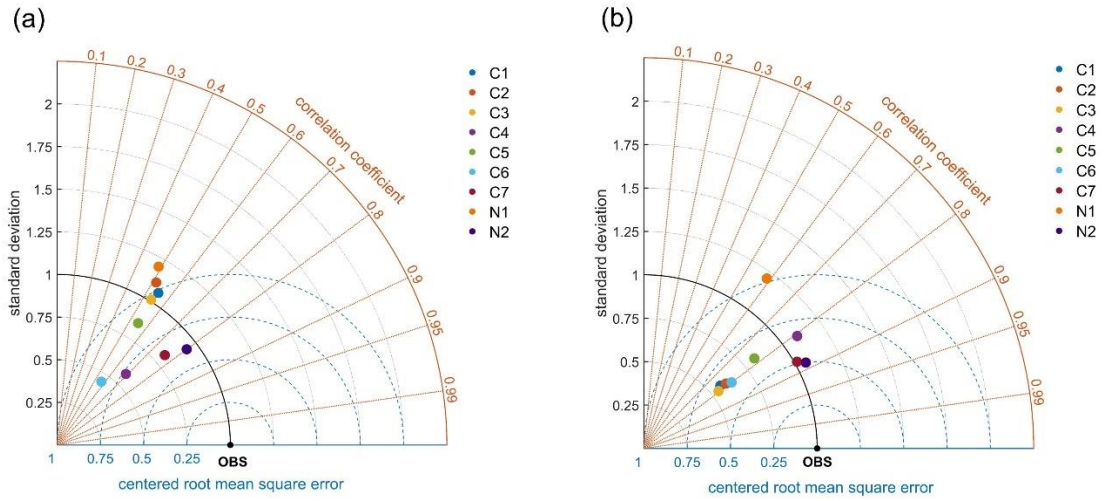

Figure 3-8 *Taylor diagrams showing a statistical assessment of radar estimated QPEs listed in table 3-1 for hourly accumulations for 297 h (a) and total event accumulations (b). (Note: Diagram summarizes three statistical performances (standard deviation, correlation coefficient, and centered root mean square error) for each radar QPE. Different colors denote different radar QPEs. The best radar QPE plots itself closer to the black arc as well as the point 'OBS', which represents agreement with gauge observations)*

3.6. Conclusions

In this study, radar-derived QPEs from rain-rate relationships using Z, Z_{DR}, and K_{DP} from WKR C-band radar at King City, ON, Canada, and the QPEs from NEXRAD S-band radar at Buffalo, New York, USA, are evaluated against rain gauge data for two watersheds in the GTA of Ontario, Canada: Humber River (semi-urban) and Don River (urban) watersheds. The objective is to assess the reliability and accuracy of WKR and

NEXRAD radar QPEs as precipitation input of hydrological models for hydrometeorological applications.

Relatively high percent detection, high correlation, low RMSE, and small percent bias suggest that the KBUF NEXRAD radar QPEs can be effectively used as supplementary precipitation forcing for hydrological models in Canadian watersheds that are covered by the US radar. The WKR radar QPEs utilizing a multi-parameter rain rate estimator using K_{DP} and Z_{DR} performs equally as KBUF NEXRAD radar QPEs. Due to the high temporal resolution, a long-term data archive, and good percent detection of WKR radar QPEs, it is possible to generate a continuous time series with less number of missing data that is often required as meteorological input for hydrological models. Therefore, WKR radar QPEs with dual-polarization algorithms can also effectively be used as precipitation input of the hydrological model for hydrometeorological applications. Because of the closeness of the watershed to the WKR radar station, it may be preferable. Spatial variations in all verification matrices are reasonably constant across the basins and, hence, can be used as a gridded precipitation input of distributed hydrological models.

Among nine radar QPEs used in this evaluation, NEXRAD Level III (DPA), WKR multi-parameter rain rate estimator using K_{DP} and Z_{DR}, and combined Z and K_{DP} algorithm are chosen for further studies. Since verification matrices are not optimum for both WKR radar and KBUF NEXRAD radar QPEs, bias correction is necessary before using selected radar QPEs as a precipitation input to hydrological models. In the future, this evaluation will be followed by proxy validation with the event-based hydrological

model run using semi-distributed and distributed hydrological models to further verify the accuracy and reliability of the radar QPE as precipitation input of hydrological models for hydrometeorological applications.

3.7. Acknowledgments

This work was funded by the Natural Science and Engineering Research Council (NSERC) Canadian FloodNet (NETGP 451456). The task for this manuscript was performed while the first author, Dayal Buddika Wijayarathne, was an intern graduate student at Observations-Based Research Section, ECCC. Hourly rain gauge measurements were collected from Toronto and Region Conservation Authority (TRCA; https://trca.ca/). The KBUF NEXRAD S-band radar QPEs were downloaded from the NOAA National Centers for Environmental Information website: https://www.ncdc.noaa.gov/has/HAS.FileAppRouter?datasetname=7000&subqueryby=STATION&applname=&outdest=FILE. The open-source software tool kit NOAA's WCT downloaded from the website: https://www.ncdc.noaa.gov/wct/ was used to process NEXRAD radar QPEs. The authors would like to thank Mr. Andre D.L. Zanchetta for his help in downloading and preprocessing NEXRAD data. The authors declare no conflict of interest.

3.8. References

Austin, P. M., and A. C. Bemis, 1950: A quantitative study of the "bright band" in radar precipitation echoes. *Journal of Meteorology*, **7**, 145–151. https://doi.org/10.1175/1520-0469(1950)007<0145:AQSOTB>2.0.CO;2.

Ayat, H., M. R. Kavianpour, S. Moazami, Y. Hong, and E. Ghaemi, 2018: Calibration of weather radar using region probability matching method (RPMM). *Theoretical and Applied Climatology*, **134**, 165–176. https://doi.org/10.1007/s00704-017-2266-7.

Aydin, K., V. N. Bringi, and L. Liu, 1995: Rain-rate estimation in the presence of hail using S-band specific differential phase and other radar parameters. *Journal of Applied Meteorology*, **34**, 404–410. https://doi.org/10.1175/1520-0450-34.2.404.

Balica, S. F., I. Popescu, L. Beevers, and N. G. Wright, 2013: Parametric and physically based modelling techniques for flood risk and vulnerability assessment: a comparison. *Environmental modelling & software*, **41**, 84–92. https://doi.org/10.1016/j.envsoft.2012.11.002.

Barge, B. L., R. G. Humphries, S. J. Mah, and W. K. Kuhnke, 1979: Rainfall measurements by weather radar: applications to hydrology. *Water Resources Research*, **15**, 1380–1386. https://doi.org/10.1029/WR015i006p01380.

Beneti, C., R. V. Calheiros, M. Sorribas, L. Calvetti, C. Oliveira, N. Rozin, and J. Ruviaro, 2019: Operational Hydrological Modelling of Small Watershed using QPE from Dual-Pol Radar in Brazil. https://doi.org/10.20944/preprints201906.0026.v1.

Berkowitz, D. S., J. A. Schultz, S. Vasiloff, K. L. Elmore, C. D. Payne, and J. B. Boettcher, 2013: Status of dual pol QPE in the WSR-88D network. 27th Conf. on Hydrology, Austin, TX. *Amer. Meteor. Soc*, **2**.

Boluwade, A., K.-Y. Zhao, T. A. Stadnyk, and P. Rasmussen, 2017: Towards Validation of the Canadian Precipitation Analysis (CaPA) for Hydrologic Modeling Applications in the Canadian Prairies. *Journal of Hydrology*, **556**, 1244-1255, https://doi.org/10.1016/j.jhydrol.2017.05.059.

Boodoo, S., D. Hudak, A. Ryzhkov, P. Zhang, N. Donaldson, D. Sills, and J. Reid, 2015: Quantitative precipitation estimation from a C-band dual-polarized radar for the 8 July 2013 flood in Toronto, Canada. *Journal of Hydrometeorology*, **16**, 2027–2044. https://doi.org/10.1175/JHM-D-15-0003.1.

Borga, M., F. Tonelli, R. J. Moore, and H. Andrieu, 2002: Long-term assessment of bias adjustment in radar rainfall estimation. *Water Resources Research*, **38**, 8–1. https://doi.org/10.1029/2001WR000555.

Bowering, E. A., A. M. Peck, and S. P. Simonovic, 2014: A flood risk assessment to municipal infrastructure due to changing climate part I: methodology. *Urban Water Journal*, **11**, 20–30. https://doi.org/10.1080/1573062X.2012.758293.

Brandes, E. A., A. V. Ryzhkov, and D. S. Zrnić, 2001: An evaluation of radar rainfall estimates from specific differential phase. *Journal of Atmospheric and Oceanic Technology*, **18**, 363–375. https://doi.org/10.1175/1520-0426(2001)018<0363:AEORRE>2.0.CO;2.

——, G. Zhang, and J. Vivekanandan, 2002: Experiments in rainfall estimation with a polarimetric radar in a subtropical environment. *Journal of Applied Meteorology*, **41**, 674–685. https://doi.org/10.1175/1520-0450(2002)041<0674:EIREWA>2.0.CO;2.

Bringi, V. N., M. A. Rico-Ramirez, and M. Thurai, 2011: Rainfall estimation with an operational polarimetric C-band radar in the United Kingdom: comparison with a gauge network and error analysis. *Journal of Hydrometeorology*, **12**, 935–954. https://doi.org/10.1175/JHM-D-10-05013.1.

Chandrasekar, V., R. Keränen, S. Lim, and D. Moisseev, 2013: Recent advances in classification of observations from dual polarization weather radars. *Atmospheric Research*, **119**, 97–111. https://doi.org/10.1016/j.atmosres.2011.08.014.

Chen, D., and A. Farrar, 2007: Evaluation of NARAD Precipitation Data for Rainfall Monitoring in Eastern Ontario, Canada. *Geomatics Solutions for Disaster Management*, 103–116. https://doi.org/10.1007/978-3-540-72108-6_8.

Chiew, F. H. S., J. Teng, J. Vaze, D. A. Post, J. M. Perraud, D. G. C. Kirono, and N. R. Viney, 2009: Estimating climate change impact on runoff across southeast

Australia: Method, results, and implications of the modeling method. *Water Resources Research*, **45**. https://doi.org/10.1029/2008WR007338.

Cloke, H. L., and F. Pappenberger, 2009: Ensemble flood forecasting: a review. *Journal of Hydrology*, **375**, 613–626. https://doi.org/10.1016/j.jhydrol.2009.06.005.

Crozier, C. L., P. I. Joe, J. W. Scott, H. N. Herscovitch, and T. R. Nichols, 1991: The king city operational doppler radar: Development, all-season applications and forecasting. *Atmosphere-Ocean*, **29**, 479–516. https://doi.org/10.1080/07055900.1991.9649414.

Dai, Q., Q. Yang, J. Zhang, and S. Zhang, 2018: Impact of Gauge Representative Error on a Radar Rainfall Uncertainty Model. *Journal of Applied Meteorology and Climatology*, **57**, 2769–2787. https://doi.org/10.1175/JAMC-D-17-0272.1.

Dalezios, N. R., 1988: Objective rainfall evaluation in radar hydrology. *Journal of Water Resources Planning and Management*, **114**, 531–546. https://doi.org/10.1061/(ASCE)0733-9496(1988)114:5(531).

Damant, C., G. L. Austin, A. Bellon, M. Osseyrane, and N. Nguyen, 1983: Radar rain forecasting for wastewater control. *Journal of Hydraulic Engineering*, **109**, 293–297. https://doi.org/10.1061/(ASCE)0733-9429(1983)109:2(293).

Dhiram, K., and Z. Wang, 2016: Evaluation on Radar Reflectivity-Rainfall Rate (ZR) Relationships for Guyana. *Sciences*, **6**, 489–499. https://doi.org/10.4236/acs.2016.64039.

Diakakis, M., G. Deligiannakis, A. Pallikarakis, and M. Skordoulis, 2016: Factors controlling the spatial distribution of flash flooding in the complex environment of a metropolitan urban area. The case of Athens 2013 flash flood event. *International journal of disaster risk reduction*, **18**, 171–180. https://doi.org/10.1016/j.ijdrr.2016.06.010.

Douglas, R. H., 1990: The stormy weather group (Canada). *Radar in Meteorology*, Springer, 61–68. https://doi.org/10.1007/978-1-935704-15-7_8.

Duchon, C. E., and G. R. Essenberg, 2001: Comparative rainfall observations from pit and aboveground rain gauges with and without wind shields. *Water Resources Research*, **37**, 3253–3263. https://doi.org/10.1029/2001WR000541.

Dufton, D. R. L., 2016: Quantifying uncertainty in radar rainfall estimates using an X-band dual polarisation weather radar. University of Leeds, 229 pp.

Einfalt, T., K. Arnbjerg-Nielsen, C. Golz, N.-E. Jensen, M. Quirmbach, G. Vaes, and B. Vieux, 2004: Towards a roadmap for use of radar rainfall data in urban drainage. *Journal of Hydrology*, **299**, 186–202. https://doi.org/10.1016/j.jhydrol.2004.08.004.

Fabry, F., and I. Zawadzki, 1995: Long-term radar observations of the melting layer of precipitation and their interpretation. *Journal of the atmospheric sciences*, 52, 838–851. https://doi.org/10.1175/1520-0469(1995)052<0838:LTROOT>2.0.CO;2.

Fassnacht, S. R., 2003: Radar precipitation for winter hydrological. Weather Radar Information and Distributed Hydrological Modelling: *Proceedings of an International Symposium (Symposium HS03) Held During IUGG 2003, the XXIII General Assembly of the International Union of Geodesy and Geophysics: at Sapporo, Japan, from 30 June to 11 July, 2003, International Assn of Hydrological Sciences, 35.*

Fortin, V., G. Roy, N. Donaldson, and A. Mahidjiba, 2015: Assimilation of radar quantitative precipitation estimations in the Canadian Precipitation Analysis (CaPA). *Journal of Hydrology*, **531**, 296–307. https://doi.org/10.1016/j.jhydrol.2015.08.003.

Fulton, R. A., J. P. Breidenbach, D.-J. Seo, D. A. Miller, and T. O'Bannon, 1998: The WSR-88D rainfall algorithm. *Weather and Forecasting*, **13**, 377–395. https://doi.org/10.1175/1520-0434(1998)013<0377:TWRA>2.0.CO;2.

Germann, U., 1999: Radome attenuation—a serious limiting factor for quantitative radar measurements? *Meteorologische Zeitschrift*, 85–90. https://doi.org/10.1127/metz/8/1999/85.

Grayman, W. M., and P. S. Eagleson, 1971: Evaluation of radar and raingage systems for flood forecasting. Ralph M. Parsons Lab, Dep. Civ. Eng, Mass. Inst. Technol, Cambridge, Mass, Tech. Rep. No. 138.

Guzman, J. A., D. N. Moriasi, M. L. Chu, P. J. Starks, J. L. Steiner, and P. H. Gowda, 2013: A tool for mapping and spatio-temporal analysis of hydrological data. *Environmental modelling & software*, **48**, 163–170. https://doi.org/10.1016/j.envsoft.2013.06.014.

Hall, W., M. A. Rico-Ramirez, and S. Krämer, 2015: Classification and correction of the bright band using an operational C-band polarimetric radar. *Journal of Hydrology*, **531**, 248–258. https://doi.org/10.1016/j.jhydrol.2015.06.011.

Han, S., and P. Coulibaly, 2017: Bayesian Flood Forecasting Methods: A Review. *Journal of Hydrology*, **551**, 340-351. https://doi.org/10.1016/j.jhydrol.2017.06.004.

Hapuarachchi, H. A. P., Q. J. Wang, and T. C. Pagano, 2011: A review of advances in flash flood forecasting. *Hydrological processes*, **25**, 2771–2784. https://doi.org/10.1002/hyp.8040.

Hubbert, J. C., M. Dixon, S. M. Ellis, and G. Meymaris, 2009: Weather radar ground clutter. Part I: Identification, modeling, and simulation. *Journal of Atmospheric and Oceanic Technology*, **26**, 1165–1180. https://doi.org/10.1175/2009JTECHA1159.1.

Jentsch, A., J. Kreyling, and C. Beierkuhnlein, 2007: A new generation of climate-change experiments: events, not trends. *Frontiers in Ecology and the Environment*, **5**, 365–374. https://doi.org/10.1890/1540-9295(2007)5[365:ANGOCE]2.0.CO;2.

Joe, P., and S. Lapczak, 2002: Evolution of the Canadian operational radar network. *ERAD, Nov., Delft, EMS, Netherlands*, 26 pp.

Kalinga, O. A., and T. Y. Gan, 2006: Semi-distributed modelling of basin hydrology with radar and gauged precipitation. *Hydrological processes*, **20**, 3725–3746. https://doi.org/10.1002/hyp.6385.

Khan, S. I., Z. Flamig, and Y. Hong, 2019: Flood Monitoring System Using Distributed Hydrologic Modeling for Indus River Basin. *Indus River Basin*, Elsevier, 335–355. https://doi.org/10.1016/B978-0-12-812782-7.00015-1.

Krajewski, W. F., and Coauthors, 2010a: Towards better utilization of NEXRAD data in hydrology: An overview of Hydro-NEXRAD. *Journal of hydroinformatics*, **13**, 255–266. https://doi.org/10.2166/hydro.2010.056.

——, G. Villarini, and J. A. Smith, 2010b: Radar-rainfall uncertainties: Where are we after thirty years of effort? *Bulletin of the American Meteorological Society*, **91**, 87–94. https://doi.org/10.1175/2009BAMS2747.1.

——, and Coauthors, 2017: Real-time flood forecasting and information system for the state of Iowa. *Bulletin of the American Meteorological Society*, **98**, 539–554. https://doi.org/10.1175/BAMS-D-15-00243.1.

Lack, S. A., and N. I. Fox, 2007: An examination of the effect of wind-drift on radar-derived surface rainfall estimations. *Atmospheric research*, **85**, 217–229. https://doi.org/10.1016/j.atmosres.2006.09.010.

Madsen, H., G. Wilson, and H. C. Ammentorp, 2002: Comparison of different automated strategies for calibration of rainfall-runoff models. *Journal of Hydrology*, **261**, 48–59. https://doi.org/10.1016/S0022-1694(01)00619-9.

Maki, M., S.-G. Park, and V. N. Bringi, 2005: Effect of natural variations in rain drop size distributions on rain rate estimators of 3 cm wavelength polarimetric radar. *Journal of the Meteorological Society of Japan. Ser. II*, **83**, 871–893. https://doi.org/10.2151/jmsj.83.871.

Marshall, J. S., and W. M. K. Palmer, 1948: The distribution of raindrops with size. *Journal of meteorology*, **5**, 165–166. https://doi.org/10.1175/1520-0469(1948)005x003C;0165:tdorwsx0003e;2.0.co;2.

Marx, A., H. Kunstmann, A. Bárdossy, and J. Seltmann, 2006: Radar rainfall estimates in an alpine environment using inverse hydrological modelling. *Advances in Geosciences*, **9**, 25–29. https://doi.org/10.5194/adgeo-9-25-2006.

Mazzarella, V., I. Maiello, R. Ferretti, V. Capozzi, E. Picciotti, P. P. Alberoni, F. S. Marzano, and G. Budillon, 2020: Reflectivity and velocity radar data assimilation for two flash flood events in central Italy: A comparison between 3D and 4D variational methods. Quarterly *Journal of the Royal Meteorological Society,* 146, 348–366.

McKee, J. L., and A. D. Binns, 2016: A review of gauge–radar merging methods for quantitative precipitation estimation in hydrology. *Canadian Water Resources Journal/Revue canadienne des ressources hydriques*, **41**, 186–203. https://doi.org/10.1080/07011784.2015.1064786.

Meischner, P., 2005: *Weather radar: principles and advanced applications*. Springer Science & Business Media, 315 pp.

Mekis, E., N. Donaldson, J. Reid, A. Zucconi, J. Hoover, Q. Li, R. Nitu, and S. Melo, 2018: An overview of surface-based precipitation observations at Environment and Climate Change Canada. *Atmosphere-Ocean*, **56**, 71–95. https://doi.org/10.1080/07055900.2018.1433627.

Mekonnen, G. B., S. Matula, F. Doležal, and J. Fišák, 2015: Adjustment to rainfall measurement undercatch with a tipping-bucket rain gauge using ground-level manual gauges. *Meteorology and Atmospheric Physics*, **127**, 241–256. https://doi.org/10.1007/s00703-014-0355-z.

Moore, R. J., A. E. Jones, D. A. Jones, K. B. Black, and V. A. Bell, 2004: Weather radar for flood forecasting: some UK experiences. *Sixth International Symposium on Hydrological Applications of Weather Radar*, Citeseer, 2–4.

Moradkhani, H., and S. Sorooshian, 2008: General review of rainfall-runoff modeling: model calibration, data assimilation, and uncertainty analysis. *Hydrological modelling and the water cycle*, 1–24. https://doi.org/10.1007/978-3-540-77843-1_1.

Natural Resources Canada, 2009: GeoBase - Land Cover, circa 2000-Vector (LCC2000-V), Accessed 26 November 2019, https://atlas.gc.ca/lcct/en/index.html.

Nerini, D., Z. Zulkafli, L.P. Wang, C. Onof, W. Buytaert, W. Lavado-Casimiro, and J.L. Guyot, 2015: A comparative analysis of TRMM–rain gauge data merging techniques at the daily time scale for distributed rainfall–runoff modeling applications. *Journal of Hydrometeorology*, **16**, 2153–2168. https://doi.org/10.1175/JHM-D-14-0197.1.

NOAA, 2018: National Climatic Data Center (NCDC), Accessed 01 June 2019, https://www.ncdc.noaa.gov/has/HAS.FileAppRouter?datasetname=7000&subqueryby=STATION&applname=&outdest=FILE.

Pachauri, R. K., and Coauthors, 2014: *Climate change 2014: synthesis report. Contribution of Working Groups I, II and III to the fifth assessment report of the Intergovernmental Panel on Climate Change*. IPCC, 168 pp.

Park, S. G., V. N. Bringi, V. Chandrasekar, M. Maki, and K. Iwanami, 2005: Correction of radar reflectivity and differential reflectivity for rain attenuation at X band. Part I: Theoretical and empirical basis. *Journal of Atmospheric and Oceanic Technology*, **22**, 1621–1632. https://doi.org/10.1175/JTECH1803.1.

PC, S., M. Maki, S. Shimizu, T. Maesaka, D.-S. Kim, D.-I. Lee, and H. Iida, 2013: Correction of reflectivity in the presence of partial beam blockage over a mountainous region using X-band dual polarization radar. *Journal of Hydrometeorology*, **14**, 744–764. https://doi.org/10.1175/JHM-D-12-077.1.

Prat, O. P., and B. R. Nelson, 2014: Evaluation of precipitation estimates over CONUS derived from satellite, radar, and rain gauge datasets (2002-2012). *HESSD*, **11**, 11489–11531. https://doi.org/10.5194/hessd-11-11489-2014.

Price, K., S. T. Purucker, S. R. Kraemer, J. E. Babendreier, and C. D. Knightes, 2014: Comparison of radar and gauge precipitation data in watershed models across varying spatial and temporal scales. *Hydrological Processes*, **28**, 3505–3520. https://doi.org/10.1002/hyp.9890.

Public Safety Canada, 2019: The Canadian Disaster Database, Accessed 13 May 2020, https://www.publicsafety.gc.ca/cnt/rsrcs/cndn-dsstr-dtbs/index-en.aspx.

Rabiei, E., and U. Haberlandt, 2015: Applying bias correction for merging rain gauge and radar data. *Journal of Hydrology*, **522**, 544–557. https://doi.org/10.1016/j.jhydrol.2015.01.020.

Ran, Q., W. Fu, Y. Liu, T. Li, K. Shi, and B. Sivakumar, 2018: Evaluation of Quantitative Precipitation Predictions by ECMWF, CMA, and UKMO for Flood Forecasting: Application to Two Basins in China. *Natural Hazards Review*, **19**, 05018003. https://doi.org/10.1061/(ASCE)NH.1527-6996.0000282.

Reggiani, P., and A. H. Weerts, 2008: A Bayesian approach to decision-making under uncertainty: An application to real-time forecasting in the river Rhine. *Journal of Hydrology*, **356**, 56–69. https://doi.org/10.1016/j.jhydrol.2008.03.027.

Richards, W. G., and C. L. Crozier, 1983: Precipitation measurement with a C-band weather radar in southern Ontario. *Atmosphere-Ocean*, **21**, 125–137. https://doi.org/10.1080/07055900.1983.9649160.

Ryzhkov, A., D. Hudak, and J. Scott, 2006: A new polarimetric scheme for attenuation correction at C band. *Proc. Fourth European Conf. on Radar in Meteorology and Hydrology*, 29–32.

——, P. Zhang, D. Hudak, J. Alford, M. Knight, and J. Conway, 2007: Validation of polarimetric methods for attenuation correction at C band. *Proc. 33rd Conf. Radar Meteorol.*

Ryzhkov, A., M. Diederich, P. Zhang, and C. Simmer, 2014: Potential utilization of specific attenuation for rainfall estimation, mitigation of partial beam blockage, and

radar networking. *Journal of Atmospheric and Oceanic Technology*, **31**, 599–619. https://doi.org/10.1175/JTECH-D-13-00038.1.

Ryzhkov, A. V., S. E. Giangrande, V. M. Melnikov, and T. J. Schuur, 2005: Calibration issues of dual-polarization radar measurements. *Journal of Atmospheric and Oceanic Technology*, **22**, 1138–1155. https://doi.org/10.1175/JTECH1772.1.

Sachidananda, M., and D. S. Zrnić, 1987: Rain rate estimates from differential polarization measurements. *Journal of Atmospheric and Oceanic Technology*, **4**, 588–598. https://doi.org/10.1175/1520-0426(1987)004<0588:RREFDP>2.0.CO;2.

Schell, G. S., C. A. Madramootoo, G. L. Austin, and R. S. Broughton, 1992: Use of radar measured rainfall for hydrologic modelling. *Canadian Agricultural Engineering*, **34**, 41–48.

Şensoy, A., G. Uysal, and A. A. Şorman, 2016: Developing a decision support framework for real-time flood management using integrated models. *Journal of Flood Risk Management,***11**, 866-883. https://doi.org/10.1111/jfr3.12280.

Seo, D.J., E. Habib, H. Andrieu, and E. Morin, 2015: Hydrologic applications of weather radar. *Journal of Hydrology*, **531**, 231–233. https://doi.org/10.1016/j.jhydrol.2015.11.010.

Sevruk, B., 1982: Methods of correction for systematic error in point precipitation measurement for operational use. Operational Hydrology Rep. 21, WMO Rep. 589, 91 pp.

Sills, D. M., and P. I. Joe, 2019: From pioneers to practitioners: A short history of severe thunderstorm research and forecasting in Canada. *Atmosphere-Ocean*, **57**, 249–261. https://doi.org/10.1080/07055900.2019.1673145.

Stellman, K. M., H. E. Fuelberg, R. Garza, and M. Mullusky, 2001: An examination of radar and rain gauge–derived mean areal precipitation over Georgia watersheds. *Weather and Forecasting*, **16**, 133–144. https://doi.org/10.1175/1520-0434(2001)016<0133:AEORAR>2.0.CO;2.

Sugier, J., P. Tabary, J. Gourley, and K. Friedrich, 2006: Evaluation of dual-polarisation technology at C-band for operational weather radar network. *EUMETNET Opera 2 Rep*., 44 pp.

Tabios III, G. Q., and J. D. Salas, 1985: A comparative analysis of techniques for spatial interpolation of precipitation 1. *JAWRA Journal of the American Water Resources Association*, **21**, 365–380. https://doi.org/10.1111/j.1752-1688.1985.tb00147.x.

Thorndahl, S., T. Einfalt, P. Willems, J. E. ek Nielsen, M.-C. ten Veldhuis, K. Arnbjerg-Nielsen, M. R. Rasmussen, and P. Molnar, 2016: Weather radar rainfall data in urban hydrology. *Hydrology and Earth System Sciences & Discussions*, 1–37. https://doi.org/10.5194/hess-21-1359-2017.

Thorndahl, S., T. Einfalt, P. Willems, J. E. Nielsen, M.-C. ten Veldhuis, K. Arnbjerg-Nielsen, M. R. Rasmussen, and P. Molnar, 2017: Weather radar rainfall data in urban hydrology. *Hydrology and Earth System Sciences*, **21**, 1359–1380. https://doi.org/10.5194/hess-21-1359-2017.

Toronto and Region Conservation Authority (TRCA), n.d.: Don River, Accessed 26 November 2019, https://trca.ca/conservation/watershed-management/don-river.

Toronto and Region Conservation Authority (TRCA), n.d.: Watershed Features - Humber River, Accessed 26 November 2019, https://trca.ca/conservation/watershed-management/humber-river/watershed-features/.

Unduche, F., H. Tolossa, D. Senbeta, and E. Zhu, 2018: Evaluation of four hydrological models for operational flood forecasting in a Canadian Prairie watershed. *Hydrological Sciences Journal*, **63**, 1133-1149. https://doi.org/10.1080/02626667.2018.1474219.

Viney, N. R., J. Perraud, J. Vaze, F. H. S. Chiew, D. A. Post, and A. Yang, 2009: The usefulness of bias constraints in model calibration for regionalisation to ungauged catchments. *18th World IMACS Congress and MODSIM09 International Congress on Modelling and Simulation, Cairns, Australia*, 13–17.

Vivekanandan, J., D. N. Yates, and E. A. Brandes, 1999: The influence of terrain on rainfall estimates from radar reflectivity and specific propagation phase observations. *Journal of Atmospheric and Oceanic Technology*, **16**, 837–845. https://doi.org/10.1175/1520-0426(1999)016<0837:TIOTOR>2.0.CO;2.

Vivoni, E. R., D. Entekhabi, R. L. Bras, V. Y. Ivanov, M. P. Van Horne, C. Grassotti, and R. N. Hoffman, 2006: Extending the predictability of hydrometeorological flood events using radar rainfall nowcasting. *Journal of Hydrometeorology*, **7**, 660–677. https://doi.org/10.1175/JHM514.1.

Wang, L.-P., S. Ochoa-Rodríguez, J. Van Assel, R. D. Pina, M. Pessemier, S. Kroll, P. Willems, and C. Onof, 2015: Enhancement of radar rainfall estimates for urban hydrology through optical flow temporal interpolation and Bayesian gauge-based adjustment. *Journal of Hydrology*, **531**, 408–426. https://doi.org/10.1016/j.jhydrol.2015.05.049.

Weber, M. E., J. Y. Cho, J. S. Herd, J. M. Flavin, W. 708 E. Benner, and G. S. Torok, 2007: The next generation multimission US surveillance radar network. *Bulletin of the American Meteorological Society*, 88, 1739–1752. https://doi.org/10.1175/BAMS-88-11-1739.

Wijayarathne, D., P. Coulibaly, S. Boodoo, and D. Sills, 2020: Evaluation of Radar-Gauge Merging Techniques to be Used in Operational Flood Forecasting in Urban Watersheds. *Water,* **12(5),** 1494. https://doi.org/10.3390/w12051494.

Xie, H., X. Zhou, J. Hendrickx, E. Vivoni, H. Guan, Y. Tian, and E. Small, 2006: Comparison of NEXRAD Stage III and gauge precipitation estimates in central New Mexico. *Journal of the American Water Resources Association*, **42**, 237–256. https://doi.org/10.1111/j.1752-1688.2006.tb03837.x.

Young, C. B., and N. A. Brunsell, 2008: Evaluating NEXRAD estimates for the Missouri River Basin: Analysis using daily raingauge data. *Journal of Hydrologic Engineering*, **13**, 549–553. https://doi.org/10.1061/(ASCE)1084-0699(2008)13:7(549).

Zahmatkesh, Z., S. Kumar Jha, P. Coulibaly, and T. Stadnyk, 2019: An overview of river flood forecasting procedures in Canadian watersheds. *Canadian Water Resources Journal/Revue canadienne des ressources hydriques*, 1–17. https://doi.org/10.1080/07011784.2019.1601598.

Zhang, J., Y. Qi, D. Kingsmill, and K. Howard, 2012: Radar-based quantitative precipitation estimation for the cool season in complex terrain: Case studies from the NOAA Hydrometeorology Testbed. *Journal of Hydrometeorology*, **13**, 1836–1854. https://doi.org/10.1175/JHM-D-11-0145.1.

Chapter 4. Evaluation of Radar-Gauge Merging Techniques to be Used in Operational Flood Forecasting in Urban Watersheds

Summary of Paper 3: Wijayarathne, D., Coulibaly, P., Boodoo, S., and Sills, D. (2020). Evaluation of Radar-Gauge Merging Techniques to be Used in Operational Flood Forecasting in Urban Watersheds. *Water*, 12(5), 1494. https://doi.org/10.3390/w12051494.

This research evaluated nine existing radar-gauge merging techniques using two dual-polarized WKR C-band Radar and two KBUF NEXRAD S-band operational Radar hourly QPEs to assess which method best suits the Humber River (semi-urban) and Don River (urban) watersheds in Canada. The impact of the quality of radar QPEs on the performance of radar-gauge merging was also examined. Moreover, the relative strength of radar-gauge merging techniques at different rain intensities and different rainfall events were evaluated.

Key findings of this research include:

- All radar-gauge merging methods outperformed radar only QPEs.
- The CDF Matching (CDFM) performed best, followed by Kriging with radar-based error correction (KRE).
- Both WKR and NEXRAD Radar QPEs improved significantly, while NEXRAD Level III (DPA) provided the best results.
- All methods performed well for low intense precipitation but deteriorated with the increasing rainfall intensities.

- Overall, all methods outperformed the Radar only QPEs for all events and performed better during the summer.

4.1. Abstract

Demand for radar Quantitative Precipitation Estimates (QPEs) as precipitation forcing to hydrological models in operational flood forecasting has increased in the recent past. It is practically impossible to get error-free QPEs due to the intrinsic limitations of weather radar as a precipitation measurement tool. Adjusting radar QPEs with gauge observations by combining their advantages while minimizing their weaknesses increases the accuracy and reliability of radar QPEs. This study deploys several techniques to merge two dual-polarized King City radar (WKR) C-band and two KBUF Next-Generation Radar (NEXRAD) S-band operational radar QPEs with rain gauge data for the Humber River (semi-urban) and Don River (urban) watersheds in Ontario, Canada. The relative performances are assessed against an independent gauge network by comparing hourly rainfall events. The Cumulative Distribution Function Matching (CDFM) method performed best, followed by Kriging with Radar-based Error correction (KRE). Although both WKR and NEXRAD radar QPEs improved significantly, NEXRAD Level III Digital Precipitation Array (DPA) provided the best results. All methods performed better for low- to medium-intensity precipitation but deteriorated with the increasing rainfall intensities. All methods outperformed radar only QPEs for all events, but the agreement is best in the summer.

Keywords: radar-gauge merging; QPE; WKR C-band radar; NEXRAD radar; hydrology; floods

4.2. Introduction

Flooding has been identified as the world's deadliest natural disaster after earthquakes and tsunamis due to the associated damage to life, property, economy, and infrastructure [1,2]. Therefore, flood mitigation procedures are essential for regions susceptible to flooding. A well-developed flood forecasting system that can deliver accurate and reliable forecasts with proper lead time is a vital part of nonstructural flood management. At present, flood forecasting and warning utilizing hydrological models to forecast river flow have a widespread application in disaster management [3,4]. In urban watersheds, the frequency and magnitude of flooding are mostly influenced by precipitation [5,6]. Therefore, the accuracy and reliability of hydrological model predictions depend heavily on the accuracy of the forcing data, especially the Quantitative Precipitation Estimates (QPEs) [7,8]. Additionally, accurate QPEs produce model parameter sets that represent watershed characteristics after hydrological model calibration. Therefore, accurate and reliable QPEs are necessary to provide runoff and streamflow estimates with high confidence [9].

Today, the precipitation input for hydrological models comes from surface rainfall gauges, weather radar, weather models, and satellite images [10,11]. Currently, the calibration of these hydrological models relies mostly on in-situ rain gauge data [5,10]. Rain gauges are trustworthy instruments for rainfall point measurements, but the rainfall variations in both space and time are not well captured [12]. Since radar produces

spatially and temporally continuous data over a large area in real-time, there is considerable interest in precipitation information derived from weather radar for a hydrological model run in operational flood forecasting [5,10].

The concept of forcing hydrological models with radar QPEs first appeared at the urban storm drainage conference in Sweden, 1984 [13]. Since then, radar QPEs have been used as precipitation forcing for hydrological models for flood forecasting applications worldwide, mainly due to the advances in radar infrastructure, computer power, and hydrological models. [14–17]. At present, different countries produce commercial weather radar products that are extensively used in operational hydrology: e.g., Next Generation Weather Radar (NEXRAD) in the USA and Radar-Online-Aneichung (RADOLAN) in Germany [18–20]. Those products provide a fixed cartesian grid with rainfall accumulation data summarized over a set time. The spatiotemporal resolution of radar QPEs has been improved recently, and therefore, the application of radar QPEs in operation hydrology has been increased. For example, the United States and European countries have used S-band radars and C-band radars with spatial resolutions of about 1000 m and 5 min temporal resolutions, mostly in operational hydrology [5]. Additionally, the X-band radar with spatial and temporal resolutions of 250 m and 1 min has been used in Japan for operational purposes [21].

Even if the radar QPEs have been used for nearly 30 years to run hydrological models, well-known artifacts associated with radar limits its operational use [22,23]. Since weather radar measures the precipitation indirectly, radar QPEs are known to be exposed to errors due to attenuation [24], radar miscalibration [25,26], ground clutter

[27], anomalous propagation [28], beam blockage [29], range degradation [30], presence of the bright band [31], variations in the drop size distribution [32], and more [16,33–36]. Numerous studies have attempted to demonstrate and quantify the potential magnitude of radar uncertainty and the resulting consequences of using radar QPE for operational hydrological modeling [34,37–41]. The studies mentioned above have identified radar QPE uncertainties related to range, Vertical Profile of Reflectivity (VPR) effects, inappropriate Z–R relationships, anomalous propagation, clutter, and visibility effects as significant sources of error in the radar-estimated rainfall that can have a profound effect on hydrological modeling confidence. Therefore, radar data must undergo careful selection and corrections where possible before using them as a precipitation source for hydrological model calibration. In contrast to these studies, Vehvilainen et al. [42] have investigated the effect of using raw radar estimated QPEs for hydrological modeling and concluded that in small catchments (<500 km^2), where the time of concentration is on the order of hours, hydrological models can benefit from raw radar-derived rainfall estimates. Previous studies have discussed several methods to reduce these errors since the start of the use of radar as precipitation estimates in hydrological applications [13,39]. The recent improvements built upon dual-polarization radar measurements have improved the accuracy and reliability of weather radar data in hydrological applications [24,43–46]. The dual-polarized radar emits and receives radar pulses in both horizontal and vertical polarization, permitting additional products such as differential reflectivity (Z_{DR}) and specific differential phase (K_{DP}) [47] that produce better precipitation estimates, particularly for extreme rainfall events [48]. Additionally, dual-polarized radar improves

the quality of radar estimated precipitation rates and total amounts by mitigating attenuation and anomalous propagation, leading to more accurate radar QPEs [33,45,49,50]. Since dual-polarized radar produces more accurate radar QPEs, it is beneficial to use dual-polarized radar QPEs over single polarized radar [33,48]. Additionally, increasing the density of the radar network reduces the uncertainties in radar QPEs by reducing the distance to the radar stations [51]. However, both methods mentioned above require significant investment.

Besides the methods mentioned above, a significant improvement has been made by adjusting radar QPEs with gauge observations (hereafter radar-gauge merging). The radar-gauge merging produces accurate, reliable, real-time QPEs that capture variations both in space and time. Radar-gauge merging to adjust radar QPEs to match with gauge observations is broadly discussed in the literature [52–54]. Previous research has shown that the radar-gauge merging is useful to improve radar QPEs that can be used as an additional source for hydrological applications [23,52,54,55]. Even though radar-gauge merging has been used in improving radar QPEs since the start of the operational use of weather radars in the 1970s, Ochoa-Rodriguez et al. [54] emphasize the lack of understanding of the full potential of application at the spatial-temporal resolutions required for urban hydrology. High-quality precipitation estimates with high temporal resolution are needed for urban hydrological applications due to small-sized urban catchments and a high degree of imperviousness in response to fast rainfall [36,54]. Hence, urban watersheds are very sensitive to the spatial and temporal variability of

rainfall, and further research is essential before using radar QPEs in operational urban hydrology with confidence.

Even though studies on radar-gauge merging are common, to date, they have not adequately addressed applicability at the resolution and scale required for urban hydrological applications. Most of the studies have focused on large-scale area applications, frequently country-wide, using a time-step above 24 h, or at temporal scales for event-based accumulation [22,51,52,56–65]. Urban hydrological studies need reliable QPEs at high spatial (a few km) and temporal (hourly or sub-hourly) resolutions [53,66]. A few studies have investigated radar-gauge merging techniques focusing on the urban scale but were limited to a single technique under limited climatological and infrastructure conditions [23,67–69]. To date, only two inter-comparison studies have been conducted focusing on urban scales [68,70]. The first study evaluated radar-gauge merging techniques based on a rain gauge network of three gauges [69]. The latter research provides an introductory understanding of the relative performances of merging methods [70]. Therefore, further research on smaller-scale urban catchments is essential [53,54]. The most recent categorization of the existing radar-gauge merging methods was introduced by Ochoa-Rodriguez et al. [54] based on the potential for urban hydrological application; 1. radar bias adjustment methods, 2. rain gauge interpolation methods using spatial radar association as additional information, and 3. radar-rain gauge integration methods. Only two preliminary studies have investigated the three categories of merging methods defined by Ochoa-Rodriguez et al. [54,68,71]. Therefore, it is beneficial to consider methods that preserve small-scale features in the merged estimates in fine scale,

the limited availability of rain gauges, and computational requirements for operational use when applying radar-gauge merging methods. Furthermore, radar-gauge merging applications using modern dual-polarization radars must be evaluated. Most of the previous studies have evaluated merging techniques using single polarized radar [51,53]. As mentioned before, the dual-polarized radars have the potential to produce more accurate and reliable radar QPE compared to single polarized radar [33,50]. As emphasized by Ochoa-Rodriguez et al. [68], the quality of initial radar products affects the relative performance of merging methods and, ultimately, the quality of merged radar precipitation estimates. Therefore, it is vital to investigate how these new dual-polarized products may impact the performance of different radar-gauge merging techniques.

In this study, different existing radar-gauge merging techniques for operational use in urban watersheds have been implemented to obtain the best estimation of precipitation in two watersheds in the Greater Toronto Area (GTA), Canada: semi-urban Humber River, and urban Don River watersheds. The operational application of radar-gauge merging in flood forecasting is not yet implemented widely in Canada [51]. This is important because a recent study conducted in the GTA reported about 94.0 mm of rainfall estimates with R(K_{DP}) algorithm using dual-polarized King City radar (WKR) through a heavy rainfall event over a 2-h period on 8 July 2013, whereas the rain gauge recorded 126 mm over the same period [72]. In the same study, an accumulation of 109.2 mm of rain is reported for the same storm event with the R(Z) algorithm using KBUF NEXRAD S-band algorithms [72]. The authors suggested the differences are caused by ground clutter contamination, path attenuation, and radome wetting. To use radar QPEs as

additional precipitation forcing for hydrological models in the GTA area, the reported differences must be minimized. In this study, the performance of two dual-polarized WKR C-band radar hourly QPEs and two KBUF NEXRAD S-band radar hourly QPEs have been improved using radar-gauge merging techniques to minimize the difference with gauge measurements. Moreover, several radar-gauge merging techniques with varying degrees of complexity have been evaluated to assess which method best suits these two urban and semi-urban watersheds in the GTA area. The merging techniques implemented include Mean Field Bias correction (MFB), Frequency and Intensity Correction (FIC), local intensity scaling (LOCI), Cumulative Distribution Function Matching (CDFM), Range-Dependent bias Adjustment (RDA), Modified Brandes Spatial Adjustment (MBSA), and Kriging with Radar-based Error correction (KRE). The MFB, RDA, MBSA, and KRE methods are often used in the literature for radar-gauge merging; however, methods CDFM, FIC, and LOCI are seldomly discussed in the literature as radar-gauge merging techniques. In addition to radar-gauge merging techniques, Ordinary Kriging (OK) was also included for the evaluation as a benchmark since it is a widely used interpolation method for hydrological applications and is often used as a reference.

This work aims to evaluate radar-gauge merging techniques using two dual-polarized WKR C-band radar and two KBUF NEXRAD S-band operational radar hourly QPEs (the first attempt to the best of our knowledge) to assess which best suits the two urban and semi-urban watersheds in the GTA, Canada. The objectives of this study are (1) to evaluate different existing radar-gauge merging techniques of various degrees of complexity to facilitate hydrological model runs for operational flood forecasting in urban

watersheds; (2) to verify the reliability and accuracy of dual-polarized radar QPEs from WKR C-band and KBUF NEXRAD S-band QPEs as an additional data source for hydrological model calibration; (3) to assess the relative strength of radar-gauge merging techniques at different rain intensities; and (4) to illustrate the performance of radar-gauge merging techniques for different rainfall events. Additionally, Section 2 provides a detailed description of the study area. Characteristics of the radar and the rain gauge network and detailed descriptions of different methods used for merging can be found in Section 3. Section 4 presents the results and discussion of the evaluation of radar-gauge methods. Section 5 draws general conclusions.

4.3. Study Area

The Humber River watershed and Don River watershed, located in the GTA, Ontario, Canada, are the two watersheds of interest in this study (Figure 4-1). Toronto and Region Conservation Authority (TRCA) currently manages both watersheds. The watersheds form part of the Great Lakes basin and have good coverage from the King City Canadian WKR C-band radar and the Buffalo KBUF NEXRAD USA S-band radar. The radar-gauge merging methods are applied on a square domain containing both watersheds (Top left: 567,172.239m E 4,883,228.030 m N; Bottom right: 647,341.150 m E 4,819,410.402 m N).

The Humber River watershed is the largest semi-urban watershed in the GTA and is home to over 800,000 people. The watershed covers an area of 911 km^2 and consists of approximately 54% rural land, 33% urban land, and 13% of urbanizing land [73]. For

further details on the Humber River watershed, readers are referred to the TRCA Watershed Features Humber River website [73].

The other watershed focused on for this study is the Don River watershed and is nearly 350 km^2 in size and home to over a million residents. It is a fully urbanized watershed, with approximately 80% developed areas [74]. Further details of the Don River watershed can be found in the TRCA Don River website [74].

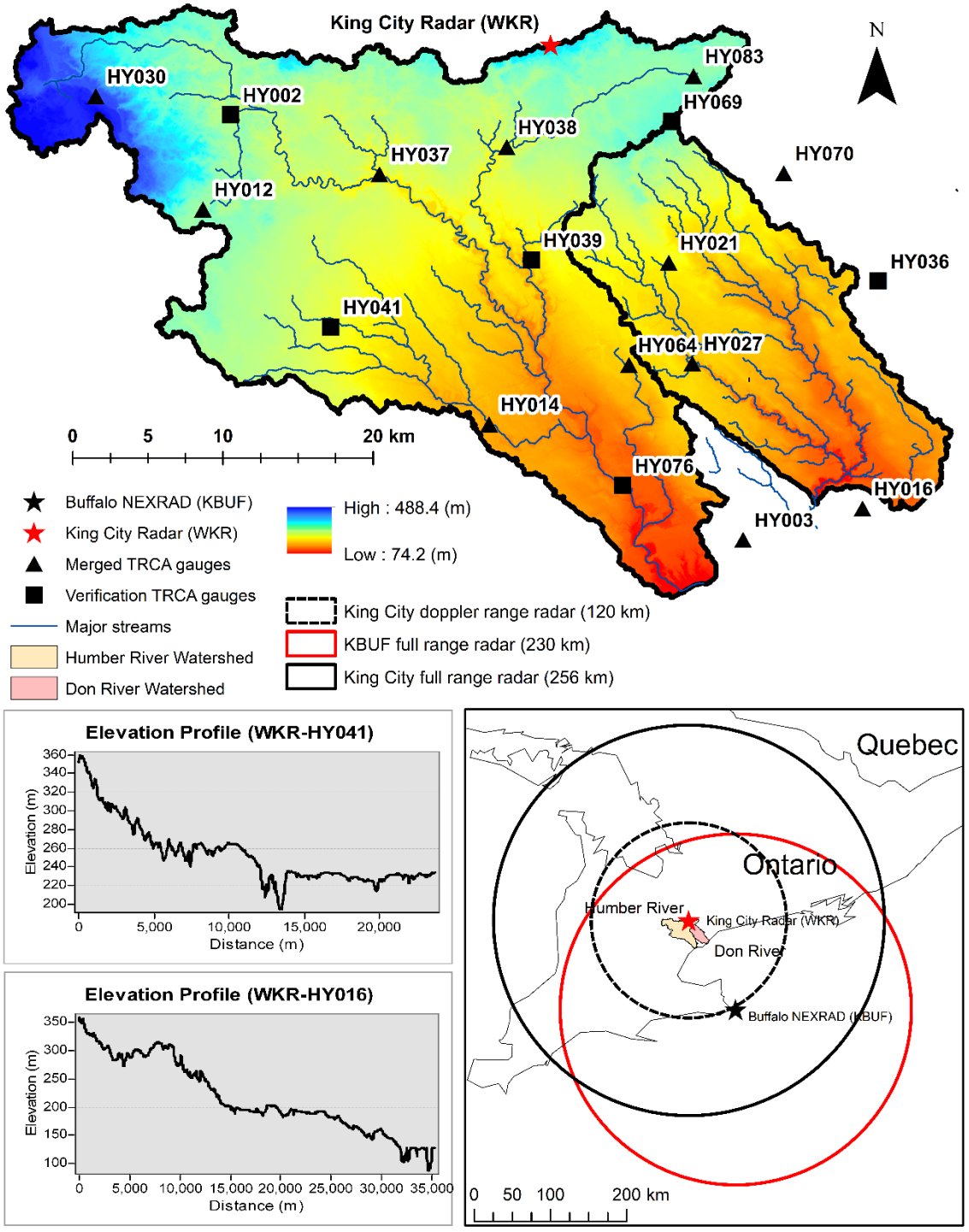

Figure 4-1 *Humber River and Don River watersheds, and coverages of the nearest radar sites (WKR and KBUF)*

4.4. Materials and Methods

4.4.1. Data

4.4.1.1. Rain Gauge Data

Hourly rainfall accumulations provided by tipping-bucket rain gauges from 2012 to 2017 were gathered from TRCA data archives. TRCA operates a dense gauge network (one gauge per ~75 km^2 in Humber River and one gauge per ~116 km^2 in the Don River) with 18 precipitation monitoring locations across the two watersheds. All TRCA gauge stations are located within ~40 km radius range of WKR Canadian C-band radar station and within the usable range (<180 km) of KBUF NEXRAD S-band radar (Figure 4-1).

4.4.1.2. King City WKR C-Band Dual-Polarized Radar QPEs

Environment and Climate Change Canada (ECCC) operates 29 weather radar stations across Canada at a full reflectivity measurement range of 256 km around the site and a Doppler range of 120 km around the site [75]. Reflectivity data for this study were collected from the King City weather radar facility located north of Toronto, Ontario (Figure 4-1). The WKR radar performs dual-polarization POLarimetric Plan Position Indicator (POLPPI) scans at 0.5-degree elevation, completed in about 1 min, every 10 min with 0.25 km range and 0.5-degree azimuth resolution [33]. Reflectivity values were corrected for attenuation using the modified ZPHI algorithm [33,76]. Radar QPEs were estimated using different rain rate estimator algorithms, R(Z), R (Z, K_{DP}), and R (K_{DP}, Z_{DR}), listed in Table 4-1. In this study, the average over 11 × 11 radar pixels around the nearest gauge location was used to limit the wind drift [77]. Considering the resolution of

radar bins, the final radar QPE grid size is about 3 km (11 × 0.25 km) × 4 km (11 × 0.5 = 5.5 deg assuming a distance of 40 km) with each grid cell containing a 10-min rainfall accumulation. Radar estimated rain rates are not time interpolated and are assumed to be constant over the scanning time interval of 10 min. To be consistent with the gauge data, the 10-min rainfall was integrated in time to derive 1-h rainfall accumulations.

4.4.1.3. KBUF NEXRAD S-Band Dual-Polarized Radar QPEs

NEXRAD Level III S-band radar QPE data from the Buffalo radar station (Latitude 42.94639 Longitude −78.72278) were downloaded from the National Centers for Environmental Information (NCEI) archives. The KBUF radar collects reflectivity values about every 6 min at 0.25 km in range and 0.5-degree in azimuth. Afterward, rain rates are calculated using the Precipitation Processing System (PPS) algorithm R = 0.017 $Z^{0.714}$. Two NEXRAD Level III one-hour precipitation products, Digital Precipitation Array (DPA), and one-hour precipitation (OHA), were used for the study (Table 4-1). The operational NEXRAD QPEs have a temporal resolution of 60 min and a spatial resolution of ~4 × 4 km [78].

Table 4-1 *List of rain-rate estimators for radar Quantitative Precipitation Estimates (QPEs)*

Radar QPE	Description	Formula	Reference
C1	Combined Z and K_{DP} algorithm using a threshold on K_{DP}	$R = 0.017Z^{0.714}$ $R = 33.8K_{DP}^{0.79}$	[79]
C2	Multi-parameter rain rate estimator using K_{DP} and Z_{DR}	$R = 37.9K_{DP}^{0.89}10^{-0.072Z_{DR}}$	[43]
N1	NEXRAD Level III (DPA)	$R = 0.017Z^{0.714}$	[59]
N2	NEXRAD Level III (OHA)	$R = 0.017Z^{0.714}$	[59]

4.4.2. Radar-Gauge Merging Methods

The following radar-gauge merging techniques were carefully chosen for this study based on extensive operational use in urban areas, the ability to be implemented, prominence in past literature, varying degrees of complexity, and several location-specific factors such as gauge density, proximity to the radar station, basin size, and time step of adjustment [51,80].

4.4.2.1. Mean Field Bias Correction (MFB)

This method removes the bias introduced through the uncertainty in the radar calibration or an erroneous coefficient in the Z-R relationship [81]. MFB assumes that the radar QPEs are affected by a uniform multiplicative error. Therefore, a single adjustment factor (C_{mfb}) is estimated (Equation (4-1) [82]) and applied to the entire radar field [82]. An alternative adjustment that depends on the mean assessment factor (C_{maf}) (Equation (4-2) [82]) is also implemented:

$$\mathrm{C_{mfb}} = \frac{\sum_{\mathrm{i=1}}^{\mathrm{N}} \mathrm{G_i}}{\sum_{\mathrm{i=1}}^{\mathrm{N}} \mathrm{R_i}} \tag{4-1}$$

$$C_{\mathrm{maf}} = \frac{1}{N} \sum_{i=1}^{N} \frac{\mathrm{G_i}}{\mathrm{R_i}} \tag{4-2}$$

where $\mathrm{C_{mfb}}$ and C_{maf} are correction factors, $\mathrm{G_i}$ and $\mathrm{R_i}$ are the gauge and corresponding radar value associated with gauge i.

4.4.2.2. Frequency and Intensity Correction (FIC)

This method maps the distribution between the radar and gauge rainfall data at a given location [83]. FIC first truncates the radar rainfall distribution at a point that

approximately replicates the long-term observed relative frequency of rainfall. Then the truncated radar rainfall intensity distribution is mapped on to a gamma distribution fitted to observed gauge intensity distribution. The frequency of the hourly radar rainfall is corrected by fitting a threshold value $\tilde{x}_R$ to truncate the empirical distribution of the radar rainfall data. The radar rainfall threshold $\tilde{x}_R$ is calculated as follows (Equation (4-3) [83]) using the empirical cumulative distribution of both gauge and radar rainfall. In this method, 0.1 mm was used as the minimum observed precipitation amount $\tilde{x}$ for an hour to be considered wet (hours with precipitation $\geq$ threshold) based on the literature [83]. Corrected radar rainfall x_i^{Cor} on hour i is calculated as in Equation (4-4) [83] by mapping the truncated radar rainfall intensity distribution $F_R(x)$ (e.g., fitted gamma or empirical distribution) to a gamma distribution fitted to observed intensity distribution $F_G(x)$.

$$\tilde{x}_R = F_R^{-1}\left(F_G(\tilde{x})\right) \tag{4-3}$$

Where $F(\cdot)$ and $F^{-1}(\cdot)$ represent a cumulative distribution function (CDF) and its inverse, R indicated radar rainfall, and G shows observed gauge rainfall

$$x_i^{Cor} = \begin{cases} F_{obs}^{-1}\left(F_R(x_i)\right), & x_i \geq \tilde{x} \\ 0, & x_i < \tilde{x} \end{cases} \tag{4-4}$$

This study considered both gamma (GG) and empirical distribution (EG) for truncated radar data, respectively. Precipitation at a location without a coincident gauge record was obtained by correction from the precipitation values from the WKR C-band grid point closest to the gauge station. For NEXRAD radar, it was obtained from the closest radar pixel to the prediction grid cell with coincidental gauge records.

4.4.2.3. Local Intensity Scaling (LOCI)

The primary step of the LOCI method is to correct the wet time-step frequency and intensity, respectively [84]. First, a model wet-hour threshold $\left(\tilde{x}_{R,h}\right)$ is determined from the hourly radar rainfall for an hour h to ensure that the threshold exceedance matches the wet-hourly frequency in the gauge observation. A correction factor $\left(x_{R,h,i}^{Cor}\right)$ is then calculated using the following equation (Equation (4-5) [84]):

$$x_{R,h,i}^{Cor} = \begin{cases} x_{R,h,i} \times \dfrac{\mu\left(x_{G,h,i} \middle| \; x_{G,h,i} > \tilde{x}_{R,h}\right)}{\mu\left(x_{R,h,i} \middle| \; x_{R,h,i} > \tilde{x}_{R,h}\right)}, & x_{R,h,i} \geq \tilde{x}_{R,h} \\ 0, & x_{R,h,i} < \tilde{x}_{R,h} \end{cases} \quad (4\text{-}5)$$

where μ is mean intensity (mm wh^{-1}) (''wh'' is a wet hour, with greater than or equal to thresh hold).

4.4.2.4. CDF Matching (CDFM)

The CDFM method uses a sorting algorithm to match the CDF of observed data (radar rainfall) to a reference data (gauge) set [85]. CDFM matches the CDF of the radar rainfall (cdf_R) based on polynomial fitting to match with the CDF of the historical gauge data(cdf_G). The radar estimated QPEs are re-scaled so that the empirical CDFs of both radar and gauge data sets match (Equation (4-6) [85]). A third-degree polynomial model is employed as follows for this purpose (Equation (4-7) [85]).

$$cdf_G(x') = cdf_R(x) \quad (4\text{-}6)$$

where x and x' are the gauge data and transformed radar rainfall data respectively

$$BR = P_1 S^3 + P_2 S^2 + P_3 S + P_4 \quad (4\text{-}7)$$

where BR is the bias-corrected radar rainfall, P indicates the coefficients of the polynomial models, and S is the raw radar rainfall.

4.4.2.5. Range-Dependent Bias Adjustment (RDA)

This method is based on the Baltic Sea Experiment (BALTEX) adjustment proposed by Michelson et al. [86] and assumes that radar biases are a function of the distance from the radar tower [87]. Range dependencies are due to beam broadening, overshooting of the beam, increasing height of the measurements, and attenuation effects [88]. The relationship between the R/G ratio and the distance from the radar station is expressed in the log-scale. The range is approximated by a second-order polynomial whose coefficients are determined through observations using the least-squares fit (Equation (4-8) [53]). The range dependent multiplicative factor is calculated from:

$$\log C_{RDA} = ar^2 + br + c \tag{4-8}$$

where r is the distance from the radar tower to the radar bin, and a, b, and c are coefficients using the least-squares fit.

4.4.2.6. Modified Brandes Spatial Adjustment (MBSA)

In opposition to MFB, the MBSA assumes that the biases are spatially dependent [57]. The MBSA distributes correction factors across the radar field. A distance-weighting scheme with a smoothing factor is used to determine the influence of a known data point on the interpolated value of a specific radar bin. The correction factors (C_i) are calculated at each gauge location at a set time step (e.g., hourly) (Equation (4-9) [53]). Then, weights (WT) for each radar bin i from each gauge location are determined following the Barnes objective analysis to produce the calibration field [89]. A negative exponential weighting (Equation (4-10) [53]) is used to calculate the weights. All correction factors are then interpolated across the entire radar field using two passes (F_1:

Equation (4-11) [53] and F_2: Equation (4-12) [53]). Finally, the spatially interpolated correction factors at each radar bin are multiplied by the radar-estimated rainfall (Equation (4-13) [53]) to get the bias-corrected radar rainfall.

$$C_i = \frac{G}{R} \tag{4-9}$$

$$WT_i = exp\left(\frac{-d^2}{EP}\right) \tag{4-10}$$

$$F_1 = \frac{\sum_{i=1}^{N}(WT_i)(G_i)}{\sum_{i=1}^{N} WT_i} \tag{4-11}$$

$$F_2 = F_1 + \frac{\sum_{i=1}^{N}(WT_i)(D_i)}{\sum_{i=1}^{N} WT_i} \tag{4-12}$$

where $D_i = C_i - F_{1,i}$

$$R_{new,i} = \left(R_{old,i}\right)(F_2) \tag{4-13}$$

4.4.2.7. Kriging

The Kriging methods determine the precipitation value at a grid point/pixel at a non-gauged location by using gauge measurements at neighboring locations [61]. In this study, two kriging methods have been implemented: Ordinary Kriging (OK) and Kriging with Radar-based Error correction (KRE). The Ordinary Kriging method interpolates the precipitation from gauge observations at several locations [90]. The KRE method uses the radar field to estimate the error of the OK that is created using gauge data [91].

Ordinary Kriging (OK)

The OK defines a variogram symbolizing the spatial variability of the observed precipitation field. First, a parametric variogram, $\gamma(h)$, is generated using the gauge measurements. Weighted contributions from surrounding gauges are then used to

calculate rainfall values at unknown points (Equation (4-14) and 4-15) [61]). After that, the OK system is produced by minimizing the estimate variance using a Lagrange multiplier μ_1 (Equation (4-16) [61]). Finally, merged rainfall values at x_0 are determined using n values obtained by solving a matrix (Equation (4-17) [61]) that formalizes the above conditions.

$$Z(x_0) = \sum_{\alpha=1}^{N} w_\alpha \, Z(x_\alpha) \tag{4-14}$$

with the condition that

$$\sum_{\propto=1}^{N} w_\propto = 1 \tag{4-15}$$

$$\sum_{\beta=1}^{N} w_\beta \, \gamma(x_\alpha - x_\beta) + \mu_1 = \gamma(x_\alpha - x_0) \; for \; a = 1, \dots, n \tag{4-16}$$

$$\begin{bmatrix} \gamma(x_1 - x_1) & \cdots & \gamma(x_1 - x_n) & 1 \\ \vdots & \ddots & \vdots & \vdots \\ \gamma(x_n - x_1) & \cdots & \gamma(x_n - x_n) & 1 \\ 1 & \cdots & 1 & 0 \end{bmatrix} \begin{bmatrix} w_1 \\ \vdots \\ w_n \\ \mu_1 \end{bmatrix} = \begin{bmatrix} \gamma(x_1 - x_0) \\ \vdots \\ \gamma(x_n - x_0) \\ 1 \end{bmatrix} \tag{4-17}$$

Kriging with Radar-Based Error Correction (KRE)

This method attempts to diminish the bias while minimizing the variance of error [53]. The KRE method combines radar and gauges by fitting gauge data into the observed precipitation field $R(s)$ based on the radar data [91]. First, gauge data are Kriged using OK to create a gauge Kriging field $G_K(s)$ to obtain the best linear unbiased rainfall estimates. Then, the radar-based Kriging precipitation filed $R_K(s)$ is generated with the same variogram using radar QPEs at corresponding gauge stations. This process produces an interpolated rainfall field that retains the mean-field of the original radar data. After

that, the deviation between observed and interpolated radar values $\varepsilon_R(s)$ is calculated at each grid point (Equation (4-18) [91]). Finally, the deviation field $\varepsilon_R(s)$ is applied to the Kriged gauge field $G_K(s)$ to obtain the merged rainfall field (Equation (4-19) [91]) that preserves mean-field deviation and the spatial structure of radar rainfall.

$$\varepsilon_R(s) = R(s) - R_K(s) \tag{4-18}$$

$$M(s) = G_K(s) + \varepsilon_R(s) \tag{4-19}$$

4.4.3. Evaluation of Radar-Gauge Merging Techniques

After Koistinen and Puhakka [92], several assumptions were made before conducting radar-gauge merging. Firstly, rain gauge data were used as a ground reference assuming they are accurate for each respective gauge location. However, gauge data can be unreliable due to human errors, irregularities of topography, wind-induced under-catch, wetting, and evaporation losses [93]. Secondly, it was assumed that there is no spatial mismatch between radar and gauge measurements and is valid for the same location in time and space. However, there is always a spatial mismatch because different volumes are sampled by point rain gauges and spatially integrated weather radar at different heights [94]. While radar samples volume above approximately 4 × 4 km surface for NEXRAD radar and 3 × 4 km for WKR radar, rain gauges measure precipitation over an eight-inch diameter surface area contributing differences in measured precipitation. Thirdly, the radar was assumed to capture relative spatial and temporal variabilities of precipitation successfully. Even if attenuation and ground clutter is addressed during signal processing, other limitations such as anomalous propagation, radar calibration errors, wind effect, growth of precipitation, variations in the Z–R relationship, presence of

hail, or other hydrometeors can affect the radar precipitation [95]. Fourthly, the assumption of constant rain rate over the scans leads to a temporal sampling error [69,96]. Finally, the relations that are made upon the comparison between gauges and radar were assumed to be valid for other locations in time and space.

Performance of nine radar-gauge merging techniques was investigated by using 18 rainfall events, totaling 278 h (i.e., all events) of rainfall that occurred in spring, summer, and fall periods from 2012 to 2017 (Table 4-2). Since the Z–R relationships for WKR C-band radar QPEs are only valid for liquid rainfall and do not account for low melting layers and possible bright band contamination, winter precipitation was excluded from the analysis [33]. Events were determined as the time where at least half of the gauges (9 out of 18) recorded a precipitation amount > 0 mm to the time where half of the gauges start re-recording zero. Additionally, intensity, availability of both radar and gauge precipitation, data continuity (limited number of missing values), reasonable accumulation of rainfall, and coverage of the watershed were considered during event selection.

Table 4-2 *Description of events.*

Event No	Start Date	UTC	End Date	UTC	Season	Duration (Hours)	Max Total Rainfall (mm)	Max Rainfall Intensity (mm/h)
1	1 June 2012	8:00	1 June 2012	23:00	Summer	16	39	28.0
2	28 May 2013	20:00	29 May 2013	8:00	Spring	14	60	39.2
3	8 July 2013	18:00	9 July 2013	2:00	Summer	9	93.8	46.8
4	31 July 2013	19:00	1 August 2013	10:00	Summer	16	50	17.6
5	28 July 2014	0:00	28 July 2014	12:00	Summer	13	85	81.0
6	6 September 2014	0:00	6 September 2014	10:00	Fall	11	52.6	21.9
7	20 April 2015	3:00	20 April 2015	19:00	Spring	17	32	6.1
8	30 May 2015	15:00	31 May 2015	23:00	Spring	33	66	19.0
9	8 June 2015	0:00	8 June 2015	13:00	Summer	14	44.2	32.0
10	27 June 2015	17:00	28 June 2015	21:00	Summer	29	57	26.0
11	28 October 2015	7:00	28 October 2015	23:00	Fall	17	49.8	11.0
12	10 November 2015	19:00	11 November 2015	11:00	Fall	17	20.4	8.0
13	13 August 2016	16:00	14 August 2016	1:00	Summer	11	45.2	28.8
14	16 August 2016	8:00	16 August 2016	19:00	Summer	12	34.4	12.8
15	23 June 2017	5:00	23 June 2017	14:00	Summer	10	65.2	25.2
16	20 July 2017	15:00	20 July 2017	17:00	Summer	3	41.6	31.4
17	27 July 2017	0:00	27 July 2017	15:00	Summer	16	15.2	7.6
18	18 November 2017	22:00	19 November 2017	8:00	Fall	11	20	11.0

The methods were evaluated by comparing the merged radar QPEs to the gauge measurements and radar only QPEs (hereafter referred to as RO) to determine what

method generates the best precipitation estimates. First, radar-gauge merging was applied for all events (278 h) at the same time to evaluate the performance of each technique for each radar QPE for an hourly time-step of accumulation. Then radar-gauge merging was separately applied for the events to represent the performance by the event. Missing gauge values were ignored during the analysis. The merged WKR QPE at the nearest gauge point or the combined NEXRAD radar pixel where the ground observation is collected was compared with the reference gauge points. As commonly practiced in hydrological studies, two-thirds of the gauges (12) were assigned for merging method implementing purpose (denoted by triangles in Figure 4-1), and the remaining six gauge stations (denoted by squares in Figure 4-1) were used for validation as reference gauges [61]. To get the maximum coverage within the watershed, stations that are located a minimum of 10 km apart from each other were selected for the verification. To assess the added value of the radar-gauge merging compared to the spatial distribution of the rain gauge data alone, the OK method was tested as a benchmark. In addition, the performance of each merging method for rainfall intensity thresholds was assessed to determine the effect of rainfall intensity on the merging methods.

The merging techniques were applied to hourly precipitation amounts to keep the spatial and temporal advantages accessible by radar as the error due to spatial and temporal variations in gauge estimates are averaged out for more extended time steps, especially at 24 h or above or event-based accumulation times. The selection of appropriate space and time scales for radar-gauge merging to remove systematic bias in urban and semi-urban watersheds is always a compromise. It heavily depends on the

specific area of interest. Even though sub-hourly data provides more reliable results during radar-gauge merging for urban watersheds, hourly precipitation was used in this study due to several reasons. Firstly, high temporal resolution data limitation is a challenge in these two watersheds. Only hourly precipitation gauge data is available from most of the TRCA gauge stations for the study period from 2012 to 2017. Additionally, available NEXRAD radar data for the study area are in hourly temporal resolution. Secondly, sub-hourly time steps can result in random errors [97]. Thirdly, adjusting radar QPEs in long-term accumulations to be applied in short term hydrological applications is often used in literature and proven to be effective [97–100]. Fourthly, the hydrological models have been improved recently; however, many of them are not yet ready to use high temporal resolution (sub-hourly) inputs because the output is always for an hour or more than that [5]. Finally, hourly streamflow simulations using hydrological models could adequately capture peak flows at the two watersheds because the calculated time of concentration of both basins is higher than one hour [101]. In terms of operational flood forecasting, streamflow and possible inundated areas along a river must be sent to the authorities and public as early as possible. High-resolution radar QPEs are costly and also could delay the flood forecasting process because of the high model computation time when it comes to real-world application [5].

The spatial resolution of the radar data used in the study may not be the optimal resolution for urban hydrological applications. High spatial resolution data limitation is challenging. Nearly 4 × 4 km resolution NEXRAD radar is available for the study area. However, Hourly NEXRAD radar with 4 × 4 km spatial resolution has shown some

potential for operational use in urban scale watersheds in the USA [102]. After pixel averaging to limit the wind drift, the resolution of WKR is ~3 ×4 km. The pixels averaging was performed following the advice of severe weather scientists at WKR radar station, who has a long time of hands-on experience on WKR radar QPEs. Even though spatial sampling error increases with pixel averaging, the effect decreases with increasing accumulation time and, therefore, relatively low at a longer time scale [52]. Moreover, on a 1261 km^2 (Humber River—911 km^2 + Don River—350 km^2) grid, the radar provides better spatial resolution than gauges. For Humber River watershed and Don River watershed, the WKR C-band radar gives the equivalent of about ~75 and ~29 rain gauges across the basins, respectively. In contrast, the rain gauges yield 12 and 3 measurements (Figure 4-1). The NEXRAD S-band radar provides the equivalent of about ~56 and ~21 rain gauges across the Humber River and Don River basins, respectively. In addition, the use of radar QPE resolution mentioned earlier might save on computation time, facilitating the operational flood forecasting.

The performance of merging techniques was assessed by calculating the Pearson's correlation coefficient (r) (Equation (4-20)), BIAS (%) (Equation (4-21)), MAE (mm) (Equation (4-22)), and RMSE (mm) (Equation (4-23)) metrics for reference gauges measuring 'true' rainfall for all events together and each event separately. A metric called RMSF (dB) (Equation (4-24)) was also calculated because the RMSE overstates relatively significant differences that may be caused by inaccurate data [80].

Correlation (r)

$$\text{Correlation} = \frac{\sum(P_G - \bar{P}_G)(P_R - \bar{P}_R)}{\sqrt{\sum (P_G - \bar{P}_G)^2 \sum (P_R - \bar{P}_R)^2}} \quad (4\text{-}20)$$

BIAS (%)

$$\text{BIAS} = \frac{\sum P_R - \sum P_G}{\sum P_G} \tag{4-21}$$

MAE (mm)

$$\text{MAE} = \frac{\sum_{i=1}^{N} |R_i - G_i|}{N} \tag{4-22}$$

RMSE (mm)

$$\text{RMSE} = \sqrt{\frac{\sum_{i=1}^{n} (P_G - P_R)^2}{N}} \tag{4-23}$$

RMSF (dB)

$$\text{RMSF} = \sqrt{\frac{\sum_{i=1}^{N} \left(10 \log \frac{R_i}{G_i}\right)^2}{N}} \tag{4-24}$$

where,

P_G is gauge measurement, $\bar{P}_G$ is average gauge measurement, P_R is radar rainfall, $\bar{P}_R$ is average radar rainfall, and N is the number of radar-gauge pairs data available.

The following flow chart (Figure 4-2) provides an overview of the methods and evaluation process for this study.

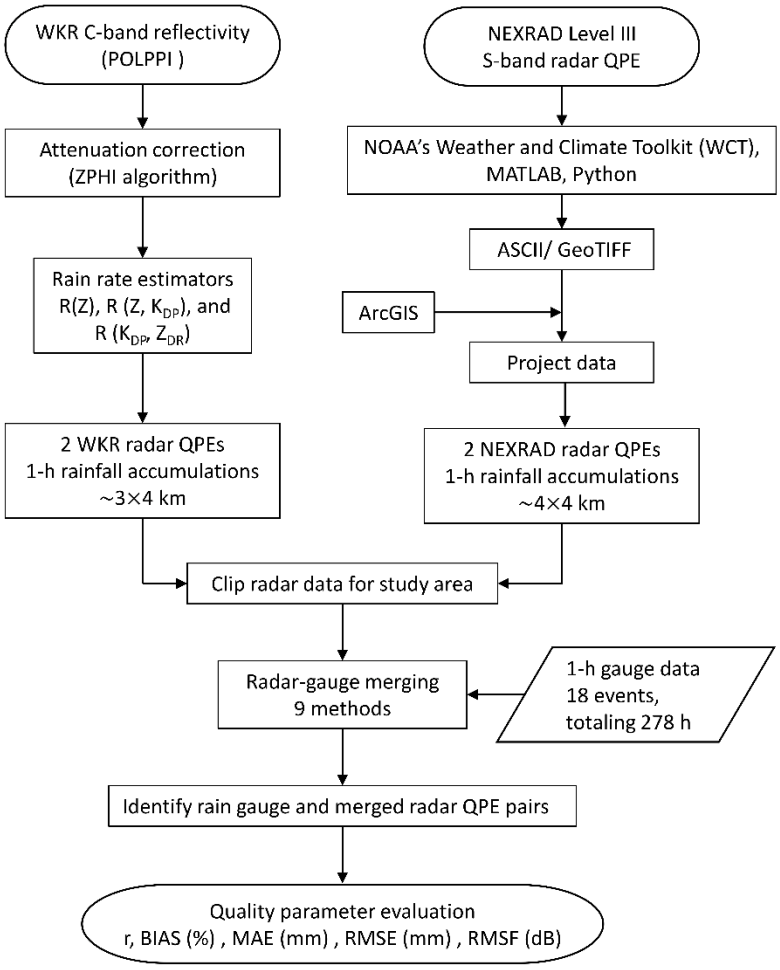

Figure 4-2 *Flow chart showing an overview of the methods and evaluation process*

4.5. Results and Discussion

Figure 4-3 shows the average RMSE (mm), MAE (mm), BIAS (%), correlation (r), and RMSF(dB) of the radar only QPE and merged radar QPE values for 278 h (i.e., all events) at grid point nearest to gauge point of King City WKR C-band radar and corresponding grid cell of KBUF NEXRAD S-band radar. The agreement between gauge observations and radar QPEs has been improved after applying radar-gauge merging; however, the degree of improvement varies for each method as well as for each radar

QPE (Figure 4-3). Overall, the CDFM method appears as the best performing method followed by KRE among nine merging techniques used in this study. Matching the CDFs of radar and gauge data sets based on polynomial fitting 1–5 was carried out to remove the systematic differences between two data sets. The CDFM method with polynomial fitting 3 appeared to perform best with the least RMSE and highest correlation for all four radar QPEs. The reported average RMSE with polynomial fitting 3 for C1, N1, C2, and N2 is 1.0 mm, 0.8 mm, 0.9 mm, and 1.7 mm, respectively. The correlation values for C1, N1, C2, and N2 recorded after CDFM with the third-degree polynomial model is 0.88, 0.91, 0.89, and 0.89, correspondingly. The existing error after applying CDFM may be caused by the random component of the radar QPE errors that are not removed by the CDFM method. Even though the CDFM method is not often used in radar-gauge merging, it has been successfully applied to bias correct different other gridded hydrological inputs to hydrological models in previous literature such as soil moisture [103–105] and snow depths [106,107]. For example, Leach et al. [106] have reported a significant reduction of average RMSE after applying CDFM bias correction for Snow Data Assimilation System (SNODAS) snow depths (67.30 mm to 38.45 mm) as well as SNODAS snow water equivalent data (SWE) (19.99 mm to 5.19 mm). A significant improvement of average NSE for SNODAS snow depths (0.24 to 0.76) and SNODAS snow water equivalent data (−5.7 to 0.55) have also been reported. Furthermore, a mean correlation of 0.87 $\pm$ 0.02 and mean RMSE of 0.05 $\pm$ 0.02 was reported after CDF matching between soil moisture and ocean salinity (SMOS) microwave radiometer and local soil moisture observations [104]. Although the CDFM method is not very common

in radar-gauge merging, results suggest that it can be successfully used to match radar QPEs with gauge observations. The KRE method shows the second-best performance in terms of matrices calculated for all events. In this study, a bounded linear function that can be fitted to the experimental variogram model was used, and the data are assumed to be isotropic. Other unbounded functions stable, exponential, and Gaussian were also explored in the study to perform Kriging. Several bounded functions, including circular, spherical, pentaspherical, were also explored with gauge observations to find the best method to be used for radar-gauge merging. The bounded linear variogram outperforms all other variogram models with a recorded correlation of 0.88, BIAS of −1.05%, RMSE of 1.7 mm, and MAE of 0.8 mm. Both KBUF NEXRAD S-band (N1 and N2) and WKR C-band radar (C1 and C2) have been enhanced after application of radar-gauge merging; nevertheless, the degree of improvement differs for each radar QPE.

In comparison with the radar only QPEs, the RMSE decrease is apparent for all the radar-gauge merging methods (Figure 4-3). The percent decrease of RMSE compared to radar only QPEs for C1, N1, C2, and N2 ranges from 79.85% to 90.50% after applying the CDFM method (Table 4-3). The NEXRAD Level III (DPA) shows the highest percent decrease, followed by WKR C-band multi-parameter rain rate estimator using K_{DP} and $Z_{DR.}$ All radar-gauge merging methods effectively reduced the RMSE by more than 50% for C1, C2, and N1 except for MFB-maf and MBSA (Table 4-3). The recorded RMSF has been reduced for all four radar QPEs after applying all radar-gauge merging methods. In contrast to RMSE, N2 shows relatively higher RMSF decrement compared to the other three radar QPEs, especially after MFB-mfb, MFB-maf, RDA, and FIC-GG with greater

than 70% (Table 4-3). As mentioned before, RMSE inflates relatively significant differences that may be caused by inaccurate data that leads to anomalous values. The anomalous reflectivity values caused by the bright band effect may have caused the discrepancies in RMSE for N2. There is a high possibility for NEXRAD to measure reflectivity at the height of the bright band because the KBUF NEXRAD measures the precipitation relatively far (~106 km) from the watershed making a discrepancy in sampling heights between KBUF NEXRAD S-band and WKR C-band reflectivity measurements.

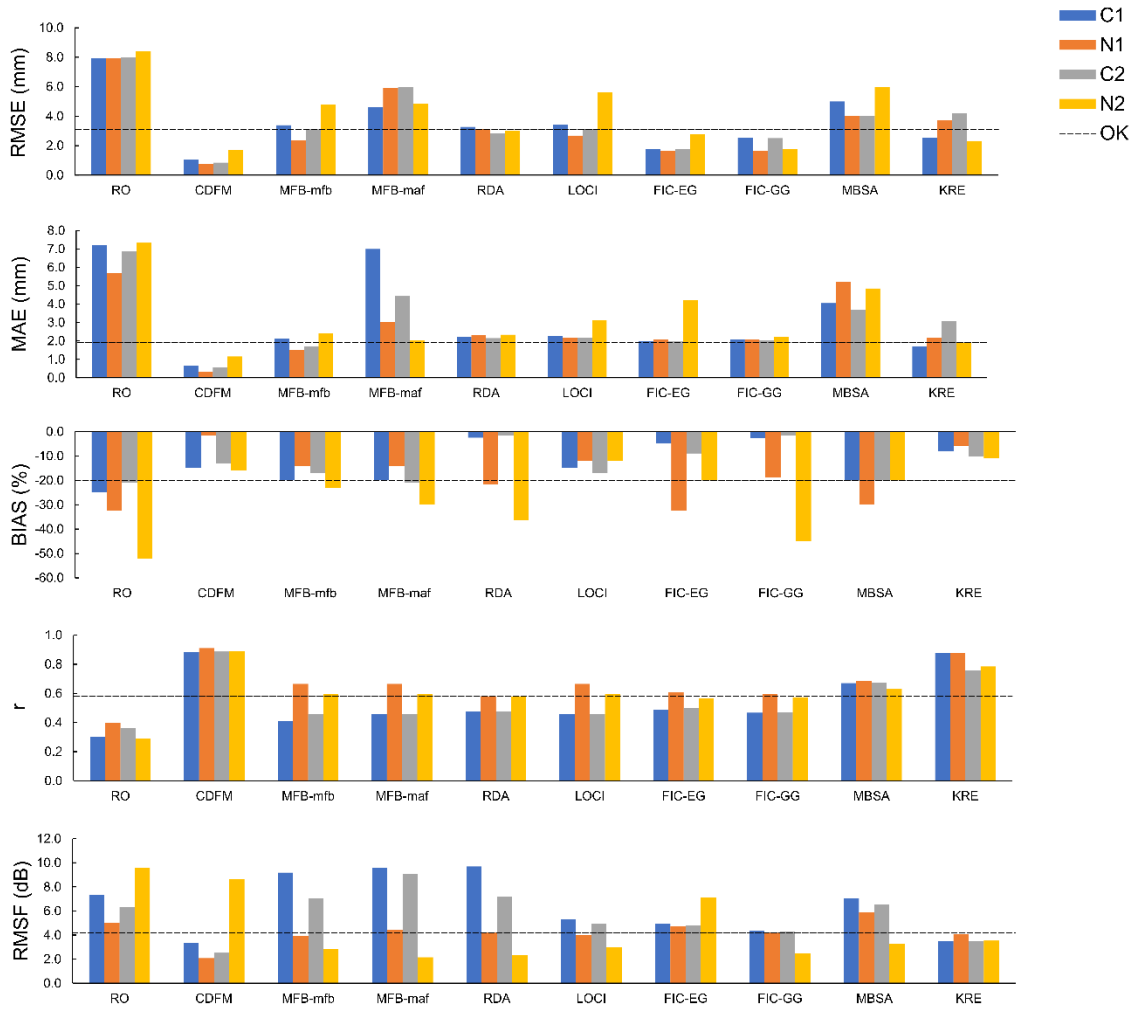

Figure 4-3 *RMSE (mm), MAE (mm), BIAS (%), correlation (r), and RMSF of all radar-gauge merging methods*

As seen in Figure 4-3, the MAE is considerably reduced after radar-gauge merging for all methods used in the study. All four radar QPEs have been improved except for MFB-mfb for C1. Reported MAE after RDA and FIC-GG merging methods are relatively similar for all radar QPEs. Reported MAE values for C1, N1, C2, and N2 are 2.21 mm, 2.32 mm, 2.15 mm, and 2.34 mm respectively after RDA and 2.07 mm, 2.08 mm, 2.03 mm, and 2.21 mm after applying FIC-GG. The highest percent decrease of

MAE is recorded after CDFM with greater than 90% decrement percent for C1, C2, and N1 (Table 4-3). Most of the methods effectively reduced the MAE (>50% percent decrease) for both WKR C-band and NEXRAD S-band radar QPEs except for MFB-maf and MBSA.

The average negative (underestimation) BIAS for all radar QPEs has been reduced after applying radar-gauge merging; however, the degree of bias reduction varies for each method as well as for each radar QPE (Figure 4-3). The BIAS is relatively higher for both KBUF NEXRAD S-band radar before and after radar-gauge merging (Figure 4-3). After radar-gauge merging, the KRE method shows low BIAS with relatively persistent (average value ranges between −5% and −15%) values for each radar QPE. The persistent bias can be adjusted through hydrological model calibration [108].

The correlation between radar QPEs and gauge measurements has considerably increased after applying radar-gauge merging techniques (Figure 4-3). The correlation values after radar-gauge merging for all four radar QPEs are relatively high and persistent for the CDFM method compared to other methods. The percent increase of r values is higher than 100% for all four radar QPEs after bias correcting using the CDFM method (Table 4-3). After the CDFM method, a relatively complex KRE method shows the highest correlations between radar and gauge measurements with reported r values of 0.88, 0.87, 0.76, and 0.78 respectively for C1, N1, C2, and N2. The percent increase of r values for all four radar QPEs for the KRE method is also higher than 100% (Table 4-3). The KRE method outperforms simple radar-gauge merging methods because it uses optimal interpolation to combine gauge and radar observations while taking the

covariance structure of the data into account to reduce bias as well as to minimize variance [52]. The MBSA method that uses a negative exponential weighing method (Barnes's objective analysis) to interpolate differences in radar and gauge measurements performs well after KRE with relatively high and consistent correlation values for all four radar QPEs (Figure 4-3). The correlation values for all four radar QPEs after application of MFB-mfb, MFB-maf, RDA, LOCI, FIC-EG, and FIC-GG methods show similar and relatively satisfactory performances with r values range from 0.40 to 0.60 and relatively high percent increments (Table 4-3). The simple methods such as MFB can significantly improve radar QPEs and therefore remains one of the most commonly used radar-gauge merging methods for operational applications, especially in many national meteorological services [52,60,65]. Contrasting the MFB adjustment, the RDA method assumes radar QPE error surges with distance from the radar tower because of beam broadening and overshooting, and therefore improves KBUF NEXRAD than WKR C-band radar QPEs (Figure 4-3).

Moreover, after radar-gauge merging, the correlation values decrease for radar QPEs as N1 > N2 > C2 ≈ C1. Among four radar QPEs, the correlation is much improved after applying bias correction for N2 compared to the other three radar QPEs and ranges from 94.97% to 206.89% (Table 4-3). For example, the correlation value of 0.29 between raw radar and gauge before bias correction is improved to 0.89, with the percent increment associated is 206.89% (Table 4-3) after applying CDFM. Apart from the CDFM method, all the other methods show a percent increment of greater than 90% for N2 (Table 4-3). Improvement is apparent for N2 after applying KRE with recorded

highest percent decrement of RMSE, BIAS, RMSF, and MAE, and the second-highest percent increment of the correlation (Table 4-3). The N2 shows the worst performances compared to other radar QPEs before radar-gauge adjustment with recorded RMSE, MAE, BIAS, r, and RMSF of 8.4 mm, 7.3 mm, −52.01%, 0.29, and 9.6 dB, respectively.

Overall, as seen in Figure 4-3, the CDFM and KRE methods perform better than gauge only OK. However, the OK method provided precipitation estimates with a similar or better magnitude of accuracy as other radar-gauge merging techniques. The OK method shows a better magnitude of accuracy than all four radars only QPEs. The estimated matrices for gauge only OK method display similar matrices to other radar-gauge merging techniques MFB, RDA, LOCI, FIC, and MBSA. As mentioned before, the rain gauge network density is relatively high for both Humber River and Don River watersheds with one gauge per 75 km^2 and one gauge per 116 km^2, respectively. The noticeable accuracy of gauge only OK is attributed to the proximity of merged gauge stations to verification gauges. The distance between the verification gauge and the nearest merged gauge in the study area varies from 3.5 km to 9.5 km. Since gauge only OK method performs better than radar only QPEs, radar QPEs must be adjusted with gauge measurements before using them as precipitation inputs to get the additional benefit added by radar QPEs.

Table 4-3 *Percentage of change of RMSE, BIAS, Correlation, RMSF, and MAE after application of radar-gauge merging methods*

Merging Method	RMSE Decrease (%)				BIAS Decrease (%)				r Increase (%)			
	C1	N1	C2	N2	C1	N1	C2	N2	C1	N1	C2	N2
CDFM	86.94	90.50	89.41	79.85	14.86	94.72	3.76	50.01	193.83	127.50	146.43	206.89
MFB-mfb	57.25	70.51	60.71	43.15	20.00	56.64	19.05	55.78	37.02	66.08	27.64	105.87
MFB-maf	42.14	25.26	25.00	22.40	20.00	56.64	10.00	42.32	52.60	66.08	27.64	105.87
RDA	58.73	60.23	64.26	63.86	89.94	32.61	92.56	30.11	49.03	54.85	32.68	99.65
LOCI	57.14	66.10	60.62	53.07	40.00	62.55	19.05	76.75	52.65	66.08	27.69	105.87
FIC-EG	77.70	79.47	78.22	66.74	96.96	10.00	94.90	61.55	62.81	51.68	39.30	94.97
FIC-GG	68.32	79.31	68.66	59.21	89.29	41.72	91.68	13.54	55.70	49.39	30.11	98.09
MBSA	37.11	49.48	50.00	28.57	20.00	7.09	4.76	61.55	123.40	70.70	86.48	116.85
KRE	68.14	53.23	57.50	78.31	67.90	71.42	51.23	78.85	191.87	118.66	111.11	170.57

Merging Method	RMSF Decrease (%)				MAE Decrease (%)			
	C1	N1	C2	N2	C1	N1	C2	N2
CDFM	54.46	58.52	59.94	9.78	91.06	94.17	91.98	84.23
MFB-mfb	24.71	21.22	11.58	70.32	70.61	73.28	75.36	67.04
MFB-maf	30.00	11.09	44.33	77.50	3.07	46.99	35.30	72.10
RDA	31.78	15.81	13.91	75.88	69.38	59.36	68.65	68.04
LOCI	28.26	19.99	21.33	69.05	68.40	61.87	68.02	57.11
FIC-EG	33.13	5.45	23.60	25.80	72.21	63.59	71.31	52.23
FIC-GG	40.52	16.38	31.87	73.81	71.35	63.59	70.34	69.80
MBSA	3.95	17.81	3.65	65.66	43.82	8.45	45.98	33.76
KRE	52.16	18.97	44.71	63.07	76.46	61.83	55.14	78.00

1.00
25.00
50.00
75.00
100.00
125.00
150.00
200.00
(%)

Figure 4-4 compares the box and whisker plots of gauge measurements with each of the radar QPEs after the application of radar-gauge merging. The interquartile range (IQR) for merged radar QPEs is at the same level as reference gauge measurements and overlaps with one another for C1, C2, and N1 for all radar-gauge merging methods. Additionally, the median of C1, C2, and N1 lies within the IQR of the gauge measurements. The first quartile, median, third quartile, and the range of C1, C2, and N1 nearly tie-up with gauge measurements, implying that all radar-gauge merging methods perform evenly well for C1, C2, and N1. The first quartile, median, third quartile, and the range of N1 after applying CDFM methods match the gauge measurements implying that N1 with the CDFM method can be used as an additional source of precipitation for hydrological model calibration with high confidence. The IQR for N2 does not overlap with reference gauge or with C1, C2, and N1 for all radar-gauge merging methods except for the KRE method. For example, after FIC-EG correction, the IQR for N2 is entirely above the reference gauge measurements as well as C1, C2, and N1. Additionally, its median always lies either below or above IQR of gauge and other radar QPEs except for KRE. Therefore, it can be concluded that radar-gauge merging methods work relatively better on C1, C2, and N1 compared to N2. However, after applying KRE, the IQR of N2 overlaps with gauge measurements and other radar QPEs. The median after KRE bias correction lies within IQR of the gauge data as well as C1, C2, and N1. Therefore, the KRE method performs well for all radar QPEs compared to other methods.

As mentioned above, the N2 QPEs are unstable for radar-gauge merging methods except for KRE. The percent detection (d) of precipitation was calculated for radar only

QPEs using the following equation to find out the capability of each radar QPE to capture the precipitation compared to gauges.

Detection (d)

$$\mathrm{d} = \frac{n_{P_R} > 0, n_{P_G} > thresh}{n_{P_G} > thresh} \times 100 \quad (4\text{-}25)$$

where,

P_G is gauge measurement, $\bar{P}_G$ is average gauge measurement, P_R is radar rainfall, $\bar{P}_R$ is average radar rainfall, $n_{P_R} > 0, n_{P_G} > thresh$, number of radar-gauge pairs that the radar records precipitation and the corresponding gauge observation exceeds the specified threshold (0 mm); and $n_{P_G} > thresh$, number of radar-gauge pairs where the gauge value exceeds the specified threshold (>0 mm).

The calculated percent detection for C1, C2, N1, and N2 are 84%, 84%, 78%, and 58%. The detection is relatively higher for WKR radar only QPEs than NEXRAD radar QPEs. The detection for N1 is better than N2. The WKR radar measures the precipitation at a distance of 37 km away from the greatest edge of the watershed and therefore shows high detection whereas the KBUF NEXRAD measures the precipitation ~106 km away from the watershed resulting lower detection of precipitation. The low detection of N2 partially causes the worst performances compared to other radar QPEs used in the study. However, the KRE method uses radar observations of rainfall to assess the errors using Kriging to interpolate between the rain gauge observations and then condition the Kriged gauge field accordingly. Unlike bias reduction methods, the KRE method uses the spatial association of the radar rainfall field to support the interpolation of gauge measurements. Since it interpolates rainfall between radar and gauges, the missing values are infilled

during the radar-gauge merging process. The spatial variability observed by the radar is retained while reducing variance using the optimal information content in the vicinity of the gauges where they provide accurate information on the exact rainfall field using Kriging interpolation. The infilling using Kriging has caused relatively significant improvement of N2 radar QPEs compared to other radar QPEs. It is beneficial, especially for hydrological model calibration, where a continuous precipitation time series is often necessary. As suggested by Zhang et al. [109], the lack of detection is difficult to address during the calibration of hydrologic models. Therefore, the KRE method is recommended if the original data suffers from missing data.

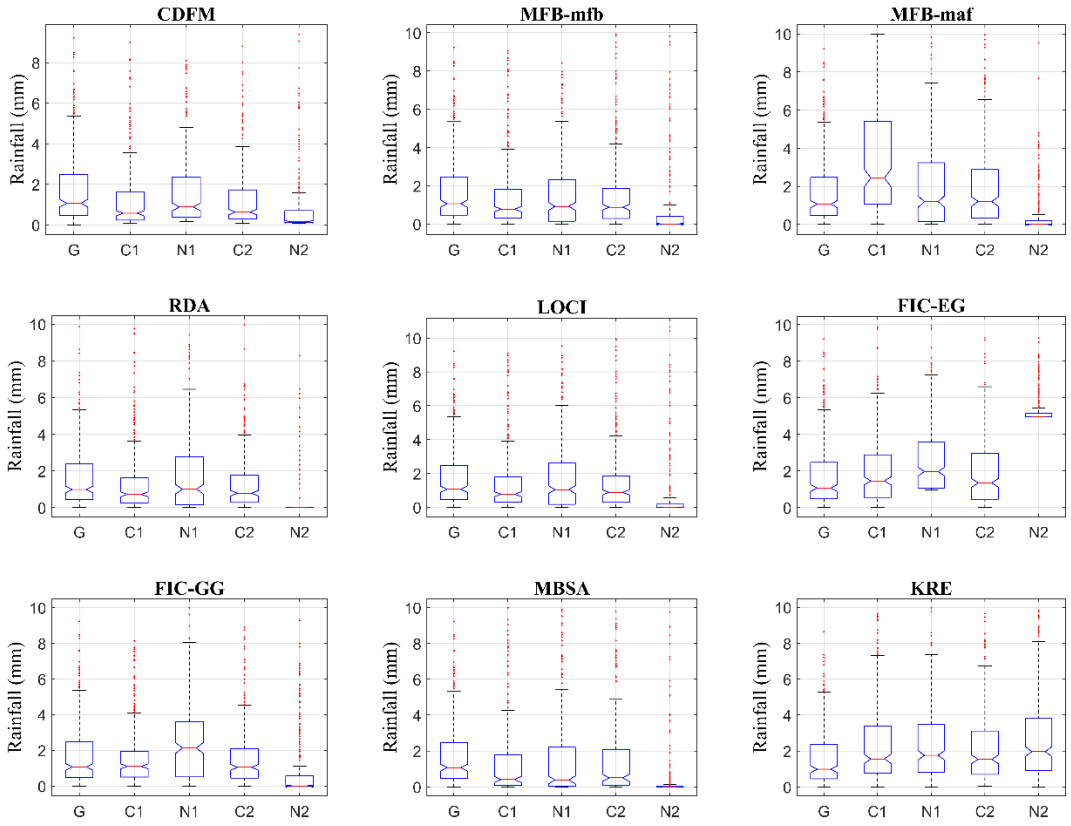

Figure 4-4 *Box plots showing the distribution of precipitation values after radar-gauge merging for Gauge (G), C1, N1, C2, and N2*

Figure 4-5 shows the hourly radar rainfall accumulations before and after radar-gauge merging for all four radar QPEs for the 278 h of analysis (i.e., all events) and plotted against the gauge hourly accumulations. The scatter plots illustrate the relative strengths of each radar-gauge merging method at different rain intensities. The unbiased radar precipitation estimates are indicated by the one-to-one line (dotted line). In general, hourly precipitation values are more clustered along the one-to-one line after the application of radar-gauge merging when compared to the radar-only QPEs. Therefore, all radar-gauge merging methods are effective in adjusting radar QPEs to match with observed gauge measures. The CDFM and KRE methods generally perform well compared to the gauge observation followed by MBSA. However, the KRE method slightly overestimates the gauge measurements. The QPEs are much closer to the one-to-one line for all four radar QPEs for precipitation intensities ranges from 1 mm/h to 10 mm/h, especially after the application of CDFM methods. The KRE method performs reasonably well for all intensities as well as for all four radar QPEs. However, the agreement is relatively low for precipitation less than 1 mm/h and has become progressively worse with higher rainfall intensities. In heavy intensity rainfall events, the path attenuation affects reflectivity values and, ultimately, radar estimates precipitation [33]. Even though attenuation is addressed using the ZPHI algorithm for all methods, the attenuation correction can be possibly overshadowed by the extensive radome attenuation at WKR C-band radar station, resulting in poor rainfall estimates [33]. The CDFM method performs reasonably well for a wide range of intensities, including intensity > 10 mm/h. However, the CDMF method overestimates lower accumulation amounts.

A similar overestimation is observed for the remaining radar-gauge merging methods as well. Even though a degree of scattering occurs between radar QPEs and gauge reported precipitation for hourly data after application of radar-gauge merging, less scatter is observed for N1 compared to C1, C2, and N2. Even though N2 shows acceptable performance after application of CDFM radar-gauge merging, some inconsistencies at the medium and higher intensities exist. This inconsistency may result due to the lack of detection of precipitation from NEXRAD S-band radar compared to WKR C-band as the two watersheds are closer to the WKR C-band radar than the KBUF NEXRAD radar. Although the WKR radar suffers from attenuation of return echoes, the detection is high as WKR radar measures the precipitation at a distance of ~37 km at the furthest edge of the watershed. For N2, the low detection has been successfully addressed by applying the KRE method as most of the values after KRE correction plotted close to the one-to-one line.

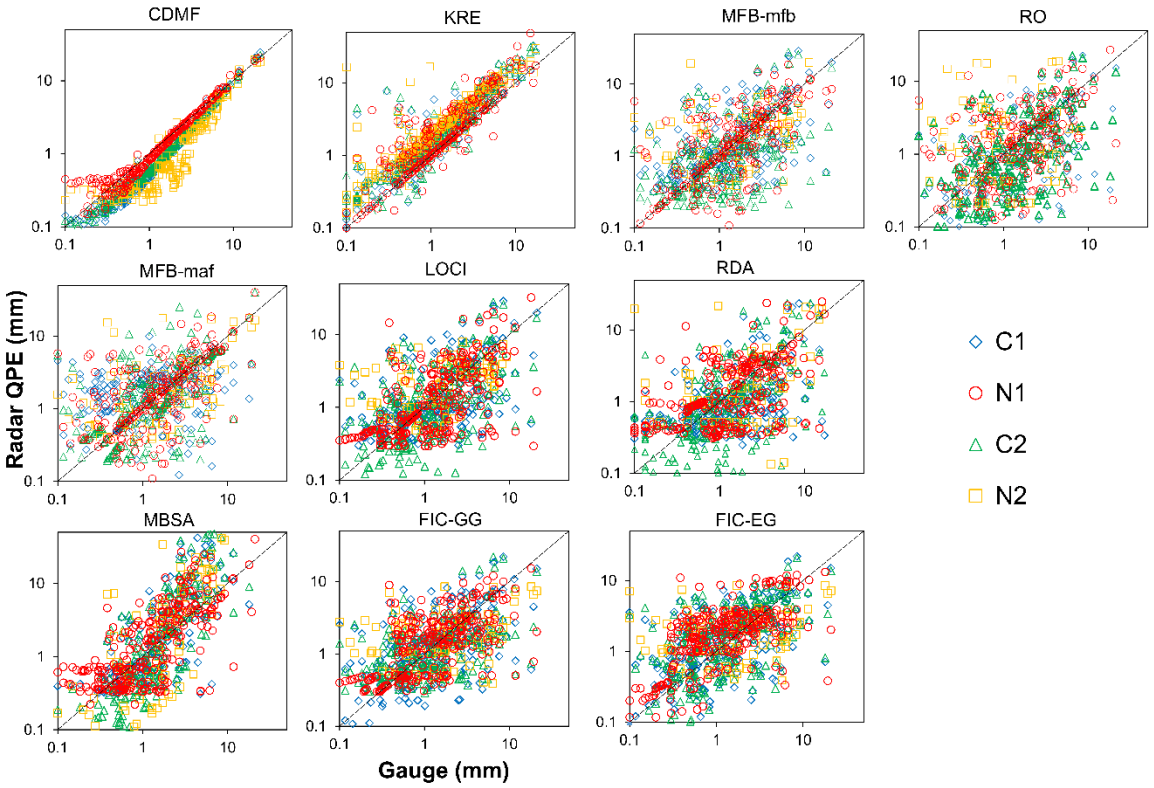

Figure 4-5 *Scatterplots of radar quantitative precipitation estimate (QPE) hourly accumulations as a function of the hourly gauge accumulations before and after radar-gauge merging (Note: both horizontal and vertical axes are in log scale)*

The average correlation between WKR C-band and KBUF NEXRAD S-band radar QPEs and gauge observations before and after radar-gauge merging for each event are presented in Figure 4-6a–d. Overall, the correlation is relatively higher for all four radar QPEs (C1: 0.24–0.96; C2: 0.25–0.96; N1: 0.45–0.97; N2: 0.10–0.94) compared to radar only QPEs (C1: 0.01–0.80; C2: 0.00–0.79; N1: 0.05–0.74; N2: 0.0–0.46) after applying radar-gauge merging methods. The correlation values vary from event to event. The average correlation for 18 events for QPEs from C1, C2, and N1 after applying the CDFM method is superior to other radar-gauge methods for all events followed by KRE

and MBSA (Figure 4-6a–c). The correlation values vary considerably between different radar QPEs as well as between different events before the application of radar-gauge merging. As can be seen in Figure 4-6, after radar-gauge merging, the correlation values are approximately similar for all radar QPEs as well as for all events, especially after CDFM. Correlation values range from 0.80 to 0.99 for all events after applying the CDFM method for C1, C2, and N1. However, for N2, the CDFM method shows some inconsistencies (Figure 4-6d), and this may be due to the lack of detection, as discussed before. The KRE method shows a higher correlation with gauge data compared to other radar-gauge merging methods followed by CDFM and MBSA for N2 (Figure 4-6d). Even though MFB, RDA, LOCI, FIC methods show higher correlation values after radar-gauge merging for 278 h (i.e., all events) compared to radar only QPEs, relatively low or no improvement is observed for each event separately for C1, C2, and N2. However, all radar-gauge merging techniques show a considerable increase in correlation values for four summer events 13, 14, 15, and 16 and relatively low but substantial improvements for summer events 3, 4, and 10 for N1 (Figure 4-6b). The radar-gauge merging is relatively effective for events in summer than fall and spring, especially for N1. The performances of radar-gauge merging methods and, eventually, the quality of merged rainfall products is affected by the quality of original radar QPE products [68]. The recorded RMSE and Correlation values before radar-gauge merging for N1 is relatively good compared to other raw radar QPEs of C1, C2, and N2. This quality of N1 radar QPEs may have affected for successful merging in N1. On the other hand, the bright band effect might have affected the quality of radar QPEs in early spring, and late fall, and

apparently, the radar-gauge merging is not able to improve the radar precipitation estimates successfully.

Figure 4-6e–h shows the average RMSE between radar-gauge hourly accumulation pairs before (RO) and after applying radar-gauge merging for radar QPEs for each event separately. Calculated RMSE shows the same trend as the correlation values and varies from event to event. Generally, the RMSE is relatively lower for all four radar QPEs compared to raw radar QPEs after applying radar-gauge merging. The average RMSE for QPEs from all four radar QPEs after applying CDFM method (C1: 0.4–12.0 mm; C2: 0.3–13.0; N1: 0.6–12.1 mm; N2: 0.0–13.0 mm) are superior to other radar-gauge methods compared to radar only QPEs (C1: 1.7–18.0 mm; C2: 3.1–15.1 mm; N1: 1.1–15.0 mm; N2: 1.2–15.0 mm) for all events. The RMSE values vary substantially between different radar QPEs as well as between different events before the application of radar-gauge merging. Even though RMSE is reduced after radar-gauge merging, RMSE is nonetheless high for high-intensity events (e.g., events 3 and 5) and relatively small in low-intensity events (e.g., events 7, 12, and 18). Although radar-gauge merging reduces the RMSE, above mentioned limitations in radar precipitation estimates [23,41] impede the accuracy and reliability of radar QPEs.

As indicated in the matrices for 278 h (i.e., all events), the gauge only OK method shows relatively better performances than radar only QPEs for separate events in terms of r and RMSE (Figure 4-6). After applying the CDFM, KRE, and MBSA merging techniques to C1, C2, and N1 show better performances than the OK method. As stated before, a relatively high dense gauge network may result in a better magnitude of

accuracy for OK than MFB, RDA, FIC, and LOCI radar-gauge merging techniques. The outperformance of rain gauge alone OK could be due to the ability of the high-density gauge network to describe the spatial variability in the precipitation field. For every event, radar QPEs adds additional value only after applying radar-gauge merging. Therefore, radar only QPEs must be adjusted with the appropriate merging technique before using them as additional precipitation source for event-based hydrological models for operational flood forecasting.

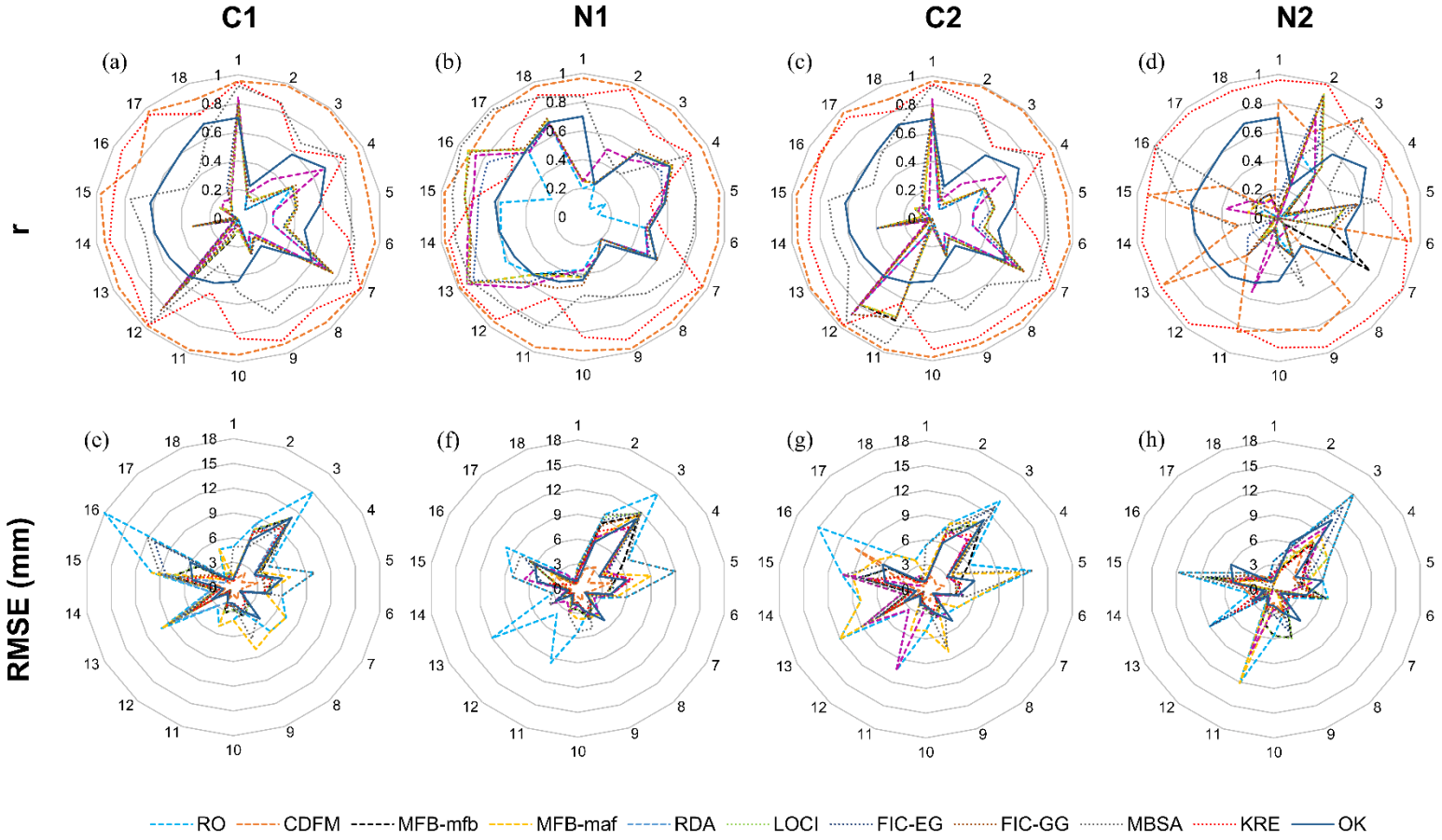

Figure 4-6 *Average correlation (a–d) and RMSE (e–h) between the hourly accumulation of merged radar QPEs and gauge measurements for each event. Note: Summer events: 1, 3, 4, 5, 9, 10, and 13-17; Spring events: 2, 7, and 8; Fall events: 6, 11, 12, and 18*

Figure 4-7 shows an example of radar-gauge merging results after applying the KRE method. The figure shows the spatial distribution of accumulated precipitation derived from radar-gauge merging using KRE for the event 3 took place from 8 July 2013 1800 UTC to 9 July 2013 0200 UTC. It compares the difference between the gauge (G), NEXRAD radar only QPEs (RO), and KRE merged QPE (KRE). The KRE precipitation field display features from both gauges and radar only QPE. Additional information is reported after applying the KRE method in the areas where the gauges' record precipitation, but the radar only QPEs is uncertain. The agreement between the precipitation recorded at the reference gauges and radar QPEs is higher than that of the radar only QPEs, especially in the South-Eastern parts of the watershed.

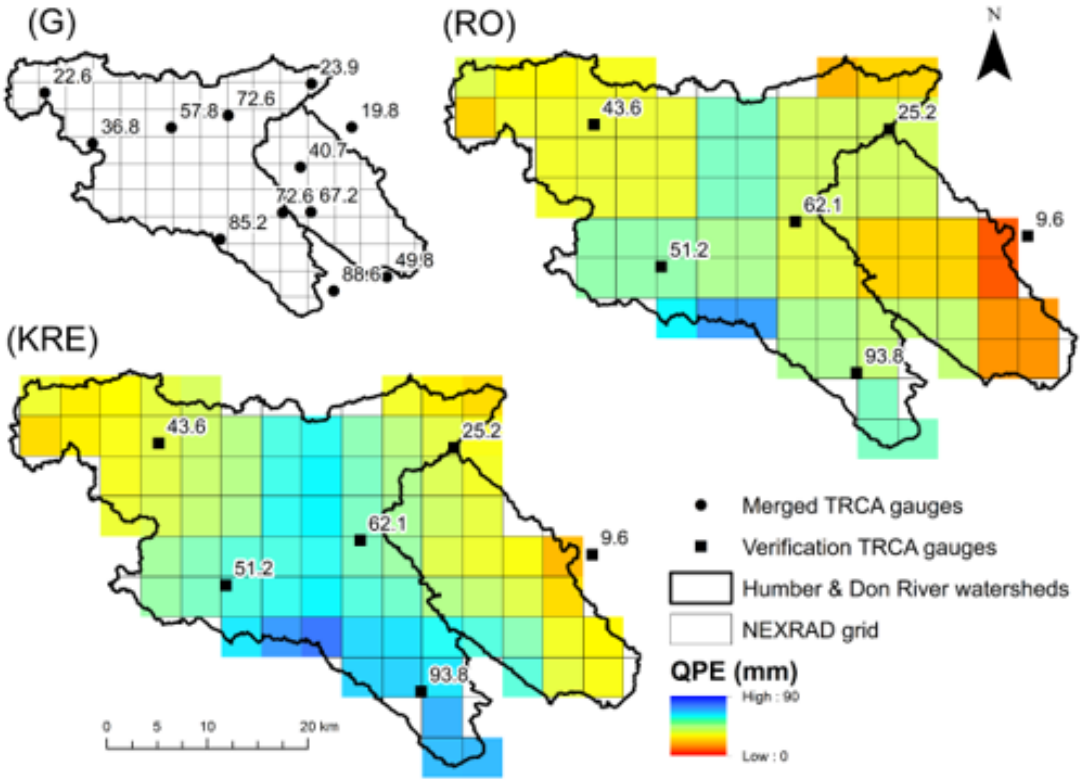

Figure 4-7 *Comparison between the gauge (G), NEXRAD radar only QPEs (RO), and KRE merged QPE (KRE) precipitation field for event 3 (8 July 2013 1800 UTC to 9 July 2013 0200 UTC) The numbers represent observed precipitations at each gauge station in mm*

Besides the factors discussed above, the selection of an optimal radar-gauge merging method is influenced by location-specific environmental and operational factors [53]. Therefore, it is vital to understand the impact of factors such as the density of the gauge network, storm characteristics, proximity to radar tower, response time (time of concentration) of the watersheds, and the time step of adjustment to select appropriate radar-gauge merging technique. The rain gauge density of the semi-urban Humber River and urban Don River watersheds are relatively high, with rain gauge densities of one gauge per ~75 km^2 and one gauge per ~116 km^2, respectively. According to McKee and

Binns [53], rain gauge density can play a significant role in determining the optimal radar-gauge merging method. Highly dense rain gauge networks can sometimes characterize the spatial variability in the rainfall field and hence adequately increase the confidence in radar-gauge merging methods. For example, Goudenhoofdt and Delobbe [52] studied the sensitivity of radar-gauge merging methods to rain gauge density and concluded that the decrease in density affects spatial adjustment methods than simple bias reduction techniques. As shown in this study, both bias reduction techniques (CDFM, MFB, MBSA, RDA) and error variance minimization techniques (KRE) produce better results because of the high dense gauge network. The characteristics of the storm, such as intensity, also affect the accuracy of radar-gauge merging [110]. The results of this study also suggest that only the CDFM method and KRE method show better agreement between observed gauge measures and merged radar QPEs for a wide range of intensities; however, the agreement is deteriorated for all other methods with increasing the intensity. Furthermore, the proximity to the radar tower affects the accuracy of radar-gauge merging in two separate ways. Firstly, the accuracy of the radar-estimated precipitation and the radar-gauge merging methods deteriorate with increasing distance from the radar tower. Secondly, low detections of KBUF NEXRAD radar compared to WKR C-band radar due to beam broadening, beam overshooting, and beam attenuation affect the raw radar QPE quality, radar-gauge merging techniques, and ultimately merged radar QPEs. After applying RDA to KBUF NEXRAD radar, a substantial improvement was observed compared to WKR C-band radar, especially in terms of correlation. As Gjertsen et al. [80] suggested, relatively small urban basins with a time of concentration on the order of hours

are highly benefitted from radar QPEs that require rainfall estimation on small spatial and temporal scales. Therefore, the time step of the radar-gauge merging plays a vital role in selecting radar-gauge merging methods for urban watersheds. For more extended periods (e.g., daily or event-based temporal resolutions), the magnitude of spatiotemporal sampling errors become stable because error fluctuations are averaged over time [53,80]. Even though the errors are reduced, short-term variations are missed affecting the accuracy of merged radar QPEs. In this study, an hourly time-step is used, because the study targets operational flood forecasting in urban watersheds where response time is on the range of hours. Since radar-gauge merging is performed in hourly time-step, spatially dependent bias correction method KRE works better than bias reduction method MFB. The variations between radar and gauges are more pronounced in shorter time steps, and therefore more weight is placed on the gauge observations when error variance methods such as KRE are used. Bias reduction methods such as MFB averaged out these variations and hence produced less accurate merged radar QPEs compared to KRE. Apart from all the above-mentioned factors, data management, and computational requirements must also be considered. The error variance methods, such as KRE, involves higher computational power than simple methods such as MFB. Because of these factors, the results from this study are transferable only between relatively small urban watersheds with similar environmental and operational factors but not between large rural basins.

4.6. Conclusions

Various methods combining QPEs from the dual-polarized WKR C-band and KBUF NEXRAD S-band operational radars and precipitation data from a rain gauge

network have been implemented for two watersheds in the GTA, Ontario, Canada—the semi-urban Humber River, and the urban Don River. A comparison of nine radar-gauge merging techniques is conducted using 18 rainfall events, occurring from 2012-2017, totaling 278 h (i.e., all events), against an independent gauge network of hourly rainfall measurements. Additionally, this study has investigated the impact of the quality and quantity of different radar QPEs on the performance of radar-gauge merging. Several statistical measures, Correlation (r), BIAS (%), MAE (mm), RMSE (mm), and RMSF (dB), have been computed to evaluate the performance of selected radar-gauge merging methods.

Based on the verification study, all radar-gauge merging methods outperformed radar only QPEs alone. However, performance varies for each radar method as well as for different radar QPEs. The CDFM method with polynomial fitting 3 is the best performing method, followed by KRE. Since the KRE method uses information from radar to interpolate gauge data, it can be effectively used to merge radar QPEs with missing gauge values. The persistent bias reported using the KRE method could be addressed adequately during hydrological model calibration. If the distance from the radar tower to gauges in the watershed changes drastically, the RDA method that takes distance from the radar tower into account during radar-gauge merging is recommended. A relatively simple MFB method shows satisfactory performances along with reduced computational demand. Since radar-gauge merging primarily addresses the systematic errors, the inevitable random error component of the radar QPE errors is responsible for most of the existing differences between merged radar QPEs and reference gauge observations. The

gauge-only OK method outperforms radar only QPEs, as well as several merged QPEs because of its ability to characterize the spatial variability in the precipitation field using the high dense gauge network.

The effectiveness of various radar-gauge merging methods and, ultimately, the quality of merged radar QPEs are affected by the quality and quantity of the radar only QPEs. Both NEXRAD S-band and WKR C-band radar QPEs have been improved after radar-gauge merging; however, the NEXRAD Level III (DPA) showed the most improvement. For that reason, all types of corrections for errors such as attenuation, VPR effect, etc. must be applied to improve raw radar QPEs before applying radar-gauge merging. Both merged NEXRAD and WKR radar QPEs show acceptable agreement between reference gauges and, therefore, can be used as an additional data source for hydrological model calibration with high confidence. All merged radar QPEs performed well in predicting for low and medium intensity precipitation from 1 mm/h to 10 mm/h. The CDFM and KRE methods show better performances for a wide range of intensities; nevertheless, performances deteriorate with the increasing rainfall intensities. The event-based evaluation points out that all merged radar QPEs outperformed radar only QPES alone for all 18 events. However, performances improve considerably after applying CDFM, KRE, and MBSA. Radar-gauge merging performed best in the summer season when contamination due to the bright band effect is minimal compared to late fall and early spring.

Since this study addresses systematic spatio-temporal errors at an hourly time step, radar-gauge merging would aid in developing accurate and continuous precipitation

data for hydrological model calibration for flood forecasting purposes at relatively small urban and semi-urban watersheds with a time of concentration on the order of hours. Although the results presented in this study provide some direction on the best methods to use for radar-gauge merging, there is no guarantee that similar performances will be obtained in all other locations in the radar domain. Therefore, it is recommended that additional information about the environmental and operational factors such as rain gauge density, rainfall intensity, proximity to radar tower, the response time of the watershed, and the time step of the radar-gauge merging, be used to select the best-merged radar estimated precipitation. In the future, evaluation of the accuracy, as well as computational demand for radar-gauge merging methods with hydrological models used for operational flood forecasting, is recommended. In addition, the radar-gauge merging methods must be re-evaluated when sub-hourly data is available.

Author Contributions: Conceptualization, D.W., P.C. and S.B.; Methodology, D.W.; Software, D.W., P.C. and S.B.; Formal analysis, D.W.; Investigation, D.W.; Resources, P.C., D.S. and S.B; Data curation, D.W., and S.B.; Writing—Original draft preparation, D.W.; Writing—Review and editing, D.W., P.C., S.B. and D.S; Visualization, D.W.; Supervision, P.C., S.B. and D.S; Project administration, P.C.; Funding acquisition, P.C. All authors have read and agreed to the published version of the manuscript.

Funding: This work was supported by the Natural Science and Engineering Research Council (NSERC) Canadian FloodNet (Grant number: NETGP 451456).

4.7. Acknowledgments:

The WKR C-band radar QPEs used in this study were collected from ECCC while the first author, Dayal Buddika Wijayarathne, was an intern graduate student at Observations-Based Research Section, King City, ECCC. The KBUF NEXRAD S-band radar QPEs were downloaded from the NOAA National Centers for Environmental Information website: https://www.ncdc.noaa.gov/has/HAS.FileAppRouter?datasetname=7000&subqueryby=STATION&applname=&outdest=FILE. Hourly rainfall data were obtained from Toronto and Region Conservation Authority (TRCA; https://trca.ca/). NEXRAD data were processed using an open-source software tool kit NOAA's WCT downloaded from the website: https://www.ncdc.noaa.gov/wct/. Thanks to Andre D.L. Zanchetta and G. Watthewaduge for their help in downloading data and method development. The authors acknowledge three reviewers for their commentaries that helped to improve the manuscript.

Conflicts of Interest: The authors declare no conflict of interest.

4.8. References

1. Balica, S.F.; Popescu, I.; Beevers, L.; Wright, N.G. Parametric and physically based modelling techniques for flood risk and vulnerability assessment: A comparison. *Environ. Model. Softw.* **2013**, *41*, 84–92, doi:10.1016/j.envsoft.2012.11.002.
2. Zahmatkesh, Z.; Kumar Jha, S.; Coulibaly, P.; Stadnyk, T. An overview of river flood forecasting procedures in Canadian watersheds. *Can. Water Resour. J. Rev. Can. Resour. Hydr.* **2019**, *44*, 213–229, doi:10.1080/07011784.2019.1601598.

3. Arduino, G.; Reggiani, P.; Todini, E. Recent advances in flood forecasting and flood risk assessment. *Hydrol. Earth Syst. Sci. Discuss. Eur. Geosci. Union* **2005**, *9*, 280–284.
4. Awol, F.S.; Coulibaly, P.; Tsanis, I.; Unduche, F. Identification of hydrological models for enhanced ensemble reservoir inflow forecasting in a large complex prairie watershed. *Water* **2019**, *11*, 2201, doi:10.3390/w11112201.
5. PC, S.; Nakatani, T.; Misumi, R. The role of the spatial distribution of radar rainfall on hydrological modeling for an urbanized river basin in Japan. *Water* **2019**, *11*, 1703, doi:10.3390/w11081703.
6. Yang, L.; Tian, F.; Niyogi, D. A need to revisit hydrologic responses to urbanization by incorporating the feedback on spatial rainfall patterns. *Urban Clim.* **2015**, *12*, 128–140, doi:10.1016/j.uclim.2015.03.001.
7. McMillan, H.; Jackson, B.; Clark, M.; Kavetski, D.; Woods, R. Rainfall uncertainty in hydrological modelling: An evaluation of multiplicative error models. *J. Hydrol.* **2011**, *400*, 83–94, doi:10.1016/j.jhydrol.2011.01.026.
8. Zhu, D.; Peng, D.Z.; Cluckie, I.D. Statistical analysis of error propagation from radar rainfall to hydrological models. *Hydrol. Earth Syst. Sci.* **2013**, *17*, 1445–1453, doi:10.5194/hess-17-1445-2013.
9. Beven, K. Towards an alternative blueprint for a physically based digitally simulated hydrologic response modelling system. *Hydrol. Process.* **2002**, *16*, 189–206, doi:10.1002/hyp.343.
10. Gilewski, P.; Nawalany, M. Inter-comparison of rain-gauge, radar, and satellite (IMERG GPM) precipitation estimates performance for rainfall-runoff modeling in a mountainous catchment in Poland. *Water* **2018**, *10*, 1665, doi:10.3390/w10111665.
11. Randall, M.; James, R.; James, W.; Finney, K.; Heralall, M. *PCSWMM Real Time Flood Forecasting–Toronto, Canada*; CUNY: New York, USA, 2014.
12. Dhiram, K.; Wang, Z. Evaluation on radar reflectivity-rainfall Rate (ZR) relationships for guyana. *Sciences* **2016**, *6*, 489–499, doi:10.4236/acs.2016.64039.

13. Thorndahl, S.; Einfalt, T.; Willems, P.; Nielsen, J.E.; ten Veldhuis, M.-C.; Arnbjerg-Nielsen, K.; Rasmussen, M.R.; Molnar, P. Weather radar rainfall data in urban hydrology. *Hydrol. Earth Syst. Sci. Discuss.* **2016**, *21*, 1359–1380, doi:10.5194/hess-21-1359-2017.
14. Beneti, C.; Calheiros, R.V.; Sorribas, M.; Calvetti, L.; Oliveira, C.; Rozin, N.; Ruviaro, J. Operational hydrological modelling of small watershed using QPE from Dual-Pol radar in brazil. *Preprints* **2019**, 2019060026, doi:10.20944/preprints201906.0026.v1.
15. Khan, S.I.; Flamig, Z.; Hong, Y. Flood Monitoring System Using Distributed Hydrologic Modeling for Indus River Basin. In *Indus River Basin*; Elsevier: Amsterdam, The Netherlands, 2019; pp. 335–355, doi:10.1016/B978-0-12-812782-7.00015-1.
16. Meischner, P. *Weather Radar: PRINCIPLES and Advanced Applications*; Springer Science & Business Media: Berlin, Germany, 2005.
17. Ran, Q.; Fu, W.; Liu, Y.; Li, T.; Shi, K.; Sivakumar, B. Evaluation of quantitative precipitation predictions by ECMWF, CMA, and UKMO for flood forecasting: Application to two basins in China. *Nat. Hazards Rev.* **2018**, *19*, 05018003, doi:10.1061/(ASCE)NH.1527-6996.0000282.
18. Krajewski, W.F.; Kruger, A.; Smith, J.A.; Lawrence, R.; Gunyon, C.; Goska, R.; Seo, B.-C.; Domaszczynski, P.; Baeck, M.L.; Ramamurthy, M.K. Towards better utilization of NEXRAD data in hydrology: An overview of Hydro-NEXRAD. *J. Hydroinf.* **2010**, *13*, 255–266, doi:10.2166/hydro.2010.056.
19. Marx, A.; Kunstmann, H.; Bárdossy, A.; Seltmann, J. Radar rainfall estimates in an alpine environment using inverse hydrological modelling. *Adv. Geosci.* **2006**, *9*, 25–29.
20. Moore, R.J.; Jones, A.E.; Jones, D.A.; Black, K.B.; Bell, V.A. Weather radar for flood forecasting: Some UK experiences. In Proceedings of the Sixth International Symposium on Hydrological Applications of Weather Radar, Citeseer, Melbourne, Australia, 2–4 February 2004; pp. 2–4.

21. PC, S.; Misumi, R.; Nakatani, T.; Iwanami, K.; Maki, M.; Maesaka, T.; Hirano, K. Accuracy of quantitative precipitation estimation using operational weather radars: A case study of heavy rainfall on 9–10 September 2015 in the East Kanto region, Japan. *J. Disaster Res.* **2016**, *11*, 1003–1016, doi:10.20965/jdr.2016.p1003.
22. Rabiei, E.; Haberlandt, U. Applying bias correction for merging rain gauge and radar data. *J. Hydrol.* **2015**, *522*, 544–557, doi:10.1016/j.jhydrol.2015.01.020.
23. Wang, L.-P.; Ochoa-Rodríguez, S.; Van Assel, J.; Pina, R.D.; Pessemier, M.; Kroll, S.; Willems, P.; Onof, C. Enhancement of radar rainfall estimates for urban hydrology through optical flow temporal interpolation and Bayesian gauge-based adjustment. *J. Hydrol.* **2015**, *531*, 408–426, doi:10.1016/j.jhydrol.2015.05.049.
24. Park, S.G.; Bringi, V.N.; Chandrasekar, V.; Maki, M.; Iwanami, K. Correction of radar reflectivity and differential reflectivity for rain attenuation at X band. Part I: Theoretical and empirical basis. *J. Atmos. Ocean. Technol.* **2005**, *22*, 1621–1632, doi:10.1175/JTECH1803.1.
25. Ayat, H.; Kavianpour, M.R.; Moazami, S.; Hong, Y.; Ghaemi, E. Calibration of weather radar using region probability matching method (RPMM). *Theor. Appl. Climatol.* **2018**, *134*, 165–176, doi:10.1007/s00704-017-2266-7.
26. Collier, C.G. Accuracy of rainfall estimates by radar, Part I: Calibration by telemetering raingauges. *J. Hydrol.* **1986**, *83*, 207–223, doi:10.1016/0022-1694(86)90152-6.
27. Hubbert, J.C.; Dixon, M.; Ellis, S.M.; Meymaris, G. Weather radar ground clutter. Part I: Identification, modeling, and simulation. *J. Atmos. Ocean. Technol.* **2009**, *26*, 1165–1180, doi:10.1175/2009JTECHA1159.1.
28. Moszkowicz, S.; Ciach, G.J.; Krajewski, W.F. Statistical detection of anomalous propagation in radar reflectivity patterns. *J. Atmos. Ocean. Technol.* **1994**, *11*, 1026–1034, doi:10.1175/1520-0426(1994)011<1026:SDOAPI>2.0.CO;2.
29. PC, S.; Maki, M.; Shimizu, S.; Maesaka, T.; Kim, D.-S.; Lee, D.-I.; Iida, H. Correction of reflectivity in the presence of partial beam blockage over a

mountainous region using X-band dual polarization radar. *J. Hydrol.* **2013**, *14*, 744–764, doi:10.1175/JHM-D-12-077.1.

30. Gabella, M.; Morin, E.; Notarpietro, R. Using TRMM spaceborne radar as a reference for compensating ground-based radar range degradation: Methodology verification based on rain gauges in Israel. *J. Geophys. Res. Atmos.* **2011**, *116*, doi:10.1029/2010JD014496.
31. Zhang, J.; Qi, Y. A real-time algorithm for the correction of brightband effects in radar-derived QPE. *J. Hydrometeorol.* **2010**, *11*, 1157–1171, doi:10.1175/2010JHM1201.1.
32. Maki, M.; Park, S.-G.; Bringi, V.N. Effect of natural variations in rain drop size distributions on rain rate estimators of 3 cm wavelength polarimetric radar. *J. Meteorol. Soc. Jpn. Ser. II* **2005**, *83*, 871–893, doi:10.2151/jmsj.83.871.
33. Boodoo, S.; Hudak, D.; Ryzhkov, A.; Zhang, P.; Donaldson, N.; Sills, D.; Reid, J. Quantitative precipitation estimation from a C-band dual-polarized radar for the 8 July 2013 flood in Toronto, Canada. *J. Hydrometeorol.* **2015**, *16*, 2027–2044, doi:10.1175/JHM-D-15-0003.1.
34. Borga, M. Accuracy of radar rainfall estimates for streamflow simulation. *J. Hydrol.* **2002**, *267*, 26–39, doi:10.1016/S0022-1694(02)00137-3.
35. Jordan, P.; Seed, A.; Austin, G. Sampling errors in radar estimates of rainfall. *J. Geophys. Res. Atmos.* **2000**, *105*, 2247–2257, doi:10.1029/1999JD900130.
36. Villarini, G.; Krajewski, W.F. Review of the different sources of uncertainty in single polarization radar-based estimates of rainfall. *Surv. Geophys.* **2010**, *31*, 107–129, doi:10.1007/s10712-009-9079-x.
37. Jayakrishnan, R.; Srinivasan, R.; Arnold, J.G. Comparison of raingage and WSR-88D Stage III precipitation data over the Texas-Gulf basin. *J. Hydrol.* **2004**, *292*, 135–152, doi:10.1016/j.jhydrol.2003.12.027.
38. Kouwen, N.; Garland, G. Resolution considerations in using radar rainfall data for flood forecasting. *Can. J. Civ. Eng.* **1989**, *16*, 279–289, doi:10.1139/l89-053.

39. Krajewski, W.F.; Villarini, G.; Smith, J.A. Radar-rainfall uncertainties: Where are we after thirty years of effort? *Bull. Am. Meteorol. Soc.* **2010**, *91*, 87–94, doi:10.1175/2009BAMS2747.1.
40. Neary, V.S.; Habib, E.; Fleming, M. Hydrologic modeling with NEXRAD precipitation in middle Tennessee. *J. Hydrol. Eng.* **2004**, *9*, 339–349, doi:10.1061/(ASCE)1084-0699(2004)9:5(339).
41. Wilson, J.W.; Brandes, E.A. Radar measurement of rainfall-A summary. *Bull. Am. Meteorol. Soc.* **1979**, *60*, 1048–1058, doi:10.1175/1520-0477(1979)060<1048:RMORS>2.0.CO;2.
42. Vehviläinen, B.; Cauwengerghs, M.K.; Cheze, J.L.; Jurczyk, A.; Moore, R.J.; Olsson, J.; Salek, M.; Szturc, J. Evaluation of operational flow forecasting systems that use weather radar. *COST717 WorkingGroup 1*, **2004**, *1*. Available online: http://www.smhi.se/cost717/doc/WDD01200408 1.pdf (accessed on 2 January 2020).
43. Bringi, V.N.; Rico-Ramirez, M.A.; Thurai, M. Rainfall estimation with an operational polarimetric C-band radar in the United Kingdom: Comparison with a gauge network and error analysis. *J. Hydrometeorol.* **2011**, *12*, 935–954, doi:10.1175/JHM-D-10-05013.1.
44. Chandrasekar, V.; Keränen, R.; Lim, S.; Moisseev, D. Recent advances in classification of observations from dual polarization weather radars. *Atmos. Res.* **2013**, *119*, 97–111, doi:10.1016/j.atmosres.2011.08.014.
45. Hall, W.; Rico-Ramirez, M.A.; Krämer, S. Classification and correction of the bright band using an operational C-band polarimetric radar. *J. Hydrol.* **2015**, *531*, 248–258, doi:10.1016/j.jhydrol.2015.06.011.
46. Sugier, J.; Tabary, P.; Gourley, J.; Friedrich, K. Evaluation of dual-polarisation technology at C-band for operational weather radar network. *EUMETNET Opera* **2006**, *2*, pp. 44*2*.
47. Dufton, D.R.L. Quantifying Uncertainty in Radar Rainfall Estimates Using an X-Band Dual Polarisation Weather Radar. Ph.D. Thesis, University of Leeds, Woodhouse, UK, 2016.

48. Ryzhkov, A.V.; Schuur, T.J.; Burgess, D.W.; Heinselman, P.L.; Giangrande, S.E.; Zrnic, D.S. The Joint Polarization Experiment: Polarimetric rainfall measurements and hydrometeor classification. *Bull. Am. Meteorol. Soc.* **2005**, *86*, 809–824, doi:10.1175/BAMS-86-6-809.
49. Berenguer, M.; Sempere-Torres, D.; Corral, C.; Sánchez-Diezma, R. A fuzzy logic technique for identifying nonprecipitating echoes in radar scans. *J. Atmos. Ocean. Technol.* **2006**, *23*, 1157–1180, doi:10.1175/JTECH1914.1.
50. Ryzhkov, A.V.; Giangrande, S.E.; Melnikov, V.M.; Schuur, T.J. Calibration issues of dual-polarization radar measurements. *J. Atmos. Ocean. Technol.* **2005**, *22*, 1138–1155, doi:10.1175/JTECH1772.1.
51. McKee, J.L.; Binns, A.D.; Helsten, M.; Shifflett, M. Evaluation of Gauge-Radar Merging Methods Using a Semi-Distributed Hydrological Model in the Upper Thames River Basin, Canada. *JAWRA J. Am. Water Resour. Assoc.* **2018**, *54*, 594–612.
52. Goudenhoofdt, E.; Delobbe, L. Evaluation of radar-gauge merging methods for quantitative precipitation estimates. *Hydrol. Earth Syst. Sci.* **2009**, *13*, 195–203.
53. McKee, J.L.; Binns, A.D. A review of gauge–radar merging methods for quantitative precipitation estimation in hydrology. *Can. Water Resour. J. Rev. Can. Resour. Hydr.* **2016**, *41*, 186–203, doi:10.1111/1752-1688.12625.
54. Ochoa-Rodriguez, S.; Wang, L.-P.; Willems, P.; Onof, C. A review of radar-rain gauge data merging methods and their potential for urban hydrological applications. *Water Resour. Res.* **2019**, doi:10.1029/2018WR023332.
55. Vieux, B.E.; Bedient, P.B. Assessing urban hydrologic prediction accuracy through event reconstruction. *J. Hydrol.* **2004**, *299*, 217–236, doi:10.1016/j.jhydrol.2004.08.005.
56. Anagnostou, E.N.; Krajewski, W.F.; Seo, D.-J.; Johnson, E.R. Mean-field rainfall bias studies for WSR-88D. *J. Hydrol. Eng.* **1998**, *3*, 149–159, doi:10.1061/(ASCE)1084-0699(1998)3:3(149).

57. Brandes, E.A. Optimizing rainfall estimates with the aid of radar. *J. Appl. Meteorol.* **1975**, *14*, 1339–1345, doi:10.1175/1520-0450(1975)014<1339:OREWTA>2.0.CO;2.
58. Cole, S.J.; Moore, R.J. Hydrological modelling using raingauge-and radar-based estimators of areal rainfall. *J. Hydrol.* **2008**, *358*, 159–181, doi:10.1016/j.jhydrol.2008.05.025.
59. Fulton, R.A.; Breidenbach, J.P.; Seo, D.-J.; Miller, D.A.; O'Bannon, T. The WSR-88D rainfall algorithm. *Weather For.* **1998**, *13*, 377–395, doi:10.1175/1520-0434(1998)013<0377:TWRA>2.0.CO;2.
60. Harrison, D.L.; Scovell, R.W.; Kitchen, M. High-resolution precipitation estimates for hydrological uses. In *Proceedings of the Institution of Civil Engineers-Water Management*; Thomas Telford Ltd.: Exeter, UK, 2009; Volume 162, pp. 125–135, doi:10.1680/wama.2009.162.2.125.
61. Jewell, S.A.; Gaussiat, N. An assessment of kriging-based rain-gauge–radar merging techniques. *Q. J. R. Meteorol. Soc.* **2015**, *141*, 2300–2313, doi:10.1002/qj.2522.
62. Nanding, N.; Rico-Ramirez, M.A.; Han, D. Comparison of different radar-raingauge rainfall merging techniques. *J. Hydroinf.* **2015**, *17*, 422–445, doi:10.2166/hydro.2015.001.
63. Seo, D.-J.; Breidenbach, J.P. Real-time correction of spatially nonuniform bias in radar rainfall data using rain gauge measurements. *J. Hydrometeorol.* **2002**, *3*, 93–111, doi:10.1175/1525-7541(2002)003<0093:RTCOSN>2.0.CO;2.
64. Sideris, I.V.; Gabella, M.; Erdin, R.; Germann, U. Real-time radar–rain-gauge merging using spatio-temporal co-kriging with external drift in the alpine terrain of Switzerland. *Q. J. R. Meteorol. Soc.* **2014**, *140*, 1097–1111, doi:10.1002/qj.2188.
65. Thorndahl, S.; Nielsen, J.E.; Rasmussen, M.R. Bias adjustment and advection interpolation of long-term high resolution radar rainfall series. *J. Hydrol.* **2014**, *508*, 214–226, doi:10.1016/j.jhydrol.2013.10.056.
66. Berne, A.; Krajewski, W.F. Radar for hydrology: Unfulfilled promise or unrecognized potential? *Adv. Water Resour.* **2013**, *51*, 357–366, doi:10.1016/j.advwatres.2012.05.005.

67. Cecinati, F.; de Niet, A.; Sawicka, K.; Rico-Ramirez, M. Optimal temporal resolution of rainfall for urban applications and uncertainty propagation. *Water* **2017**, *9*, 762, doi:10.3390/w9100762.
68. Ochoa-Rodriguez, S.; Wang, L.; Bailey, A.; Schellart, A.; Willems, P.; Onof, C. Evaluation of radar-rain gauge merging methods for urban hydrological applications: Relative performance and impact of gauge density. *UrbanRain15 Proc. Rainfall Urban Nat. Syst.* **2015**, doi:10.3929/ethz-a-010549004.
69. Wang, L.; Ochoa-Rodriguez, S.; Onof, C.; Willems, P. Singularity-sensitive gauge-based radar rainfall adjustment methods for urban hydrological applications. *Hydrol. Earth Syst. Sci.* **2015**, *19*, 4001–4021, doi:10.5194/hess-19-4001-2015.
70. Wang, L.-P.; Ochoa-Rodríguez, S.; Simões, N.E.; Onof, C.; Maksimović, Č. Radar–raingauge data combination techniques: A revision and analysis of their suitability for urban hydrology. *Water Sci. Technol.* **2013**, *68*, 737–747, doi:10.2166/wst.2013.300.
71. Kumar, A.; Binns, A.D.; Gupta, S.K.; Singh, V.P.; McKee, J.L. Analysing the Performance of Various Radar-Rain Gauge Merging Methods for Modelling the Hydrologic Response of Upper Thames River Basin, Canada. In Proceedings of the World Environmental and Water Resources Congress, West Palm Beach, FL, USA, 22–26 May 2016; pp. 359–371, doi:10.1061/9780784479858.037.
72. Boodoo, S.; Hudak, D.; Ryzhkov, A.; Zhang, P.; Donaldson, N.; Reid, J. Quantitative precipitation estimation (QPE) from C-band dual-polarized radar for the July 8th 2013 flood in Toronto, Canada. Presented at ERAD 2014 - the Eighth European Conference on Radar in Meteorology and Hydrology, Garmisch-Partenkirchen, Germany, 1–5 September 2014; ID 322.
73. Watershed Features—Humber River. Toronto and Region Conservation Authority (TRCA). Available online: https://trca.ca/conservation/watershed-management/humber-river/watershed-features/ (accessed on 26 November 2019).

74. Don River. Toronto and Region Conservation Authority (TRCA). Available online: https://trca.ca/conservation/watershed-management/don-river/ (accessed on 26 November 2019).
75. Mekis, E.; Donaldson, N.; Reid, J.; Zucconi, A.; Hoover, J.; Li, Q.; Nitu, R.; Melo, S. An overview of surface-based precipitation observations at environment and climate change Canada. *Atmos. Ocean* **2018**, *56*, 71–95, doi:10.1080/07055900.2018.1433627.
76. Ryzhkov, A.; Zhang, P.; Hudak, D.; Alford, J.; Knight, M.; Conway, J. Validation of polarimetric methods for attenuation correction at C band. In Proceedings of the Proceedings 33rd Conferevce Radar Meteorol, Cairns, Australia, 6 August 2007.
77. Lack, S.A.; Fox, N.I. An examination of the effect of wind-drift on radar-derived surface rainfall estimations. *Atmos. Res.* **2007**, *85*, 217–229, doi:10.1016/j.atmosres.2006.09.010.
78. Reed, S.M.; Maidment, D.R. Coordinate transformations for using NEXRAD data in GIS-based hydrologic modeling. *J. Hydrol. Eng.* **1999**, *4*, 174–182, doi:10.1061/(ASCE)1084-0699(1999)4:2(174).
79. Brandes, E.A.; Zhang, G.; Vivekanandan, J. Experiments in rainfall estimation with a polarimetric radar in a subtropical environment. *J. Appl. Meteorol.* **2002**, *41*, 674–685, doi:10.1175/1520-0450(2002)041<0674:EIREWA>2.0.CO;2.
80. Gjertsen, U.; Salek, M.; Michelson, D.B. Gauge adjustment of radar-based precipitation estimates in Europe. In Proceedings of the Proceedings of ERAD, Visby, Sweden, 6–10 September 2004; Volume 7.
81. Hitschfeld, W.; Bordan, J. Errors inherent in the radar measurement of rainfall at attenuating wavelengths. *J. Meteorol.* **1954**, *11*, 58–67, doi:10.1175/1520-0469(1954)011<0058:EIITRM>2.0.CO;2.
82. Borga, M.; Tonelli, F.; Moore, R.J.; Andrieu, H. Long-term assessment of bias adjustment in radar rainfall estimation. *Water Resour. Res.* **2002**, *38*, 8-1–8-10, doi:10.1029/2001WR000555.

83. Ines, A.V.; Hansen, J.W. Bias correction of daily GCM rainfall for crop simulation studies. *Agric. For. Meteorol.* **2006**, *138*, 44–53, doi:10.1016/j.agrformet.2006.03.009.
84. Schmidli, J.; Frei, C.; Vidale, P.L. Downscaling from GCM precipitation: A benchmark for dynamical and statistical downscaling methods. *Int. J. Clim.* **2006**, *26*, 679–689, doi:10.1002/joc.1287.
85. Drusch, M.; Wood, E.F.; Gao, H. Observation operators for the direct assimilation of TRMM microwave imager retrieved soil moisture. *Geophys. Res. Lett.* **2005**, *32*, doi:10.1029/2005GL023623.
86. Michelson, D.; Andersson, T.; Koistinen, J.; Collier, C.G.; Riedl, J.; Nielsen, A.; Overgaard Persson, T. *BALTEX Radar Data Centre Products and Their Methodologies*; SMHI: North Köping, Sweden, 2000.
87. Michelson, D.B.; Koistinen, J. Gauge-radar network adjustment for the Baltic Sea Experiment. *Phys. Chem. Earth Part B Hydrol. Ocean. Atmos.* **2000**, *25*, 915–920, doi:10.1016/S1464-1909(00)00125-8.
88. Andrieu, H.; Creutin, J.D. Identification of vertical profiles of radar reflectivity for hydrological applications using an inverse method. Part I: Formulation. *J. Appl. Meteorol.* **1995**, *34*, 225–239, doi:10.1175/1520-0450(1995)034<0225:IOVPOR>2.0.CO;2.
89. Barnes, S.L. A technique for maximizing details in numerical weather map analysis. *J. Appl. Meteorol.* **1964**, *3*, 396–409, doi:10.1175/1520-0450(1964)003<0396:ATFMDI>2.0.CO;2.
90. Goovaerts, P. *Geostatistics for Natural Resources Evaluation*; Oxford University Press on Demand: Oxford, UK, 1997.
91. Sinclair, S.; Pegram, G. Combining radar and rain gauge rainfall estimates using conditional merging. *Atmos. Sci. Lett.* **2005**, *6*, 19–22, doi:10.1002/asl.85.
92. Koistinen, J.; Puhakka, T. An improved spatial gauge-radar adjustment technique. In Proceedings of the 20th Conference on Radar Meteorology, Boston, MA, USA, 30 November–3 December 1981; pp. 179–186.

93. Mekonnen, G.B.; Matula, S.; Doležal, F.; Fišák, J. Adjustment to rainfall measurement undercatch with a tipping-bucket rain gauge using ground-level manual gauges. *Meteorol. Atmos. Phys.* **2015**, *127*, 241–256, doi:10.1007/s00703-014-0355-z.
94. Steiner, M.; Smith, J.A.; Burges, S.J.; Alonso, C.V.; Darden, R.W. Effect of bias adjustment and rain gauge data quality control on radar rainfall estimation. *Water Resour. Res.* **1999**, *35*, 2487–2503, doi:10.1029/1999WR900142.
95. Seo, D.-J.; Habib, E.; Andrieu, H.; Morin, E. Hydrologic applications of weather radar. *J. Hydrol.* **2015**, *531*, 231–233, doi:10.1016/j.jhydrol.2015.11.010.
96. Seo, B.-C.; Krajewski, W.F. Correcting temporal sampling error in radar-rainfall: Effect of advection parameters and rain storm characteristics on the correction accuracy. *J. Hydrol.* **2015**, *531*, 272–283, doi:10.1016/j.jhydrol.2015.04.018.
97. Smith, J.A.; Baeck, M.L.; Villarini, G.; Welty, C.; Miller, A.J.; Krajewski, W.F. Analyses of a long-term, high-resolution radar rainfall data set for the Baltimore metropolitan region. *Water Resour. Res.* **2012**, *48*, doi:10.1029/2011WR010641.
98. Ciach, G.J.; Krajewski, W.F.; Villarini, G. Product-error-driven uncertainty model for probabilistic quantitative precipitation estimation with NEXRAD data. *J. Hydrometeorol.* **2007**, *8*, 1325–1347, doi:10.1175/2007JHM814.1.
99. Smith, B.; Rodriguez, S. Spatial analysis of high-resolution radar rainfall and citizen-reported flash flood data in ultra-urban New York City. *Water* **2017**, *9*, 736, doi:10.3390/w9100736.
100. Villarini, G.; Krajewski, W.F. Inference of spatial scaling properties of rainfall: Impact of radar rainfall estimation uncertainties. *IEEE Geosci. Remote Sens. Lett.* **2009**, *6*, 812–815, doi:10.1109/LGRS.2009.2025891.
101. Fang, X.; Thompson, D.B.; Cleveland, T.G.; Pradhan, P.; Malla, R. Time of concentration estimated using watershed parameters determined by automated and manual methods. *J. Irrig. Drain. Eng.* **2008**, *134*, 202–211, doi:10.1061/(ASCE)0733-9437(2008)134:2(202).

102. Bedient, P.B.; Holder, A.; Benavides, J.A.; Vieux, B.E. Radar-based flood warning system applied to Tropical Storm Allison. *J. Hydrol. Eng.* **2003**, *8*, 308–318, doi:10.1061/(ASCE)1084-0699(2003)8:6(308).
103. Brocca, L.; Hasenauer, S.; Lacava, T.; Melone, F.; Moramarco, T.; Wagner, W.; Dorigo, W.; Matgen, P.; Martínez-Fernández, J.; Llorens, P. Soil moisture estimation through ASCAT and AMSR-E sensors: An intercomparison and validation study across Europe. *Remote Sens. Environ.* **2011**, *115*, 3390–3408, doi:10.1016/j.rse.2011.08.003.
104. Kornelsen, K.C.; Coulibaly, P. Data-based disaggregation of SMOS soil moisture. In Proceedings of the 2014 IEEE Geoscience and Remote Sensing Symposium, Quebec City, QC, Canada, 13–18 July 2014; pp. 3334–3337, doi:10.1109/IGARSS.2014.6947194.
105. Reichle, R.H.; Koster, R.D. Bias reduction in short records of satellite soil moisture. *Geophys. Res. Lett.* **2004**, *31*, doi:10.1029/2004GL020938.
106. Leach, J.M.; Kornelsen, K.C.; Coulibaly, P. Assimilation of near-real time data products into models of an urban basin. *J. Hydrol.* **2018**, *563*, 51–64 doi:10.1016/j.jhydrol.2018.05.064.
107. Zahmatkesh, Z.; Tapsoba, D.; Leach, J.; Coulibaly, P. Evaluation and bias correction of SNODAS snow water equivalent (SWE) for streamflow simulation in eastern Canadian basins. *Hydrol. Sci. J.* **2019**, *64*, 1541–1555, doi:10.1080/02626667.2019.1660780.
108. Reed, S.; Schaake, J.; Zhang, Z. A distributed hydrologic model and threshold frequency-based method for flash flood forecasting at ungauged locations. *J. Hydrol.* **2007**, *337*, 402–420, doi:10.1016/j.jhydrol.2007.02.015.
109. Zhang, H.; Li, D.; Wang, X.; Jiang, X. Quantitative evaluation of NEXRAD data and its application to the distributed hydrologic model BPCC. *Sci. China Technol. Sci.* **2012**, *55*, 2617–2624, doi:10.1007/s11431-012-4918-2.

110. Smith, J.A.; Baeck, M.L.; Meierdiercks, K.L.; Miller, A.J.; Krajewski, W.F. Radar rainfall estimation for flash flood forecasting in small urban watersheds. *Adv. Water Resour.* **2007**, *30*, 2087–2097, doi:10.1016/j.advwatres.2006.09.007.

Chapter 5. Integration of Radar QPEs into HEC-RTS Framework for Improved Hydrological Model Calibration for Streamflow Simulation and Flood Inundation Mapping

Summary of Paper 4: Wijayarathne, D., Coulibaly, P., Boodoo, S., and Sills, D. (2020). Integration of Radar QPEs into HEC-RTS Framework for Improved Hydrological Model Calibration for Streamflow Simulation and Flood Inundation Mapping. *Journal of Hydrometeorology*, under review.

The effect of Radar Quantitative Precipitation Estimates (QPEs) on hydrological model calibration for streamflow simulation and flood mapping was evaluated in this study for an urban watershed. To improve the calibration of model parameters, event-based hydrological model run was performed by integrating KBUF NEXRAD S-band and WKR C-band radar QPEs. Then the results from hydrological modeling was compared to assess how Radar QPE forcing affect the streamflow simulation accuracy. Finally, hydrological-hydraulic HEC models were integrated within the Hydrologic Engineering Center- Real-Time Simulation (HEC-RTS) framework to develop flood extent maps.

Key findings of this research include:

- All model performance indices were improved after the application of bias correction and therefore, hydrological model calibration can be enhanced through radar-gauge merging.
- In addition, bias-corrected Radar QPEs are helpful for running gauge-calibrated hydrological models.

- Streamflow simulations and flood maps created through bias-corrected Radar QPEs could be effectively used for improving flood forecasting in Canada.
- HEC-RTS framework with bias-corrected Radar QPEs could be used to produce flood forecast maps.
- Flood forecasting and management in urbanized areas could be affectively achieved by using Radar rainfall estimates.

5.1. Abstract

Flood forecasting is essential to minimize the impacts and costs of floods, especially in urbanized watersheds. Radar rainfall estimates are becoming increasingly popular in flood forecasting because they provide the much needed real-time spatially distributed precipitation information. The current study evaluates the use of Radar Quantitative Precipitation Estimates (QPEs) in hydrological model calibration for streamflow simulation and flood mapping in an urban setting.

S-band and C-band Radar QPEs were integrated into event-based hydrological models to improve the calibration of model parameters. Then, rain gauge and Radar precipitation estimates performance were compared for hydrological modeling in an urban watershed to assess the effects of Radar QPE forcing on streamflow simulation accuracy. Finally, flood extent maps were produced using coupled hydrological-hydraulic models integrated within the Hydrologic Engineering Center- Real-Time Simulation (HEC-RTS) framework.

Radar-gauge merging can enhance the hydrological model calibration as all model performance indices were improved when bias correction was applied. Bias-corrected Radar QPEs are also useful for running hydrological models calibrated using gauge data. It is shown that flood forecast maps can be produced with the HEC-RTS framework using the bias-corrected Radar QPEs. Canadian flood forecasting systems could be effectively updated by integrating bias-corrected Radar QPEs to simulate streamflow and produce flood inundation maps. Radar rainfall estimates could be effectively used to forecast flood in urbanized areas for effective flood management and mitigation.

5.2. Introduction

Flooding is one of the most significant natural hazards given its potential for lost of lives and catastrophic socio-economic impacts (Jonkman and Vrijling 2008; Jonkman and Kelman 2005). Over the past decades, the frequency of flooding has increased due to population growth and climate change (Tol 2016; Jonkman and Vrijling 2008; Zhang et al. 2018). In Canada, floods are often mentioned as the most frequent natural hazard to life, property, economy, and environment (Bowering et al. 2014). The estimated total cost of floods in Canada was almost 36 billion CAD from 1900 to 2016 (Public Safety Canada 2019). During the past few years, significant urban floods such as the 8th July 2013 flash flood in Toronto (Boodoo et al. 2015; Sills et al. 2016) have increased the demand for flood mitigation measures in Canada to minimize the damage (Han and Coulibaly 2019).

Standard flood mitigation measures are divided into two main categories: structural and nonstructural measures (Thampapillai and Musgrave 1985). Structural measures are mainly the construction of flood control structures that require a significant capital investment (Mays 2010). Nonstructural measures include flood forecasting, and these measures are a more effective and affordable alternative to reducing the negative impacts of flooding (WMO, 2006). A flood forecasting system that can deliver accurate and reliable forecasts with appropriate lead time is a critical part of nonstructural flood management (Nagai 2003; Reed et al. 2007; Unduche et al. 2018). According to the United Nations, flood damage can be reduced up to 35 % if a flood is adequately forecasted in advance (Pilon 2002). Various flood forecasting systems with varying complexities are being used worldwide to forecast floods in advance. Community Hydrologic Prediction System (CHPS) in the USA, European Flood Forecasting System (EFFS) in Europe, National Flood Forecasting System (NFFS) in England, and Flood Early Warning System (FEWS) in Scotland (Cranston and Tavendale 2012; De Roo et al. 2003; Roe et al. 2010; Werner et al. 2009) are some of the examples. Hydrological and hydraulic models are critical parts of such flood forecasting systems (Teal and Allan 2017).

Hydrological and hydraulic modeling approaches were used to forecast river flows and flood extent over decades (Arduino et al. 2005; Awol et al. 2019; Han and Coulibaly 2017; Leach et al. 2018; Wijayarathne and Coulibaly 2020; Che and Mays 2015). These models represent different hydrological processes in the hydrologic cycle, such as precipitation, evapotranspiration, infiltration, interception, and runoff using a set of model

parameters. Hydrological models calculate streamflow using inputs such as precipitation, temperature, soil moisture, and topography (Devia et al. 2015). Hydraulic models that simulate flood extent and inundation levels in the flood plain and surrounding areas use output from the hydrological models (Aksoy et al. 2016). Among all meteorological inputs, precipitation is the primary forcing for hydrological models (Devia et al. 2015). Therefore, the efficiency of flood forecasting systems where hydrological and hydraulic models are embedded is mainly determined by the accuracy and reliability of precipitation inputs (Larson and Peck 1974).

Surface rainfall gauges or weather Radar provide precipitation input for the hydrological models (Randall et al. 2014). Rain gauges are believed to be accurate instruments for precipitation point measurements even though they suffer from both random errors (e.g. poor gauge site conditions, human errors, inadequate network density, and by the exposure to prevailing winds) and systematic errors (e.g. wind-induced under-catch, wetting, and evaporation losses) (Sevruk 1982). At present, the calibration of a hydrological model mostly relies on in-situ rain gauge data (McMillan et al. 2011; Moreno et al. 2012). However, this approach often fails to adequately capture spatial and temporal variations (Dhiram and Wang 2016). Weather Radar produces spatially and temporally continuous data over a large area, including regions with sparse gauge point observation networks (Thorndahl et al., 2016), and its use can help address this shortcoming.

With the worldwide development of Radar infrastructure and data processing methods, the interest in real-time, spatially distributed precipitation information derived

from weather Radar over conventional rainfall gauges is notable (Şensoy et al. 2016). The ability to capture the spatial variation of precipitation has contributed to Radar playing an essential role in meteorological studies (Doviak 1993). However, Radar Quantitative Precipitation Estimates (QPEs) are known to be suffering from errors arising from the measurements and reflectivity-rain intensity conversion process (Dai et al. 2018). Attenuation, miscalibration, ground clutter, anomalous propagation, beam blockage, range degradation, the presence of a bright band, variations in precipitation drop-size distribution, radome wetting etc., can cause errors in reflectivity measurements and eventually Radar QPEs (Boodoo et al. 2015; Borga 2002; Borga et al. 2006; Jordan et al. 2000; Meischner 2005). Therefore, it is not practically possible to obtain error-free Radar QPEs when weather Radar is used as a precipitation measurement tool.

The first appearance of Radar QPEs as precipitation input to hydrological models was reported at the urban storm drainage conference in Sweden, 1984 (Thorndahl et al., 2016). The applications of weather Radar from a hydrological perspective have developed considerably since then, especially with the advances in computer power and expansion of new hydrological models (Beneti et al., 2019; Khan et al., 2019; Meischner, 2005; Ran et al., 2018; Thorndahl et al., 2016). In Canada, research in weather Radar began after the Second World War under the project Stormy Weather (Douglas 1990; Sills and Joe 2019). Weather Radars were subsequently used for various hydrological studies in the Canadian context (Bellon and Austin 1984, 1978; Bellon and Zawadzki 1994; Bellon et al. 1980; Germann and Zawadzki 2004; Hassan et al. 2019; Germann and Zawadzki 2002; Huang et al. 2010; Hudak et al. 2008, 2002; Brown et al. 2007; Barge et al. 1979;

Chen and Farrar 2007; Sills and Joe 2019; Wijayarathne et al. 2020a). The main applications of weather Radar in Canada include determining the type of precipitation, precipitation features and structure, operational forecasting such as weather forecasts and snow depth predictions, for operational weather warnings and as a tool to validate atmospheric models (Sills and Joe 2019). However, the use of Radar QPEs as an input to hydrological models is not a typical application in Canada, and previous studies were limited to the model WATFLOOD (Wijayarathne et al. 2020, unpublished manuscript). Therefore, Radar QPEs in operational flood forecasting is not yet implemented widely in Canada, and there are some challenges to overcome (McKee et al. 2018).

For flood forecasting in urban and semi-urban watersheds where response time is in hours, Radar QPEs with high temporal and spatial resolution are needed to calibrate and run hydrological models. Relatively small-sized urban and semi-urban catchments with a high degree of imperviousness respond to rainfall relatively quickly and hence are very sensitive to the spatial and temporal variability of rainfall (Ochoa-Rodriguez et al., 2019; Villarini & Krajewski, 2010). Therefore, hydrological models calibrated using selected events (e.g., severe or extreme weather spanning a few hours) are advantageous. Even though Radar QPEs produce real-time, spatially, and temporally continuous precipitation data, the intrinsic errors associated with Radar measurements and eventually Radar QPEs are the main reason for the limited use of Radar QPEs in operational flood forecasting (Wang et al. 2015). A significant improvement in Radar QPEs was observed after the introduction of dual-polarization technology and prototype algorithms in Canada (Bringi et al. 2011; Chandrasekar et al. 2013; Hall et al. 2015; Sugier et al. 2006; Boodoo

et al. 2015; Ryzhkov et al. 2005), with dual-polarized approaches producing more accurate Radar QPEs than is possible with single-polarized Radar. In addition to dual-polarization, a significant improvement to Radar QPEs is possible via adjustment of values to match rain-gauge observations (radar-gauge merging) (Goudenhoofdt and Delobbe 2009; Ochoa-Rodriguez et al. 2019; Vieux and Bedient 2004; Wang et al. 2015; Wijayarathne et al. 2020b). Radar-gauge merging combines the advantages of both gauge and Radar QPEs while minimizing their weaknesses to produce accurate and reliable Radar QPEs (McKee and Binns 2016). With the invention of methods to retrieve, compute, view, bias-correct, and manage Radar QPEs, it is possible to implement flood early warning system to issue real-time flood forecasts for operational use. For that reason, Radar QPEs should go through careful selection, a comprehensive evaluation, and corrections where necessary before using them as precipitation forcing for the hydrological model in operational flood forecasting. Further research is essential to fill these niche areas before using Radar QPEs for operational flood forecasting in urban and semi-urban watersheds with confidence.

The current study involves implementing a flood forecasting framework that allows connecting hydrological and hydraulic models in one platform using both rain gauge and weather Radar QPEs derived from USA and Canadian weather Radar to assess the benefit of Radar QPEs in flood forecasting. Firstly, the impact of radar-gauge merging on Radar QPE accuracy and reliability, and eventually, streamflow simulations were examined. Secondly, the use of Radar QPEs to improve hydrological model parameters' calibration was tested by integrating weather Radar QPEs to event-based hydrological

models focusing on flood forecasting. An inter-comparison of rain gauge and Radar QPE performance for hydrological modeling in an urban watershed was performed to assess the effects of various precipitation forcing on streamflow simulation accuracy. Finally, hydrological and hydraulic models were integrated within one framework to generate flood inundation maps to examine the impact of Radar QPEs on flood forecasting potential in an urban setting.

5.3. Study area

The Mimico Creek watershed used in this study (Figure 5-1) is a part of the Great Lakes basin and lies between the Humber River and Etobicoke Creek watersheds (TRCA Report Cards 2020). It is currently managed by the Toronto and Region Conservation Authority (TRCA). The Mimico Creek starts at Brampton and flows through Mississauga and Toronto in the Greater Toronto Area (GTA) of Ontario (Natural Resources Canada 2016). It flows about 33 km through urban neighborhoods and discharges into Lake Ontario. More than 60% of the creek is artificially channelized, leading to rapid urban stormwater runoff resulting sometimes in flooding (TRCA Report Cards 2020). The watershed covers 77 km^2 and is home to over 100,000 people (TRCA 2020). It is heavily urbanized, with approximately 90% urban area and 10% natural cover (Figure 5-1) (Ontario GeoHub 2020). Predominant soil types are poorly drained clays and clay loams (TRCA 2009). The combination of impervious urban areas with poorly drained clay soil make the watershed particularly susceptible to flooding. Further details on Mimico Creek watershed can be found on the TRCA Watershed Features Etobicoke and Mimico website (TRCA 2020). The watershed has excellent coverage from both

Canadian King City (WKR) C-band Radar and USA Buffalo (KBUF) Next Generation Weather Radar (NEXRAD) S-band Radar (Figure 5-1).

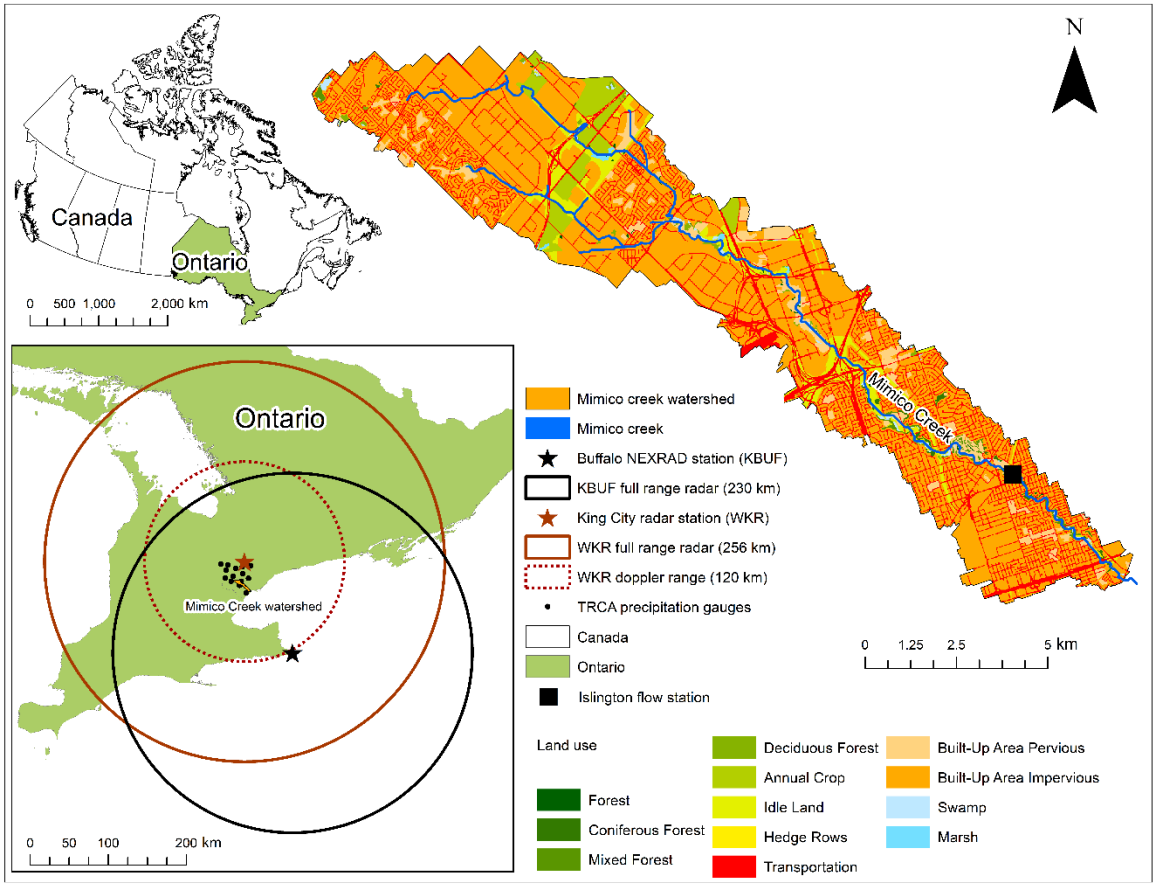

Figure 5-1 *Mimico Creek watershed in GTA, and coverages of the Canadian WKR and USA KBUF NEXRAD Radar sites.*

5.4. Data/Hydrological and Hydraulic models

5.4.1. Hydrometeorological and hydrometric data

Sub-hourly (5-15 min) rainfall accumulations and temperature reported at fourteen hydrometeorological stations from 2013 to 2018 were gathered from TRCA data archives. All TRCA rain gauges are located within the Doppler range (<180 km) of the KBUF

NEXRAD S - band Radar and the dual-polarized Doppler range (<120 km) of the WKR C-band Radar station (Figure 5-1). It is assumed that TRCA rain gauges characterize the precipitation distribution over the entire watershed. This assumption is valid due to the relatively small size of the watershed and relatively high rain gauge density of one gauge per ~75 km^2 (Wijayarathne et al. 2020b). Sub-hourly (5-15 min) streamflow data from 2013 to 2018 recorded by Water Survey of Canada (compiled at https://wateroffice.ec.gc.ca/search/historical_e.html) were collected from a long-term flow gauge named "Islington" (ID: 02HC033) (Figure 5-1). Both precipitation and streamflow data were aggregated to obtain a 15 min rainfall time series for analysis.

5.4.2. Radar QPEs

5.4.2.1. King City (WKR) C-band Radar QPEs

The WKR C-band Radar station has a conventional reflectivity measurement range of 256 km and a dual-polarization Doppler range of 120 km (Figure 5-1). Radar reflectivity data, gathered from Environment and Climate Change Canada (ECCC) archives, include dual-polarization POLarimetric Plan Position Indicator (POLPPI) scans in 10-minute cycles at the lowest (0.5°) elevation (Boodoo et al. 2015). The data resolution is 0.25 km by 0.5° in azimuth (Wijayarathne et al. 2020a). The modified ZPHI algorithm was used to correct reflectivity values for attenuation (Ryzhkov et al. 2007). The Radar pixel nearest to the gauge location was extracted. Wijayarathne et al. (2020a) evaluated the performance of WKR C-band Radar QPEs derived using seven Z-R relationships to verify the reliability and accuracy for operational use in the GTA, ON,

Canada and reported the best performance from the relationship $R = aK_{DP}^{b}10^{cZ_{DR}}$. Therefore, in this study, the rainfall rate was calculated for a K_{DP} (specific differential phase)-Z_{DR} (differential reflectivity) rate relationship $R = aK_{DP}^{b}10^{cZ_{DR}}$, where a=37.9, b=0.89, c=-0.072 (Bringi and Chandrasekar 2001). This is applied only if K_{DP} values are greater than 0.1 deg/km; otherwise, R (Z) is used, i.e., $Z=200R^{1.6}$ (Marshall and Palmer 1948). Therefore, in effect, the rates are derived as a composite of these two relationships. To be consistent with the gauge and streamflow data, the 10-min rainfall accumulations were resampled using time interpolation to derive 15-min rainfall accumulations using Hydrologic Engineering Center Data Storage System Visual Utility Engine (HEC-DSSVue).

5.4.2.2. Buffalo (KBUF) NEXRAD S-band Radar QPEs

Level III NEXRAD S-band Radar reflectivities from the KBUF NEXRAD station were downloaded from the archives of the National Centers for Environmental Information (NCEI) (NOAA 2018). The Radar QPEs were derived using the Precipitation Processing System (PPS) algorithm $R = 0.017\ Z^{0.714}$ (Fulton et al. 1998) and reflectivity values collected every 5-10 min and having resolution 0.25 km in range and 0.5° in azimuth. The Digital Precipitation Array (DPA) QPE accumulation on the 4.7625 km Hydrologic Rainfall Analysis Projection (HRAP) grid was selected for the analysis after a NEXRAD QPE evaluation for GTA watersheds by Wijayarathne et al. (2020a). National Oceanic and Atmospheric Administration's (NOAA's) Weather and Climate Toolkit (WCT), ArcGIS 10.6.1, MATLAB, and Python scripts were used for further processing of NEXRAD QPEs (Guzman et al. 2013; Wijayarathne et al. 2020a). The first previously

recorded value at each 15 min interval was extracted, and rain rates were assumed to be constant across the time of interest.

5.4.3. Hydrological and hydraulic models

5.4.3.1. Hydrologic Engineering Center's Hydrologic Modeling System (HEC-HMS)

The HEC-HMS hydrological model was developed by the Hydrologic Engineering Center of the US Army Corps of Engineers to simulate both continuous and event-based hydrological processes in a dendritic watershed in both space and time (Darbandsari and Coulibaly 2020; Wijayarathne and Coulibaly 2020). It allows users to select from a list of methods that can model different components in runoff generation (i.e., rainfall loss, direct runoff, river routing, base flow, and routing processes) (Cunderlik and Simonovic 2004). Precipitation, temperature, and calibrated parameters are the Major input to the HEC-HMS model. For further details on the HEC-HMS model, readers are referred to the HEC-HMS user manual (US Army Corps of Engineers 2020a). In this study, the HEC-HMS version 4.2.1 model implemented for the Mimico Creek watershed by TRCA (Zahmatkesh et al. 2020, unpublished manuscript) was used. For urban sub-basins, the model used the Soil Conservation Service (SCS) curve number and SCS Unit Hydrograph as the loss and transform methods, respectively. Clark Unit Hydrograph method was used as the transform method for sub-basins with natural cover. The other parameters such as Manning's n, curve number, imperviousness, etc., were considered unspecified to determine during model calibration. To represent prevailing

stormwater management facilities, reservoir routing components were also added to the HEC-HMS model.

5.4.3.2. Hydrologic Engineering Center's River Analysis System (HEC-RAS)

The HEC-RAS hydraulic model was developed by the Hydrologic Engineering Center of the US Army Corps of Engineers to simulate both one and two-dimensional and combined one/two-dimensional flow in open channels and floodplains (Ezz 2018; Hicks and Peacock 2005). The model can produce flood extent and water levels using resulting peak flows from hydrological models (Hashemyan et al. 2015). The RAS Mapper portion of the HEC-RAS software performs flood inundation mapping for flood forecasting applications (Brunner et al. 2015). Further details on the HEC-RAS model can be found in the HEC-RAS user manual (US Army Corps of Engineers 2020b). For this study, the HEC-RAS model developed for Mimico Creek watershed by TRCA was used (Zahmatkesh et al. 2020, unpublished manuscript).

5.4.3.3. Hydrologic Engineering Center- Real-Time Simulation (HEC- RTS)

The HEC-RTS is a framework that assimilates different HEC products making it possible to develop a flood forecasting system by integrating HEC models in one platform (US Army Corps of Engineers 2020c). HEC-RTS connects the hydrological model HEC-HMS with the hydraulic model HEC-RAS and HEC-RAS mapper to generate flood inundation maps (Charley et al. 2012). Rainfall-runoff processes for a selected watershed are simulated using the HEC-HMS model component. One and two-dimensional, steady, and unsteady flow routing in streams are executed using the HEC-

RAS model component. RAS mapper component of the HEC-RTS framework generates flood inundation maps using peak flows from HEC-HMS. Therefore, HEC-RTS can support operational flood forecasting by combining hydrological and hydraulic models in one common framework (Vyas and John 2016). For further details on the HEC-RTS model, readers are referred to the HEC-RTS user manual (US Army Corps of Engineers 2020c).

5.5. Methods

5.5.1. Hydrological model calibration and validation

5.5.1.1. Selection of precipitation events

Since this study focuses on flood forecasting in a fully urbanized catchment, the hydrological model must be calibrated and validated to simulate extreme events. Therefore, an event-based model calibration approach was used to calibrate the hydrological model (Awol et al. 2018). Given that the time of concentration of the watershed is relatively low (~4 hours), 15-minute time steps were used for hydrological simulations (Fang et al. 2008). Consistent with previous storm events reported in the GTA with the potential for flooding, events with rainfall accumulation > 20 mm (corresponding to a 2-year return period storm) were considered during the event selection (TRCA Flood Risk Management 2020). Other criteria such as precipitation intensity, percent detection, availability of both Radar and gauge precipitation, missing value percentage, and sufficient discharge at the watershed outlet were also considered during event selection (Wijayarathne et al. 2020b, a). As Z–R relationships for WKR C-

band Radar QPEs do not account for bright band contamination, precipitation during the winter season was excluded from the study (Boodoo et al. 2015; Wijayarathne et al. 2020a). Consequently, eighteen precipitation events occurred during spring, summer, and fall periods from 2013 to 2018 were screened to select significant storm events with the potential of flooding to perform calibration and validation of hydrological models and stormwater runoff simulation (Table 5-1).

Table 5-1 *Description of events.*

Event #	Start time (UTC)	End time (UTC)	Season	Cumulative rainfall (mm)	Peak flow (m^3s^{-1})
1	28 May 2013 0915	29 May 2013 0800	Spring	35.2	36.6
2	31 Jul 2013 2220	01 Aug 2013 1005	Summer	42.5	30.2
3	27 Jul 2014 2300	28 Jul 2014 0930	Summer	35.5	51.5
4	20 Apr 2015 0305	20 Apr 2015 1305	Spring	24	39.4
5	31 May 2015 0315	31 May 2015 1000	Spring	21.2	39.3
6	08 Jun 2015 0455	08 Jun 2015 1025	Summer	29	42.7
7	27 Jun 2015 1810	28 Jun 2015 0255	Summer	34	56.4
8	10 Aug 2015 1625	10 Aug 2015 2040	Summer	43.5	79
9	28 Oct 2015 0950	28 Oct 2015 1435	Fall	21.9	56.8
10	10 Nov 2015 19:55	11 Nov 2015 0040	Fall	21.7	18.5
11	13 Aug 2016 1615	13 Aug 2016 2000	Summer	27	74.7
12	23 Jun 2017 0435	23 Jun 2017 1405	Summer	47.5	110.7
13	20 Jul 2017 1515	20 Jul 2017 1700	Summer	23.8	65.2
14	24 Jun 2018 0930	24 Jun 2018 1515	Summer	27.2	49.7
15	22 Jul 2018 0825	22 Jul 2018 1355	Summer	26.7	20.6
16	17 Aug 2018 0540	17 Aug 2018 1225	Summer	52.2	31.82
17	21 Aug 2018 1105	21 Aug 2018 1935	Summer	39.8	59.55
18	10 Sep 2018 0810	10 Sep 2018 2040	Fall	25.8	36.38

5.5.1.2. Bias correction of Radar QPEs

Firstly, Radar estimated precipitation data were bias-corrected using the Cumulative Distribution Function Matching (CDFM) radar-gauge merging method to increase accuracy and reliability before using them as precipitation input to hydrological, hydraulic models (Wijayarathne et al. 2020a). The impact of radar-gauge merging on accuracy and reliability of Radar QPEs was assessed by comparing the nearest gauge point for WKR QPEs and Radar pixel where the gauge is located for NEXRAD QPEs (Wijayarathne et al. 2020a). The correlation coefficient (r, Eq. 5-1) (value of 1 for a perfect fit) and Root Mean Square Error (RMSE, Eq. 5-2) (value of 0 for a perfect fit) were calculated between radar-gauge pairs for each event.

Correlation (r)

$$r = \frac{\sum(P_G - \bar{P}_G)(P_R - \bar{P}_R)}{\sqrt{\sum (P_G - \bar{P}_G)^2 \sum (P_R - \bar{P}_R)^2}} \quad (5\text{-}1)$$

RMSE (mm)

$$rmse = \sqrt{\frac{\sum_{i=1}^{n}(P_G - P_R)^2}{n}} \quad (5\text{-}2)$$

Where,

P_G gauge measurement

$\bar{P}_G$ average gauge measurement

P_R radar rainfall

$\bar{P}_R$ average radar rainfall

n number of radar-gauge pairs

Secondly, to further assess the impact of radar-gauge merging on the accuracy and reliability of Radar QPEs, a proxy validation was performed using the HEC-HMS hydrological model from TRCA (McKee et al. 2018). The previously calibrated model

parameters determined using gauge data were employed during the model run (Chu and Steinman 2009). Precipitation input to the HEC-HMS model was modified according to five different scenarios: i) Gauge data (G-G); ii) WKR C-band Radar QPEs (G-C); iii) WKR C-band Radar QPEs bias-corrected with CDFM (G-C-B); iv) NEXRAD S-band Radar QPEs (G-N); v) NEXRAD S-band Radar QPEs bias-corrected with CDFM (G-N-B). The agreement between observed and simulated streamflow was evaluated by calculating Pearson's correlation coefficient (r, Eq. 5-3), Root Mean Square Error (RMSE, Eq. 5-4), Percent BIAS (PBIAS, Eq. 5-5), Mean Absolute Error (MAE, Eq. 5-6), Kling-Gupta Efficiency (KGE, Eq. 5-7), Nash Sutcliffe Efficiency (NSE, Eq. 5-8), Volume Error (VE, Eq. 5-9), and Modified Peak Flow Criterion (MPFC, Eq. 5-10). The optimal value of PBIAS is 0. Positive values indicate model overestimation, whereas negative values show model underestimation (Wijayarathne and Coulibaly 2020). MAE values range from 0 to ∞ where lower values indicate better performances (Willmott and Matsuura 2005). KGE value ranges between -∞ and 1, with one indicating perfect fit (Gupta et al. 2009). NSE values spanning between -∞ and 1, with 1 being the optimal value. Values between 0 and 1 are considered acceptable (Nash and Sutcliffe 1970; Moriasi et al. 2007). The value of VE ranges from 0 to ∞ , and better performances show values close to 0 (Samuel et al. 2011). MPFC focuses on peak flows, and a value of 1 reveals a perfect fit (Coulibaly et al. 2001).

Correlation (r)

$$r = \frac{\sum_{i=1}^{n}\left(\widehat{Q}_i - \bar{\widehat{Q}}\right)\left(Q_i - \widehat{Q}_i\right)}{\sqrt{\sum_{i=1}^{n}\left(Q_i - \widehat{Q}_i\right)^2 * \sum_{i=1}^{n}\left(\widehat{Q}_i - \bar{\widehat{Q}}\right)^2}} \quad (5\text{-}3)$$

RMSE (mm)

$$RMSE = \sqrt{\frac{\sum_{i=1}^{n}\left(Q_i - \widehat{Q}_i\right)^2}{n}} \quad (5\text{-}4)$$

PBIAS (%)

$$PBIAS = \left[\frac{\sum_{i=1}^{n}\left(\widehat{Q}_i - Q_i\right) * (100)}{\sum_{i=1}^{n}(Q_i)}\right] \quad (5\text{-}5)$$

MAE (mm)

$$MAE = \frac{\sum_{i=1}^{n}\left|\widehat{Q}_i - Q_i\right|}{n} \quad (5\text{-}6)$$

KGE

$$KGE = 1 - \sqrt{(r-1)^2 + (\alpha-1)^2 + (\beta-1)^2} \quad (5\text{-}7)$$

NSE

$$NSE = 1 - \frac{\sum_{i=1}^{n}\left(Q_i - \widehat{Q}_i\right)^2}{\sum_{i=1}^{n}(Q_i - \bar{Q})^2} \quad (5\text{-}8)$$

VE

$$VE = \frac{\sum_{i=1}^{n}\widehat{Q}_i - \sum_{i=1}^{n}Q_i}{\sum_{i=1}^{n}Q_i} \quad (5\text{-}9)$$

MPFC

$$MPFC = 1 - \frac{\left[\sum_{i=1}^{n_p}\left(Q_{pi} - \hat{Q}_{pi}\right)^2 Q_{pi}^2\right]^{1/4}}{\left(\sum_{i=1}^{n_p}Q_{pi}^2\right)^{1/2}} \quad (5\text{-}10)$$

Where,

Q_i observed flow at i^{th} data point

$\bar{Q}$ mean observed flow

$\widehat{Q}_i$ simulated flow at i^{th} data point

$\bar{\widehat{Q}}$ mean simulated flow

n number of data points

n_p number of peak flows that are greater than 75 percentiles of observed flow

Q_{pi} observed peak flows

$\hat{Q}_{pi}$ simulated peak flows

r linear correlation coefficient

α measure of relative variability

β bias (ratio of simulated and observed values)

NSE_{log} NSE calculated using the log streamflow values (for low flows)

NSE_{sqr} NSE calculated using the squared streamflow values (for high flows)

5.5.1.3. Model recalibration and validation

In the hydrological model run analysis above, the existing HEC-HMS model from TRCA was used to evaluate the impact of radar-gauge merging on streamflow simulation. It is worth noting that the model's calibrated parameters were determined using historical gauge data, and therefore, the performances can be biased toward gauge data. In order to address this issue, HEC-HMS hydrological model was recalibrated using both WKR King City C-band Radar QPEs and KBUF S-band Radar QPEs to evaluate the effects of different Radar QPEs on hydrological model calibration and streamflow simulation. The following scenarios listed in Table 5-2 were considered during the recalibration. Scenarios 1 to 5 used gauge data, Radar only QPEs, and merged Radar QPEs during calibration and validation. Flood forecasting systems usually encompass hydrological models calibrated and validated using historical gauge data. To examine the advantage of using bias-corrected Radar QPEs to run the hydrological models with optimum parameters obtained using gauge data, two additional scenarios (scenarios 6 and 7) were also considered in the study.

Table 5-2 *HEC-HMS model run scenarios during calibration and validation.*

Scenario	Calibration	Validation/ model run
1) G-G	Gauge	Gauge
2) C-C	C-band radar QPEs	C-band radar QPEs
3) N-N	NEXRAD	NEXRAD
4) C-C-B	C-band radar QPEs + CDFM	C-band radar QPEs + CDFM
5) N-N-B	NEXRAD + CDFM	NEXRAD + CDFM
6) G-C-B	Gauge	C-band radar QPEs + CDFM
7) G-N-B	Gauge	NEXRAD + CDFM

The HEC-HMS model was calibrated against observed 15 min steam flow recorded at Islington (ID: 02HC033) flow gauge downstream. Two-thirds of the number of selected events (12) were assigned for model calibration, and the remaining number of events (6) were used for validation purposes. A total of 240 parameters were chosen to be optimized via calibration of the HEC-HMS model (Zahmatkesh et al. 2020, unpublished manuscript). The Dynamically Dimensioned Search (DDS) optimization algorithm (Tolson and Shoemaker 2008) was used to determine optimal parameter sets for each calibration event by maximizing the Nash Sutcliffe Efficiency objective function (Samuel et al. 2011) within Optimization Software Toolkit (OSTRICH) (Matott 2016). An average value of the parameters resulting after calibration for each event was calculated and used as the calibrated parameter list. Finally, the performances of calibrated model parameters were verified using selected validation events. Model performances were evaluated based on standard model performance statistics during each calibration and validation scenarios, as mentioned above.

5.5.2. Flood inundation mapping

This part of the research involved setting up the HEC-RTS platform for the Mimico Creek watershed using both Radar QPEs and gauges to assess the benefit of radar-derived rainfall for flood forecasting. First, existing hydrological (HEC-HMS) and hydraulic (HEC-RAS) models were integrated into the HEC-RTS framework using the setup module in HEC-RTS. Hydrometeorological data were transferred from an ArcHydro geo-database time series to Hydrologic Engineering Center-Data Storage System (HEC-DSS) software and eventually to HEC-HMS as hydrometeorological inputs. HEC-RTS links HEC-HMS and HEC-RAS, and therefore each model is executed in a coordinated manner. Simulated streamflow from HEC-HMS hydrological model was inputted to HEC-RAS using DSS data exchange software to produce flood inundation maps. Finally, flood inundation depths and extent boundaries were generated through the RAS mapper component of HEC-RAS within the HEC-RTS framework. The HEC-RTS framework was used to produce flood inundation maps that correspond to the seven model run scenarios listed in Table 5-2 for 8th July 2013 flash flood event in Toronto. The probability of flooding for each cell on the inundation maps was calculated and, flood probability maps were prepared using ArcGIS.

5.6. Results and discussion

5.6.1. Bias-correction of Radar QPEs

The correlation (r) improved for both WKR C-band and KBUF S-band Radar QPEs after applying radar-gauge merging (Table 5-3). The RMSE decreased for both

WKR C-band and KBUF S-band Radar QPEs after adjusting Radar QPEs to match gauge observations. Overall, the accuracy and reliability of both WKR C-band and KBUF S-band Radar QPEs improved after applying the CDFM radar-gauge merging method. The random component of the error causes the existing mismatch (Wijayarathne et al. 2020b).

Table 5-3 *Evaluation results for Radar QPEs before and after radar-gauge merging.*

Radar QPE	r		RMSE (mm)	
	Before	After	Before	After
WKR C-Band radar QPEs	0.21	0.65	5.25	0.83
KBUF S-band radar QPEs	0.08	0.61	2.32	0.99

A comparison of hydrological model performance statistics of the streamflow simulation at Islington hydrometric station using gauge measurements, Radar only QPEs, and merged Radar QPEs as precipitation input is presented in Figure 5-2 and 5-3. The statistics indicate that the radar-gauge merging has a considerable effect on the accuracy of simulated stream flows. According to the previous literature, the uncertainty in the precipitation forcing is the most problematic in hydrological modeling (Her et al. 2019). Since the optimal model parameters in the existing HEC-HMS model were determined using gauge data during its calibration, the model performance statistics calculated between observed and simulated flow using the gauge as precipitation input (G-G) were used as the reference to perform evaluations.

Figure 5-2 shows the average correlation (r), RMSE (m^3s^{-1}), BIAS (%), and MAE (m^3s^{-1}) between observed and simulated streamflow using gauges, Radar only QPEs, and merged Radar QPEs as precipitation input to the HEC-HMS model. The streamflow simulations using gauge data appeared to perform best with relatively higher prediction accuracy than Radar QPEs. The intrinsic errors associated with reflectivity measurement

and reflectivity– rain intensity conversions cause errors in Radar QPEs (Dai et al. 2018). Errors can be induced to the Radar estimated precipitation by radome wetting, beam filling, partial beam blocking, Radar miscalibration, vertical air motion, evaporation, advection, attenuation, ground Clutter, and variability of the drop size distribution (Wijayarathne et al. 2020a; Seo et al. 2015). These biases can propagate through the hydrological model leading to uncertainties in streamflow simulations (Fornasiero et al. 2005). However, the model performance could be influenced by the gauge data as the model was calibrated using gauge data.

Overall, the model performances were improved using merged Radar QPEs compared to Radar only QPEs for both WKR C-band and KBUF S-band Radar QPEs. The agreement between observed and simulated streamflow using WKR C-band Radar QPEs is relatively low compare to the KBUF S-band Radar QPEs, according to RMSE, MAE, and BIAS (Figure 5-2). However, the correlation is relatively higher for WKR C-band Radar QPEs. Interestingly, the C-band Radar QPEs overestimated the streamflow both before and after radar-gauge merging while S-band QPEs underestimated the streamflow. In general, radar-only QPEs are known to underestimate precipitation, especially during heavy precipitation events (Smith et al. 2007; Duchon and Essenberg 2001). The significant ground clutter caused by highly developed infrastructure in the fully urbanized Mimico Creek watershed strongly contaminates and inflates the reflectivity values leading to higher Radar reflectivity values and consequently QPEs (Torres and Warde 2014). Since C-band Radar attenuates more than S-band Radar owing to its shorter wavelength, the WKR Radar is expected to underestimate precipitation,

especially in heavy rain events (Boodoo et al. 2015). The Mimico Creek watershed is located much closer to the WKR Radar station (<40 km radius, Figure 5-1), and hence detects precipitation closest to the ground and hence the gauge location. Therefore, extensive radome attenuation could result in low rainfall estimates (Germann 1999). Even though path attenuation was addressed during the study, the attenuation correction could be dominated by the extensive ground clutter at WKR, leading to higher reflectivity values and subsequently overestimated stream flows. Also, the season of the year where the precipitation event was recorded can influence the Radar QPEs (Prat and Nelson 2014). The bright band contamination could produce significantly high reflectivity values, causing overestimating QPEs especially during early spring and late fall. In contrast to the WKR Radar, the KBUF Radar detects precipitation over the study area at a distance of more than 100 km away from the Radar station. This distance results in rainfall detection at a higher elevation leading to underestimated precipitation (Young and Brunsell 2008).

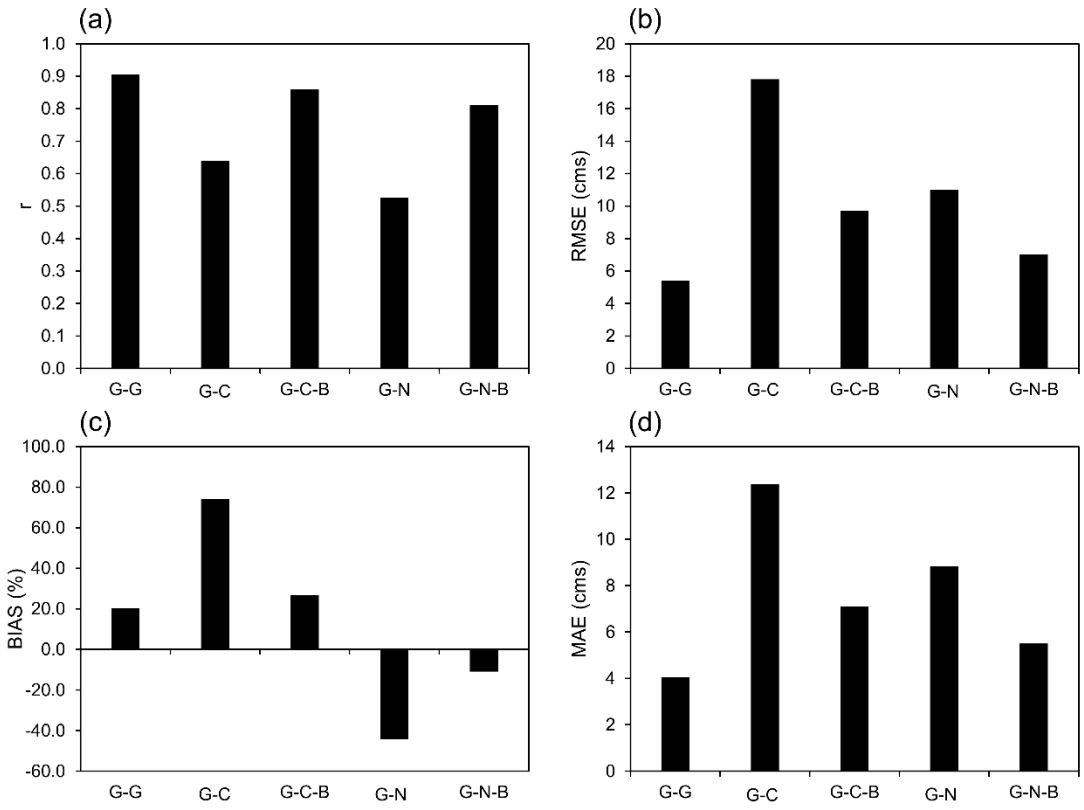

Figure 5-2 *Model performance for Radar QPEs before (G-C and G-N) and after (G-C-B and G-N-B) radar-gauge merging: (a) correlation coefficient-r, (b) root mean square error-RMSE, (c) percent bias-PBIAS, and (d) mean absolute error-MAE (Note: cms =* m^3s^{-1}*)*

Figure 5-3 presents the box plots of four model efficiency indices: NSE, KGE, VE, and MPFC. In comparison to radar-only QPEs (for both WKR C-band and KBUF S-band), merged-radar QPEs provide reasonably accurate simulated streamflow for all rainfall events. The intrinsic errors associated with Radar produce relatively poor Radar QPEs leading to less accurate streamflow simulations than with merged-radar QPEs. The medians of the performance indices for both WKR C-band and KBUF S-band Radar remained much closer to the medians of the reference gauge and sometimes even within

the interquartile range (IQR) after applying the bias correction. The first quartile, median, and third quartile of performance indices calculated for simulated streamflow using both WKR and KBUF Radar were the same as gauges after radar-gauge merging compared to the Radar only QPEs. Also, IQRs of performance indices were reduced after the bias correction of Radar QPEs, implying that radar-gauge merging helps enhance predicted streamflow accuracy.

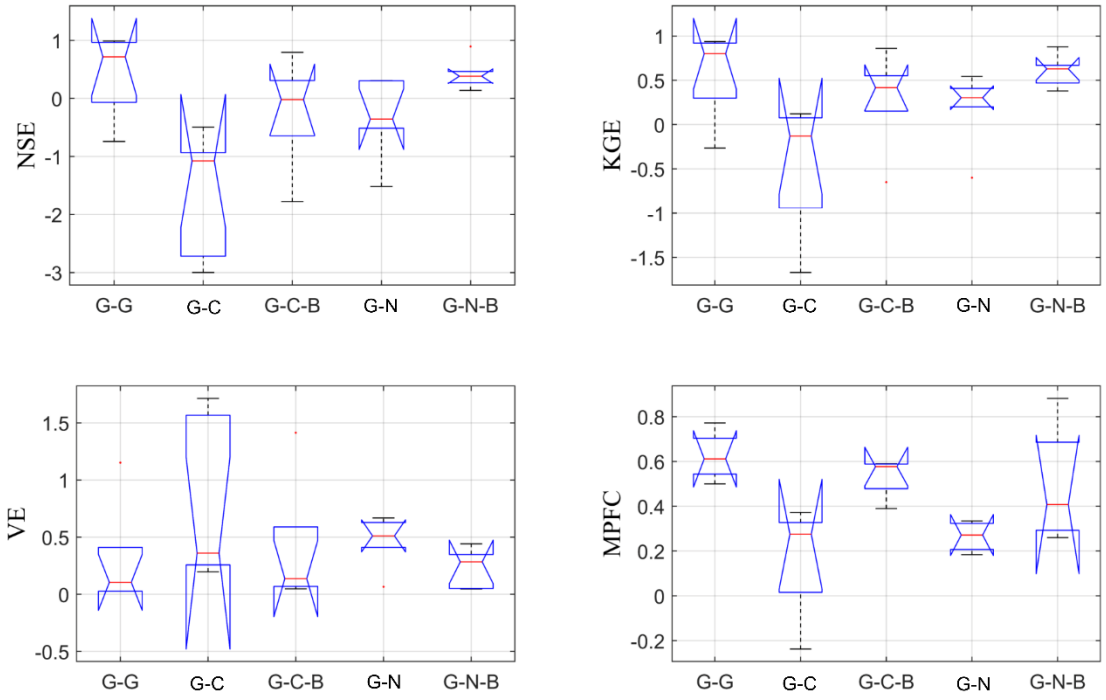

Figure 5-3 *Box plots showing model performance criteria for Radar QPEs before (G-C and G-N) and after (G-C-B and G-N-B) radar-gauge merging: (a) Nash Sutcliffe Efficiency-NSE, (b) Kling-Gupta Efficiency-KGE, (c) Volume Error-VE, and (d) Modified Peak Flow Criterion-MPFC*

5.6.2. Model calibration and validation

Figure 5-4 presents the average event-based model performance statistics for the streamflow simulation at the Islington flow station downstream of Mimico Creek watershed during the calibration period. The performance matrices calculated between observed and simulated flow using a model calibrated with gauge data (G-G) were used to reference Radar QPE performance evaluation. The calculated correlation values varied depending on the event and were relatively higher for all calibration scenarios that involved merged Radar QPEs (C-C-B:0.48-0.95; N-N-B:0.47-0.96) compared to scenarios with Radar only QPEs (C-C:0.03-0.96; N-N:0.25-0.98). Therefore, in comparison to models calibrated with Radar only QPEs for both WKR C-band and KBUF S-band, models calibrated with merged Radar QPEs provided reasonably accurate simulated stream flows. As shown in Figure 5-4, RMSE values also varied considerably between both different events and calibration scenarios. Similar to correlation, calibration scenarios involving merged Radar QPEs (C-C-B and N-N-B) showed better performances than scenarios with Radar only QPEs (C-C and N-N). The corresponding RMSE values were relatively low and nearly similar for models calibrated using merged Radar QPEs (4.39-33.82 $m^3s^{-1}$and 5.43-22.08 m^3s^{-1} for C-C-B and N-N-B, respectively) than the models calibrated with Radar only QPEs (7.35-45.39 $m^3s^{-1}$and 7.96-33.51 m^3s^{-1} for C-C and N-N, respectively). The MAE followed the same trend as RMSE with relatively lower values for calibration scenarios with merged Radar QPEs (C-C-B:3.13-22.78 m^3s^{-1}; N-N-B:3.93-22.06 m^3s^{-1}) and relatively raised errors for scenarios using Radar only QPEs (C-C:5.60-46.50 m^3s^{-1}; N-N:6.20-55.71 m^3s^{-1}). Consistent with the correlation,

hydrological models calibrated with bias-corrected Radar QPEs (C-C-B and N-N-B) performed better than models calibrated with Radar only QPEs (C-C and N-N) concerning error measurements. The average negative and positive bias percentages estimated for scenarios with Radar only QPEs were significantly reduced using the merged Radar QPEs for both WKR C-band and KBUF S-band Radar during calibration. Hydrological models calibrated with bias-corrected Radar QPEs produced results with relatively low bias values (-40.27% - 141.36% and -62.82 % - 42.05 % for C-C-B and N-N-B, respectively) compared to results from the models calibrated with radar-only QPEs (2.62-173.00 % and -66.76-122.81 % for C-C and N-N, respectively; Figure 5-4). Calculated hydrological model performance indices, KGE, NSE, VE, and MPFC, also supported that radar-gauge merging improves the accuracy and reliability of Radar QPEs and subsequently calibration of hydrological models. The KGE values were relatively better for models calibrated using merged Radar QPEs (C-C-B:-0.35-0.82; N-N-B:-0.26-0.67) compared to models calibrated a with Radar only QPEs (C-C:-2.08-0.41; N-N:-2.63-0.45). The NSE followed KRE with values range from -2.08-0.73, -1.32-0.66, -22.30- 0.04, and -12.37-0.24 for C-C-B, N-N-B, C-C, and N-N, respectively revealing better performance for merged Radar QPEs. Reported volume errors also supported the notion that models calibrated with merged Radar QPEs perform better than models calibrated with Radar only QPEs with reported VE values of 0.03-0.76, 0.03-0.67, 0.04-1.72, and 0.06-1.71 for C-C-B, N-N-B, C-C, and N-N, respectively. The MPFC values were better for calibrated models with bias-corrected Radar QPEs (C-C-B:0.26-0.72; N-

N-B:0.04-0.69) compared to the models calibrated with Radar only QPEs (C-C:0.01-0.27; N-N:0 -0.64).

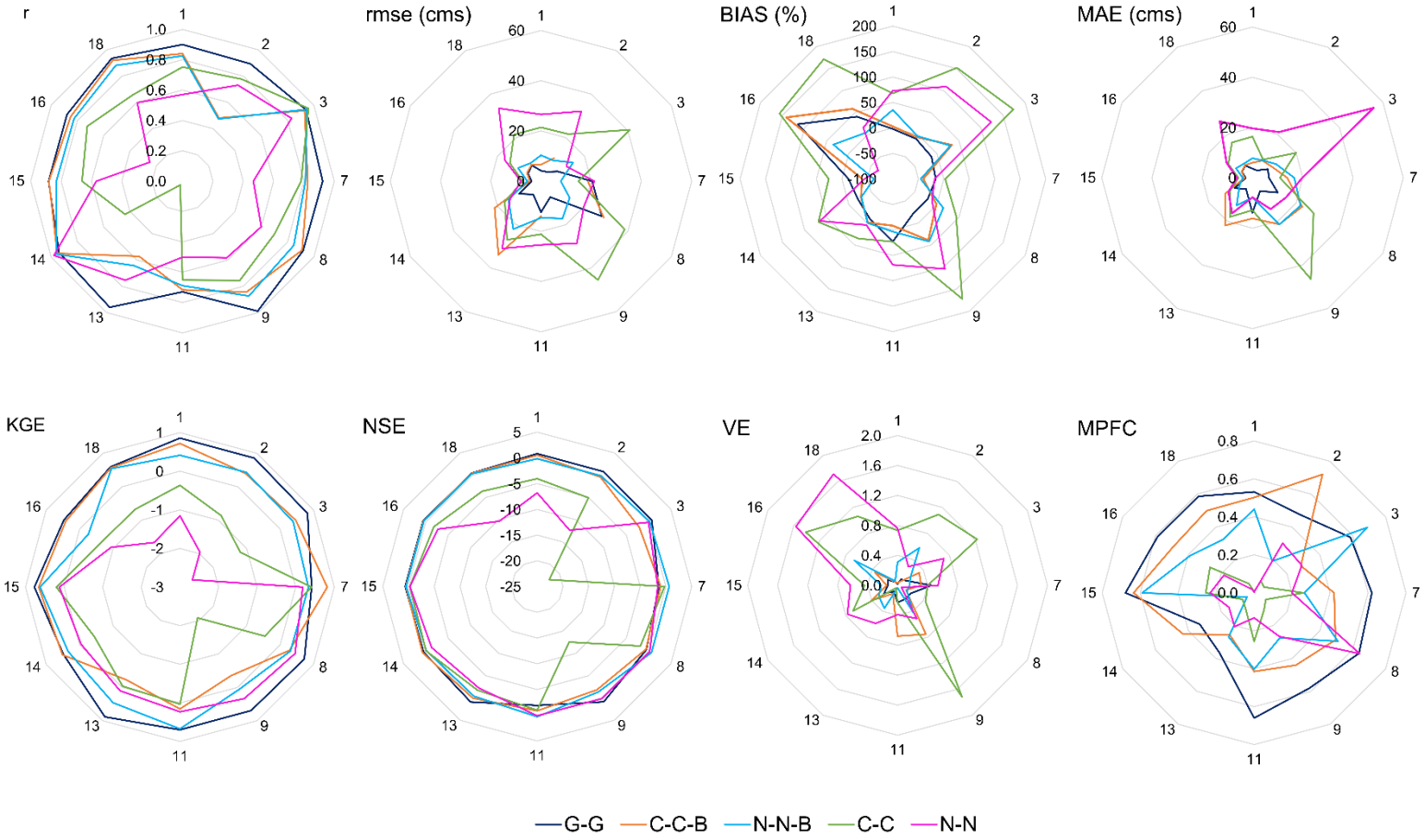

Figure 5-4 *Average correlation (r), RMSE (m^3s^{-1}), BIAS (%), MAE (m^3s^{-1}), KGE, NSE, VE, and MPFC between observed and simulated streamflow at Islington flow station downstream of Mimico Creek watershed during calibration (Note: cms = m^3s^{-1})*

Figure 5-5 compares the box plots of observed and simulated streamflow at Islington flow station downstream of Mimico Creek watershed using gauge data, Radar only QPEs, and merged Radar QPEs for seven model run scenarios listed in Table 5-2 during validation. The median and IQR of simulated flows using gauge data as the precipitation input to the hydrological model calibrated with gauge data (G-G) matched the observed flow relatively well compared to the Radar QPEs. On the contrary, hydrological models calibrated and validated with Radar only QPEs (C-C and N-N) showed the least match with the observed streamflow. The inherent errors associated with Radar QPEs during data acquisition and processing can cause errors leading to less accurate Radar QPEs and subsequently erroneous simulated stream flows. However, hydrological models calibrated and validated with KBUF S-band Radar only QPEs performed better than the models calibrated with WKR C-band Radar only QPEs. The anomalously high reflectivity values resulted from ground clutter, and bright band contamination during spring and fall might have resulted in overestimated QPEs leading to less accurate streamflow simulations. Even though the hydrological model calibrated with Radar only QPEs showed relatively low performances, the agreement between observed and simulated streamflow increased after applying radar-gauge merging. In comparison to Radar only QPEs scenarios (C-C and N-N), hydrological models calibrated with merged Radar QPEs (C-C-B and N-N-B) provided considerably accurate simulated streamflow for all events. Surprisingly, when hydrological models were calibrated with gauge data and then run with bias-corrected Radar QPEs (G-C-B and G-N-B), similar or better performance was observed than the models calibrated with merged Radar QPEs (C-

C-B and N-N-B). The medians of simulated streamflow for both G-C-B and G-N-B calibration scenarios remained much closer to the medians of the observed and G-G and most of the time within the IQR of observed streamflow. The overall performance of model run scenarios varies from best performance to worst as G-G > G-C-B ≅ G-N-B > C-C-B ≅ N-N-B > C-C ≅ N-N.

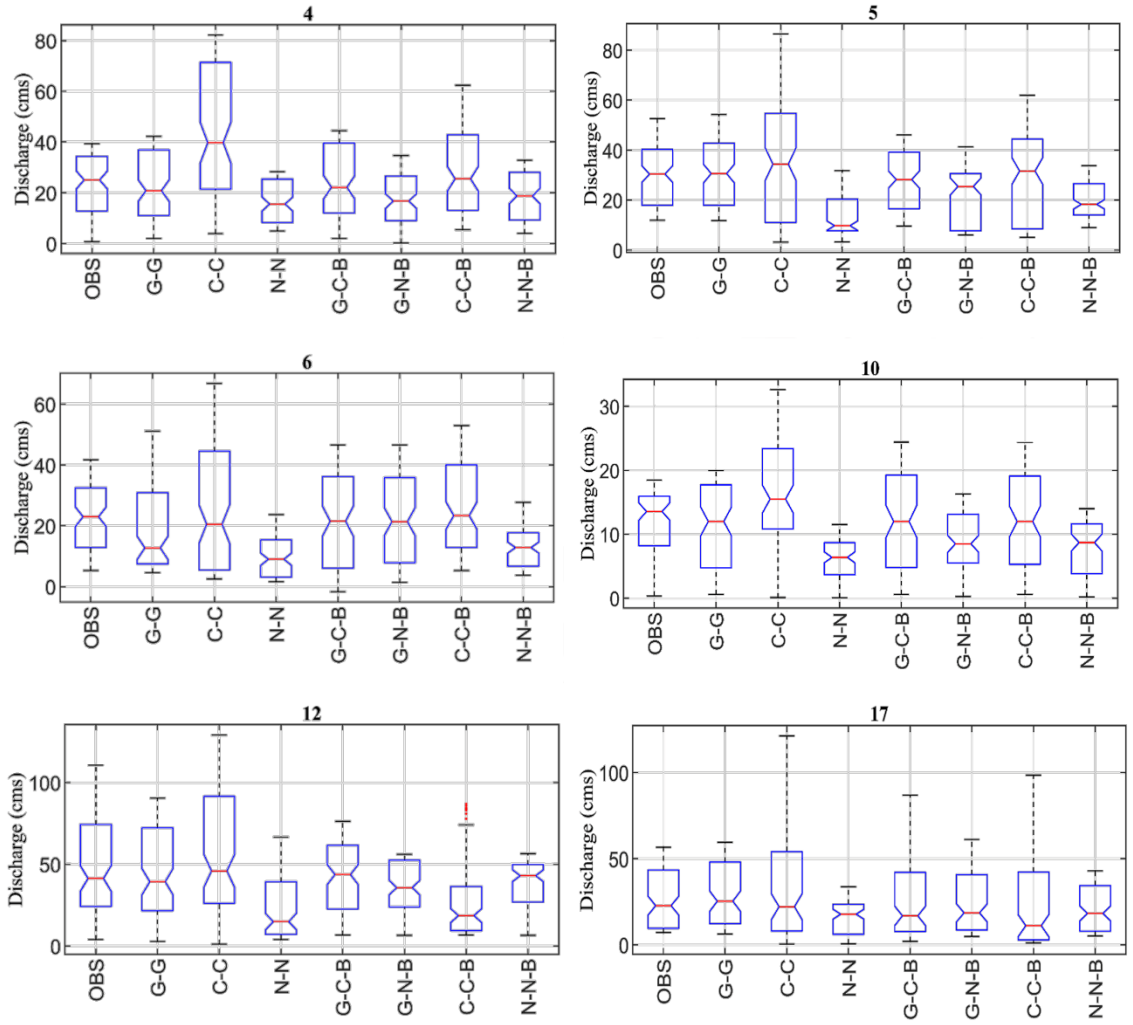

Figure 5-5 *Box plots of observed and simulated streamflow for model run scenarios during validation*

Figure 5-6 shows observed and simulated hydrographs for the seven model run scenarios (Table 5-2) using gauges, Radar only QPEs, and merged Radar QPEs as precipitation input to the HEC-HMS model validation events. The simulated peak streamflow's magnitude and timing closely matched with models calibrated with merged Radar QPEs for both WKR C-band and KBUF S-band Radar QPEs compared to the models calibrated with Radar only QPEs. Similar to the previous results, hydrological models calibrated with gauge data and run with bias-corrected Radar QPEs (G-C-B and G-N-B) performed better than the models calibrated and run with merged Radar QPEs (C-C-B and N-N-B). The similarity of hydrographs from the HEC-HMS model runs using bias-corrected Radar QPEs are statistically demonstrated in Figure 5-7. A comparison of hydrological model performance statistics calculated for seven calibration scenarios listed in Table 5-2 is shown in Figure 5-7. All four indices were significantly improved after the application of radar-gauge merging using the CDFM radar-gauge merging method. Similar to the previous results, G-C-B and G-N-B performed better than C-C-B and N-N-B, implying that merged Radar QPEs can be successfully used to run hydrological models which were calibrated using gauge data for flood forecasting purposes.

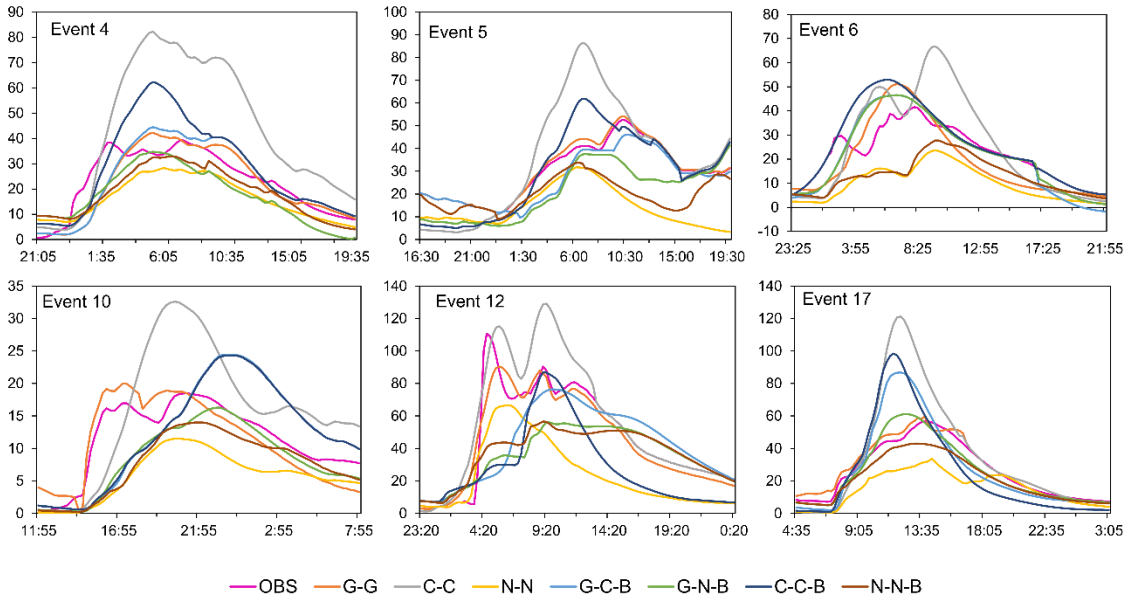

Figure 5-6 *Hydrographs of streamflow for model run scenarios during validation*

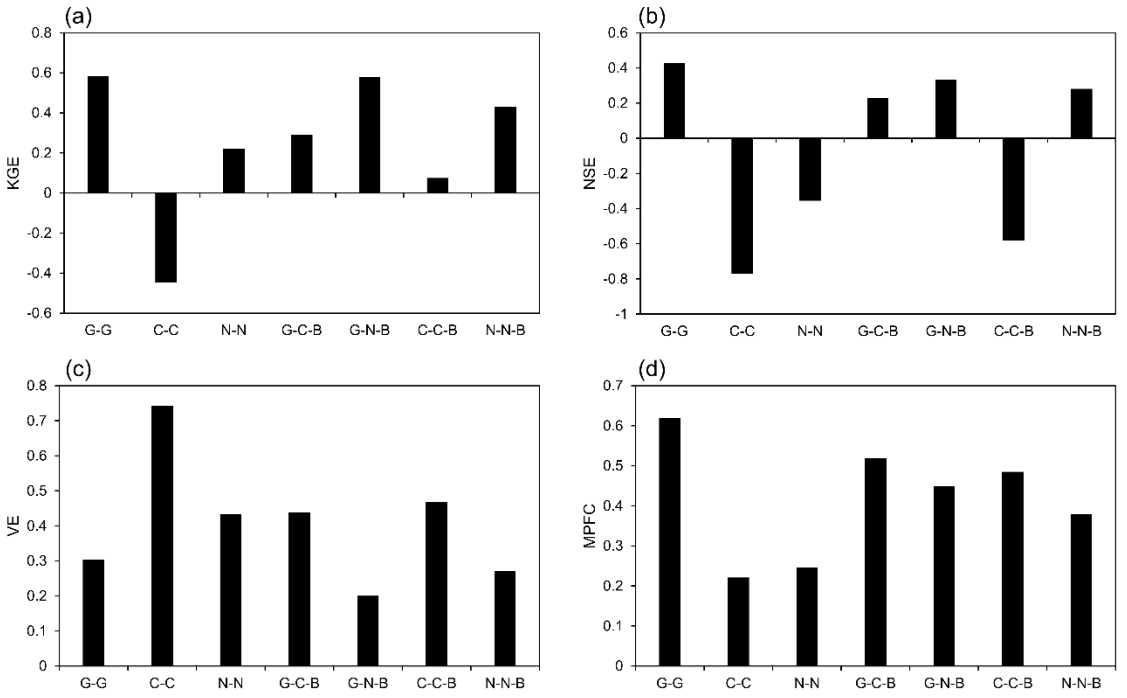

Figure 5-7 *Hydrological model performance criteria for validation events: (a) Kling-Gupta Efficiency-KGE, (b) Nash Sutcliffe Efficiency-NSE, (c) Volume Error-VE, and (d) Modified Peak Flow Criterion-MPFC*

To further assess the effect of Radar QPEs on hydrological model simulations, Taylor diagrams were drawn using three statistical parameters (standard deviation, correlation coefficient, and centered root mean square error) calculated for the validation events (Figure 5-8). The simulated streamflow using gauge data as precipitation input to a model calibrated using gauge data (G-G) performed best as they are plotted closest to the black arc and the point "OBS". The model run scenarios that involved bias-corrected Radar QPEs during calibration were plotted relatively closer to the black curve as well as the point "OBS", revealing their better performances compared to the models calibrated with Radar only QPEs. Also, hydrological models calibrated with gauge data but validated with merged Radar QPEs (G-C-B and G-N-B) performed better, showing the ability to use bias-corrected Radar to run existing hydrological models for operational flood forecasting.

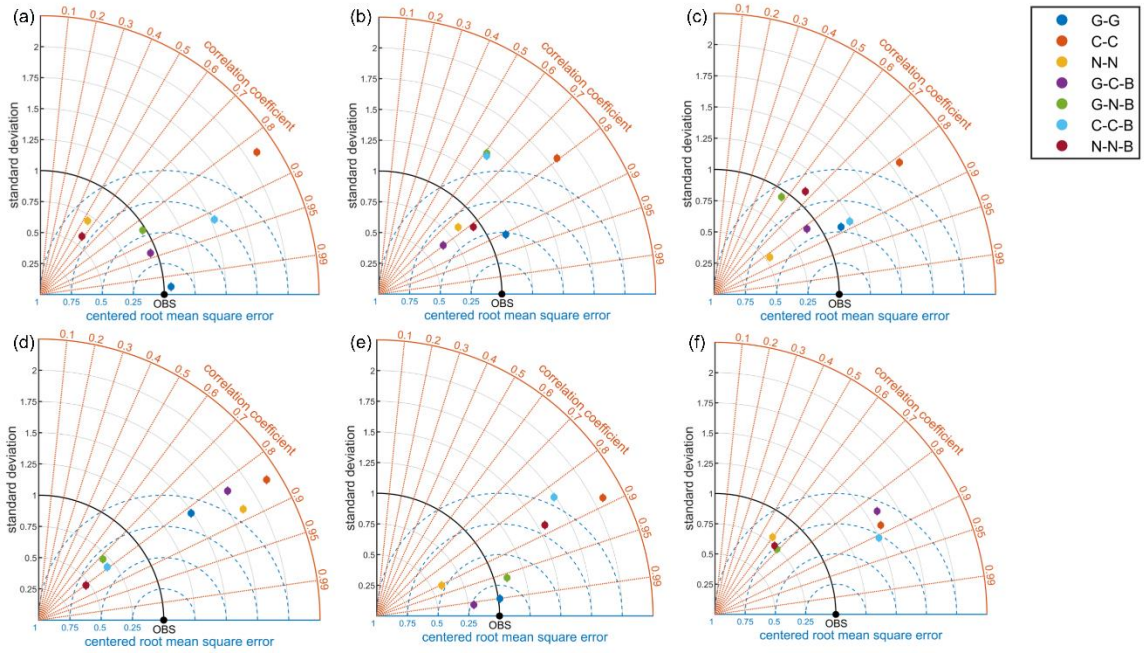

Figure 5-8 *Taylor diagrams showing a statistical comparison between observed and simulated streamflow for all model run scenarios during validation [Note: Taylor diagram summarizes standard deviation, correlation coefficient, and centered root mean square error for each calibration scenario for validation events. Different colors denote different model run scenarios. The best scenario plots itself closer to the black arc as well as the point 'OBS' (observed flow)]*

5.6.3. Flood inundation mapping

Figure 5-9 shows the flood extent maps produced using HEC-HMS and HEC-RAS models within the HEC-RTS framework for the 8th July 2013 Toronto flood. Precipitation input from gauges, Radar only QPEs, and merged Radar QPEs along with calibrated model parameters from the seven calibration scenarios were used to generate flood inundation maps. Flood extent maps corresponding to a selected part of the downstream part of the watershed are shown in Figure 5-9. The flood extent was mapped using peak flows recorded at each junction of the Mimico Creek. The flood extent using gauge data as precipitation input to HEC-RTS was considered as the reference. The area under inundation determined using the bias-corrected Radar QPEs (G-C-B and G-N-B)

agreed well with the flood extent using gauge data compared to the Radar only QPEs (C-C and N-N; Figure 5-9). For example, a relatively large submerged area in Figure 5-9 (C) that resulted from Radar only C-band QPEs reflects the overestimation of precipitation due to excessive ground clutter. The extent of the flood-prone area generated by RAS Mapper using the outflow from the hydrological models calibrated with gauge data but ran with merged Radar QPEs (G-C-B and G-N-B) performed better, revealing the ability to use bias-corrected Radar to run existing hydrological models for operational flood forecasting.

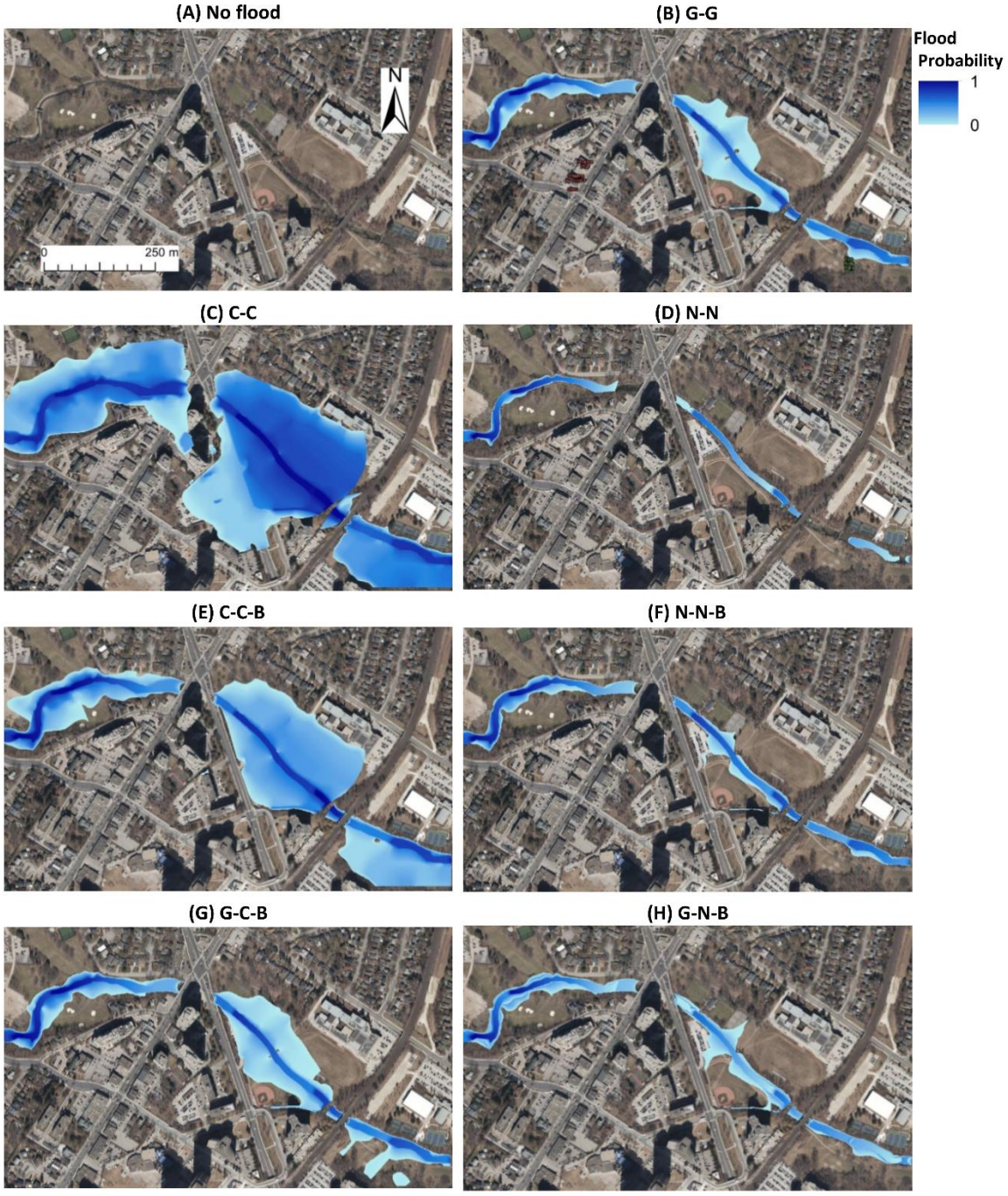

Figure 5-9 *Simulated flood inundation corresponding to the model run scenarios using the HEC-RTS framework*

5.7. Conclusions

This research integrates the HEC-HMS hydrological model and HEC-RAS hydraulic model into the HEC-RTS framework to assess the potential of Radar QPEs for flood forecasting. It is shown that radar-gauge merging enhances the accuracy and reliability of both Canadian WKR C-band and US NEXRAD KBUF S-band dual-polarized Radar QPEs and, subsequently, the streamflow simulations' accuracy. Bias-corrected Radar QPEs improved all hydrological model performance indices when compared to radar-only QPEs during model recalibration. This indicates that the radar-gauge merging can enhance the hydrological models' calibration. Therefore, Radar QPEs can be used as precipitation input to hydrometeorological models for the areas where precipitation gauges are sparse. As Radar provides real-time spatially distributed precipitation information, it can be used as precipitation input for hydrological and hydraulic models for flood forecasting purposes in small urban watersheds where response time is only a few hours. Furthermore, it is found that bias-corrected Radar QPEs can be effectively used to run hydrological models initially calibrated using gauge data. The majority of the Canadian flood forecasting agencies use hydrological models calibrated and validated using gauge data (Zahmatkesh et al. 2019). However, due to lack of long-term Radar data archives, and the high cost and the time required to recalibrate existing models, updating the existing hydrological models using bias-corrected Radar QPEs is recommended to simulate streamflow input to hydraulic models to produce flood inundation maps. Furthermore, the HEC-RTS framework can be used to produce flood extent maps using bias-corrected Radar QPEs for future storm events. These maps could

be used to make appropriate decisions and take immediate actions to reduce human and economic losses. However, simulated flood depths must be validated with the high watermark in the regional flood level maps before operational use. In the future, the HEC-RTS framework could be upgraded to an automated Flood Early Warning Systems (FEWS) using methods available in HEC-RTS to retrieve, compute, view, and manage real-time Canadian and NEXRAD Radar precipitation data to issue real-time flood forecasts for operational use.

5.8. Acknowledgments

The authors thank the Natural Science and Engineering Research Council (NSERC) Canadian FloodNet project for financially support this research (NETGP-451456). The authors would like to thank Dr. Z. Zahmatkesh and Dr. S. Han for providing the recalibrated HEC-HMS model. The authors are also grateful to Mr. Andre D.L. Zanchetta for his NEXRAD Radar QPE acquisition and processing assistance. TRCA provided both the HEC-HMS and HEC-RAS model and hydrometeorological data used in this study. The WKR C-band Radar QPEs and KBUF NEXRAD S-band Radar QPEs were collected from the Observations-Based Research Section, King City, ECCC, and NOAA National Centers for Environmental Information data archives. The authors declare no conflict of interest.

5.9. References

Aksoy, H., V. S. O. Kirca, H. I. Burgan, and D. Kellecioglu, 2016: Hydrological and hydraulic models for determination of flood-prone and flood inundation areas. *Proc. Int. Assoc. Hydrol. Sci.*, **373**, 137–141, https://doi.org/10.5194/piahs-373-137-2016.

Arduino, G., P. Reggiani, and E. Todini, 2005: Recent advances in flood forecasting and flood risk assessment, hal-00304828.

Awol, F. S., P. Coulibaly, and B. A. Tolson, 2018: Event-based model calibration approaches for selecting representative distributed parameters in semi-urban watersheds. *Adv. Water Resour.*, **118**, 12–27, https://doi.org/10.1016/j.advwatres.2018.05.013.

——, ——, I. Tsanis, and F. Unduche, 2019: Identification of Hydrological Models for Enhanced Ensemble Reservoir Inflow Forecasting in a Large Complex Prairie Watershed. *Water*, **11**, 2201, https://doi.org/10.3390/w11112201.

Barge, B. L., R. G. Humphries, S. J. Mah, and W. K. Kuhnke, 1979: Rainfall measurements by weather radar: applications to hydrology. *Water Resour. Res.*, **15**, 1380–1386, https://doi.org/10.1029/WR015i006p01380.

Bellon, A., and G. L. Austin, 1978: The evaluation of two years of real-time operation of a short-term precipitation forecasting procedure (SHARP). *J. Appl. Meteorol.*, **17**, 1778–1787, https://doi.org/10.1175/1520-0450(1978)017<1778:TEOTYO>2.0.CO;2.

——, and ——, 1984: The accuracy of short-term radar rainfall forecasts. *J. Hydrol.*, **70**, 35–49, https://doi.org/10.1016/0022-1694(84)90112-4.

——, and I. Zawadzki, 1994: Forecasting of hourly accumulations of precipitation by optimal extrapolation of radar maps. *J. Hydrol.*, **157**, 211–233, https://doi.org/10.1016/0022-1694(94)90106-6.

——, S. Lovejoy, and G. L. Austin, 1980: Combining satellite and radar data for the short-range forecasting of precipitation. *Mon. Weather Rev.*, **108**, 1554–1566, https://doi.org/10.1175/1520-0493(1980)108<1554:CSARDF>2.0.CO;2.

Beneti, C., R. V. Calheiros, M. Sorribas, L. Calvetti, C. Oliveira, N. Rozin, and J. Ruviaro, 2019: Operational Hydrological Modelling of Small Watershed using QPE from Dual-Pol Radar in Brazil, *Preprints* 2019, 2019060026, https://doi: 10.20944/preprints201906.0026.v1.

Boodoo, S., D. Hudak, A. Ryzhkov, P. Zhang, N. Donaldson, D. Sills, and J. Reid, 2015: Quantitative precipitation estimation from a C-band dual-polarized radar for the 8 July 2013 flood in Toronto, Canada. *J. Hydrometeorol.*, **16**, 2027–2044, https://doi.org/10.1175/JHM-D-15-0003.1.

Borga, M., 2002: Accuracy of radar rainfall estimates for streamflow simulation. *J. Hydrol.*, **267**, 26–39, https://doi.org/10.1016/S0022-1694(02)00137-3.

——, S. Degli Esposti, and D. Norbiato, 2006: Influence of errors in radar rainfall estimates on hydrological modeling prediction uncertainty. *Water Resour. Res.*, **42**, https://doi.org/10.1029/2005WR004559.

Bowering, E. A., A. M. Peck, and S. P. Simonovic, 2014: A flood risk assessment to municipal infrastructure due to changing climate part I: methodology. *Urban Water J.*, **11**, 20–30, https://doi.org/10.1080/1573062X.2012.758293.

Bringi, V. N., and V. Chandrasekar, 2001: *Polarimetric Doppler weather radar: principles and applications*. Cambridge university press.

Bringi, V. N., M. A. Rico-Ramirez, and M. Thurai, 2011: Rainfall estimation with an operational polarimetric C-band radar in the United Kingdom: comparison with a gauge network and error analysis. *J. Hydrometeorol.*, **12**, 935–954, https://doi.org/10.1175/JHM-D-10-05013.1.

Brown, R. A., T. A. Niziol, N. R. Donaldson, P. I. Joe, and V. T. Wood, 2007: Improved detection using negative elevation angles for mountaintop WSR-88Ds. Part III:

Simulations of shallow convective activity over and around Lake Ontario. *Weather Forecast.*, **22**, 839–852, https://doi.org/10.1175/WAF1019.1.

Brunner, G. W., S. S. Piper, M. R. Jensen, and B. Chacon, 2015: Combined 1D and 2D hydraulic modeling within HEC-RAS. *World Environmental and Water Resources Congress 2015*, 1432–1443, https://doi.org/10.1061/9780784479162.141.

Chandrasekar, V., R. Keränen, S. Lim, and D. Moisseev, 2013: Recent advances in classification of observations from dual polarization weather radars. *Atmospheric Res.*, **119**, 97–111, https://doi.org/10.1016/j.atmosres.2011.08.014.

Charley, W., B. Moran, and J. LaRosa, 2012: Model Integration for Real-Time Flood Forecasting Inundation Mapping for Nashville Tributaries. *AGUFM*, **2012**, H43A–1310.

Che, D., and L. W. Mays, 2015: Development of an optimization/simulation model for real-time flood-control operation of river-reservoirs systems. *Water Resour. Manag.*, **29**, 3987–4005, https://doi.org/10.1007/s11269-015-1041-8.

Chen, D., and A. Farrar, 2007: Evaluation of NARAD Precipitation Data for Rainfall Monitoring in Eastern Ontario, Canada. *Geomat. Solut. Disaster Manag.*, 103–116, https://doi.org/10.1007/978-3-540-72108-6_8.

Chu, X., and A. Steinman, 2009: Event and continuous hydrologic modeling with HEC-HMS. *J. Irrig. Drain. Eng.*, **135**, 119–124, https://doi.org/10.1061/(ASCE)0733-9437(2009)135:1(119).

Coulibaly, P., F. Anctil, and B. Bobee, 2001: Multivariate reservoir inflow forecasting using temporal neural networks. *J. Hydrol. Eng.*, **6**, 367–376, https://doi.org/10.1061/(ASCE)1084-0699(2001)6:5(367).

Cranston, M. D., and A. C. Tavendale, 2012: Advances in operational flood forecasting in Scotland. *Proceedings of the Institution of Civil Engineers-Water Management*, Vol. 165 of, Thomas Telford Ltd, 79–87, https://doi.org/10.1680/wama.2012.165.2.79.

Cunderlik, J., and S. P. Simonovic, 2004: *Calibration, verification and sensitivity analysis of the HEC-HMS hydrologic model*. Department of Civil and Environmental Engineering, The University of Western Ontario.

Dai, Q., Q. Yang, J. Zhang, and S. Zhang, 2018: Impact of Gauge Representative Error on a Radar Rainfall Uncertainty Model. *J. Appl. Meteorol. Climatol.*, **57**, 2769–2787, https://doi.org/10.1175/JAMC-D-17-0272.1.

Darbandsari, P., and P. Coulibaly, 2020: Inter-comparison of lumped hydrological models in data-scarce watersheds using different precipitation forcing data sets: Case study of Northern Ontario, Canada. *J. Hydrol. Reg. Stud.*, **31**, 100730, https://doi.org/10.1016/j.ejrh.2020.100730.

De Roo, A. P., and Coauthors, 2003: Development of a European flood forecasting system. *Int. J. River Basin Manag.*, **1**, 49–59, https://doi.org/10.1080/15715124.2003.9635192.

Devia, G. K., B. P. Ganasri, and G. S. Dwarakish, 2015: A review on hydrological models. *Aquat. Procedia*, **4**, 1001–1007, https://doi.org/10.1016/j.aqpro.2015.02.126.

Dhiram, K., and Z. Wang, 2016: Evaluation on Radar Reflectivity-Rainfall Rate (ZR) Relationships for Guyana. *Sciences*, **6**, 489–499, https://doi.org/10.4236/acs.2016.64039

Douglas, R. H., 1990: The stormy weather group (Canada). *Radar in Meteorology*, Springer, 61–68, https://doi.org/10.1007/978-1-935704-15-7_8.

Doviak, R. J., 1993: *Doppler radar and weather observations*. Courier Corporation.

Duchon, C. E., and G. R. Essenberg, 2001: Comparative rainfall observations from pit and aboveground rain gauges with and without wind shields. *Water Resour. Res.*, **37**, 3253–3263, https://doi.org/10.1029/2001WR000541.

Ezz, H., 2018: Integrating GIS and HEC-RAS to model Assiut plateau runoff. *Egypt. J. Remote Sens. Space Sci.*, **21**, 219–227, https://doi.org/10.1016/j.ejrs.2017.11.002.

Fang, X., D. B. Thompson, T. G. Cleveland, P. Pradhan, and R. Malla, 2008: Time of concentration estimated using watershed parameters determined by automated and manual methods. *J. Irrig. Drain. Eng.*, **134**, 202–211, https://doi.org/10.1061/(ASCE)0733-9437(2008)134:2(202).

Fornasiero, A., P. P. Alberoni, R. Amorati, L. Ferraris, and A. C. Taramasso, 2005: Effects of propagation conditions on radar beam-ground interaction: impact on data quality, hal-00297387, version 1.

Fulton, R. A., J. P. Breidenbach, D.-J. Seo, D. A. Miller, and T. O'Bannon, 1998: The WSR-88D rainfall algorithm. *Weather Forecast.*, **13**, 377–395, https://doi.org/10.1175/1520-0434(1998)013<0377:TWRA>2.0.CO;2.

Germann, U., 1999: Radome attenuation—a serious limiting factor for quantitative radar measurements? *Meteorol. Z.*, 85–90, https://doi.org/10.1127/metz/8/1999/85.

——, and I. Zawadzki, 2002: Scale-dependence of the predictability of precipitation from continental radar images. Part I: Description of the methodology. *Mon. Weather Rev.*, **130**, 2859–2873, https://doi.org/10.1175/1520-0493(2002)130<2859:SDOTPO>2.0.CO;2.

——, and ——, 2004: Scale dependence of the predictability of precipitation from continental radar images. Part II: Probability forecasts. *J. Appl. Meteorol.*, **43**, 74–89, https://doi.org/10.1175/1520-0450(2004)043<0074:SDOTPO>2.0.CO;2.

Goudenhoofdt, E., and L. Delobbe, 2009: Evaluation of radar-gauge merging methods for quantitative precipitation estimates. *Hydrol. Earth Syst. Sci.*, **13**, 195–203, https://doi.org/10.5194/hess-13-195-2009, 2009.

Gupta, H. V., H. Kling, K. K. Yilmaz, and G. F. Martinez, 2009: Decomposition of the mean squared error and NSE performance criteria: Implications for improving hydrological modelling. *J. Hydrol.*, **377**, 80–91, https://doi.org/10.1016/j.jhydrol.2009.08.003.

Guzman, J. A., D. N. Moriasi, M. L. Chu, P. J. Starks, J. L. Steiner, and P. H. Gowda, 2013: A tool for mapping and spatio-temporal analysis of hydrological data. *Environ. Model. Softw.*, **48**, 163–170, https://doi.org/10.1016/j.envsoft.2013.06.014.

Hall, W., M. A. Rico-Ramirez, and S. Krämer, 2015: Classification and correction of the bright band using an operational C-band polarimetric radar. *J. Hydrol.*, **531**, 248–258, https://doi.org/10.1016/j.jhydrol.2015.06.011.

Han, S., and P. Coulibaly, 2017: Bayesian Flood Forecasting Methods: A Review. *J. Hydrol.*, https://doi.org/10.1016/j.jhydrol.2017.06.004.

——, and ——, 2019: Probabilistic Flood Forecasting Using Hydrologic Uncertainty Processor with Ensemble Weather Forecasts. *J. Hydrometeorol.*, **20**, 1379–1398, https://doi.org/10.1175/JHM-D-18-0251.1.

Hashemyan, F., M. R. Khaleghi, and M. Kamyar, 2015: Combination of HEC-HMS and HEC-RAS models in GIS in order to Simulate Flood (Case study: Khoshke Rudan river in Fars province, Iran). *Res. J. Recent Sci. ISSN*, **2277**, 2502.

Hassan, D., P. A. Taylor, and G. A. Isaac, 2019: Solid snowfall rate estimation using a C-band radar. *Meteorol. Appl.*, **26**, 64–73, https://doi.org/10.1002/met.1737.

Her, Y., S.-H. Yoo, J. Cho, S. Hwang, J. Jeong, and C. Seong, 2019: Uncertainty in hydrological analysis of climate change: multi-parameter vs. multi-GCM ensemble predictions. *Sci. Rep.*, **9**, 1–22, https://doi.org/10.1038/s41598-019-41334-7.

Hicks, F. E., and T. Peacock, 2005: Suitability of HEC-RAS for flood forecasting. *Can. Water Resour. J.*, **30**, 159–174, https://doi.org/10.4296/cwrj3002159.

Huang, G.-J., V. N. Bringi, R. Cifelli, D. Hudak, and W. A. Petersen, 2010: A methodology to derive radar reflectivity–liquid equivalent snow rate relations using C-band radar and a 2D video disdrometer. *J. Atmospheric Ocean. Technol.*, **27**, 637–651, https://doi.org/10.1175/2009JTECHA1284.1.

Hudak, D., B. Currie, P. Rodriguez, S. G. Cober, I. Zawadzki, G. A. Isaac, and M. Wolde, 2002: Cloud phase detection in winter stratiform clouds using Polarimetric Doppler Radar. *Proc. ERAD*, 90–94.

Hudak, D., P. Rodriguez, and N. Donaldson, 2008: Validation of the CloudSat precipitation occurrence algorithm using the Canadian C band radar network. *J. Geophys. Res. Atmospheres*, **113**, https://doi.org/10.1029/2008JD009992.

Jonkman, S. N., and I. Kelman, 2005: An analysis of the causes and circumstances of flood disaster deaths. *Disasters*, **29**, 75–97, https://doi.org/10.1111/j.0361-3666.2005.00275.x.

Jonkman, S. N., and J. K. Vrijling, 2008: Loss of life due to floods. *J. Flood Risk Manag.*, **1**, 43–56, https://doi.org/10.1111/j.1753-318X.2008.00006.x.

Jordan, P., A. Seed, and G. Austin, 2000: Sampling errors in radar estimates of rainfall. *J. Geophys. Res. Atmospheres*, **105**, 2247–2257, https://doi.org/10.1029/1999JD900130.

Khan, S. I., Z. Flamig, and Y. Hong, 2019: Flood Monitoring System Using Distributed Hydrologic Modeling for Indus River Basin. *Indus River Basin*, Elsevier, 335–355, https://doi.org/10.1016/B978-0-12-812782-7.00015-1.

Larson, L. W., and E. L. Peck, 1974: Accuracy of precipitation measurements for hydrologic modeling. *Water Resour. Res.*, **10**, 857–863, https://doi.org/10.1029/WR010i004p00857.

Leach, J. M., K. C. Kornelsen, and P. Coulibaly, 2018: Assimilation of near-real time data products into models of an urban basin. *J. Hydrol.*, https://doi.org/10.1016/j.jhydrol.2018.05.064.

Marshall, J. S., and W. M. K. Palmer, 1948: The distribution of raindrops with size. *J. Meteorol.*, **5**, 165–166, https://doi.org/10.1175/1520-0469(1948)005<0165:TDORWS>2.0.CO;2.

Matott, L. S., 2016: OSTRICH–An Optimization Software Toolkit for Research Involving Computational Heuristics. *Doc. Users Guide Cent. Comput. Res. State Univ. N. Y. Buffalo N. Y. USA*.

Mays, L. W., 2010: *Water resources engineering*. John Wiley & Sons.

McKee, J. L., and A. D. Binns, 2016: A review of gauge–radar merging methods for quantitative precipitation estimation in hydrology. *Can. Water Resour. JournalRevue Can. Ressour. Hydr.*, **41**, 186–203, https://doi.org/10.1080/07011784.2015.1064786.

——, ——, M. Helsten, and M. Shifflett, 2018: Evaluation of Gauge-Radar Merging Methods Using a Semi-Distributed Hydrological Model in the Upper Thames River Basin, Canada. *JAWRA J. Am. Water Resour. Assoc.*, **54**, 594–612, https://doi.org/10.1111/1752-1688.12625.

McMillan, H., B. Jackson, M. Clark, D. Kavetski, and R. Woods, 2011: Rainfall uncertainty in hydrological modelling: An evaluation of multiplicative error models. *J. Hydrol.*, **400**, 83–94, https://doi.org/10.1016/j.jhydrol.2011.01.026.

Meischner, P., 2005: *Weather radar: principles and advanced applications*. Springer Science & Business Media.

Moreno, H. A., E. R. Vivoni, and D. J. Gochis, 2012: Utility of quantitative precipitation estimates for high resolution hydrologic forecasts in mountain watersheds of the Colorado Front Range. *J. Hydrol.*, **438**, 66–83, https://doi.org/10.1016/j.jhydrol.2012.03.019.

Moriasi, D. N., J. G. Arnold, M. W. Van Liew, R. L. Bingner, R. D. Harmel, and T. L. Veith, 2007: Model evaluation guidelines for systematic quantification of accuracy in watershed simulations. *Trans. ASABE*, **50**, 885–900, https://doi: 10.13031/2013.23153.

Nagai, A., 2003: Hydrologic Modeling of Rainfall-runoff Process and Its Application to Real-time Flood Forecasting. *Present Situat. OnThe Water Resour. Water Relat.*

Disaster Role Agro-Environ. Educ., 111–118. [Available online at https://pdfs.semanticscholar.org/cc11/b928840c5e5573df97473a59e26bcda8d750.pdf]

Nash, J. E., and J. V. Sutcliffe, 1970: River flow forecasting through conceptual models part I—A discussion of principles. *J. Hydrol.*, **10**, 282–290, https://doi.org/10.1016/0022-1694(70)90255-6.

Natural Resources Canada, 2016: Mimico Creek. Government of Canada, accessed 09October 2020, http://www4.rncan.gc.ca/search-place-names/unique.php?id=FDUYH&output=xml.

NOAA, 2018: NEXRAD Data Archive, Inventory and Access. Accessed 1st June 2019, https://www.ncdc.noaa.gov/nexradinv/.

Ochoa-Rodriguez, S., L.-P. Wang, P. Willems, and C. Onof, 2019: A review of radar-rain gauge data merging methods and their potential for urban hydrological applications. *Water Resour. Res.*, https://doi.org/10.1029/2018WR023332.

Ontario GeoHub , 2020: Southern Ontario Land Resource Information System (SOLRIS) 3.0., accessed 09October 2020, https://geohub.lio.gov.on.ca/datasets/0279f65b82314121b5b5ec93d76bc6ba.

Pilon, P. J., 2002: *Guidelines for reducing flood losses*. United Nations International Strategy for Disaster Reduction (UNISDR).

Prat, O. P., and B. R. Nelson, 2014: Evaluation of precipitation estimates over CONUS derived from satellite, radar, and rain gauge datasets (2002-2012). *HESSD*, **11**, 11489–11531, https://doi.org/10.5194/hessd-11-11489-2014.

Public Safety Canada, 2019: The Canadian Disaster Database. Accessed 13th May 2020, https://www.publicsafety.gc.ca/cnt/rsrcs/cndn-dsstr-dtbs/index-en.aspx.

Ran, Q., W. Fu, Y. Liu, T. Li, K. Shi, and B. Sivakumar, 2018: Evaluation of Quantitative Precipitation Predictions by ECMWF, CMA, and UKMO for Flood Forecasting:

Application to Two Basins in China. *Nat. Hazards Rev.*, **19**, 05018003, https://doi.org/10.1061/(ASCE)NH.1527-6996.0000282.

Randall, M., R. James, W. James, K. Finney, and M. Heralall, 2014: PCSWMM Real Time Flood Forecasting–Toronto, Canada.

Reed, S., J. Schaake, and Z. Zhang, 2007: A distributed hydrologic model and threshold frequency-based method for flash flood forecasting at ungauged locations. *J. Hydrol.*, **337**, 402–420, https://doi.org/10.1016/j.jhydrol.2007.02.015.

Roe, J., and Coauthors, 2010: NOAA's community hydrologic prediction system. *Proceedings from the 4th Federal Interagency Hydrologic Modeling Conference*.

Ryzhkov, A., P. Zhang, D. Hudak, J. Alford, M. Knight, and J. Conway, 2007: Validation of polarimetric methods for attenuation correction at C band. *Proc. 33rd Conf. Radar Meteorol*.

Ryzhkov, A. V., T. J. Schuur, D. W. Burgess, P. L. Heinselman, S. E. Giangrande, and D. S. Zrnic, 2005: The Joint Polarization Experiment: Polarimetric rainfall measurements and hydrometeor classification. *Bull. Am. Meteorol. Soc.*, **86**, 809–824, https://doi.org/10.1175/BAMS-86-6-809.

Samuel, J., P. Coulibaly, and R. A. Metcalfe, 2011: Estimation of continuous streamflow in Ontario ungauged basins: comparison of regionalization methods. *J. Hydrol. Eng.*, **16**, 447–459, https://doi.org/10.1061/(ASCE)HE.1943-5584.0000338.

Şensoy, A., G. Uysal, and A. A. Şorman, 2016: Developing a decision support framework for real-time flood management using integrated models. *J. Flood Risk Manag.*, https://doi.org/10.1111/jfr3.12280.

Seo, D.-J., E. Habib, H. Andrieu, and E. Morin, 2015: Hydrologic applications of weather radar. *J. Hydrol.*, **531**, 231–233, https://doi.org/10.1016/j.jhydrol.2015.11.010.

Sevruk, B., 1982: Methods of correction for systematic error in point precipitation measurement for operational use.

Sills, D. M. L., Ashton, A., Knott, S., Boodoo, S., Bélair, S., Klaassen, J., & Yang, H., 2016: A billion dollar flash flood in Toronto – challenges for forecasting and nowcasting (pp. 1–15, Paper 5B.5A). In Extended Abstracts, 28th AMS Conference on Severe Local Storms Portland, OR, Amer. Meteorol. Soc.

Sills, D. M., and P. I. Joe, 2019: From pioneers to practitioners: A short history of severe thunderstorm research and forecasting in Canada. *Atmosphere-Ocean*, 57, 249–261, https://doi.org/10.1080/07055900.2019.1673145.

Smith, J. A., M. L. Baeck, K. L. Meierdiercks, A. J. Miller, and W. F. Krajewski, 2007: Radar rainfall estimation for flash flood forecasting in small urban watersheds. *Adv. Water Resour.*, **30**, 2087–2097, https://doi.org/10.1016/j.advwatres.2006.09.007.

Sugier, J., P. Tabary, J. Gourley, and K. Friedrich, 2006: Evaluation of dual-polarisation technology at C-band for operational weather radar network. *EUMETNET Opera*, **2**, [Available online at http://www.knmi.nl/opera/opera2/OPERA_2006_05_Evaluation_of_dual_polarization_technology.pdf.]

Teal, M. J., and R. Allan, Creating a Flood Warning System for the San Diego River Using HEC-RTS Software. *World Environmental and Water Resources Congress 2017*, 263–272, https://doi.org/10.1061/9780784480601.023.

Thampapillai, D. J., and W. F. Musgrave, 1985: Flood damage mitigation: A review of structural and nonstructural measures and alternative decision frameworks. *Water Resour. Res.*, **21**, 411–424, https://doi.org/10.1029/WR021i004p00411.

Thorndahl, S., T. Einfalt, P. Willems, J. E. ek Nielsen, M.-C. ten Veldhuis, K. Arnbjerg-Nielsen, M. R. Rasmussen, and P. Molnar, 2016: Weather radar rainfall data in urban hydrology. *Hydrol. Earth Syst. Sci. Discuss.*, 1–37, https://doi.org/10.5194/hess-21-1359-2017.

Tol, R. S., 2016: The impacts of climate change according to the IPCC. *Clim. Change Econ.*, **7**, 1640004, https://doi.org/10.1142/S2010007816400042.

Tolson, B. A., and C. A. Shoemaker, 2008: Efficient prediction uncertainty approximation in the calibration of environmental simulation models. *Water Resour. Res.*, **44**, https://doi.org/10.1029/2007WR005869.

Torres, S. M., and D. A. Warde, 2014: Ground clutter mitigation for weather radars using the autocorrelation spectral density. *J. Atmospheric Ocean. Technol.*, **31**, 2049–2066, https://doi.org/10.1175/JTECH-D-13-00117.1

TRCA, 2009: *Final Report: Hydrologic Modelling Mimico Creek*. Toronto and Region Conservation Authority. [Available online at https://trca.ca/app/uploads/2016/07/Final-Report-Hydrologic-Modeling-Mimico-Creek-Dec-2009.pdf.]

TRCA, 2020: WATERSHED FEATURES – ETOBICOKE & MIMICO .Toronto andRegion Conservation Authority, accessed 09October 2020, https://trca.ca/conservation/watershed-management/etobicoke-mimico-creek/watershed-features/.

TRCA Flood Risk Management, 2020: MODELLING REFERENCES SECTION. Toronto and Region Conservation Authority, accessed 11October 2020, https://trca.ca/conservation/flood-risk-management/modeling-references-section/.

TRCA Report Cards, 2020: Mimico Creek Watershed .Toronto and Region Conservation Authority, accessed 09October 2020, https://reportcard.trca.ca/watershed-report-cards/mimico-creek/.

Unduche, F., H. Tolossa, D. Senbeta, and E. Zhu, 2018: Evaluation of four hydrological models for operational flood forecasting in a Canadian Prairie watershed. *Hydrol. Sci. J.*, https://doi.org/10.1080/02626667.2018.1474219.

US Army Corps of Engineers, 2020a: HEC-HMS. US Army Corps of Engineers-Hydrologic Engineering Center, accessed 10th October 2020, https://www.hec.usace.army.mil/software/hec-hms/.

US Army Corps of Engineers, 2020b: HEC-RAS. US Army Corps of Engineers-Hydrologic Engineering Center, accessed 10th October 2020, https://www.hec.usace.army.mil/software/hec-ras/features.aspx.

US Army Corps of Engineers, 2020c: HEC-RTS. US Army Corps of Engineers-Hydrologic Engineering Center, accessed 10th October 2020, https://www.hec.usace.army.mil/software/hec-rts/features.aspx.

Vieux, B. E., and P. B. Bedient, 2004: Assessing urban hydrologic prediction accuracy through event reconstruction. *J. Hydrol.*, **299**, 217–236, https://doi.org/10.1016/j.jhydrol.2004.08.005.

Villarini, G., and W. F. Krajewski, 2010: Review of the different sources of uncertainty in single polarization radar-based estimates of rainfall. *Surv. Geophys.*, **31**, 107–129, https://doi.org/10.1007/s10712-009-9079-x.

Vyas, A., and S. John, 2016: A Real-Time Decision Support System for River Basin Management. *MATEC Web of Conferences*, Vol. 57 of, EDP Sciences, 05002, https://doi.org/10.1051/matecconf/20165705002.

Wang, L.-P., S. Ochoa-Rodríguez, J. Van Assel, R. D. Pina, M. Pessemier, S. Kroll, P. Willems, and C. Onof, 2015: Enhancement of radar rainfall estimates for urban hydrology through optical flow temporal interpolation and Bayesian gauge-based adjustment. *J. Hydrol.*, **531**, 408–426, https://doi.org/10.1016/j.jhydrol.2015.05.049.

Werner, M., M. Cranston, T. Harrison, D. Whitfield, and J. Schellekens, 2009: Recent developments in operational flood forecasting in England, Wales and Scotland. *Meteorol. Appl. J. Forecast. Pract. Appl. Train. Tech. Model.*, **16**, 13–22, https://doi.org/10.1002/met.124.

Wijayarathne, D., S. Boodoo, P. Coulibaly, and D. Sills, 2020a: Evaluation of Radar Quantitative Precipitation Estimates (QPEs) as an Input of Hydrological Models for Hydrometeorological Applications. *J. Hydrometeorol.*, **21**, 1847–1864, https://doi.org/10.1175/JHM-D-20-0033.1.

——, P. Coulibaly, S. Boodoo, and D. Sills, 2020b: Evaluation of Radar-Gauge Merging Techniques to be Used in Operational Flood Forecasting in Urban Watersheds. *Water*, **12**, 1494, https://doi.org/10.3390/w12051494.

Wijayarathne, D. B., and P. Coulibaly, 2020: Identification of hydrological models for operational flood forecasting in St. John's, Newfoundland, Canada. *J. Hydrol. Reg. Stud.*, **27**, 100646, https://doi.org/10.1016/j.ejrh.2019.100646.

Willmott, C. J., and K. Matsuura, 2005: Advantages of the mean absolute error (MAE) over the root mean square error (RMSE) in assessing average model performance. *Clim. Res.*, **30**, 79–82, https://doi.org/10.3354/cr030079.

WMO, 2006. WMO flood Forecasting Initiative: Final Report of the Synthesis Conference on Improved Meteorological and Hydrological Forecasting.

Young, C. B., and N. A. Brunsell, 2008: Evaluating NEXRAD estimates for the Missouri River Basin: Analysis using daily raingauge data. *J. Hydrol. Eng.*, **13**, 549–553, https://doi.org/10.1061/(ASCE)1084-0699(2008)13:7(549).

Zahmatkesh, Z., S. Kumar Jha, P. Coulibaly, and T. Stadnyk, 2019: An overview of river flood forecasting procedures in Canadian watersheds. *Can. Water Resour. JournalRevue Can. Ressour. Hydr.*, 1–17, https://doi.org/10.1080/07011784.2019.1601598.

Zhang, W., G. Villarini., G. A. Vecchi, & J. A. Smith, 2018: Urbanization exacerbated the rainfall and flooding caused by hurricane Harvey in Houston. Nature, 563(7731), 384–388, https://doi.org/10.1038/s41586-018-0676-z.

Chapter 6. Conclusions and Recommendations

6.1. Conclusions

The main research objective was to select, evaluate, and apply Radar QPEs as a precipitation input for hydrological models for operational flood forecasting in urban and semi-urban watersheds in Canada. The study areas in this research covers the Humber River (semi-urban), Don River (urban), and Mimico Creek (urban) watersheds situated in the GTA, Ontario. The findings of this research will benefit future applications of real-time Radar QPEs in FEWS. The primary outcomes of the four thesis chapters are summarized as follows:

6.1.1. Use of weather Radar for operational hydrology in Canada

- This chapter reviews the literature on applications of weather Radars in Canadian hydrology. This provides an overview of Canadian weather Radar networks, different Radar only QPEs, Radar assimilated QPEs, hydrological applications, challenges, recommendations, and potential future research.
- C-band, S-band, and X-band Radar collected using both ground-based and portable Radar mounted on aircraft were used to determine the precipitation type, features, structure, and moisture transport, to predict weather and snow depth, to issue operational weather warnings, and to validate atmospheric models.
- Multi-radar QPEs such as CaPA, NMQ, and MRMS are produced by merging Radar QPEs with the ground observations, forecasts from the weather prediction models, and satellite observations.

- The main challenges identified are the intrinsic errors in Radar measurements, variability in *Z-R* relationship, inadequate gauge network, the ongoing development of the Radar infrastructure, existing C-band Radar network, and the complex geography.
- Potential future research includes identification of prospective Radar QPEs, evaluation of existing Radar QPEs, assessing radar-gauge merging techniques, and developing a method to integrate real-time Radar QPEs in FEWS.

6.1.2. Evaluation of Radar QPEs

- This study evaluates seven Canadian WKR C-band dual-polarized Radar QPEs and two US KBUF NEXRAD S-band Radar QPEs over two watersheds in the GTA of Ontario, Canada, to verify the reliability and accuracy as an additional precipitation data source for hydrological model calibration.
- Both WKR C-band and NEXRAD S-band Radar QPEs can be effectively used as supplementary precipitation data sources for hydrological model calibration in the Humber River (semi-urban) and Don River (urban) watersheds.
- NEXRAD Level III (DPA) performs best, followed by WKR multi-parameter in estimating the rain rate using K_{DP} and Z_{DR}.
- High percent detection and temporal resolution and long-term data archive of WKR Radar QPEs enable continuous time series of precipitation data that facilitate hydrological model calibration.

- Both WKR and NEXRAD Radar can be used as a gridded precipitation input to semi-distributed and distributed hydrological models where the basins are typically discretized into sub-catchments, HRUs.

6.1.3. Verification of radar-gauge merging techniques

- This research evaluates radar-gauge merging techniques, the impact of the type of Radar QPEs on the performance, relative strength of techniques at different rain intensities, and different rainfall events in the Humber River (semi-urban) and Don River (urban) watersheds in GTA, Canada.
- Both WKR C-band and NEXRAD S-band Radar QPEs are improved; however, the accuracy is influenced by the type and quality of raw radar QPEs, distance from the radar station, and the rainfall intensity.
- All radar-gauge merging methods outplayed Radar only QPEs with the best performance from the CDFM method followed by the KRE.
- The NEXRAD Level III (DPA) is most improved among four Radar QPEs.
- Since the KRE method uses optimal interpolation to merge gauge and Radar QPES, it can facilitate hydrological model calibration by providing a continuous precipitation time series.
- As the RDA method considers distance from the Radar tower to the gauge stations during the merging process, it is recommended if there is a considerable difference in the distance between the Radar and gauge stations.

- If the computational demand is a limiting factor, a relatively simple MFB method is recommended.
- Random errors mostly cause the remaining differences between merged Radar QPEs and reference gauge observations.
- The accuracy of raw Radar products influences the performance of radar-gauge merging methods and, eventually, the accuracy of merged Radar QPEs.
- All methods performed relatively well for low-intensity precipitation. However, performances are decreased with increasing intensities.
- CDFM and KRE perform best for individual events, followed by MBSA with better performance in the summer.

6.1.4. Integration of Radar QPEs into HEC-RTS Framework

- This study evaluates the use of Radar QPEs for flood foresting by integrating the HEC-HMS hydrological model and HEC-RAS hydraulic models into the HEC-RTS model framework.
- Both accuracy and reliability of Canadian WKR C-band and NEXRAD KBUF S-band dual-polarized Radar QPEs are improved by the radar-gauge merging, and therefore, the accuracy of streamflow simulation is also enhanced.
- Gauge-calibrated hydrological models can be run effectively using the bias-corrected Radar QPEs.
- Flood extent maps for future storm events could be produced using the HEC-RTS framework with the bias-corrected Radar QPEs, and these maps could be

effectively used for decision making and for taking immediate actions to reduce human and economic losses.

6.1.5. General conclusion and contributions from the thesis

The general conclusions from the thesis are summarized as follows:

- Weather Radar is an essential source of precipitation information that provides real-time, spatially distributed data for the hydrological and hydraulic models for flood forecasting and is especially useful for small, urban watersheds with short response times.
- NEXRAD S-band Radar QPEs can be used as precipitation source in Canadian watersheds located within the Radar range.
- Radar-gauge merging improved both WKR and NEXRAD Radar QPEs; however, radar-gauge merging is greatly influenced by the type and quality of raw radar QPEs, distance from the radar station, and the rainfall intensity.
- The Canadian flood forecasting agencies commonly use hydrological models that are both calibrated and validated using gauge data. Therefore, running the existing hydrological models using bias-corrected Radar QPEs is recommended for streamflow simulation to produce flood extent maps.
- Floods could be successfully predicted with a framework built through integrated hydrological and hydraulic models using bias-corrected Radar QPEs.

6.2. Future works and Recommendations

The research work presented in this thesis is an initial step in the process of developing a robust method to incorporate real-time Radar QPEs in the Canadian Adaptive Flood Forecasting and Early Warning System (CAFFEWS) (*Floodnet—NSERC Network—Enhanced flood forecasting and management capacity in Canada*, 2020). Therefore, great efforts are still needed to achieve this goal. Relatively small and impervious urban watersheds respond to rainfall relatively fast and, therefore, is sensitive to the temporal and spatial resolution of precipitation (Ochoa-Rodriguez et al., 2019; Villarini et al., 2008). Hence, following up on Chapter 3 of this thesis, the evaluation of Radar QPEs should be extended to evaluate Radar QPEs with spatial-temporal resolutions of the order of 1 km and 1-5 min whenever data is available. Another QPE of considerable interest and requiring ongoing evaluation is multi Radar, multi-sensor precipitation (e.g., NMQ, and MRMS) with a spatial and temporal resolution of 1 km and 2 min across Southern Canada and 2 km resolution CaPA (Fortin et al., 2015; Nasab, 2017). Methods to access and evaluate multi Radar, multi-sensor precipitation on selected watersheds are anticipated. The evaluation has yet to be performed in diverse watersheds in terms of size, physiography, and hydrology. For example, it would be more beneficial to use Radar QPEs in large rural watersheds vulnerable to flooding with sparse rain gauge density (Unduche et al., 2018). Moreover, the existing ECCC C-band Radar is being upgraded to dual-polarized S-band Radar, starting with Radisson, SK. As of October 2020, fourteen C-band Radar stations have been replaced since February 28, 2017. Future

research should evaluate newly deployed S-band polarimetric Radars for precipitation estimates and, subsequently, hydrological modeling.

Another topic of considerable interest would be to test radar-gauge merging using radar-rain gauge integration methods (Ochoa-Rodriguez et al., 2019). In addition to the methods discussed in Chapter 4, the Bayesian (BAY) data merging method that integrates gauge and Radar data to minimize the overall estimation uncertainty using a Kalman filter and weighted average of Radar and gauge values could be assessed (Todini, 2001). It is necessary to search for methods to minimize computational cost since radar-rain gauge integration methods are computationally demanding. Similarly, Radar QPEs could be assimilated and blended with other precipitation sources to improve the accuracy of forecasts using Bayesian ensemble flood forecasting with a multi-model approach (Awol et al., 2019; Han & Coulibaly, 2019).

Finally, an automated flood forecasting framework with a robust method to retrieve, compute, view, and manage real-time Canadian and NEXRAD Radar precipitation data could be implemented. The methods available in HEC-RTS to retrieve, compute, view, and manage real-time Canadian and NEXRAD Radar precipitation data, and could be used to upgrade the HEC-RTS framework into an automated FEWS to issue real-time flood forecasts for operational applications in the future. Freely available windows based “Getrealtime” software could be used for retrieval, computation, viewing, and managing real-time NOAA and Canadian Radar for continuous flood monitoring (*GetMyRealtime water data*, 2019). Moreover, the “GetNexrad” tool, which computes the basin area average rainfall time series in real-time, could possibly be used to view and

download real-time NEXRAD Radar rainfall (*GetNexrad Radar*, 2017). NEXRAD Radar data can easily be preprocessed using a freely available, prebuilt NOAA tool kit (*NOAA's Weather and Climate Toolkit (Viewer and Data Exporter)*, 2020). Real-time hydrological modeling has been dramatically improved in recent years with the development of the NEXRAD Radar system and linkage of NEXRAD with the GIS system (Yerramilli, 2012; Zhang et al., 2012). GIS provides a platform for the automated processing of the NEXRAD and allows for rapid data display (Xie et al., 2005). Also, NEXRAD Validation and Calibration software (NEXRAD-VC), which is freely available, would be an excellent tool to preprocess NXERAD data (Zhang & Srinivasan, 2010). NEXRAD-VC is developed as an extension of ArcGIS to facilitate spatial precipitation estimates and provides a user-friendly GIS tool for batch processing of NEXRAD data. Therefore, further research is needed to develop a robust system that provides real-time Radar QPEs for flood forecasting to mitigate flood hazards in Canada.

6.3. References

Available Resources | Compute Canada. (2020). Retrieved October 27, 2020, from https://www.computecanada.ca/research-portal/accessing-resources/available-resources/.

Awol, F. S., Coulibaly, P., Tsanis, I., & Unduche, F. (2019). Identification of Hydrological Models for Enhanced Ensemble Reservoir Inflow Forecasting in a Large Complex Prairie Watershed. *Water*, *11*(11), 2201. https://doi.org/10.3390/w11112201.

FloodNet—NSERC Strategic Research Network—Enhanced flood forecasting and management capacity in Canada. (2020). Retrieved October 27, 2020, from http://www.nsercfloodnet.ca/

Fortin, V., Roy, G., Donaldson, N., & Mahidjiba, A. (2015). Assimilation of radar quantitative precipitation estimations in the Canadian Precipitation Analysis (CaPA). *Journal of Hydrology*, *531*, 296–307. https://doi.org/10.1016/j.jhydrol.2015.08.003.

GetMyRealtime water data. (2019). Retrieved October 27, 2020, from http://getmyrealtime.com/

GetNexrad Radar. (2017). Retrieved October 27, 2020, from http://getmyrealtime.com/GetNexradHelp.aspx

Güntner, A., Olsson, J., Calver, A., & Gannon, B. (2001). Cascade-based disaggregation of continuous rainfall time series: The influence of climate. *Hydrology and Earth System Sciences Discussions*, *5*(2), 145–164. hal-00304590.

Han, S., & Coulibaly, P. (2019). Probabilistic Flood Forecasting Using Hydrologic Uncertainty Processor with Ensemble Weather Forecasts. *Journal of Hydrometeorology*, *20*(7), 1379–1398. https://doi.org/10.1175/JHM-D-18-0251.1.

Nasab, A. R. (2017). *Improving Hydrologic Prediction Via Data Assimilation, Data Fusion and High-resolution Modeling* [PhD Thesis]. University of Texas at Arlington.

NOAA's Weather and Climate Toolkit (Viewer and Data Exporter). (2020). Retrieved October 27, 2020, from https://www.ncdc.noaa.gov/wct/

Ochoa-Rodriguez, S., Wang, L.-P., Willems, P., & Onof, C. (2019). A review of radar-rain gauge data merging methods and their potential for urban hydrological applications. *Water Resources Research*. https://doi.org/10.1029/2018WR023332.

Olsson, J. (1995). Limits and characteristics of the multifractal behaviour of a high-resolution rainfall time series. *Nonlinear Processes in Geophysics*, *2*(1), 23–29. hal-00301758.

Olsson, Jonas. (1998). Evaluation of a scaling cascade model for temporal rainfall disaggregation. *Hydrology and Earth System Sciences Discussions*, *2*(1), 19–30. hal-00304453.

Rebora, N., Ferraris, L., von Hardenberg, J., & Provenzale, A. (2006). RainFARM: Rainfall downscaling by a filtered autoregressive model. *Journal of Hydrometeorology*, *7*(4), 724–738. https://doi.org/10.1175/JHM517.1.

Todini, E. (2001). A Bayesian technique for conditioning radar precipitation estimates to rain-gauge measurements. *Hydrology and Earth System Sciences Discussions*, *5*(2), 187–199. hal-00304593.

Unduche, F., Tolossa, H., Senbeta, D., & Zhu, E. (2018). Evaluation of four hydrological models for operational flood forecasting in a Canadian Prairie watershed. *Hydrological Sciences Journal*, *just-accepted*. https://doi.org/10.1080/02626667.2018.1474219.

Villarini, G., Serinaldi, F., & Krajewski, W. F. (2008). Modeling radar-rainfall estimation uncertainties using parametric and non-parametric approaches. *Advances in Water Resources*, *31*(12), 1674–1686. https://doi.org/10.1016/j.advwatres.2008.08.002.

Xie, H., Zhou, X., Vivoni, E. R., Hendrickx, J. M., & Small, E. E. (2005). GIS-based NEXRAD Stage III precipitation database: Automated approaches for data processing and visualization. *Computers & Geosciences*, *31*(1), 65–76. https://doi.org/10.1016/j.cageo.2004.09.009.

Yerramilli, S. (2012). A hybrid approach of integrating HEC-RAS and GIS towards the identification and assessment of flood risk vulnerability in the city of Jackson, MS. *American Journal of Geographic Information System*, *1*(1), 7–16. https://doi:10.5923/j.ajgis.20120101.02.

Zhang, H., Li, D., Wang, X., & Jiang, X. (2012). Quantitative evaluation of NEXRAD data and its application to the distributed hydrologic model BPCC. *Science China Technological Sciences*, 1–8. https://doi.org/10.1007/s11431-012-4918-2.

Zhang, X., & Srinivasan, R. (2010). GIS-based spatial precipitation estimation using next generation radar and raingauge data. *Environmental Modelling & Software*, *25*(12), 1781–1788. https://doi.org/10.1016/j.envsoft.2010.05.012.

Appendix A: Identification of Hydrological Models for Operational Flood Forecasting in St. John's, Newfoundland, Canada

Summary of Paper 5: Wijayarathne, D.B., and Coulibaly, P. (2019). Identification of hydrological models for operational flood forecasting in St. John's, Newfoundland. *Journal of Hydrology: Regional Studies,* 27, 100646. https://doi.org/10.1016/j.ejrh.2019.100646.

St. John's is the capital city of NL and has had the most reported floods over the past five decades among 98 communities in NL. Due to the increasing population over the last decades, flood damage has become a rising problem. From 1962 to 2011, more than 267 communities in Newfoundland were affected by flooding, causing average annual damage of about $8 to $22 million. Even though St John's is the most vulnerable to flooding in the NL province, a proper tool to forecast floods in advance is currently not available. Therefore, further studies must be conducted to propose a suitable operational flood forecasting method in St. John's, Newfoundland.

In this study, five hydrological models in varying complexity (lumped, semi-distributed, and fully-distributed) were first set-up, calibrated, and validated using historical data to identify the best model(s) for operational flood forecasting at Waterford River watershed in St. John's, Newfoundland. Then, deterministic forecasts were performed to verify the potential of the selected hydrological models for operational use. Key findings of this research include:

- All five models were satisfactory in simulating streamflow.

- The SAC-SMA and GR4J models equally outperformed the other three models for all low, medium, and peak flows.
- The SAC-SMA and GR4J models performed better for peak flows, followed by HEC-HMS.
- The SAC-SMA and GR4J models performed well for up to 1–3 days ahead forecasts.
- Ensemble forecasting using continuous, multiple hydrological models is recommended.

A.1. Abstract

Study region: Waterford River watershed, St. John's, Newfoundland and Labrador (NL), Canada.

Study focus: This study investigates five hydrological models to identify adequate model(s) for operational flood forecasting at Waterford River watershed. These models included three lumped conceptual models (SAC-SMA: Sacramento Soil Moisture Accounting, GR4J: modèle du Génie Rural à 4 paramètres Journalier, and MAC-HBV: McMaster University Hydrologiska Byråns Vattenbalansavdelning), a semi-distributed model (HEC-HMS: Hydrologic Engineering Center's Hydrologic Modeling System) and a fully distributed physically-based model (WATFLOOD: University of Waterloo Flood Forecasting System). The best model(s) were chosen by comparison of performance criteria. To verify the potential of the best performing hydrological models for operational use, deterministic hydrologic forecasts were performed.

New Hydrological Insights for the Region: All five models are capable of simulating streamflow reasonably well in both calibration and validation periods. The SAC-SMA and GR4J models perform equally well and perform better than the other three models for all low, medium, and peak flows. The SAC-SMA and GR4J models generally perform better for peak flows, followed by HEC-HMS. Streamflow forecast experiment using deterministic weather prediction shows that SAC-SMA, GR4J, and HEC-HMS models perform well for up to 1 to 3 days ahead forecasts and are recommended for operational use. However, due to the good performance of all five models, an ensemble forecasting using continuous, multiple hydrological models is also recommended.

Keywords: Waterford River watershed, flood forecasting, hydrological models, deterministic forecast

A.2. Introduction

Floods are one of the deadliest disasters in the world and the most common and frequent natural hazard to life, property, the economy, and the environment in Canada. Flood mitigation measures and an enhanced flood forecasting system are critical parts of flood management. An accurate flood forecasting system can deliver precise and reliable forecasts with appropriate lead time. Hydrological modeling is being used to forecast river flows for years, and a well-developed flood forecasting system can deliver precise and reliable forecasts with appropriate lead time (Nagai, 2003; Reed et al., 2007; Unduche et al., 2018).

Flood damage has become a growing problem in Newfoundland and Labrador (NL), Canada, due to the increasing population density close to water bodies over the last decades (Sheppard, 2018). The results of the "Flood Risk and Vulnerability Analysis Project" completed on June 13, 2012, have emphasized the need for a robust method to forecast floods to minimize future flood damage and related expenses in Newfoundland (Innes and Nimmrichter, 2012). According to the report, more than 267 communities in Newfoundland had been affected by flooding in the last decades, causing significant economic loss and infrastructure damages. The average annual damage caused by flood-related impacts is estimated to be about $8 to $22 million over the period 1962-2011. The cost of estimated damages may be even higher as some of the floods were recorded with no information on the estimated cost of damages.

St. John's is the capital and the largest city of NL and is located on the Avalon Peninsula, the east side of the island of Newfoundland. According to Innes and Nimmrichter (2012), St. John's has had the most reported floods (73 out of 650) over the period 1950 to 2011 among 98 communities in NL. The same study has identified and ranked communities in Newfoundland according to their exposure to the physical hazards, vulnerability to direct impacts of flooding, and indirect flooding impacts and isolation over the last decade (2000 – 2011). It was found that St John's is the most vulnerable to flooding, and therefore further study and funding had been recommended.

Several hydrological modeling studies have been conducted in the Waterford River watershed in St. John's for different purposes. A series of studies on water quality and quantity in the Waterford River watershed was conducted by the Canadian

Government and Province of NL over the period from 1980 to 1985. After the five-year-long project, the "Urban Hydrology Study of the Waterford River Basin: Flood Study (UHS-WRB)" was published in 1988 (Smith, 1988). The study mainly focused on the effects of urbanization between 1973 and 1981 on peak flows. An event-based, simple, and single hydrological model "HYdrologic Model" (HYMO) was implemented to simulate the 1:20 and 1:100 Annual Exceedance Probability (AEP) flows. After that, a hydraulic model was developed using three sections of the Waterford river channel and was fed with the flows simulated by the hydrological model to indicate the change in the storm runoff as a result of future urbanization. Following the study, it was concluded that urbanization has increased flows; however, change in the volume of direct runoff is not significant. A study entitled "Simulation of the effects of urbanization on basin streamflow" was conducted as a part of the aforementioned comprehensive investigations of the effect of urbanization on peak-flows (Ng and Marsalek, 1989). Continuous simulation of streamflow was performed utilizing the "Hydrological Simulation Program—Fortran" (HSPF) model to evaluate the effects of future urban development on annual streamflow and peak flows. According to the simulation results, streamflow volumes are not affected much, but flow peaks and the incidence of flooding has increased significantly. In 1988, the "Waterford River Area- Hydrotechnical Study" was completed as a joint effort between the Water Resources Division of the Department of Environment and Lands and Fenco Newfoundland Ltd (Gray, 1988). Several flood risk maps were developed using flows simulated from "Quality/Quantity Simulation Model" (QUALHYMO) and "Hydrologic Engineering Center" (HEC-2) models. In 1998, the

Water Resources Management Division (WRMD) of the Department of Environment and Labor conducted a study entitled “Updated Flood Extents for the Waterford River” as an update for the Fenco Newfoundland study in 1988. The 1:20 and 1:100 AEP flood flows from the 1988 study were re-examined along with annual instantaneous peak flow up to 1996. Existing flood risk maps were updated using a hydraulic model “Hydrologic Engineering Center River Analysis System” (HEC-RAS). The most recent update of flood risk maps was conducted in 2015 under the study entitled “Waterford River Area Flood Risk Mapping Study” by CBCL Ltd with the collaboration of the WRMD of the Department of Municipal Affairs and Environment (Sheppard, 2018). The objective of this study was to update flood risk maps to accurately predict the long-term effect of climate change in St. John’s area. Coupled hydrologic-hydraulic models “Hydrologic Engineering Center’s Hydrologic Modeling System” (HEC-HMS) and HEC-RAS were used in the study. A comprehensive set of flood risk maps had been produced to predict the long-term effect of climate change on floods in St. John’s area. Moreover, the study emphasizes the need to implement a flood forecasting system that can allow local authorities to receive flood warnings to respond promptly in the event of a potential flood.

Limited studies have been conducted on hydrological modeling in the Waterford River watershed in St. John’s, and the models used in these studies are relatively simple. Most of these studies were mainly focused on investigating the effects of urbanization on peak flows and streamflow volumes. The rest of the studies were focused on developing flood risk maps rather than operational flood forecasting. These studies have used hydrological modeling approaches to develop flood maps, and these maps had been used

for decision-making purposes. However, none of these studies have investigated developing hydrological models that can be used in operational flood forecasting. This study has evaluated the use of five hydrological models in varying complexity (lumped, semi-distributed, and fully-distributed) to propose a suitable method for operational flood forecasting in St. John's, Newfoundland.

A.3. Study Area

The study was conducted in the Waterford River watershed in St. John's, NL (Figure A-1). The Waterford river starts at the eastern part of the rapidly growing town of Paradise and is originated from Bremigan's Pond and Nevilles Pond. The river takes a meandering course through the City of Mount Pearl and into the City of St. John's. In St. John's, the river flows through the Waterford Valley before it discharges into the western end of St. John's Harbor. It flows approximately 15 km from the origin before it meets the Atlantic Ocean at the western part of St. John's Harbor. The river has a drainage basin area of about 70 km^2 that covers St. John's Harbor and three municipalities: The City of St. John's, the City of Mount Pearl, and the Town of Paradise (Figure A-1). The only hydrometric station located along the river reach is "Waterford River at Kilbride" (Station ID 02ZM008) and is operated as a collaborative effort of Water Survey of Canada and WRMD, NL.

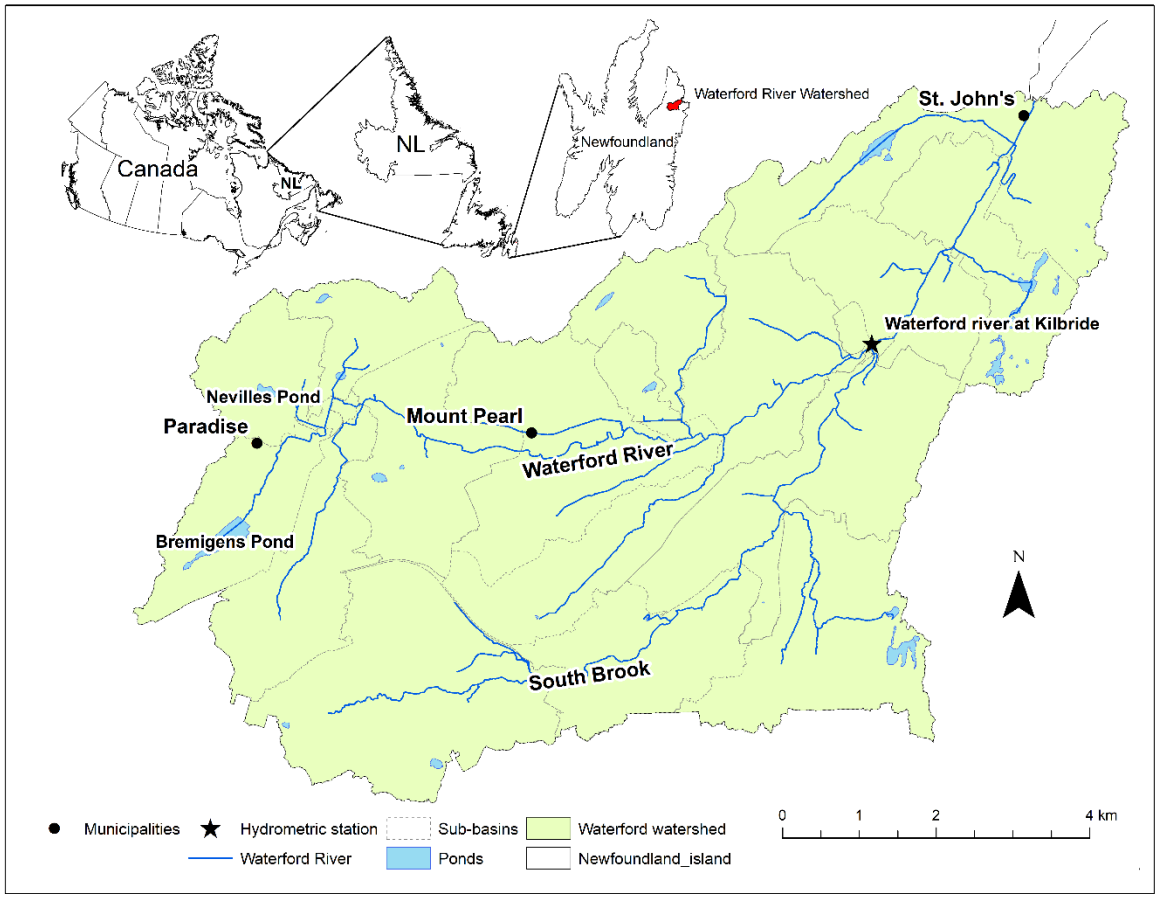

Figure A-1 *Location map of the Waterford River watershed*

The watershed is semi-urban and provides a home for about 108,860 individuals at the time of the 2016 census ("Statistics - Newfoundland & Labrador Statistics Agency," n.d.). Land uses and features of the study area include urban areas, forest, water bodies, wetlands, barren lands, deforested areas, and open areas (Figure A-2a, Natural Resources Canada, 2009). The urban areas encompass residential, commercial, and industrial areas and transportation corridors. The surface elevation in the watershed ranges from 1 to 262 m above sea level (Figure A-2b). The soil is coarse to moderately coarse-textured, stony, acid to extremely acid, and low natural fertility soil (Heringa,

1981). This soil is developed from the materials derived from the underlying coarse-textured Precambrian sedimentary rocks (Batterson, 1984). These soils are characterized as rapid surface drainage. The whole area was glaciated, and as a result, most of the area is underlain by a till (Heringa, 1981). The till deposit lies beneath the surface and contains pockets of clay with low permeability. Therefore, this till deposit acts as an aquitard allowing the accumulation of standing water, which contributes to the surface runoff. A combination of impervious urban areas, impervious till, and poorly drained soils cause poor internal drainage and eventually results in a highly flood-prone area.

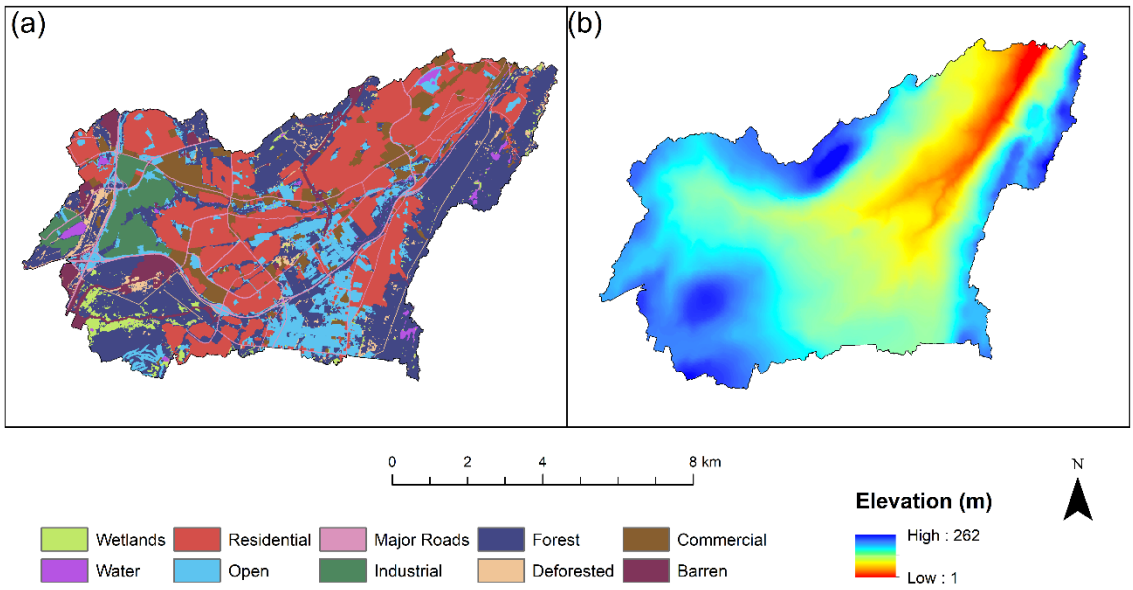

Figure A-2 *Land use (a) (Natural Resources Canada, 2009) and topography (b) of Waterford River watershed.*

The average daily temperature of the area is 4°C (Environment Canada, 2017). The average annual precipitation is 1416 mm on the average over 296 days in the year (Environment Canada, 2017). The minimum and maximum instantaneous flows recorded at "Waterford River at Kilbride" were 0.3 and 45.2 m^3s^{-1} (Environment Climate Change

Canada, 2017). High-intensity rainfall events are frequent throughout the year (Innes and Nimmrichter, 2012). The leading cause of flooding in the area is recognized as rainfall followed by events related to coastal processes such as storm surge and waves (Innes and Nimmrichter, 2012).

A.4. Data and Methods

A.4.1. Hydrometeorological and hydrometric data

Daily climate data recorded at four Environment Canada (EC) weather stations were downloaded from the EC website from 2006 - 2015 (Table A-1). This period contained the least amount of missing values, both in precipitation and temperature. Missing values in precipitation data were infilled using Canadian Precipitation Analysis (CaPA) data. There is a long-term flow gauge named "Waterford River at Kilbride" located downstream of the confluence of South Brook and Waterford river (Figure A-1). This station is operated by the Water Survey of Canada and in operation since 1974. A complete time series of flow data is available on both EC's and WRMD's websites. WRMD is using data from this Gauge station in hydrological modeling. Daily streamflow data were collected from the HYDAT database and narrowed to a 10-year time series spanning from 2006 to 2015 to be consistent with available climate data.

Table A-1 *Details of hydrometeorological and hydrometric stations.*

Station Name	ID	Operated by	Latitude (N)	Longitude (W)	Elevation (m)	Type of Data	Years of operation
Hydrometric station							
Waterford River at Kilbride	02ZM008	WSC	47°31’44”	52°44’42”	33	Daily	1974-2018
Hydrometeorological stations							
St. John’s West Climate	8403603	EC	47°30’48”	52°47’00”	110	Daily	2010-2019
St. John’s A	8403506	EC	47°37’20”	52°44’34”	140.5	Daily	1942-2012
St. john’s Intl A	8403505	EC	47°37’07”	52°45’09”	140.5	Daily	2012-2019
St. John’s West CDA CS	8403605	EC	47°30’56”	52°47’05”	114	Daily	1996-2007

A.4.2. Hydrological models

Five hydrological models with complexity ranging from simple lumped models to a fully- distributed were chosen for the investigation to identify adequate model(s) for operational flood forecasting in the Waterford River watershed in St. John's, NL. These models include, modèle du Génie Rural à 4 paramètres Journalier (GR4J), McMaster University Hydrologiska Byråns Vattenbalansavdelning (MAC-HBV), Sacramento Soil Moisture Accounting (SAC-SMA), Hydrologic Engineering Center's Hydrologic Modeling System (HEC-HMS), and University of Waterloo Flood Forecasting System (WATFLOOD). These hydrological models were implemented, calibrated, and validated to simulate the flow at Waterford River at Kilbride hydrometric station.

A.4.2.1. GR4J model

GR4J is a simple conceptual hydrological model that runs with four parameters (Perrin et al., 2003). Inputs to the original model include precipitation, evapotranspiration, and the optimized set of parameters. In this study, the model was modified to include the two components: a simplified "Thornwaite" formula to account for daily potential evapotranspiration using temperature and a degree-day snow routine to determine Snow Water Equivalent (SWE) following Samuel et al. (2011). Therefore, the temperature time series was inputted instead of the calculated evapotranspiration. Hence, the final modified model includes nine parameters that are listed in Table B-1 in the Appendix. The range of each of these parameters listed in Table B-1 was obtained from the previous literature based on the land use, soil, climate, morphology, and vegetation in the watershed. For a

detailed description of the GR4J model, the interested readers may refer to the journal article by Perrin et al. (2003).

A.4.2.2. MAC-HBV

MAC-HBV model is a lumped conceptual rainfall-runoff model which had been extensively used in hydrological studies (Leach et al., 2018; Razavi and Coulibaly, 2017; Samuel et al., 2011). It is a modified version of the original HBV model (Bergström, 1976) to provide a better performance, especially flow estimation at ungauged sites in Canada (Samuel et al., 2011, 2012). There are 15 parameters in MAC-HBV and incorporates a degree-day snow routine, a soil moisture routine, a nonlinear response function, and a routing routine. Parameters and their ranges obtained from the literature for the MAC-HBV model are listed in Table B-2 in the Appendix. Further details of the MAC-HBV model are presented in Samuel et al. (2011, 2012).

A.4.2.3. SAC-SMA

SAC-SMA is a conceptual watershed model that is widely used by the National Weather Services, USA, in operational flood forecasting since its development by Burnash et al. in 1973. There are 19 input parameters within the model. Those parameters and their ranges gathered from literature are listed in Table B-3 in the Appendix. Water accumulation in the catchment is represented using five storages; two upper zones (tension and free water storages) and three lower zones (tension water storage, and primary and supplementary free water storages) (Koren et al., 2004; Samuel et al., 2014). SWE was determined using the degree day snow routine (Samuel et al., 2014). The same

evapotranspiration calculation method used in MAC-HBV is applied in SAC-SMA to account for daily potential evapotranspiration. A detailed description of SAC-SMA is available in Burnash et al. (1973).

A.4.2.4. HEC-HMS

HEC-HMS is a hydrological model developed by the Hydrologic Engineering Center of the US Army Corps of Engineers. It is designed to simulate complete hydrological processes in a dendritic watershed in both space and time (US Army Corps of Engineers, 2016). HEC-HMS comprises six different in-built algorithms to represent different components in runoff generation; meteorological, rainfall loss, direct runoff, river routing, base flow, and reservoir (Cunderlik and Simonovic, 2004). Further details of the HEC-HMS model can be found in the HEC-HMS user manual (US Army Corps of Engineers, 2016). Twenty-three sub-basins were delineated using Light Detection and Ranging (LiDAR) and used in the semi-distributed HEC-HMS model. Inputs to the HEC-HMS model include precipitation, temperature, the monthly average of evapotranspiration, and calibrated parameters. The simplified 'Thornwaite' formula was used to calculate daily potential evapotranspiration using temperature. The calibrated parameters in the existing model were used in this study to simulate flows, as suggested by Chu and Steinman in 2009. Parameters of the HEC-HMS model and range of them extracted from previous literature are listed in the Appendix in Table B-4. Since calibrated parameters of the existing HEC-HMS model were gathered from WRMD, parameter ranges are not mentioned in the table.

A.4.2.5. WATFLOOD

WATFLOOD is a physically-based distributed hydrological model that has been extensively used in flood forecasting since its first introduction in 1973 (Kouwen, 1973). The model subdivides the watershed into Group Response Units (GRUs), assuming surface areas with similar land use to have similar hydrological responses (Kouwen et al., 1993). The runoff response from each GRU was calculated considering processes such as interception, evaporation, infiltration, interflow, recharge, baseflow, overland and channel routing, snow accumulation, and ablation (Kouwen, 2016). Ten river and basin parameters, 11 surface hydrological parameters, and 14 snowmelt parameters for each GRU were used in WATFLOOD. Parameter ranges for each of the land cover classes were gathered from the previous literature and used during the calibration. Since the number of parameters is relatively large, only optimized parameters and parameter ranges for forest land cover class were listed in table B-5 in the Appendix. It uses Green Kenue, a GIS-based data processing, and visualization tool, as the graphical user interface for data pre and post-processing. Further details on WATFLOOD are included in Kouwen (1973).

A.4.3. Model calibration and validation

Selected models were calibrated against observed daily streamflow time series for seven years over the period 2006-01-01 to 2012-12-31. Models were validated against data for three years over the period 2013-01-01 to 2015-12-31 for model comparison. Data recorded in the first year (2006) were used for model warm-up. Dynamically

Dimensioned Search (DDS; Tolson and Shoemaker, 2008) optimization algorithm was used to determine optimal parameter sets for all models. The optimal parameter sets were found by maximizing Nash Sutcliffe Efficiency (NSE, Eq A-1) objective functions that address mean, low, and high flows at the same time (Samuel et al., 2011). Optimization Software Toolkit (OSTRICH) was used to automate the processes of model calibration. OSTRICH is a model-independent, Windows-based program that is designed to perform optimization without the need for any other additional software (Matott, 2016). OSTRICH currently supports 36 optimization and calibration algorithms; 7 Deterministic (Local Search), 13 Heuristic (Global Search), 3 Multi-Objective Optimization and Multi-Criteria Calibration, 1 Hybrid (Heuristic + Deterministic), and 4 Sampling Algorithms (Uncertainty-based Optimization).

Even though sub-daily precipitation is preferred for model calibration and validation, especially for flood forecasting, daily precipitation data were used in this study due to several reasons. Data limitation is a challenge in this regional context. Only daily precipitation data is publicly available from EC for the study period of 2006 to 2015. The flood management authority for this watershed (WRMD) had been using daily data for long term hydrological studies. The attempt to derive high temporal resolution precipitation from observed daily precipitation using numerous approaches proposed in the literature (Güntner et al., 2001; Olsson, 1995) was not possible because there was no hourly precipitation data to validate the disaggregated precipitation directly. Since disaggregation can introduce more errors, the original daily data were used for model calibration and validation. After considering climate, basin morphology, drainage pattern,

and historical flood records, Gray (1988) suggested that the flood is resulted in the Waterford River watershed by synoptic rainfall events with durations of about two days. Therefore, daily streamflow simulations generated by the hydrological models could adequately capture peak flows at the Waterford River at Kilbride hydrometric station. However, it is noteworthy that daily peak flow can be different from hourly peak flow. The proposed hydrological models will need to be re-calibrated for use with sub-daily data when they become available.

A.4.4. Model performance criteria

The fitness of simulated flows to the observed flows was evaluated based on common model performance statistics. It is important to note that the performance of evaluation criteria varies according to the targeted portion (low, mean, and peak flows) of the hydrograph. The model performance criteria used in this study are listed below:

***Nash Sutcliffe Efficiency (NSE)*:** (Eq A-1) NSE only for peak flows was calculated for evaluation of peak flows, and it is denoted as PNSE. The value of 1 indicates a perfect fit (Nash and Sutcliffe, 1970). Values between 0.0 and 1.0 are generally viewed as acceptable levels of performance, whereas NSE>0.50 is considered satisfactory (Moriasi et al., 2007).

Correlation coefficient (r): (Eq A-2) value of 1 indicates a perfect fit.

***Kling-Gupta Efficiency (KGE)*:** (Eq A-3) ranges from $-\infty$ to 1, with one being the optimal value (Gupta et al., 2009).

***Percent Bias (PBIAS)*:** (Eq A-4) optimal value of PBIAS is 0.0, with low-magnitude values indicating accurate model simulation. Positive values indicate model overestimation bias, and negative values indicate model underestimation bias.

***PFC (Peak Flow Criterion)*:** (Eq A-5) focuses on the accuracy of predicting peak flows (Ribeiro et al., 1998). The value of 1 indicates no correlation and value of zero for a perfect fit. The Modified Peak Flow Criterion (MPFC) is used in this study for consistency (i.e., 1 for the perfect fit).

RMSE-observations standard deviation ratio (RSR): (Eq A-6) RSR standardizes RMSE using the observations standard deviation making it a better tool for model inter-comparisons (Moriasi et al., 2007). Values of 0 are optimal, with lower values indicate good model performance (Moriasi et al., 2007).

Equations

$$NSE = 1 - \frac{\sum_{i=1}^{n}\left(Q_i - \widehat{Q}_i\right)^2}{\sum_{i=1}^{n}(Q_i - \bar{Q})^2} \quad \text{(A-1)}$$

$$r = \frac{\sum_{i=1}^{n}\left(\widehat{Q}_i - \bar{\widehat{Q}}\right)(Q_i - \widehat{Q}_i)}{\sqrt{\sum_{i=1}^{n}\left(Q_i - \widehat{Q}_i\right)^2 * \sum_{i=1}^{n}\left(\widehat{Q}_i - \bar{\widehat{Q}}\right)^2}} \quad \text{(A-2)}$$

$$KGE = 1 - \sqrt{(r-1)^2 + (\alpha - 1)^2 + (\beta - 1)^2} \quad \text{(A-3)}$$

$$PBIAS = \left[\frac{\sum_{i=1}^{N}(\widehat{Q}_i - Q_i) * (100)}{\sum_{i=1}^{N}(Q_i)}\right] \quad \text{(A-4)}$$

$$MPFC = 1 - \frac{\left[\sum_{i=1}^{n_p}(Q_{pi} - \hat{Q}_{pi})^2 Q_{pi}^2\right]^{1/4}}{\left(\sum_{i=1}^{n_p} Q_{pi}^2\right)^{1/2}} \quad \text{(A-5)}$$

$$RSR = \frac{RMSE}{STDEV_{(Q_i)}} = \frac{\left[\sqrt{\sum_{i=1}^{N}(Q_i - \widehat{Q}_i)^2}\right]}{\left[\sqrt{\sum_{i=1}^{N}\left(Q_i - \bar{\hat{Q}}\right)^2}\right]} \quad \text{(A-6)}$$

Where,

Q_i	observed flow at i^{th} data point
$\bar{Q}$	mean observed flow
$\widehat{Q}_i$	simulated flow at i^{th} data point
$\bar{\hat{Q}}$	mean simulated flow
n	number of data points
n_p	number of peak flows that are greater than 75 percentiles of observed flow
Q_{pi}	observed peak flows
$\hat{Q}_{pi}$	simulated peak flows
r	linear correlation coefficient

α	measure of relative variability
β	bias (ratio between the simulated and observed values)
NSE_{log}	NSE calculated using the log streamflow values (for low flows)
NSE_{sqr}	NSE found using the squared streamflow values (for high flows)

A.5. Results and Discussion

A comparison of the model performance statistics for the streamflow simulation at the "Waterford river at Kilbride" hydrometric station for the calibration and validation periods is summarized in Tables A-2 and A-3, respectively. The SAC-SMA model appears to perform well in simulating stream flows, with the best prediction accuracy during the calibration period (KGE =0.85 and r = 0.87). Relatively low RMSE (1.48 m^3s^{-1}) and SRS (0.49) statistics suggest that the SAC-SMA model is capable of simulating stream flows more accurately regarding errors. Even though SAC-SMA performs well, the negative PBIAS suggests that the model slightly underestimates the flow during the calibration. Relatively high MPFC (0.79) and PNSE (0.62) reveals that the SAC-SMA model can capture not only low and medium-range flows but also peak flows well. The GR4J model also has similar performance results (KGE = 0.82 and r =0.85) as compared to SAC-SMA for both low and medium-range flows. However, the GR4J model underpredicts flows more than SAC-SMA based on the percentage PBIAS values (-1.96% and -5.71% for SAC-SMA and GR4J, respectively). Statistics for peak flows suggest that the GR4J performs equally as the SAC-SMA model in capturing peak flows in the calibration period. Even though the performances are lower than SAC-SMA and GR4J models, KGE, r, and RMSE statistics indicate that the MAC-HBV, HEC-HMS, and

WATFLOOD models also can provide satisfactory (KGE >0.5) results during the calibration period for both low and medium-range flows. All three models underpredict observed flows, but the HEC-HMS model's performance is relatively better than MAC-HBV and WATFLOOD regarding underprediction (Table A-2). Peak flow statistics indicate that the MAC-HBV, HEC-HMS, and WATFLOOD models can provide reasonably good results where HEC-HMS performs relatively better. In general, all five models provide adequate results, but SAC-SMA and GR4J outperform the other three models in the calibration period.

A similar trend was observed during the validation for all low, medium-range, and peak flows of all five models. In contrast to the calibration period, the SAC-SMA, GR4J, and HEC-HMS models appear to slightly overpredict observed flows during the validation period (Table A-3). The MAC-HBV, HEC-HMS, and WATFLOOD models have similar performance for both low and medium-range flows, but WATFLOOD performs relatively better in the validation period for all flows. In general, the SAC-SMA and the GR4J models appear the best performing for all flows in both calibration and validation periods. The MAC-HBV, HEC-HMS, and WATFLOOD models perform reasonably well for low to medium-range flows but underestimate peak flows in both calibration and validation periods.

Table A-2 *Comparison of hydrological model performances in simulating streamflow in Waterford River watershed during the calibration period (note: the best model performance and the second-best model performance are indicated by* ***underlined bold*** *and* ***bold****, respectively)*

Model	Calibration						
	All flows					Peak flow	
	KGE	r	RMSE (m^3s^{-1})	PBIAS (%)	RSR	MPFC	PNSE
SAC-SMA	**0.85**	**0.87**	**1.48**	**-1.96**	**0.49**	**0.79**	**0.62**
GR4J	**0.82**	**0.85**	**1.61**	-5.71	**0.53**	**0.77**	**0.53**
MAC-HBV	0.62	0.72	2.13	-10.05	0.70	0.71	0.38
HEC-HMS	0.75	0.79	2.12	**-4.27**	0.70	0.75	0.44
WATFLOOD	0.64	0.71	2.24	-10.81	0.74	0.70	0.32

Table A-3 *Comparison of hydrological model performances in simulating streamflow in Waterford River watershed during the validation period (Note: the best model performance and the second-best model performance are indicated by* ***underlined bold*** *and* ***bold,*** *respectively)*

Model	Validation						
	All flows					Peak flow	
	KGE	r	RMSE (m^3s^{-1})	PBIAS (%)	RSR	MPFC	PNSE
SAC-SMA	**0.82**	**0.84**	**1.50**	**2.27**	**0.60**	**0.80**	**0.44**
GR4J	**0.81**	**0.82**	**1.54**	7.62	**0.62**	**0.77**	0.36
MAC-HBV	0.65	0.68	1.91	-10.73	0.77	0.68	0.32
HEC-HMS	0.67	0.75	2.00	**5.62**	0.80	0.76	0.37
WATFLOOD	0.66	0.72	1.76	-10.60	0.71	0.70	**0.39**

To further assess the general model performances, scatter plots of observed vs. simulated flows for each model for calibration and validation periods are used (Figure A-3). Data are more clustered along the 45° line in the case of both SAC-SMA and GR4J models. The SAC-SMA and GR4J models generally perform well for all low, medium, and high flows in both calibration and validation periods. The HEC-HMS model performs reasonably well for most flows in both calibration and validation periods, except for overestimating at low flows. MAC-HBV performs well for low flows but shows some inconsistencies at medium and high flows in both calibration and validation periods. The WATFLOOD also performs reasonably well for low flows in both calibration and validation period but with a clear underestimation at medium-range and high flows in the calibration period. However, WATFLOOD performs relatively better in the validation period, especially for high flows compared to calibration. The scatterplots also show that the results are more dispersed from the 45° line with increasing flows for all models. In general, the SAC-SMA and the GR4J models show better performance for all flows in both calibration and validation periods. On the other hand, the HEC-HMS model captures most of the peaks during both calibration and validation period and hence competes with SAC-SMA and GR4J. The WATFLOOD and MAC-HBV models perform reasonably well for low to medium-range flows but underestimate peak flows in both calibration and validation periods.

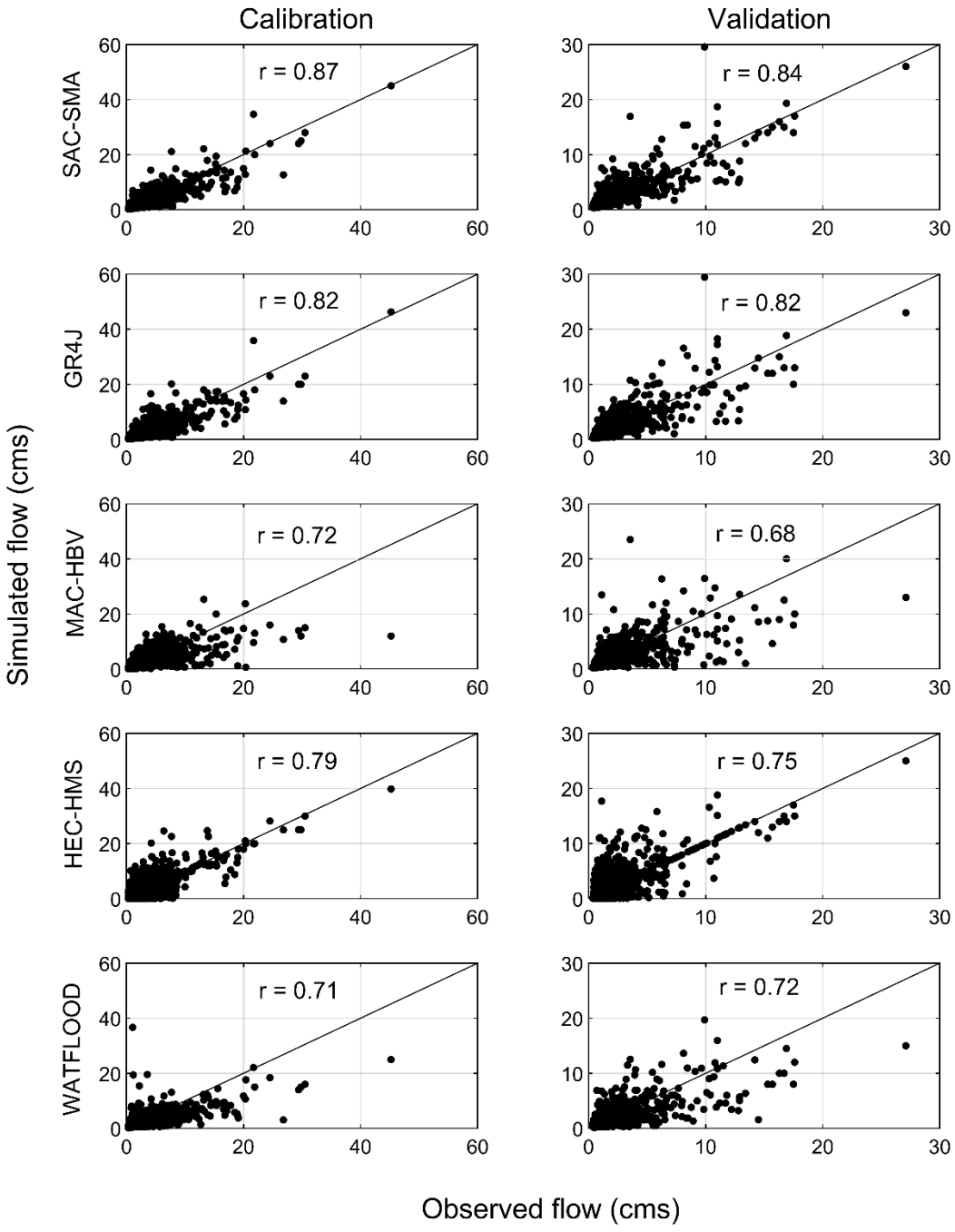

Figure A-3 *Scatter plots of observed and simulated flows using SAC-SMA, GR4J, MAC-HBV, HEC-HMS, and WATFLOOD for the calibration period (2007 to 2012) and the validation period (2013 -2015)*

Hydrographs of observed and simulated stream flows are shown for the year 2011 for calibration and 2015 for the validation period in Figures A-4 and A-5, respectively. SAC-SMA model appears effective at simulating the magnitude and timing of all stream flows better than other models during the calibration period. The same trend is observed during the validation period for SAC-SMA but shows some inconsistencies in the early months of the year. The GR4J model is also able to capture all flows as accurately as the SAC-SMA model during the calibration period except towards the end of the year. The agreement between observed and simulated flows in both rising limbs and falling limbs of the hydrographs is more accurate for both SAC-SMA and GR4J models during the validation period. The other models tend to underpredict or overpredict observed flows and are not able to capture the rising and falling limbs of the hydrograph accurately as SAC-SMA and GR4J. Therefore, the hydrographs and model performances indicate that the SAC-SMA and the GR4J models to provide better streamflow simulations.

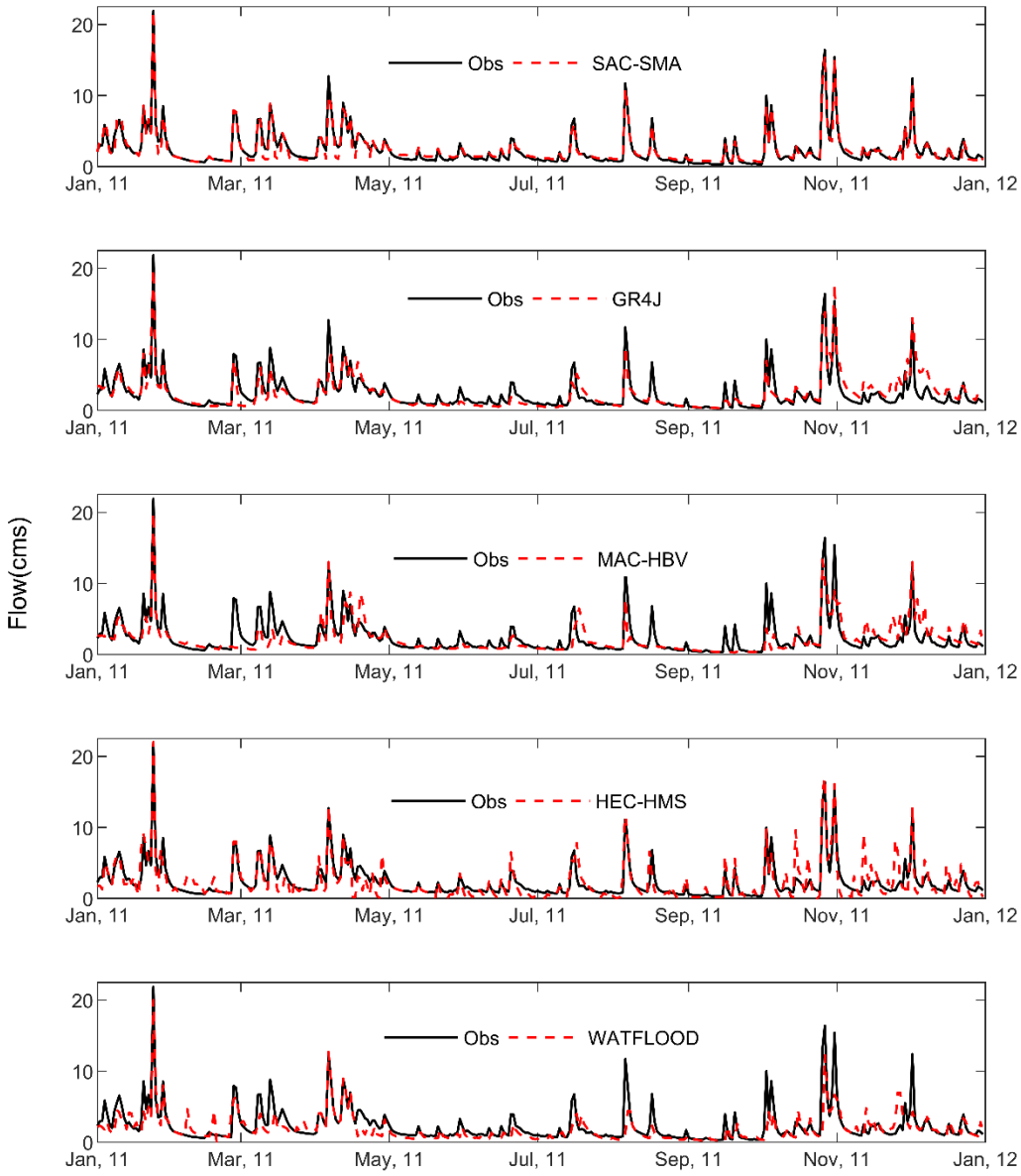

Figure A-4 *Hydrographs of streamflow for the calibration period (only for 2011) (Note: Obs: observed flow)*

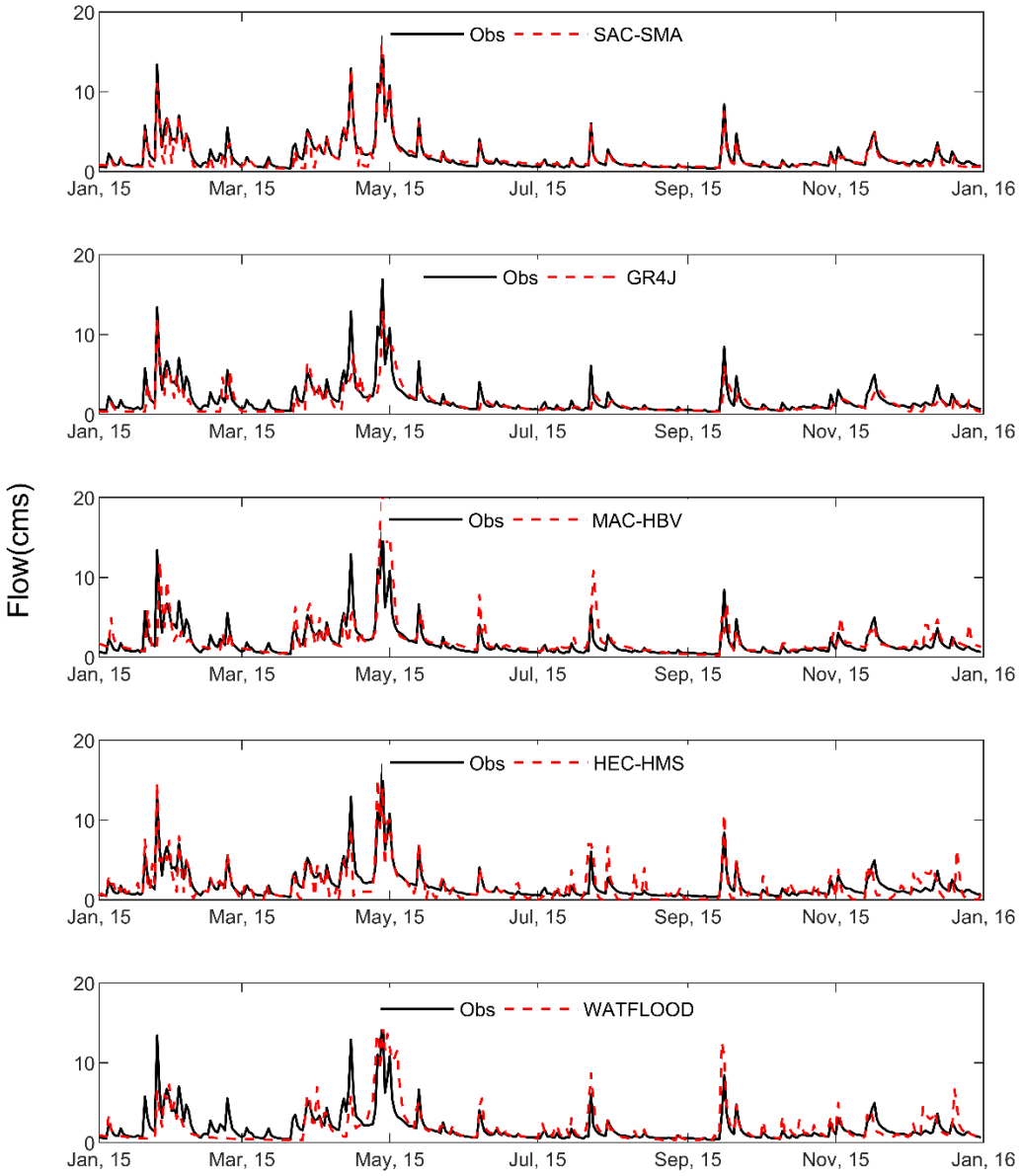

Figure A-5 *Hydrographs of streamflow for the validation period (only for 2015) (Note: Obs: observed flow)*

For further analysis, Taylor diagrams are used to select the best model based on three statistical parameters; standard deviation, correlation coefficient, and centered root

mean square error for both calibration and validation periods (Figure A-6). Similarly to the results discussed above, the GR4J and SAC-SMA models perform competitively well as they are plotted closest to the black arc as well as the point "OBS". The MAC-HBV, HEC-HMS, and WATFLOOD models also closely follow GR4J and SAC-SMA models indicating comparatively good performance.

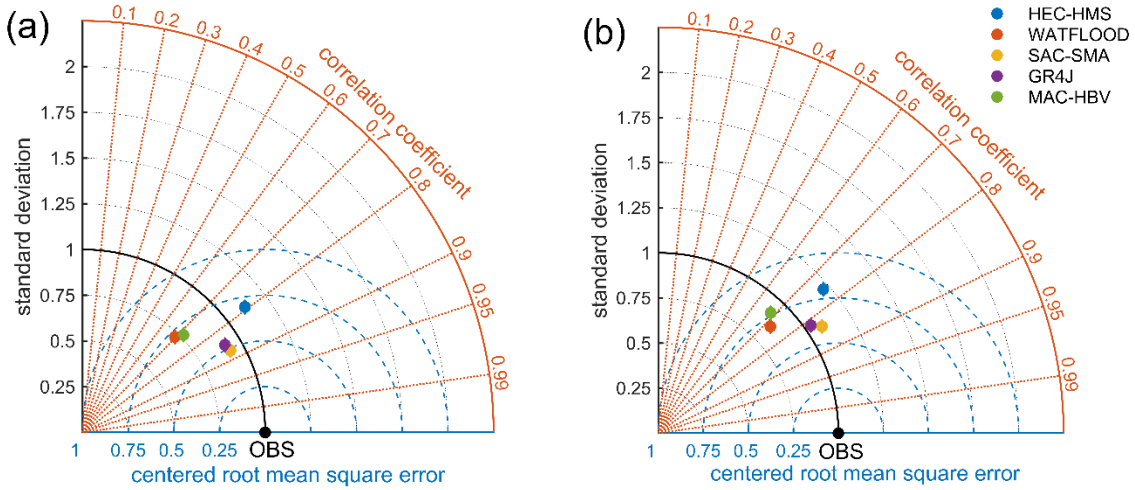

Figure A-6 *Taylor diagrams showing a statistical assessment of simulated flows from five hydrologic models SAC-SMA, GR4J, MAC-HBV, HEC-HMS, and WATFLOOD for the calibration (a) and validation period (b) (Note: Diagram summarizes three statistical performances (standard deviation, correlation coefficient, and centered root mean square error) for each model. Different colors denote different models. The best model plots itself closer to the black arc as well as the point 'OBS' (observed flow), which represents agreement with observations).*

Apart from model simulation accuracy, some other factors which affect model selection for operational streamflow forecasting were also considered in this study. Model simulation time, user-friendliness, input data requirement, and availability were also evaluated along with the model simulation accuracy as a requirement for forecasting.

When all models run on computers with similar computational power, no significant time difference observed between the five models.

A significant difference in user-friendliness was experienced among the models used in this study. The HEC-HMS model has its own data preprocessing tool called "HEC-DSSVue" and user-friendly Graphical User Interface (GUI). HEC-DSSVue is a Java-based program that can be used to process observed meteorological data for input to HEC-HMS. HEC-DSSVue produces observed meteorological time series formatted for compatibility with HEC-HMS. All three lumped models do not have a GUI, and original MATLAB codes were run in MATLAB software in the study. The "Geen Kenue" software was used to pre and post-processing data for WATFLOOD, even though it does not have a prebuilt GUI interface. Therefore, data preprocessing, input-output, visualization, and model forcing is relatively easy with HEC-HMS compared to the other four models.

When considering the complexity and input data requirement, all three lump models are advantageous as they only require temperature and precipitation as model forcing. The fully distributed WATFLOOD model only requires land cover as an additional input other than temperature and precipitation. On the other hand, the semi-distributed HEC-HMS model requires more basin characteristics, which result in difficulties in model implementation.

The availability of hydrologic models may also play a role in model selection for operational forecasting. All the HEC-models are freely available at the US Army Corps of Engineers website via www.hec.usace.army.mil/software/hec-hms/downloads.aspx. The GR4J model is also available as a pre-built full R package "airGR" where R is free software available to the public. Calculated evapotranspiration is a requirement for the

original GR4J model. Evapotranspiration also could be calculated using the pre-built R package "Evapotranspiration" using 21 different formulations, including Penman, Penman-Monteith FAO 56, Priestley-Taylor and Morton formulations. Therefore, the use of the GR4J model is advantageous over other models and has openings for further development. The other three models used in this study are not freely available and hence is a disadvantage.

A.6. Operational flow forecasting

To verify the potential of the best performing hydrological models for operational streamflow forecasting in the Waterford River watershed, deterministic hydrologic forecasts were performed. The SAC-SMA, GR4J, and HEC-HMS hydrological models were used to simulate the streamflow for forecast ranges of 1 to 5 days ahead. The HEC-HMS model was run as the benchmark model. Flows were simulated for six months from 2017-06-01 to 2017-12-31 on a daily time step. The simulation was limited to only six months because the observed flow data were available only up to 31 December 2017. Global Deterministic Prediction System (GDPS) meteorological forecasts archived in Canadian Surface Prediction ARchive (CaSPAr) (https://caspar-data.ca/) were used to force the selected hydrological models. GDPS forecast weather variables are available in daily time step, and therefore, daily time streamflow simulations for up to five days ahead were generated using selected hydrologic models. Forecasted GDPS meteorological data (precipitation and temperature) were assessed before forcing the hydrological models to verify the quality of archived meteorological data. This assessment was performed using observed precipitation and temperature for two years from 2017-06-01 to 2019-06-01

recorded at “St. john’s Intl A” and “St. John’s West Climate” EC weather station in St. John’s, NL. The evaluation was performed by first overlying observation gauge points on GDPS forecast grids and then by comparing corresponding GDPS pixel value with the observed gauge value. To evaluate the quality of forecast meteorological data, the correlation coefficient and RMSE were chosen, as shown in table A-4. Average forecast weather variables corresponding to “St. john’s Intl A” and “St. John’s West Climate” EC weather stations were used as input for hydrologic model runs.

Table A-4 *Evaluation results of GDPS forecasts*

	r					RMSE				
Lead time (days ahead)	1	2	3	4	5	1	2	3	4	5
Precipitation	0.82	0.63	0.56	0.35	0.29	5.40	8.00	8.61	11.80	13.87
Temperature	0.98	0.95	0.88	0.85	0.81	1.86	2.74	3.60	3.38	4.50

The statistics show that the temperature forecasts for the study area performed well and better than precipitation forecasts (Table A-4). For the precipitation, correlation is significant for short lead times. On the other hand, temperature shows a significant correlation for all lead times up to 5 days ahead. In both cases, performance decreases with increasing lead time. RMSE follows a similar pattern as the correlation coefficient for both precipitation and temperature. Overall, the results suggest that the GDPS data perform well only for short lead times for precipitation while it performs well for longer lead times for temperature.

The results of the forecasting flow using SAC-SMA, GR4J, and HEC-HMS are presented in Table A-5, A-6, and A-7, respectively. Both SAC-SMA and GR4J models perform reasonably well for up to 1 to 3 day ahead forecasts. The agreement between

observed and simulated flows in both the rising limbs and the falling limbs of the hydrographs (Figure A-7) is more accurate for both SAC-SMA and GR4J models for one day ahead forecasts. The benchmark model, HEC-HMS, does not perform equally well for all flows when compared to the SAC-SMA and GR4J models. The HEC-HMS model performs relatively well for the peak flows as the SAC-SMA and GR4J models (Figure A-7). As expected, based on the forecast evaluation results, the performance decreases with increasing lead time (Figure A-7). The average time of concentration of the watershed was calculated to be about 10.8 hours (Smith, 1988). GDPS daily forecasts are released in 6-hour intervals a day (time of 00:00, 06:00, 12:00, and 18:00). Therefore, daily streamflow forecasts using hydrological models can be issued in 6-hour time intervals. Hence, the methods used in this study can capture most of the peaks adequately.

Table A-5 *Model performances for streamflow forecast up to 5 days forecasts using SAC-SMA model*

SAC-SMA	All flows					Peak flow	
	KGE	r	RMSE (m^3s^{-1})	PBIAS (%)	RSR	MPFC	PNSE
1	**0.75**	**0.91**	**0.92**	**17.91**	**0.38**	**0.60**	**0.67**
2	**0.46**	**0.87**	**1.23**	**29.63**	**0.51**	**0.58**	**0.28**
3	**0.42**	**0.74**	**1.34**	**63.21**	**0.85**	**0.41**	**0.12**
4	-0.28	0.58	3.52	84.25	1.90	0.32	0.08
5	-2.42	0.42	5.23	217.10	4.71	0.22	-0.92

Table A-6 *Model performances for streamflow forecast up to 5 days forecasts using GR4J model*

GR4J	All flows					Peak flow	
	KGE	r	RMSE (m^3s^{-1})	PBIAS (%)	RSR	MPFC	PNSE
1	**0.65**	**0.90**	**1.00**	**36.08**	**0.40**	**0.60**	**0.50**
2	**0.42**	**0.85**	**1.53**	**38.80**	**0.69**	**0.48**	**0.12**
3	**0.23**	**0.72**	**3.33**	**72.48**	**0.84**	**0.45**	**0.06**
4	-0.52	0.57	4.23	92.00	2.31	0.33	0.01
5	-2.52	0.23	5.63	221.96	4.78	0.12	-1.02

Table A-7 *Model performances for streamflow forecast up to 5 days forecasts using HEC-HMS model.*

HEC-HMS	All flows					Peak flow	
	KGE	r	RMSE (m^3s^{-1})	PBIAS (%)	RSR	MPFC	PNSE
1	**0.42**	**0.85**	**2.42**	**43.59**	**0.61**	**0.58**	**0.32**
2	**0.22**	**0.72**	**3.07**	**60.48**	**0.93**	**0.32**	**0.07**
3	**0.10**	**0.57**	**4.94**	**92.60**	**1.36**	**0.31**	**0.01**
4	-1.15	0.13	5.37	181.00	2.89	0.12	-1.02
5	-3.25	0.01	7.35	414.32	3.96	0.08	-2.00

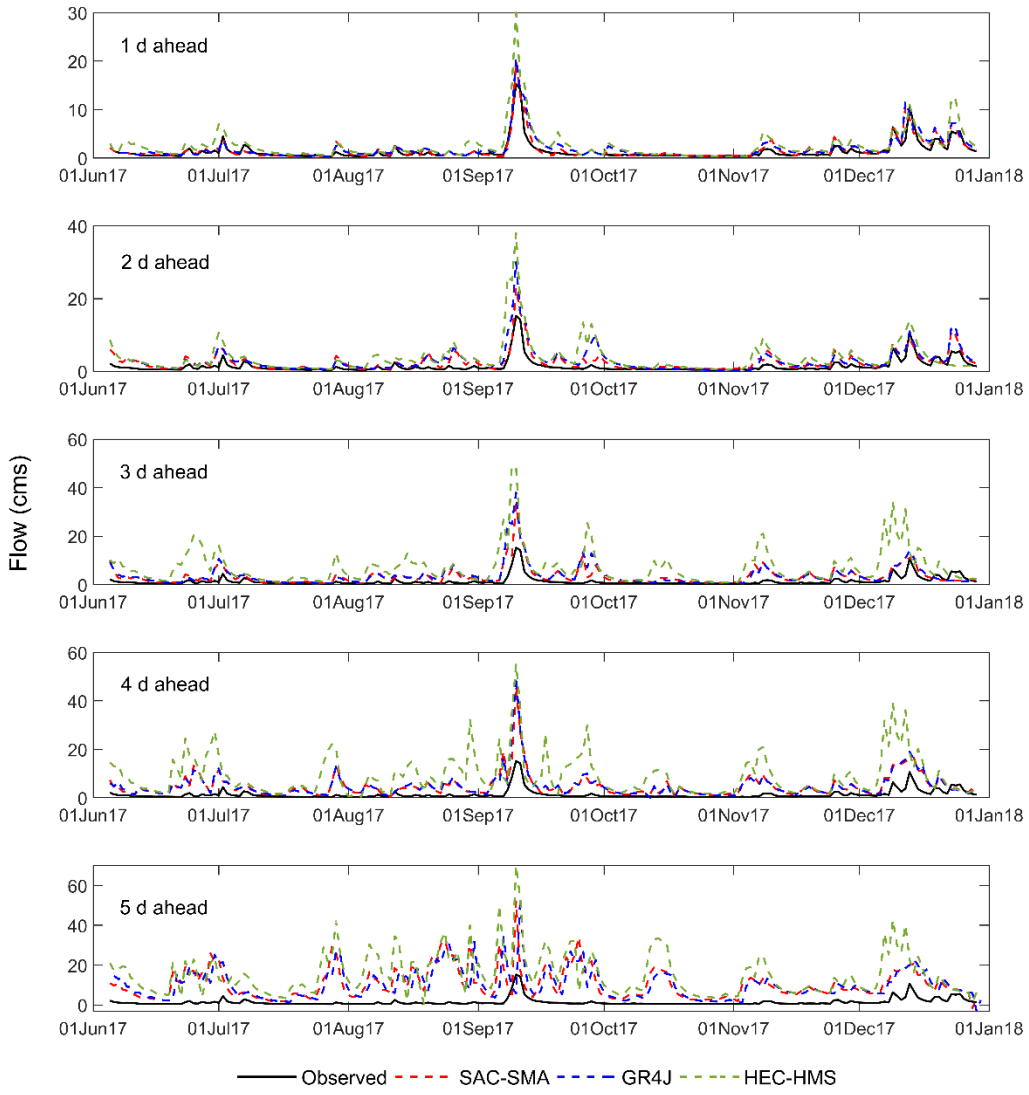

Figure A-7 *Hydrographs of streamflow for 1 to 5 days ahead forecasts using SAC-SMA, GR4J, and HEC-HMS*

A.7. Conclusions

From the results presented in this paper, it can be concluded that all five models are capable of simulating streamflow reasonably well. The SAC-SMA and GR4J models perform equally well and perform better than the other three models in both calibration and validation periods for all low, medium, and peak flows. The SAC-SMA and GR4J models generally perform better for peak flows, followed by HEC-HMS. The WATFLOOD and MAC-HBV models perform better in simulating low flows but underpredict high flows. The results from the statistics, hydrographs, scatter plots, and Taylor diagrams indicate that the best performing models are SAC-SMA and GR4J, followed by HEC-HMS. Forecasting model runs using GDPS meteorological forecasts have been verified by their accuracy in forecasting the observed streamflow in the Waterford River watershed. If a single model to be used for forecasting, the GR4J model can be recommended. Relatively smaller basin size, less input data requirement, efficiency in computational timing, freely available R-package makes GR4J as the best model to be used in operational flood forecasting in the Waterford River basin in St. John's, NL. However, due to the good performance of all five models, an ensemble streamflow forecast using continuous, multiple hydrological models for operational forecasting is also recommended. The resultant flows for hydrological models can be used as forcing data for existing hydraulic models at WRMD to produce user-friendly flood risk maps to be delivered via social media to the public. The use of existing knowledge gathered through a long time of hands-on experience of forecasters along with

hydrological and hydraulic model runs will produce more accurate operational flood forecasting for St. John's, NL.

A.8. Acknowledgments

The work for this manuscript was performed while the first author, Dayal Buddika Wijayarathne, was an intern graduate student at Water Resources Management Division, Department of Municipal Affairs and Environment, Government of Newfoundland and Labrador. The authors would like to thank Dr. Amir Ali Khan, Dr. Nicholas Kouwen, and Mr. Mohammad Khayer for their help in collecting the required data, implementing models, and contributions to various aspects of this research. The authors are also grateful to the Canadian Surface Prediction ARchive (CaSPAr) system from where forecast data were downloaded.

A.9. Appendix

Table B-1 *Model parameters in GR4J model.*

Parameter	Description	Range	Units
xl	Capacity of the production soil store	1 to 1500	mm
x2	Water exchange coefficient	-10 to 5	mm
x3	Capacity of the routing store	1 to 500	mm
x4	Time parameter for unit hydrographs	0.5 to 4	days
tr	Rainfall threshold temperature	0 to 2.5	℃
scf	Snow correction factor	0.4 to 1.6	-
dff	Degree day factor	0 to 5	$mmday^{-1}℃^{-1}$
rcr	Rainfall correction factor	0.5 to 1.5	-
athorn	A constant for Thornthwaite's equation	0.1 to 0.3	-

Table B-2 *Description of MAC-HBV model parameters.*

Parameter	**Description**	**Range**	**Units**
tr	Rain threshold	0 to 2.5	℃
scf	Snow correction factor	0.4 to 1.6	-
ddf	Degree-day factor	0 to 5	$mmday^{-1}℃^{-1}$
athorn	Coefficient of a simplified version of Thornthwaite's formula	0.1 to 0.3	-
fc	Maximum soil box water content	50 to 800	mm
flp	Limit for potential evaporation	0.1 to 0.9	-
beta	A non-linear parameter controlling runoff generation	0 to 10	-
k0	Flow recession coefficient	1 to 30	day
lsuz	A threshold value to control response routing	1 to 100	mm
k1	Flow recession coefficient in the upper soil reservoir	30 to 100	day
cperc	Constant percolation rate parameter	0.01to 6	$mmday^{-1}$
k2	Flow recession coefficient in the lower soil reservoir	100 to 500	day
maxbas	Runoff distribution parameter	1to 20	day
rcr	Rainfall correction factor	0.5 to 1.5	-
alpha	Non-linearity coefficient	0.5 to 1.25	-

Table B-3 *Description of SAC-SMA model parameters.*

Parameter	Description	Range	Units
uztwm	Upper-zone tension water maximum storage	1 to 150	mm
uzfwm	Upper-zone free water maximum storage	1 to 150	mm
lztwm	Lower-zone tension water maximum storage	1 to 500	mm
lzfpm	Lower-zone free water primary maximum storage	1 to 1000	mm
lzfsm	Lower-zone free water supplemental maximum storage	1 to 1000	mm
adimp	Additional impervious area	0 to 0.4	-
uzk	Upper-zone free water lateral depletion rate	0.1 to 0.5	day^{-1}
lzpk	Lower-zone primary free water lateral depletion rate	0.1 to 0.5	day^{-1}
lzsk	Lower-zone supplemental free water lateral depletion rate	0.01 to 0.25	day^{-1}
zperc	Maximum percolation rate	1 to 250	-
rexp	Exponent of the percolation equation	1 to 5	-
pctim	Impervious fraction of the watershed area	0 to 0.9	-
pfree	Fraction percolating from upper to lower zone free water storage	0 to 0.6	-
rq	Residence time parameters of quick flow	0 to 0.99	-
ddf	Degree day factor	0 to 5	$mmday^{-1}°C^{-1}$
scf	Snowfall correction factor	0.4 to 1.6	-
tr	Upper threshold temperature to distinguish between rainfall and snowfall	0 to 2.5	°C
athorn	A constant for Thornthwaite's equation	0.1 to 0.3	-
rcr	Rainfall correction factor	0.5 to 1.5	-

Table B-4 *Description of HEC-HMS model parameters.*

Component	Symbol	Parameter	Units
Snow	*tmax*	Upper temperature threshold	$^{\circ}C$
	tmin	Lower temperature threshold	$^{\circ}C$
	tcrt	Critical temperature for snowmelt	$^{\circ}C$
	mr	Snowmelt rate	$mm^{\circ}C^{-1}day^{-1}$
Precipitation loss	*ss*	Surface storage capacity	mm
	if	Infiltration rate	$mmday^{-1}$
	is	Initial soil storage	-
	us	Soil storage capacity	mm
	ts	Tension zone capacity	mm
	sp	Soil percolation rate	$mmday^{-1}$
	g1i	Initial ground water 1 storage	-
	g1s	Groundwater 1 storage capacity	mm
	g1p	Ground water 1 percolation rate	$mmday^{-1}$
	g1c	Ground water 1 storage coefficient	days
	g2i	Initial groundwater 2 storage	-
	g2p	Groundwater 2 percolation capacity	$mmday^{-1}$
	g2c	Groundwater 2 percolation rate	days
	ai	Impervious sub-basin area	-
	as	Sub-basin area	km^2
Direct runoff	*tc*	Time of concentration	days
	st	Storage coefficient	days
River routing	*so*	Storage-outflow	m^3s^{-1}
	si	Number of sub-reaches	-
Baseflow	*b1s*	Baseflow 1 storage coefficient	day
	b1r	Baseflow 1 number of reservoirs	-
	b2s	Baseflow 2 storage coefficient	day
	b2r	Baseflow 2 number of reservoirs	-

Table B-5 *Optimized parameters of WATFLOOD model for forest land cover class.*

Hydrological Parameters			
Parameter	Description	Range	Units
rec	interflow coefficient	0.5×10^{-3} to 0.1	-
ak	infiltration coefficient bare ground	0.04 to 20	-
akfs	infiltration coefficient snow covered ground	0.04 to 20	-
retn	upper zone retention	0.1×10^{-1} to 0.3	mm
ak2	recharge coefficient bare ground	0.1×10^{-3} to 0.1	-
ak2fs	recharge coefficient snow covered ground	0 to 0.1	-
River and basin parameters			
lzf	Lower zone drainage function parameter	0.1×10^{-6} to 0.1×10^{-3}	-
pwr	Lower zone drainage function exponent	0.3 to 4	-
R2n	River channel Manning's n	0.1×10^{-1} to 0.1	-
kcond	Conductivity of the wetland (bank)-channel interface	0.1 to 0.9	-
theta	Porosity the wetland or channel bank	0.1 to 0.6	-
Snow parameters			
fm	melt factor	0.5×10^{-1} to 0.5	$mm^{\circ}C^{-1}day^{-1}$
base	base temperature for melt calculations	-5 to 5	$^{\circ}C$
sublime_rate	sublimation rate	-0.5×10^{-1} to 0.5	$mmday^{-1}$

A.10. References

Batterson, M.J., 1984. Surficial Geology of the Waterford River Basin. St Johns Nfld. Urban Hydrol. Study Waterf. River Basin Tech. Rep. No UHS WRB 1.

Bergström, S., 1976. Development and Application of a Conceptual Runoff Model for Scandinavian Catchments. Department of Water Resources Engineering, Lund Institute of Technology, University of Lund.

Burnash, R.J.C., Ferral, R.L., McGuire, Robert A., McGuire, Richard A., 1973. A Generalized Streamflow Simulation System: Conceptual Modeling for Digital Computers. U.S. Department of Commerce, National Weather Service, and State of California, Department of Water Resources.

Chu, X., Steinman, A., 2009. Event and continuous hydrologic modeling with HEC-HMS. J. Irrig. Drain. Eng. 135, 119–124.

Cunderlik, J., Simonovic, S.P., 2004. Calibration, verification and sensitivity analysis of the HEC-HMS hydrologic model. Department of Civil and Environmental Engineering, The University of Western Ontario.

Environment and Climate Change Canada, 2017. Canadian Climate Normals [WWW Document]. URL http://climate.weather.gc.ca/climate_normals/ (accessed 8.13.18).

Environment Canada, 2017. Environment and Climate Change Canada - Weather and Meteorology – Weather Tools – FAQ [WWW Document]. URL https://ec.gc.ca/meteo-weather/default.asp?lang=En&n=108C6C74-1#wsA0744309 (accessed 8. 13.18).

Gray, E., 1988. Waterford River Area- Hydrotechnical Study (Project report No. 48160-C2-380000). St. John's.

Güntner, A., Olsson, J., Calver, A., Gannon, B., 2001. Cascade-based disaggregation of continuous rainfall time series: the influence of climate. Hydrol. Earth Syst. Sci. Discuss. 5, 145–164.

Gupta, H.V., Kling, H., Yilmaz, K.K., Martinez, G.F., 2009. Decomposition of the mean squared error and NSE performance criteria: Implications for improving hydrological modelling. J. Hydrol. 377, 80–91.

Heringa, P.K., 1981. Soils of the Avalon Peninsula, Newfoundland. Research Branch Agriculture Canada.

Hydrologic modeling system HEC-HMS technical reference manual (2016). US Army Corps of Engineers, Hydrologic Engineering Center.

Innes, J.C., Nimmrichter, P., 2012. Flood Risk and Vulnerability Analysis Project (Final project report No. #TA1112733). Water Resources Management Division, Newfoundland.

Koren, V., Reed, S., Smith, M., Zhang, Z., Seo, D.-J., 2004. Hydrology laboratory research modeling system (HL-RMS) of the US national weather service. J. Hydrol. 291, 297–318.

Kouwen, N., 2016. WATFLOOD/CHARM Canadian Hydrological And Routing Model. Dep. Civ. Eng. Univ. Waterloo Waterloo Ont. Can.

Kouwen, N., 1973. WATERSHED MODELLING USING A SQUARE GRID TECHNIQUE.

Kouwen, N., Soulis, E.D., Pietroniro, A., Donald, J., Harrington, R.A., 1993. Grouped response units for distributed hydrologic modeling. J. Water Resour. Plan. Manag. 119, 289–305.

Leach, J.M., Kornelsen, K.C., Coulibaly, P., 2018. Assimilation of near-real time data products into models of an urban basin. J. Hydrol.

Matott, L.S., 2016. OSTRICH–An Optimization Software Toolkit for Research Involving Computational Heuristics. Doc. Users Guide Cent. Comput. Res. State Univ. N. Y. Buffalo N. Y. USA.

Moriasi, D.N., Arnold, J.G., Van Liew, M.W., Bingner, R.L., Harmel, R.D., Veith, T.L., 2007. Model evaluation guidelines for systematic quantification of accuracy in watershed simulations. Trans. ASABE 50, 885–900.

Nagai, A., 2003. Hydrologic Modeling of Rainfall-runoff Process and Its Application to Real-time Flood Forecasting. Present Situat. OnThe Water Resour. Water Relat. Disaster Role Agro-Environ. Educ. 111–118.

Nash, J.E., Sutcliffe, J.V., 1970. River flow forecasting through conceptual models part I—A discussion of principles. J. Hydrol. 10, 282–290.

Ng, H.Y.F., Marsalek, J., 1989. Simulation of the effects of urbanization on basin streamflow 1. JAWRA Journal of the American Water Resources Association 25, 117–124.

Natural Resources Canada, 2009. GeoBase - Land Cover, circa 2000-Vector (LCC2000-V).

Olsson, J., 1995. Limits and characteristics of the multifractal behaviour of a high-resolution rainfall time series. Nonlinear Process. Geophys. 2, 23–29.

Perrin, C., Michel, C., Andréassian, V., 2003. Improvement of a parsimonious model for streamflow simulation. J. Hydrol. 279, 275–289.

Razavi, T., Coulibaly, P., 2017. An evaluation of regionalization and watershed classification schemes for continuous daily streamflow prediction in ungauged watersheds. Can. Water Resour. JournalRevue Can. Ressour. Hydr. 42, 2–20.

Reed, S., Schaake, J., Zhang, Z., 2007. A distributed hydrologic model and threshold frequency-based method for flash flood forecasting at ungauged locations. J. Hydrol. 337, 402–420.

Ribeiro, J., Lauzon, N., Rousselle, J., Trung, H.T., Salas, J.D., 1998. Comparaison de deux modèles pour la prévision journalière en temps réel des apports naturels. Can. J. Civ. Eng. 25, 291–304.

Samuel, J., Coulibaly, P., Dumedah, G., Moradkhani, H., 2014. Assessing model state and forecasts variation in hydrologic data assimilation. J. Hydrol. 513, 127–141.

Samuel, J., Coulibaly, P., Metcalfe, R.A., 2012. Identification of rainfall-runoff model for improved baseflow estimation in ungauged basins. Hydrol. Process. 26, 356–366. https://doi.org/10.1002/hyp.8133

Samuel, J., Coulibaly, P., Metcalfe, R.A., 2011. Estimation of continuous streamflow in Ontario ungauged basins: comparison of regionalization methods. J. Hydrol. Eng. 16, 447–459.

Sheppard, G., 2018. Waterford River Area Flood Risk Mapping Study (Final project report). Water Resources Management Division, St. John's.

Smith, D.A., 1988. Watersehd Modelling Report HYMO, 1988 (Main report No. DAS/0639D). St. John's.

Statistics - Newfoundland & Labrador Statistics Agency [WWW Document], n.d. URL https://www.stats.gov.nl.ca/statistics/Census2016/ (accessed 10.7.19).

Tolson, B.A., Shoemaker, C.A., 2008. Efficient prediction uncertainty approximation in the calibration of environmental simulation models. Water Resour. Res. 44.

Unduche, F., Tolossa, H., Senbeta, D., Zhu, E., 2018. Evaluation of four hydrological models for operational flood forecasting in a Canadian Prairie watershed. Hydrol. Sci. J.